Synthesis and Development of One-part Rock-based Geopolymers for Well Cementing Applications

by

Mohamed Omran

Thesis submitted in fulfilment of
the requirements for the degree of
PHILOSOPHIAE DOCTOR
(PhD)

Faculty of Science and Technology
University of Stavanger
Fall 2023

University of Stavanger
NO-4036 Stavanger
NORWAY
www.uis.no

©2023 Mohamed Omran

ISBN: 978-82-8439-185-4
ISSN: 1890-1387
PhD: Thesis UiS No. 717

To my family; especially my parents,
for all the support and motivation!

Acknowledgements

This research has been mostly done at the University of Stavanger, at the Department of Energy and Petroleum Engineering (IEP). I would like to thank all my colleagues in SWIPA Lab for their great support, especially Sondre Hjelm, Dr. Mohammadreza Kamali, Dr. Fawzi Chamssine, Mya Chordar, and Dr. Sajjad Yousefi Oderji. I would like to thank all the staff and engineers at IEP including Øystein Arild, Norbert Puttkamer, Hilde Jonsbråten, Caroline Rudd, Jostein Djuve, Kim Vorland, Inger Johanne Olsen, Sivert Drangeid, and Samdar Kakay.

I would like to gratefully thank my supervisors Professor Mahmoud Khalifeh and Professor Arild Saasen for all their help and massive support in my PhD and for allowing me to lead this project.

I would like to acknowledge the Research Council of Norway for financing this work. Furthermore, I would like to thank the industrial partners for this project: Aker BP, TotalEnergies, and ConocoPhillips for their feedback and support. Many thanks go to Laurent Delabroy, and Gunnar Lende for their valuable input throughout the project.

I also gratefully acknowledge the staff and engineers of the Microlab in the faculty of Civil Engineering & Geosciences at the Delft University of Technology, especially Professor Guang Ye and Dr. Xiujiao Qiu, for their hospitality that made my visit very beneficial and joyful.

Finally, I would like to thank my incredible family, my dad, my mom, my sisters, my love, and my amazing friends for their support throughout my challenges during this journey.

I dedicate this work to you all.

Mohamed Omran

Stavanger – July 2023

Preface

A one-part or Just Add Water (JAW) geopolymer system is an environmental- and user-friendly alternative to Ordinary Portland Cement (OPC) and conventional geopolymers. It helps with producing lower CO_2 emissions avoiding OPC processing and eliminating the need for unnecessary liquid transportation for conventional geopolymers. A one-part geopolymer is ideal for large-scale deployment of geopolymers in well-cementing applications. It can help with quality control processes and reduce the need for extensive end-user knowledge of the chemistry involved.

Accordingly, this study is to design a successful one-part naturally occurring (i.e., unprocessed nor pre-processed) granite-based geopolymer formulation. It aims to understand all possible impacts on the performance of these geopolymers of the utilized components including precursors, activators, water content and chemical admixtures. It is also to take into account petroleum engineering standards.

This research is part of the SafeRock Project which is in collaboration between the University of Stavanger and operator and service companies. Additionally, it is done with a tight collaboration with academic institutes including Delft University of Technology (TU Delft, Netherlands), Universidade Federal do Rio de Janeiro (UFRJ, Brazil) and University of Oklahoma (OU, United States).

The outcomes of this thesis have been published in seven scientific articles: four journal papers, two peer-reviewed conferences, one SPE conference, and a filed patent application in Norway and a PCT application in Europe. This section is composed of a brief description of the published articles and their scientific findings. The outcomes of this research can be summarized as the following:

Paper I shows the normalization of a Norwegian grounded granite in the solid phase by slag, microsilica, potassium silicates and alkali-metal hydroxides. It illustrates the synthesis of a one-part granite-based geopolymer for well-cementing applications (JAW). It reveals the chemical composition of granite needs normalization. Fluid-state properties at 50 ℃ and solid-state properties at 70 ℃ are investigated. These investigations include pumpability, strength development, mineralogy, and morphology.

Papers II and III present monitoring and screening of the modified JAW mixes after the utilisation of various chemical admixtures to improve the early-age strength development at 70 ℃ of bottom-hole static temperature. Mechanical, chemical and mineralogical properties of the one-part geopolymers are investigated.

Papers IV and V study the influence of different superplasticizers on the rheology of these granite-based geopolymers at 20 and 50 ℃ of bottom-hole circulating temperatures.

Papers VI and VII illustrate various early-age characteristics of the screened and developed samples including their chemical, physical, mechanical, mineralogical, and morphological properties at 20 and 50 ℃ at bottom-hole circulating temperatures. Additionally, Paper VII further investigates and characterizes the aged JAW properties at 20 and 50 ℃ at bottom-hole circulating temperatures for up to two months of curing.

Appendix 10 is a filed patent in Norway and Europe titled ONE-PART GEOPOLYMER COMPOSITION – ref. P31562NO – June 2022.

List of Publications

I. Omran, M., Hjelm, S., Khalifeh, M., & Salehi, S. (2023a). Synthesis of sustainable one-part geopolymers for well cementing applications. Geoenergy Science and Engineering, 227, 211822. https://doi.org/10.1016/j.geoen.2023.211822.

II. Omran, M., & Khalifeh, M. (2022a). Development of Low Carbon Dioxide Intensive Rock-Based Geopolymers for Well Cementing Applications – One-Part Geopolymer, in: Volume 10: Petroleum Technology. Paper presented at the ASME 2022 41st International Conference on Ocean, Offshore and Arctic Engineering, Hamburg, Germany, 5–10 June. https://doi.org/10.1115/OMAE2022-78535.

III. Omran, M., & Khalifeh, M. (2023a). Development of one-part rock-based Geopolymers for downhole cementing applications. Journal of Energy Resources Technology, 145(10). https://doi.org/10.1115/1.4062250.

IV. Omran, M., Khalifeh, M., & Hjelm, S. (2022a). Role of Zeta Potential on Rheology of One-Part Geopolymer Slurries: Influence of Superplasticizers. In Annual Transactions of the Nordic Rheology Society, Vol. 30. Nordic Rheology Society.

V. Omran, M., Khalifeh, M., & Saasen, A. (2022b). Influence of Activators and Admixtures on Rheology of Geopolymer Slurries for Well Cementing Applications. Paper presented at the SPE Asia Pacific Oil & Gas Conference and Exhibition, Adelaide, Australia, 17–19 October. SPE-210698-MS. https://doi.org/10.2118/210698-MS.

VI. Omran, M., Paiva, M., & Khalifeh, M. (2023b). Design and early age performance of sustainable one-part geopolymers for well cementing. SPE Journal, 1–18. https://doi.org/10.2118/215825-pa.

VII. Omran, M., Khalifeh, M., & Paiva, M. (2023c). Aging and Temperature Effects on the Performance of Sustainable One-part Geopolymers Developed for Well-Cementing Applications. SPE Journal, SPE-217993-PA.

VIII. Qiu, X., Omran, M., Guang, Y., & Khalifeh, M. (2024). Numerical microstructure simulation of one-part geopolymer for wellbore applications. (To be submitted to a scientific journal in 2023-2024).

IX. Omran, M., & Khalifeh, M. (2022b). A filed patent in Norway titled: ONE-PART GEOPOLYMER COMPOSITION – ref. P31562NO – June 2022. (Under Examination)

Table of Contents

Acknowledgements iv

Preface v

List of Publications vii

1. Introduction 1
   - 1.1 Background of this research 1
     - 1.1.1 Well Cementing 1
     - 1.1.2 CO_2 Emission from OPC Production 4
     - 1.1.3 Conventional Geopolymers 5
     - 1.1.4 One-part Geopolymers 6
2. Objectives and Scope of the Research 11
   - 2.1 Strategy and Outline of this Research 11
3. Geopolymerization State-of-the-Art 13
   - 3.1 Geopolymerization Reaction 13
     - 3.1.1 Dissolution of Geopolymers 15
     - 3.1.2 Kinetics of Geopolymerization 18
     - 3.1.3 Reaction Products of Geopolymers 20
4. Materials 23
   - 4.1 Granite-based Precursor 23
   - 4.2 Activators and Chemical Admixtures 30
5. Methodology 33
   - 5.1 Formulations & Mix Design 33
   - 5.2 Slurry Preparation 34
   - 5.3 Analytical Methodologies 35
   - 5.4 Slurry Properties 36
     - 5.4.1 Workability and Thickening Time 36
     - 5.4.2 Density and Rheology 36
     - 5.4.3 Static Fluid Loss 37
     - 5.4.4 pH and Zeta Potential 37
     - 5.4.5 Inductively Coupled Plasma 37
     - 5.4.6 Differential Scanning Calorimeter 38
   - 5.5 Mechanical and Micro-structural Properties 38

5.5.1 Uniaxial Compressive Strength (UCS) 38
5.5.2 Sonic Strength Development 38
5.5.3 Hydraulic Sealability 39
5.5.4 X-Ray Diffraction (XRD) 39
5.5.5 Fourier-transform Infrared Spectroscopy (FTIR) 40
5.5.6 Scanning Electron Microscopy (SEM) 40
6. Results and Discussion 41
6.1 Normalization of Granite and Synthesis of the JAW Paste 41
6.1.1 Consistency and Thickening Time 42
6.1.2 Uniaxial and Sonic Strength Development 45
6.1.3 Compositional Analysis XRD 47
6.2 Screening and Developing JAW 49
6.2.1 Effect of Water Content 49
6.2.2 Screening of Chemical Admixtures 52
6.2.3 Effect of ZnO 53
6.2.4 Effect of Superplasticizers 55
6.3 Characterization of the JAW System - Short-term 58
6.3.1 Dissolution of JAW 59
6.3.2 Kinetics of JAW 62
6.3.3 Workability of JAW-b vs JAW-Z 65
6.4 Preliminary Study on Aging of JAW 67
6.4.1 Uniaxial & Sonic Strength Development 67
6.4.2 Hydraulic Sealability and Morphology of Geopolymer Plug 71
6.4.3 Fourier Transform Infrared Spectroscopy (FTIR) and X-ray Diffraction (XRD) 73
7. Summary & Conclusion 79
7.1 Summary 79
7.2 Conclusion 80
7.2.1 Normalization of Granite and Synthesis of the JAW Paste 80
7.2.2 Screening and Developing JAW 80
7.2.3 Short-term Characterization of the Developed JAW 81
7.2.4 Preliminary Study on Aging of JAW 81
8. Recommendations 83
9. Reference 85
10. Appendices 103

Appendix 1 – Extended UCA & UCS Profiles 103
Appendix 2 – Additional Structural Characterizations..... 105
Appendix 3 – Paper I..... 108
Appendix 4 – Paper II 119
Appendix 5 – Paper III..... 120
Appendix 6 – Paper IV..... 128
Appendix 7 – Paper V 136
Appendix 8 – Paper VI..... 137
Appendix 9 – Paper VII 155
Appendix 10 – A Filed Patent in Norway 182

Table of Figures

Figure 1: Well barriers inside the wellbore [11]. 2
Figure 2: Steps of the research plan. 12
Figure 3: Infographic showing examined properties of the granite-based JAW system 12
Figure 4: Geopolymerization process steps: a) geopolymer precursor, b) dissolution and formation of monomers and dimers, c) reorganization and condensation, and d) geopolymerization. (Paper VII) 14
Figure 5: Schematic diagrams illustrate of the dissolution of aluminosilicate materials [60] 16
Figure 6: Initial exothermal peak on the calorimetric curve was observed as an exothermic dissolution [73]. 19
Figure 7: Two exothermic peaks in the heat flow were observed from fly ash and slag in combination with different activator moduli and fly ash/slag mass ratio [76]. 19
Figure 8: NASH gel structure [72] 20
Figure 9: C(N)ASH gel structure [72]. 22
Figure 10: Size distribution of precursors; granite and GGBFS in water dispersions while microsilica in isopropanol dispersion. (Paper VI) 27
Figure 11: XRD mineralogical characterization of the raw materials. (A) Albite, (Ak) Akermanite, (B) Biotite, (Ch) Chlorite, (M) Microcline, (O) Oligoclase, (Q) Quartz and (Sp) Spinel. 28
Figure 12: SEM images of the precursors: a) granite at magnitude 1.0 K X, b) GGBFS at magnitude 1.0 K X, c) microsilica at magnitude 16.0 K X. (Paper I) 30
Figure 13: The applied testing strategy for JAW design. 35
Figure 14: Consistency development profile of the granite-based geopolymers slurries at 50℃ BHCT. (Paper I) 43
Figure 15: Consistency development profile of the two neat one-part granite-based geopolymers recipes at 50 ℃ BHCT. (Paper I) 43
Figure 16: 1-day UCS data for heat cured samples, 70 ℃. (Paper I) 45
Figure 17: Sonic strength development for GGBFS-0%, JAW-a and JAW-b. (Paper I) 46

Figure 18: Three vertical sample pictures (4 x 4 cm); a) GGBFS-47% (without horizontal cracks), b) GGBFS-50% (a small horizontal crack on the surface), c) GGBFS-60% (with observable large horizontal cracks) after heat curing at 70 ℃ for 1-day (Paper I) 47
Figure 19: XRD patterns of selected mixtures after 7 days of heat curing at 70℃ BHST, Q: Quartz, A: Albite, M: Microcline, B: Biotite. (Paper I) 48
Figure 20: Effect of water content on 1-Day UCS of the JAW system at 70 ℃ BHST. (Paper III) 50
Figure 21: UCA for JAW with two different water content; SS: sonic strength, TT: transit time; JAW-b (33% w/s) and JAW-b-35 (35% w/s). (Paper II) 50
Figure 22:Effect of water content on the consistency of JAW at 50 ℃ BHCT; JAW-b (33% w/s) and JAW-b-35 (35% w/s) 51
Figure 23: The effect of 0.14 wt.% chemical admixtures on 1- and 7-Day UCS at 70 ℃ BHST; Please consult the text for a description of the different samples. (Papers II and III) 52
Figure 24:Effect of ZnO on JAW for 1-Day UCS at 70 ℃ BHST (Papers II and III). 53
Figure 25: Sonic strength profile of JAW-b (neat) & JAW-Z (JAW-b + 0.86 wt.% ZnO). (Paper VI). 54
Figure 26: (a) Shear stress - Shear rate curves of JAW-Z with 1 wt.% superplasticizer, (b) consistency profile of JAW-Z with 1 wt.% superplasticizer at 50 ℃ BHCT. AX: Auxilchem Naphthalene-based powder, Ns: Sodium Poly-Naphthalene- sulphonate powder, Ls: Sodium Lignosulfonate. (Paper VI) 56
Figure 27: Uniaxial compressive strength of JAW-Z with 1 wt.% superplasticizer after 1- and 7-day at 70 ℃ BHST. 57
Figure 28: ICP analysis (Dissolution) of the pore solutions of JAW-b vs JAW-Z. (Paper VII) 60
Figure 29: XRD mineralogical characterization of JAW-b (neat) and JAW-Z (JAW-b + 0.86 wt.% ZnO of the precursor). (A) Albite, (Kh) Potassium containing species/crystals, (KZh) Zinc containing species/crystals, (M) Microcline and (Q) Quartz. (Paper VI) 62
Figure 30: Differential scanning calorimetry data of Granite vs GGBFS; (a) heat rate (b) energy release. (Paper VI) 63

Figure 31: Differential scanning calorimetry data of the developed JAW; (a) heat rate (b) energy release; JAW-b & JAW-Z. (Paper VII).. 65
Figure 32: Consistency of the slurries (a) JAW-b and (b) JAW-Z. (Paper VII) 66
Figure 33: UCS data for JAW-b vs JAW-Z for up to two months of curing. (Paper VII) 68
Figure 34: UCA profiles for JAW and JAW-Z up to two months; JAW-b (neat) & JAW-Z (JAW-b + 0.86 wt.% ZnO). (Paper VII). 69
Figure 35: JAW dissolution behavior between 0.5-28 days. 70
Figure 36: Hydraulic Sealability for JAW after 7-day & 28-day and JAW-Z after 7-day. (Paper VII) 71
Figure 37: a) SEM image of early-age JAW mix, b) SEM image of aged JAW mix, c) Top view of the sealability cell after gas breakthrough of the aged JAW. (Paper VII)..... 72
Figure 38: FTIR patterns of JAW-b and JAW-Z at 25 and 70 ℃. (Paper VII) 74
Figure 39: XRD patterns: a) JAW-b and b) JAW-Z, both cured at 25 ℃ BHST. 1: Quartz, 2: Microcline, 3: Albite, 4: Potassium containing species/crystals, 5: Zinc containing species/crystals. (Paper VII) 75
Figure 40: XRD patterns: a) JAW-b and b) JAW-Z, both cured at 70 ℃ BHST. 1: Quartz, 2: Microcline, 3: Albite, 4: Potassium containing species/crystals, 5: Zinc containing species/crystals. (Paper VII) 76
Figure 41: Extended UCA data for JAW-b vs JAW-Z. 103
Figure 42: Extended UCS data for JAW-b Vs JAW-Z. 104
Figure 43: SEM after curing at 25 ℃ BHST, Magnification of 10 K.X. Results of curing time up to two months. The red arrow points towards unreacted particles..... 105
Figure 44: SEM after curing at 70 ℃ BHST, Magnification of 10 K.X. Results of curing time up to two months. The red arrow points towards unreacted particles..... 106
Figure 45: FTIR patterns from 1500-500 cm^{-1} of JAW-b and JAW-Z at 25 and 70 ℃..... 107

List of Tables

Table 1: List of relevant publications considering JAW geopolymers and alkali-activated materials. 7
Table 2: Chemical composition of the precursors. (Paper I) 26
Table 3: Physical properties of the components. (Paper I) 26
Table 4: Electrokinetic potential of the precursors. (Paper VII) 27
Table 5: Granite`s mineralogy obtained from Rietveld quantification. (Paper VI) 29
Table 6: List of the main chemical admixtures used in this study. 31
Table 7: Chemical composition of the selected granite-based precursors mix. 34
Table 8: JAW geopolymer formulation investigated in this study. 34
Table 9: Mix design for one-part AAM mixes. 42
Table 10: XRD crystallinity quantification of JAW samples using “EVA v5” software. (Paper I) 48
Table 11: Yield stress and API Gel-strength results of JAW with 1 wt.% superplasticizer. (Paper VI) 57
Table 12: Zeta potential measurements of JAW with 1 wt.% superplasticizer. (Paper VI) 57
Table 13: Formulations of JAW-b and JAW-Z. (Paper VII) 59
Table 14: ICP evaluation for JAW components (Paper VI). 59
Table 15: ICP evaluation for JAW recipes (Paper VI) 60

1. Introduction

This chapter offers the essential background for this research, encompassing the objectives of well cementing, and presenting key aspects of both conventional and one-part geopolymers.

1.1 Background of this research

1.1.1 Well Cementing

In the context of oil and gas exploration and production, the successful planning and construction of wells are of utmost importance. These wells must be able to address a range of challenges, including drilling fluid-related issues, maintaining wellbore stability, optimizing operational parameters, and particularly, ensuring effective well cementing. Nowadays, annular cement and cement plug have new and diverse challenges, leading to significant increases in the number of reported well integrity issues rooted in the failure of cement and/or cementing operations [1-5].

Most of the related literature focuses on potential problems and challenges that must be overcome to ensure proper zonal isolation. These challenges of well cementing include but are not limited to highly deviated wells, deepwater offshore applications, high-pressure high-temperature (HPHT) wells, dealing with annular pressure build-up, as well as cement contamination and shrinkage at downhole conditions [6-11].

Oil well cement is usually used as an annular barrier or as a plug for slot-recovery or abandonment purposes, see Figure 1. In the context of well cementing, the successful placement of barrier material is mainly a function of downhole conditions and operational parameters. After the successful placement of cement, the hardened cement sheath serves as a

physical barrier. Ensuring the long-term integrity of the cement sheath at downhole conditions is a must.

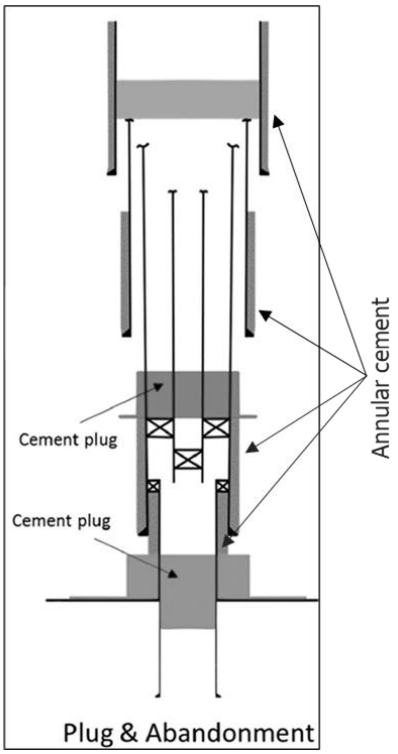

Figure 1: Well barriers inside the wellbore [11].

Regardless of the intended purpose of the well, whether for geo-energy extraction (e.g., oil and gas, geothermal), or carbon capture, utilization, and storage (CCUS), ensuring optimal production or injection hinges on maintaining the well integrity [4, 11].

NORSOK-D-010 [12] defines the term “well integrity” as the technical, operational, and organizational activities undertaken to consolidate all components of the well, and thereby minimize the likelihood of uncontrolled fluid flow from/to formation during the well's lifecycle. Zonal isolation materials are exposed to harsh downhole conditions. These barrier materials should be properly designed and selected to

withstand chemical, thermal, and mechanical stresses. Additionally, other operational factors including pressure and temperature variation, corrosive agents, erosion, and fatigue, must also be considered during the design and selection of such materials. Various issues can affect the well integrity throughout the lifecycle of a well during various phases, including well construction, production, intervention, and post-abandonment stages [11-13].

NORSOK-D-010 [12] specified the well cementing material to have different functions including but not limited to providing zonal isolation by preventing formation fluid migration among wellbore strata, protecting and sealing casing from corrosion, and mechanically supporting the wellbore structure in place. In addition, well placement of cement is important to avoid any migrations or contaminations to the surface aquifer by any produced hydrocarbons or other hazardous fluids. Thus, it should also hinder any further environmental issues [11-13].

The American Petroleum Institute (API) established standards to evaluate the effectiveness of cement and various additives for well cementing applications. Many additives were investigated and are available to enhance and regulate the performance of well cementing materials such as Ordinary Portland Cement (OPC). This trend evolves to reduce the risk of cement sheath failures [14-16]. These well cementing materials should successfully fill the annular gap between the casing and formation, and/or the space between two different casing strings, as shown in Figure 1. After its well placement, cement should solidify and seal off the annular space [14-16].

OPC has been the prime material used for zonal isolation and well abandonment in the oil and gas industry for more than a century. This wide utilization of OPC is primarily due to its global manufacturing infrastructure, locally available raw materials, established chemistry and reliability, and cost-effectiveness known as viability [10, 17-18]. Despite the well-developed knowledge of OPC chemistry, many studies

reported technical limitations in its short- and long-term properties including cement shrinkage, gas influx (i.e., permeable), durability issues with aging, and instability at high temperatures and in a corrosive downhole environment [19-20], especially under the harsh conditions of oil and gas wells [10, 21].

1.1.2 CO_2 Emission from OPC Production

The primary environmental limitation associated with the utilization of Ordinary Portland Cement (OPC) lies in its production process, which contributes significantly to global carbon dioxide (CO_2) emissions. This can be attributed to factors such as the decomposition of carbonates and high consumption of fossil fuels, accounting for up to 8% of CO_2 emissions [22]. Thus, the use of any other supplementary cementitious materials is important to avoid or minimize the CO_2 emissions from the process. These challenges and limitations serve as strong motivation for the development of new cementitious materials that have lower, or net-zero carbon footprints. Such materials are crucial to meet global targets for reducing carbon dioxide emissions [23-24].

Fantilli et al. [25] highlighted that the carbon footprint of the cement industry is expected to get even higher due to the rapid increase in global demand. However, they did not include the efforts made by the cement industry to decarbonize the process. Of these one may refer to a blend of pozzolanic materials, re-cycling of concrete elements, energy efficiency improvements, etc. Despite these efforts, there is a pressing on the cement industry for a green shift, aiming to reduce carbon dioxide emissions through the adaption of environmentally friendly alternatives to Portland cement. Hence, various ongoing research projects are focusing on developing novel cementing materials that address the potential shortcomings of traditional well cement operations in the Oil and Gas industry [3-5]. One of these alternative materials proposed to replace oilwell cement is geopolymers [26].

1.1.3 Conventional Geopolymers

The difference between geopolymers and alkali-activated materials and their categorization is disputable, and they have been discussed in different scientific articles [27-30]. Considering two-part alkali-activated materials (AAM) or geopolymers, they have been found to have outstanding chemo-physical properties that can outperform at downhole conditions while having significantly lower CO_2 emissions per ton of produced material (70-80%) when compared to API class G oilwell cement [31-32]. Hence, research is needed to tailor the utilization of geopolymers and to fully understand the principles that govern their chemistry [27, 33].

The use of AAM technology can provide a broader range of environmentally friendly cementitious products and decrease CO_2 emissions without competing with OPC on a global scale. Despite fulfilling the required rheological and pumpability characteristics and possessing excellent mechanical properties, they are not utilized in the oil and gas industry in comparison to OPC [1-5]. This limited adoption could be attributed to various factors but not limited to the uncontrolled thickening time, unknown long-term properties, and a lack of large-scale results in real-life downhole conditions [34-35].

Alkali-activated materials including conventional geopolymers are formed by mixing raw materials, or so-called precursors, with activators, in a highly alkaline medium. The activators are high pH solutions, which are typically alkali metal hydroxide solutions, either alone or in combination with alkali metal silicates. However, the precursors can be naturally amorphous minerals, fuel ashes, and/or in combination with industrial wastes, demolition wastes, and red mud waste [36].

Geopolymer precursors can also be derived from processed naturally occurring sources such as aplite, norite, and granite to produce rock-based geopolymer mixes [37-40]. Eventually, they are combined with industrial by-products such as Ground Granulated Blast Furnace Slag

(GGBFS). The practical application of geopolymers has been proposed as early as 2008 for well-cementing applications, with reports of laboratory and yard tests [41-42].

1.1.4 One-part Geopolymers

In the context of oil and gas applications, logistical and environmental challenges besides health and safety concerns associated with the transportation and handling of highly reactive alkaline solutions for activating conventional two-part geopolymers can present obstacles to their field implementation. Hence, transportation of the liquid activator phase in large quantities can lead to additional carbon dioxide emissions when compared to using a single-phase geopolymer powder system, i.e., one-part geopolymers [43]. These limitations and concerns highlight the importance of developing one-part geopolymers as a critical strategy for their use in oilwell cementing operations, which would promote their commercialization [44-45].

A one-part geopolymer product would be the user-friendly alternative while having lower CO_2 emission and eliminating the need for unnecessary transportation of the liquid activator used in conventional geopolymers [43]. A one-part process is ideal for the large-scale deployment of geopolymers. To better understand the progress done in the field of one-part geopolymers and alkali-activated materials, research has been done on relevant publicly available scientific documents. Table 1 presents previously published papers revealing the development of the one-part geopolymers and alkali-activated materials (AAM).

Table 1: List of relevant publications considering JAW geopolymers and alkali-activated materials.

Authors	Precursors & Significant Outputs
Wan-En et al. [43]	• A high calcium content (Class C) fly ash was activated by mixing anhydrous solid sodium silicates, sodium hydroxide and sodium carbonate, at different water contents. • The utilization of Na_2SiO_3 and Na_2CO_3 without NaOH gave the optimum performance with better fluidity, longer setting time and highest compressive strength due to the incorporation of Na_2CO_3 that reduced water demand.
Hajimohammadi et al. [46]	• A geothermal silica as a Si-rich source was utilized as a reactive precursor after being purified and milled. It was activated by various concentrations of solid sodium aluminate and water-to-solid ratios. • Crystalline products of the geopolymer system were increased by lowering the water content. • Geopolymerization reaction can be hindered by the aluminum content in the system though the sorption of aluminum onto the silica surface and then slow down its dissolution.
Ma et al. [47]	• An ultra-fine fly ash sinking beads (FASB) mixed GGBFS were activated by hydrous and anhydrous sodium silicates. • The activation by anhydrous sodium silicate gave the best performance with having the highest compressive strength and the lowest porosity if it is compared with the hydrous ones. • The hydrous activator showed longer acceleration period and lower heat release rate than the anhydrous activated geopolymer. • It also resulted in the presence of micro-cracks which was identified as an additional shortcoming for the hydrous activated geopolymers.
Ke et al. [48]	• An alkali-thermal activation development for an aluminium- and calcium-rich red mud based one-part system was examined. • Na-rich aluminosilicate salts provided enough alkalis during their dissolution, and then enhanced the reactivity. • Shortcomings due to the excess of alkalis in the system that resulted in limited strength development and efflorescence were identified.

Hajimohammadi & van Deventer [49]	• A low calcium content (Class F) fly ash was activated by solid sodium silicates and sodium hydroxide at various concentrations and different water contents. • The dense microstructure of the one-part geopolymers was a result of having a high Si/Al ratio in the binder design. • To achieve optimal mechanical performance, the geopolymer design needed to have low water content and high participation of Si in the final geopolymer gel.
Hajimohammadi et al. [50]	• A reactive geothermal silica precursor was milled and then activated by solid sodium aluminate. The mix was seeded with various types of oxide nanoparticles. • Unlike the unseeded mix design, the seeded one-part geopolymer mix with nanoparticles of zinc oxide showed an improvement in mechanical properties, particularly during the early-age performance. • This process enhanced the dissolution of silica and controlled the silica release rates in the initially aluminum-rich reaction mixture. It also enhanced the nucleation stage of the geopolymer though hindering the sorption of aluminum on the silica surface.
Luukkonen et. al. [100]	• A review paper on different formulations of one-part alkali-activated materials. • It shows the development of one-part AAM may have greater potential than the conventional two-part AAM, especially in cast-in-situ applications. • It presents various recent studies and results of these AAM with different types of precursors, solid activators, chemical admixtures. • It also illustrates their effects on mechanical, chemical, and physical properties, besides their environmental impacts.

Motivated by that, this research is to design a new viable and sustainable one-part granite-based geopolymer. It focuses on thoroughly evaluating the early age and long-term properties of these designed mixes.

Moreover, this study includes but not limited to investigating the geopolymerization process under downhole conditions. It is studying each stage of the geopolymerization process starting from the characterization of dissolution, reorganization, and then polycondensation processes, integrating them with a wide range of physical and chemical characterizations. Additionally, this study is to take into account downhole operational conditions and petroleum engineering standards.

2. Objectives and Scope of the Research

The main objective of this research is to synthesize and develop a sustainable one-part granite-based geopolymer to eliminate concerns associated with the liquid hardener used in conventional two-part geopolymers. This is done either with a hybrid activator or completely a solid phase activator. This activator should be blended with naturally occurring solid powder of granite as a precursor, i.e., non-processed granite powder. It may help with enabling a successful synthesis and design of a one-part geopolymer formulation. Accordingly, this one-part geopolymer design will be examined and investigated for oilwell cementing applications.

2.1 Strategy and Outline of this Research

This doctoral project implements systematic and scientific methodologies that imply various possible screenings and solutions including the following steps:

1. Normalization of a Norwegian grounded granite in solid phase by slag, microsilica, potassium silicates and alkali-metal hydroxides, all in powder form.
2. Monitoring and screening the modified mixes.
3. Analysing various early-age characteristics of the screened samples including chemical, physical, mechanical, mineralogical, and morphological properties.
4. Afterwards, properties of the aged geopolymers are characterized as well as the role of contributing parameters.

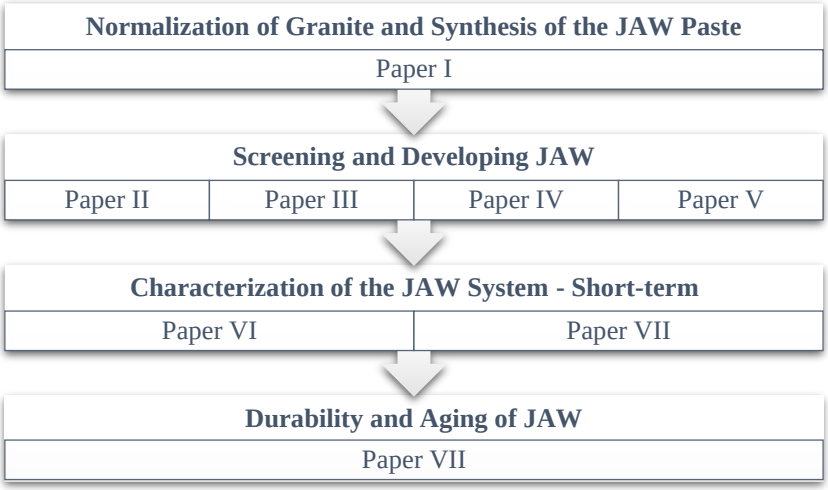

Figure 2: Steps of the research plan.

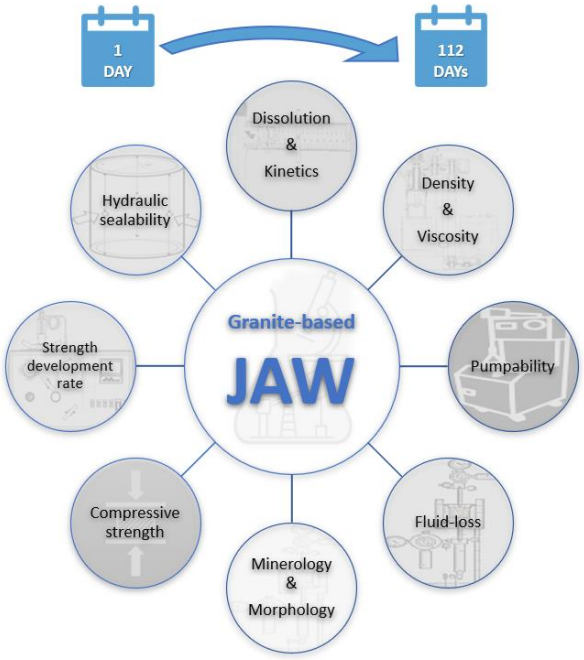

Figure 3: Infographic showing examined properties of the granite-based JAW system.

3. Geopolymerization State-of-the-Art

This chapter presents the current state-of-the-art for the complexity of geopolymer systems including Just Add Water (JAW) geopolymerization reactions. Moreover, the chemical characteristics of geopolymers are introduced, including their dissolution process, geopolymerization reaction kinetics and the expected geopolymer products.

3.1 Geopolymerization Reaction

In 1975, Joseph Davidovits introduced the concept of geopolymers and coined the term "geopolymer". He presented them as materials that are characterized by being formed in long repeating chains of tetrahedral Al_2SiO_5 polymer-like structure. Various types of alkali-activators* and hardeners have been reported and studied in literature to solidify the raw materials, i.e., geopolymeric precursors. The activators provide the highly alkaline medium needed to initiate the dissolution of precursors, while hardeners bind precursors [51-54].

The dissolution of these complex mineralogical structures can lead to the formation of various 3-D aluminosilicate structures through transportation, nucleation, and polycondensation [51-54]. Pacheco-Torgal et al. [55] investigated the geopolymerization reaction and presented it as a dissolution of the precursors in the alkaline solution at high pH, followed by the transport and reorganization of silica and alumina tetrahedra, condensation in dimers and oligomers, and then polymerization of the aluminosilicate network as shown in Figure 4.

* From a scientific point of view, the reader should differentiate between hardener and activator.

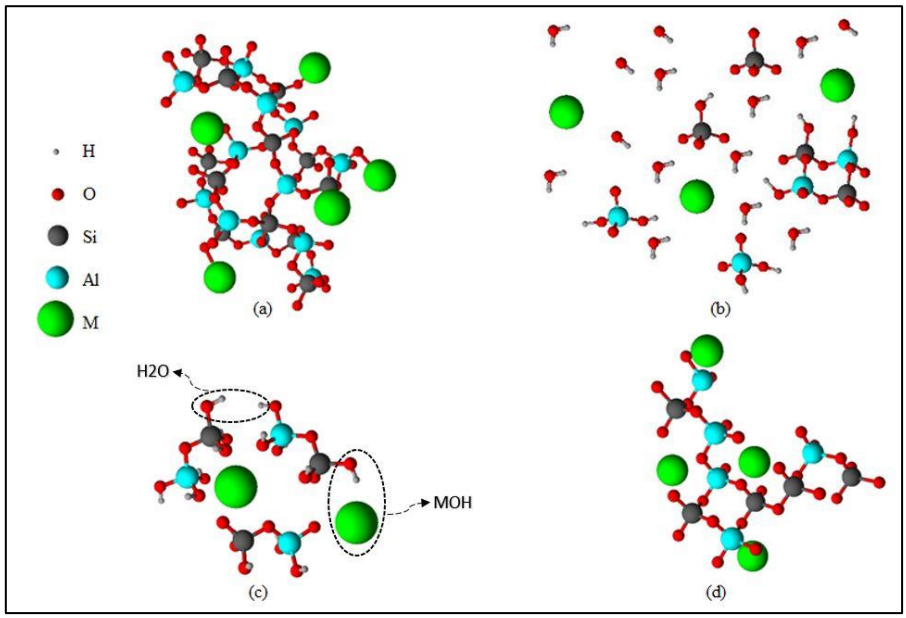

Figure 4: Geopolymerization process steps: a) geopolymer precursor, b) dissolution and formation of monomers and dimers, c) reorganization and condensation, and d) geopolymerization. (Paper VII)

Polymerization of aluminosilicates requires free tetrahedral SiO^{-}_{4} and AlO^{-}_{4} ions. These free tetrahedral ions bond in units through oxygen atoms and then form repetitive chains such as poly-sialates, poly-sialate-siloxo, and/or poly-sialate-disiloxo structures. Komnitsas [56] defined the geopolymerization reactions as the following:

$$(Si_2O_5.Al_2O_2)_n + H_2O + OH^- \rightarrow Si(OH)_4 + Al(OH)^{4-} \quad (1)$$

$$Si(OH)_4 + Al(OH)^{4-} \rightarrow \left(-\underset{\underset{O}{|}}{\overset{|}{Si}} - O - \underset{\underset{O}{|}}{\overset{|}{Al}} - O - \right) n + 4\,H_2O \quad (2)$$

The products of this reaction are water and solidified aluminosilicate matters.

3.1.1 Dissolution of Geopolymers

In the case of one-part geopolymer systems (i.e., Just Add Water; JAW geopolymers), the presence of water (as the only liquid phase) and having the right water-to-binder ratio are essential for having the optimum geopolymer formulation and properties. Water content is very crucial parameter to initiate the dissolution of the solid activator to provide the required alkaline medium for the geopolymerization reaction [46, 57]. Hajimohammadi & van Deventer [49] investigated the kinetics of low calcium fly ash JAW geopolymer. They observed that the dissolution of their precursor was increased with having higher alkalinity from the solid activator. However, the dissolution was significantly decreased with increasing the water to binder ratio (i.e., water content).

Although geopolymers are made of aluminosilicate elements where silicon and aluminium make up the structural framework, alkali and alkali earth metals such as calcium and magnesium are modifying elements to this framework. The available studies of the pore solutions and chemical kinetics of JAW alkali-activated materials are scarce and even much fewer on rock-based geopolymer pastes. As shown in Figure 5, the dissolution process of aluminosilicate precursors is divided into four steps [58-60].

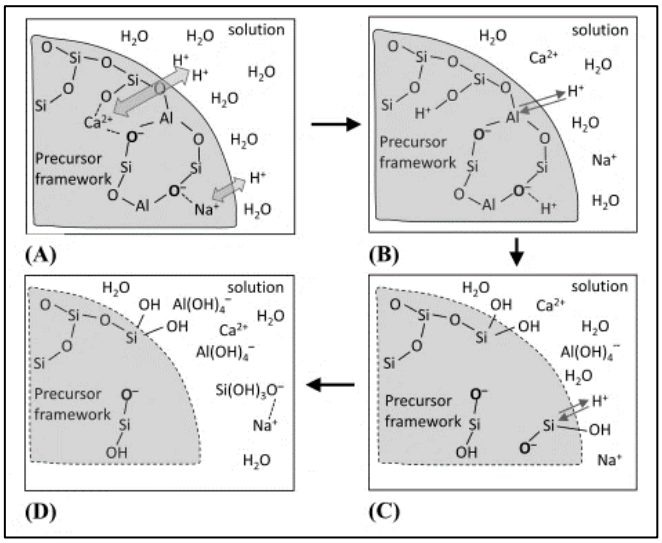

Figure 5: Schematic diagrams illustrate of the dissolution of aluminosilicate materials [60]

Metal/proton exchange reactions are initially started by dissolving the alkali and alkali earth metals from the surface of the aluminosilicate source. Then, aluminium-to-oxygen bonds start hydrolysis, followed by breaking silicon-to-oxygen bonds. Finally, the aluminosilicate framework keeps releasing more aluminium and silicon into the alkaline solution and the tetrahedral aluminosilicate source is gradually dissolved [60].

Oelkers & Gislason [61] studied the dissolution process of the aluminosilicate precursors. They found out that tetrahedrally coordinated aluminium can dissolve much faster and easier than tetrahedrally coordinated silicon. It is more difficult to break silicon-to-oxygen bonds if they are compared with aluminium-to-oxygen bonds. The hydrolysis of aluminium to oxygen bonds favours the dissolution of the partially coordinated silicon where this partially coordinated silicon dissolves much faster than the fully coordinated ones. Thus, the dissolution of the framework of aluminosilicate materials starts with the initial dissolution of a fraction of aluminium and then the dissolution of silicon adjoins the dissolved aluminium. This is the reason that quartz

(crystal form) is more robust when it comes to dissolution in an alkaline medium compared to amorphous silica.

Others experimentally investigated the dissolution rate of aluminosilicate as a function of aluminium content [62]. They showed higher dissolution rates of the aluminosilicate precursors such as fly ash and metakaolin, with higher aluminium content. In other words, the dissolution of aluminosilicate materials within different alkaline mediums indicates the preferential release of aluminium over silicon [62-64].

The dissolved aluminium and silicon from the aluminosilicate framework generate aluminate and silicate species through the hydrolysis step. The hydrolysed silicon and aluminium can be present in the forms of silicic acids $[SiO(OH)_3]^-$, $[SiO_2(OH)]^{-2}$ and Aluminate ion $[Al(OH)_4]^-$ in the pore solution [63-65]. While the ratio of $[SiO(OH)_3]^-$ to $[SiO_2(OH)]^{-2}$ can be decreased by increasing the pH of pore solution. Unlike the dissolution of OPC, the dissolution of geopolymer pastes can produce hundred times higher free silicon and alkali metals contents and ten times lower calcium content [66].

Swaddle [67] and Duxson et al. [68] studied the elements produced from aluminosilicate materials in various alkaline solutions. These produced elements existed in the form of aqueous species for using Si-NMR (nuclear magnetic resonance) spectroscopy. Their studies revealed the distribution of silicon in different forms of aqueous species with the alkaline medium by showing that the silicon was incorporated into two silicate species of monomeric and non-monomeric species. These monomeric and non-monomeric species are dependent on the modulus ratio of the alkaline medium. The higher the modulus ratio of the alkaline medium (SiO_2/M_2O, M= Na^+ or K^+) the higher the number of silicate centre coordinated (Q_n). This leads to a lower percentage of the total available silicon elements in the solution, and then more non-

monomeric silicate species. NMR Q_n represents a silicate centre coordinated to n other tetrahedral centres of silicon.

3.1.2 Kinetics of Geopolymerization

Isothermal calorimetry and differential scanning calorimeter are common techniques used for investigating the reaction kinetics of alkali-activated materials. The kinetics of OPC and high calcium content AAM is either partially or entirely based on the hydration reaction while geopolymers (i.e., low calcium AAM) are more chemically complex materials that show several reaction stages with different reaction mechanisms. So, the application of calcium-based cement (i.e., calcium based cementitious materials) knowledge and its thermodynamics may not be directly relevant.

Unlike conventional geopolymers, Just Add Water (JAW) geopolymers activation process is slower since it is mainly dependant on adding water first to the solid mixture. Afterwards, the system starts to move from neutral to a higher alkaline medium. Accordingly, it is slowing down the geopolymerization kinetics [48, 69-70]. Additionally, it is worth noticing that the type and chemical composition of alkaline activators and aluminosilicate sources have great impact on the reaction kinetics [71-72].

Researchers studied the reaction kinetics of low calcium alkali-activated fly ash and metakaolin by sodium silicate and sodium hydroxide activators between 25 to 80°C [73-75]. These studies observed only one peak on the calorimetric curve as an exothermic dissolution of the precursor and the formation of reaction products proceeded concurrently, see Figure 6. In addition, the effect of temperature on the reaction rate was observable whereas the cumulative heat of the system is impacted. It showed very small reaction rates of fly ash at low temperatures. While after increasing the temperature, the calorimetric peak had a larger

exothermic amplitude. This shows that the higher the temperature, the higher the reaction rates of alkali-activated aluminosilicate sources.

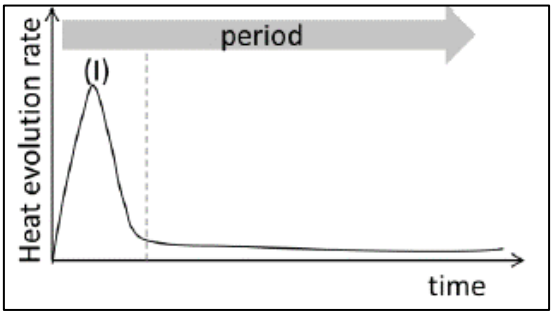

Figure 6: Initial exothermal peak on the calorimetric curve was observed as an exothermic dissolution [73].

Other researchers studied the reaction kinetics of geopolymers made of fly ash and slag in combination with different molar ratios of activators and fly ash/slag mass ratio [69-70, 76]. They observed two exothermic peaks in the heat flow, see Figure 7. The first calorimetric peak was right after mixing and was more directed to the initial wetting and dissolution of the solid activator and then aluminosilicate sources. The second peak was observed after 6 to 24 hours and more directed the formation of geopolymerization reaction products. An induction period occurred between the two peaks and lasted up to 10 hours [76].

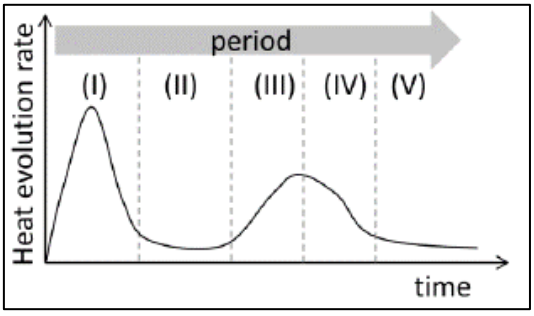

Figure 7: Two exothermic peaks in the heat flow were observed from fly ash and slag in combination with different activator moduli and fly ash/slag mass ratio [76].

Their calorimetric signs showed a clear effect of slag on the reaction rates; the higher the slag content the faster and larger the two peaks' amplitudes. Moreover, increasing the slag content results in higher heat flow in the dissolution phase. While with lower slag content, the second calorimetric peak was lowered, shifted, and delayed the formation of the geopolymerization reaction products or gels. On the other hand, an increase in the activator molar ratio led to a decrease in the two calorimetric peaks' intensities. The lower the activator moduli, the more intensive dissolution of the aluminosilicate sources and the faster and more intensive the geopolymerization reactions [69-70, 72, 76].

3.1.3 Reaction Products of Geopolymers

Studies investigated the primary geopolymerization reaction products of low calcium-content alkali-activated materials and JAW geopolymers [46, 49, 70, 77-78]. Their primary reaction product is a three-dimensional hydrous type of gel of alkali-aluminosilicate (denoted as M-A-S-H, where M can be Na^+ or K^+) gels[†]. Figure 8 presents a schematic representation of M-A-S-H gels (where M=Na^+ is an example).

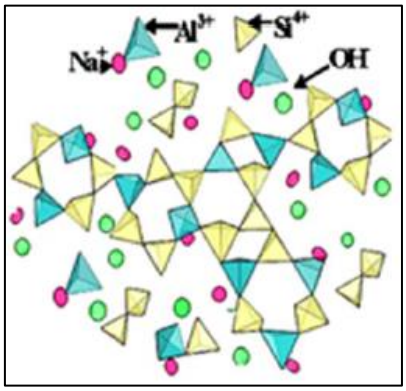

Figure 8: NASH gel structure [72].

[†] Note that gels are amorphous.

The three-dimensional structure M-A-S-H gels have tetrahedrally coordinated silicon and aluminium which are linked by oxygen bonds. The alkali cations of Na^+ and K^+ balance the tetrahedra aluminium negative charge. It is worth noticing that these gels depend on the curing conditions, curing time and alkaline activator [79]. It should be respected that gels are an indication of incomplete and/or ongoing geopolymerization reaction [80].

Others studied the effect of curing time and curing conditions on the reaction products of the low calcium-content alkali-activated materials. Fernandez Jimenez et al. [81] examined the M-A-S-H gels formed from an alkali-activated fly ash paste, which was cured at 85°C for 5 hours up to 7 days. During the first 5 hours of curing, the tetrahedra silicon in the M-A-S-H gels were attached by four tetrahedra aluminium. After 7 days of curing, these tetrahedra silicon were attached by two or three tetrahedra aluminium. It is also reported that the influence of increasing the curing temperature leads to increasing the M-A-S-H gels degree of crosslinking and long-range ordering [82-83].

Reaction products of hybrid geopolymers were also studied in the literature. In the case of slag-based geopolymers in which the slag content is ≥ 50%, formed C-(M-)A-S-H gels as the main binding product in addition to tracers of M-A-S-H gels. While in hybrid geopolymers with lower than 50% slag content, (C-(M-)A-S-H) gels were found [70, 84-85]. Figure 9 shows a schematic representation of the C-(M-)A-S-H gel structure (M=Na^+ or K^+).

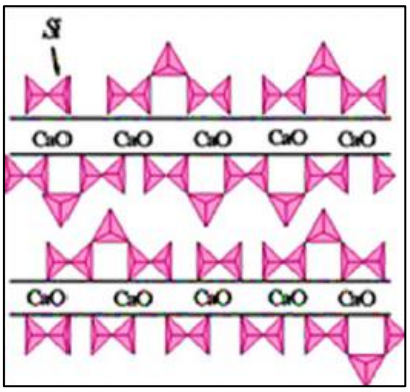

Figure 9: C(N)ASH gel structure [72].

4. Materials

4.1 Granite-based Precursor

One of the most common and available rock types found on Earth is Granite. It is an igneous rock and has wide differences in its characteristics and mineralogy dependent on the surrounding conditions and environment. Its main rock characteristic is mineral crystals and contains a combination of quartz, feldspar, mica, hornblendes, albite and/or pyroxene [86]. Different types of granite have been studied and investigated in literature with different classification systems [87-91].

Commonly, granite can be found at which two continental plates have collided. According to the tectonic movements, granite accessibility and location can be easy to be revealed around the globe [86]. Granite in some continents has high alkali feldspars while in other continents it has a mix of alkali feldspars and plagioclase. Brazil, China, Canada, Italy, India, Sweden, and Norway are some of the many large exporters of granite globally [87-88].

In Norway and Sweden, granite can be found in the Sveconorwegian orogenic belt. In the south of Norway, granite deposits are very large, especially around the southern coast. Many types of granite can be found in Norway such as Larvikite, Gneiss and Drammensgranitt. They are composed of monzonite, migmatite, biotite, etc. Each granitic rock type can be made up of various compositions and minerals including but not limited to feldspar, quartz, plagioclase, etc [88, 92].

According to the Geological Survey of Norway, granite can be classified as a massive structure and a rich aluminosilicate source [93]. On the other hand, it is considered as a non-reactive material and highly rich in crystalline minerals [92-94]. It has been used as an aggregate for cement or as a sustainable concrete filler [95]. Due to its low reactivity, one may

refer to applying some activation mechanisms for granite including chemical, thermal, and/or mechanical processes.

This study focuses on synthesizing and developing granite-based geopolymers whereas the base of the geopolymer system is granite. Due to its chemical composition, a granite powder was normalized with microsilica and slag to introduce amorphous content and cations to the mixture. This normalization is to modify the chemical and amorphous content of the precursor phase towards more favorable reactive geopolymerization conditions using slag and microsilica. Hence, the used precursors were ground granite (local granite from Sandnes, Norway), a rock-based material and aluminosilicate-rich source; ground granulated blast furnace slag (from Sweden), a calcium silicate material rich in aluminium and magnesium; and microsilica (from Elkem Norway) which is pure amorphous silica.

Microsilica (MS) was needed to balance the reactive Si/Al ratio in the mixture. The used microsilica was a highly amorphous and reactive silica with 95.5 wt.% purity. It was used to provide the early free silica that can enhance geopolymeric systems by supporting their early strength development and decreasing the permeability of the rock-based geopolymers [5, 26]. The reason behind using microsilica for rock-based geopolymers has been thoroughly studied by Khalifeh [26].

Ground granulated blast furnace slag (GGBFS) is an industrial by-product from steel industry. It is characterized by containing large amounts of amorphous silicates, alumina silicates, calcium and sometimes magnesium oxides [96]. This by-product plays a huge role in alkali-activated materials (AAM). In geopolymers, GGBFS is commonly used as combined-, or stand-alone in the precursor phase. It is usually utilized as a partial replacement for precursors like fly ash, rice husk ash and red mud which have low calcium and magnesium content to improve their geopolymeric performance [96-98].

Accordingly, GGBFS is regarded as an early strength enhancer or what is commonly known as a strength booster precursor for AAM and geopolymers. It is amorphous and rich in calcium content that can support the geopolymeric network though creating interconnected hydrates [99-104]. GGBFS hydrates like C-S-H and C-A-S-H are gels formed after the dissolution of GGBFS in water or alkaline medium. These hydrates can act as primary binding products within the geopolymeric system [99-104].

Unlike GGBFS, granite has a very low calcium content, i.e., granite is rich in aluminosilicate and poor in calcium. To achieve the required early-age well-cementing properties from the geopolymer, partial replacement of the granite by GGBFS and microsilica is necessary. Both are considered as composition normalizers to the total weight of the granite-based precursor [105-106] and combinations of these and the solid activator are labelled as the neat sample.

Table 2 presents the chemical composition of each precursor using XRF analysis, Paper I. Table 3 shows their physical properties including the specific gravity at 25℃ using Ultrapyc 3000 Helium pycnometer from Anton Paar, Paper I. Figure 10 illustrates their particle size distributions (PSD) and specific surface areas (SSA) using a Malvern Mastersizer 3000 particle size analyzer with size limitations over 3000 microns and with laser diffraction in water dispersion for granite and GGBFS while in isopropanol dispersion for microsilica, Paper VI. Table 4 illustrate the electrokinetic potential of the precursors using a Zetasizer Nano ZS (Malvern) equipped with a laser source, Paper VII.

Table 2: Chemical composition of the precursors. (Paper I)

Chemical composition (wt.%)	Granite	GGBFS	Microsilica
SiO_2	73.44	35.78	95.50
Al_2O_3	13.33	12.72	0.70
Fe_2O_3	2.06	0.18	0.30
MgO	0.44	12.77	0.50
CaO	1.12	33.74	0.40
Na_2O	3.12	0.55	0.40
K_2O	5.11	0.82	1.00
TiO_2	0.23	2.23	0.00
MnO	0.04	0.58	0.00
LOI*	0.90	0.30	2.00
*** Loss on ignition**			

Table 3: Physical properties of the components. (Paper I)

Physical properties	SG (g/cm^3)	d_{10} (µm)	d_{50} (µm)	d_{90} (µm)	SSA (m^2/kg)
Granite	2.63	3.52	21.1	131	631
GGBFS	2.90	2.79	15.9	46.6	944
Microsilica	2.29	0.19	0.34	0.60	19320

***SG: specific gravity; d10, d50, d90: particle size distribution percentiles; SSA: specific surface area.**

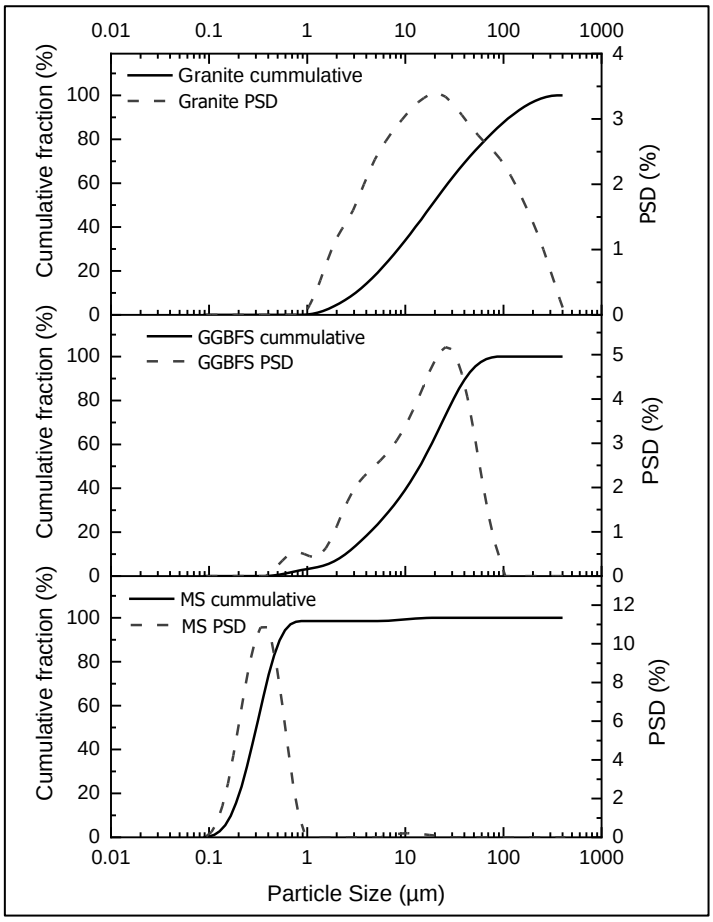

Figure 10: Size distribution of precursors; granite and GGBFS in water dispersions while microsilica in isopropanol dispersion. (Paper VI)

Table 4: Electrokinetic potential of the precursors. (Paper VII)

Material / Powder	Particle Refractive Index	Zeta Potential (mV)	Standard Deviation of Zeta Potential (mV)
Granite	1.59	-9.61	±1.74
GGBFS	1.52	-20.77	±3.00
Microsilica	1.46	-33.53	±0.33

XRD patterns of the precursors are shown in Figure 11. Granite has a very high crystalline content. Its mineralogy has been reinterpreted and quantified in Table 5 and Paper VI. Since GGBFS and microsilica exhibit mainly amorphous profiles, compared to granite, no Rietveld refinement was conducted for them. Hence, GGBFS contains a minor amount of akermanite and spinel that could be barely detected [106].

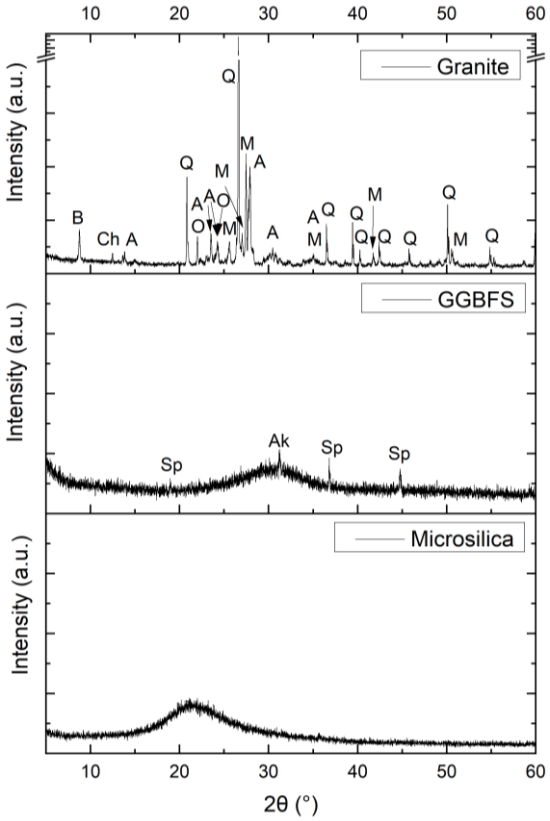

Figure 11: XRD mineralogical characterization of the raw materials. (A) Albite, (Ak) Akermanite, (B) Biotite, (Ch) Chlorite, (M) Microcline, (O) Oligoclase, (Q) Quartz and (Sp) Spinel.

Table 5: Granite`s mineralogy obtained from Rietveld quantification. (Paper VI)

Minerals	Granite (%wt/wt)
Feldspar	44.3
Quartz	30.4
Plagioclase	5.1
Muscovite	4.9
Biotite	3.5
Chlorite	11.8
Grand Total	100.0

The precursors` morphology and microstructure were examined prior to mixing at ambient conditions using scanning electron microscopy (SEM), see Figure 12 and Paper I. These characterizations and analyses for the precursors show that granite has the largest particle size distribution (PSD), the highest crystalline content, and more irregular shapes than GGBFS and microsilica as shown in Figures 10-12, respectively.

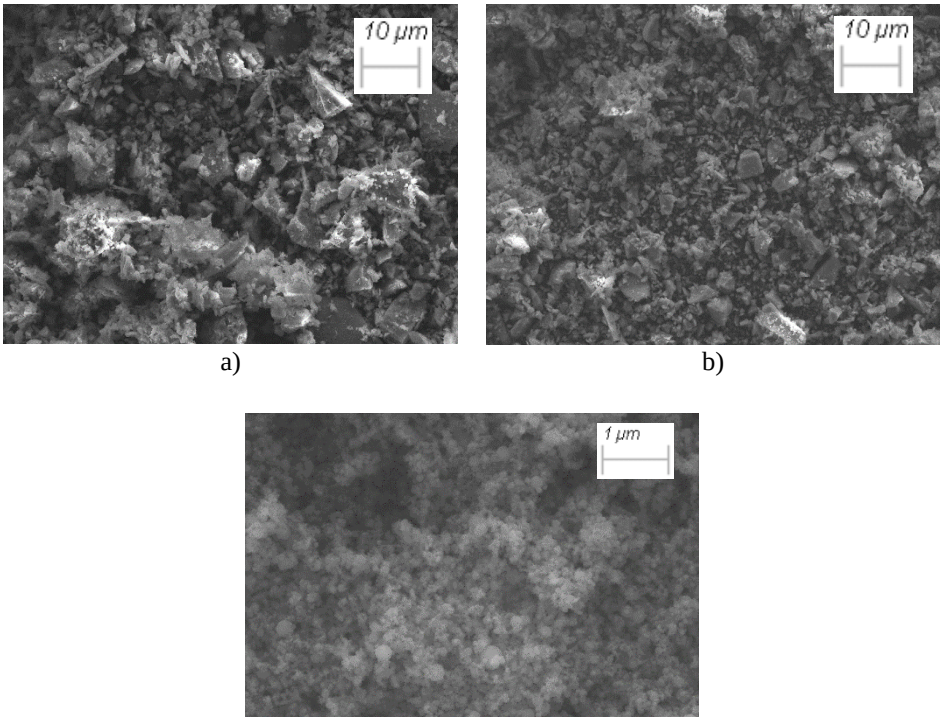

a) b)

c)

Figure 12: SEM images of the precursors: a) granite at magnitude 1.0 K X, b) GGBFS at magnitude 1.0 K X, c) microsilica at magnitude 16.0 K X. (Paper I)

4.2 Activators and Chemical Admixtures

The main utilized solid activator was potassium silicate (K_2SiO_3) anhydrous powder with a molar ratio of 3.9. Potassium hydroxide (KOH) pellets were used to lower the solid activator molar ratio between 2.0-2.4. These pellets were 99 wt.% pure KOH. The reason behind using a potassium-based activator than a sodium-based one has been presented by Khalifeh [26].

Furthermore, various chemical admixtures were investigated in this study. These chemical admixtures were in solid powders used and added separately to the geopolymer precursor directly to the dry blend, all in solid phase. Each chemical admixture was used for its expected role and

effect on the investigated granite-based geopolymer mixes. Table 6 provides a list of the main utilized chemical admixtures and their references. These admixtures are either partially or completely soluble in water and/or in alkaline medium.

Table 6: List of the main chemical admixtures used in this study.

Chemical Admixture	Chemical Formula	State / Purity	Purpose	Function Reference
Potassium Hydroxide	KOH	Pellet / +99%	Accelerator	Activator & Accelerator [28, 80, 100, 132]
Sodium Hydroxide	NaOH	Pellet / +99%	Accelerator	Activator & Accelerator [28, 80, 100, 132]
Calcium Oxide	CaO	Powder / +99%	Accelerator	Admixture & Accelerator [5, 80, 100, 132]
Sodium Aluminate	$NaAlO_2$	Powder / +99%	Accelerator	Activator [46, 100]
Calcium Carbonate	$CaCO_3$	Powder / +99%	Accelerator	Accelerator [5, 80]
Aluminum Hydroxide	$Al(OH)_3$	Powder / +99%	Accelerator	Reactive precursor [107]
Zinc Oxide	ZnO	Powder / +99%	Accelerator	Admixture [50, 100, 123]
Sodium Poly-Naphthalene-sulphonate powder	N/A (commercial)	Powder / N/A	Superplasticizer	Superplasticizer [108, 109]
Auxilchem Naphthalene-based powder	N/A (NS 181, commercial)	Powder / N/A	Superplasticizer	Superplasticizer [108, 109]
Di-Sodium Tetraborate Decarbonate	$Na_2B_4O_710H_2O$	Powder / +99%	Superplasticizer	Superplasticizer [108, 110]
Sodium Lignosulfonate	N/A (commercial)	Powder / N/A	Superplasticizer	Retarder & Superplasticizer [100, 109, 110]

5. Methodology

5.1 Formulations & Mix Design

In this research, the synthesized one-part granite-based system entails mix design and mixing various parameters including but not limited to the granite-based precursor, water content, chemical admixtures, curing temperature and curing duration. Just Add Water (JAW) mix design was prepared in a stepwise manner, considering several parameters. These parameters included varying concentrations of GGBFS, ranging from 0 to 90 wt.%, different concentrations of microsilica, ranging from 0 to 5 wt.%, diverse concentrations of solid activator, ranging from 10 to 20 wt.%, various concentrations of chemical admixtures, ranging from 0 to 1.5 wt.% of the total solid phase, and different concentrations of deionized water, ranging from 30 to 40 wt.% of the total weight of the solid phase.

This research mainly focuses on the successfully synthesized mix designs that could achieve a minimum compressive strength of 500 psi (i.e., around 3 MPa) within the first 24 hours of curing. While the rest were considered neither effective nor efficient throughout the early screening phase. These other mixes could not develop sufficient strength to set within 24 hours nor achieve the minimum requirements of the API standards [14-16]. Therefore, they are not presented in this dissertation.

The successfully synthesized design is a granite-based mix that was adjusted by incorporating GGBFS and microsilica to account for the remaining weight of the precursor. Considering API standards [14-16], the following selected mixes were considered promising neat and developed JAW recipes for well-cementing applications. Table 7 presents the chemical composition of the investigated granite-based precursors` mix. Table 8 shows the effectively formulated geopolymer mix design investigated in this work.

Table 7: Chemical composition of the selected granite-based precursors mix.

Chemical composition (wt.%)	**SiO_2**	**Al_2O_3**	**Fe_2O_3**	**MgO**	**CaO**	**Na_2O**	**K_2O**	**TiO_2**	**LOI***
Precursor Mix	56.6	12.5	1.1	6.2	16.5	1.8	2.9	1.2	0.6

*** Loss on ignition.**

Table 8: JAW geopolymer formulation investigated in this study.

Components	**Precursor**			**Solid Activator**		**Liquid**
Composition (% bwop*)	Granite	GGBFS	MS	K_2SiO_3 / TP**	KOH / TP	Water / TSP***
JAW****	48.6	47.1	4.3	0.21	0.04	0.33

*** By weight of precursor mixture (granite, GGBFS and MS).**
**** Ratios to the total precursor content (TP = Granite + GGBFS + MS).**
***** By weight of the total mixture of all solid components (TSP = Precursors + Solid Activators).**
****** JAW has the same precursor mixture for neat and modified mixes with chemical admixtures.**

5.2 Slurry Preparation

In the first step, all dry phases were blended in a closed container by hand shaking. Afterwards, the well-blended solid phase was introduced to a certain amount of deionized water to prepare the slurries in accordance with API RP 10B-2 [15]. The recommended practice includes using a high-shear commercial lab blender for mixing cement slurries in 50 seconds. The solid phase was added to water during the first 15 seconds at 4000 RPM and then the slurry was mixed for additional 35 seconds at 12000 RPM [15]. This procedure was followed to ensure a fixed amount of mixing energy to be given to the slurry and to ensure the reproducibility of the experiments.

5.3 Analytical Methodologies

Various analytical methods were utilized in laboratory scale tests for synthesizing and screening towards the desired JAW formulation which could follow and fulfil the specifications specified in relevant API standards [14-16]. The approach considers that first an acceptable neat recipe must be synthesized. Hence, chemical admixture(s) could be introduced to the neat mix design to modify the properties of interest.

Accordingly, series of properties were tested in accordance with standards defined for well cements [14-16]. Oil and Gas industrial standards and recommended practices were used to provide credibility and comparable procedures related to geopolymers vs OPC products. The testing strategy shown in Figure 13 was followed to characterize the slurry.

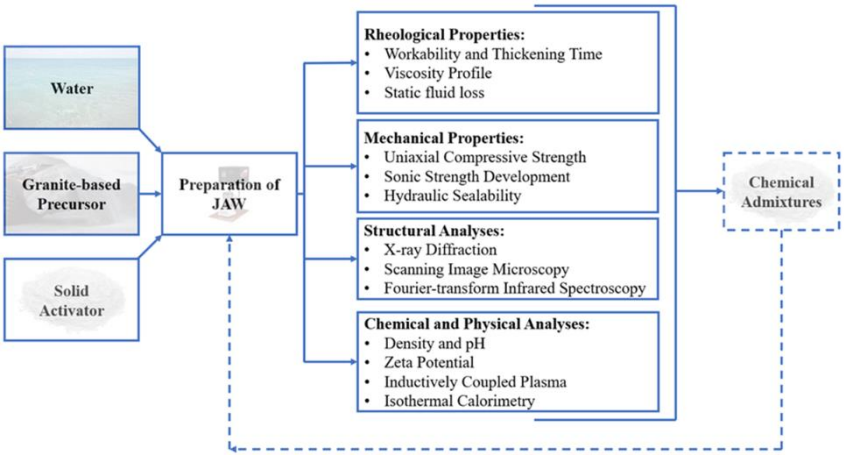

Figure 13: The applied testing strategy for JAW design.

5.4 Slurry Properties

5.4.1 Workability and Thickening Time

After the slurry preparation using an OFITE Model 20 Constant Speed Blender, each geopolymer mix was conditioned in an atmospheric consistometer. An atmospheric consistometer was used for conditioning and estimating the thickening time for all mixes between 20 to 50℃ Bottom Hole Circulating Temperature (BHCT). This temperature range was selected to simulate the conditions for BHCT that correspond to 25 to 70℃ Bottom Hole Static Temperature (BHST). The ramp-up rate for conditioning and thickening time measurements was selected to be 1℃/min and the conditioning duration was selected to be at 30 minutes in total. This conditioning duration was selected to ensure equipment safety.

The thickening time of the investigated slurries was measured from the initial consistency point until reaching the consistency at 40 Bearden units (Bc). The consistency profiles were tested to reach between 40-50 Bc. All the examined slurries of the JAW system set and harden rapidly, typically within minutes, once they reach a consistency between 40-50 Bc. This range was selected to provide a comparable benchmark for all mixes, to match the operational criteria and to ensure equipment safety.

5.4.2 Density and Rheology

Prior to density and viscosity measurements, all slurries were conditioned. A pressurized mud balance was used to estimate slurry density [15]. A viscosity-gel VG-meter was used to measure the viscosity and evaluate the rheological behavior of the slurries including the API Gel-Strength measurements. This viscometer apparatus was equipped with a cup and a heater to control the test temperature. Following API procedures, rotational speeds of 5.1, 10.2, 51, 102, 170, 340, and 511 s^{-1} were used in ascending (ramp up) and descending (ramp

down) orders, and then average values were reported for each shear rate [15].

5.4.3 Static Fluid Loss

After conditioning the slurries, an API HPHT static fluid-loss test cell was used to measure the fluid loss of the slurry at 6.9 MPa and 25℃ [15]. The cell was equipped with a sieve, a mesh gird of 250 micros and a hardened filter (to ensure clear filtrate for further analysis). All fluid loss tests were running up to 30 minutes unless the blow-out was experienced earlier. Afterwards, the produced fluids (i.e., filtrates; pore solutions) were collected, sampled and then examined for pH and Inductively Coupled Plasma Mass Spectroscopy (ICP-MS).

5.4.4 pH and Zeta Potential

pH and zeta potential of all mixes were measured after mixing the components right prior to conditioning the slurries. A Mettler Toledo pH meter equipped with an electrode, was used to measure the pH for slurries and pore solutions. Zetasizer Nano ZS Malvern equipped with a laser source of wavelength 633 nm at a scattered angle of 13° was used to estimate the zeta potential of the mixes through Electrophoretic Light Scattering (ELS) mode.

5.4.5 Inductively Coupled Plasma

The dissolution of each solid component and their mixes were analyzed by inductively coupled plasma-mass-spectrometry (ICP-MS) at ambient conditions. ICP MS tests were performed after mixing the components in the alkaline medium. Additionally, the examined pore solution samples of JAW mixes for ICP-MS tests were extracted after performing the static fluid-loss test at 6.9 MPa and 25 ℃.

5.4.6 Differential Scanning Calorimeter

Due to the limited access to an isothermal calorimetry apparatus, a Differential Scanning Calorimeter (DSC) was used instead at constant temperature. DSC tests were performed to study the heat evolution of JAW raw components and JAW mixes in the alkaline medium. The DSC tests were conducted at 20-50℃ (note the BHCT) for up to 180 minutes.

5.5 Mechanical and Micro-structural Properties

5.5.1 Uniaxial Compressive Strength (UCS)

Right after conditioning, all samples were cured at a controlled curing temperature (i.e., in an oven) at 25 and 70 ℃ BHST. All specimens were cured in closed or sealed cylindrical plastic molds to avoid any possible water evaporations. Following API 10B-2 [15], all cured specimens were cured in cylindrical molds with a slenderness height-to-length ratio of 2. JAW specimens were cured for 1 to 112 days interval. Uniaxial compressive strength (UCS) tests were measured using an MTS Criterion C45.105 Load frame mechanical tester and Toni Technik-H mechanical tester at loading rates between 7-30 kN/min. The loading rates were fixed and selected based on the curing duration and the sensitivity of the mixes. Additionally, at least three specimens were provided per each mix design at each curing duration and condition.

5.5.2 Sonic Strength Development

Non-destructive (i.e., sonic) strength development of the specimens was measured following API RP 10B-2 [15]. A high-pressure high temperature (HPHT) ultrasonic cement analyzer (UCA) was used at the confined downhole conditions of 13.7 MPa and 70 ℃ for up to two months. The UCA equipment measures the sonic waves' transit time throughout the slurry by means of transducers. The recorded transit time

is used to estimate the sonic compressive strength of the slurries using pre-defined and custom algorithms.

The built-in algorithms and correlations depend on the chemistry of the material under examination. In this research, a new algorithm was generated based on the testing conditions of the JAW system. This new algorithm was generated by integrating UCS and transit time results at different time intervals to develop a new polynomial equation for estimating the strength development of JAW system. The developed correlation is found in Paper II.

5.5.3 Hydraulic Sealability

A hydraulic sealability test setup of a cylindrical steel tube (KF HUP S355J2H) was used to examine the hydraulic sealability of the JAW mix. This mix was cured at 25℃ and 34.5 bar for 7-28 days. After curing inside the cylindrical steel tube, bottom of the test cell was connected to nitrogen gas and then the gas was injected into the system. The setup was also connected to a separator, flowmeters, and a data logging system. Increments of 5 bar pressure steps were applied to the cell to examine sealing ability of the hardened JAW system. Hence, any production or breakthrough of gas bubbles along the contact area or through the geopolymer plug was registered as leakage and failure pressure.

5.5.4 X-Ray Diffraction (XRD)

Crystallography of the hardened JAW specimens was examined by using X-ray diffraction (XRD). XRD analysis was performed on the remains of each crushed geopolymer specimen after performing UCS tests on the final day of aging (7 days – 2 months). These UCS remains were ground and dried in an oven at 30°C overnight, and then they were kept in a vacuum dryer for 1 day to maximize the removal of moisture. A CuKα radiation Bruker-AXS Micro-diffractometer D8 Advance XRD setup

was employed, selecting a 2theta (2θ) range between 5-92 º with 1 º /min step and 0.010 ° increment step.

Due to the complexity of JAW's chemical composition and random distribution of the raw minerals, this study was mainly focused on presenting the main detectable peaks of the XRD patterns. EVA v5 Bruker software was used to identify crystalline phases of the precursors and pastes. Hence, the obtained XRD patterns and TOPAS v5 Bruker software were used and integrated for the Rietveld quantification analysis.

5.5.5 Fourier-transform Infrared Spectroscopy (FTIR)

An Agilent Cary 630 Fourier Transform Infrared (FTIR) spectrometer was used to analyze the powdered pastes. Aliquots from the samples prepared for XRD tests, the FTIR spectra were collected and analyzed in a transmittance mode between 600-4000 cm^{-1}.

5.5.6 Scanning Electron Microscopy (SEM)

The morphology of the precursors and pastes was examined by employing Scanning Electron Microscopy (SEM) technique. SEM analyses were done using an SEM model Gemini Supra 35VP (ZEISS). Prior to coating, all samples were dried the same way as the samples for XRD. All SEM samples were small pieces of ~2 mm thickness and were coated with 10 nm palladium plasma to prevent charging before running SEM tests.

6. Results and Discussion

6.1 Normalization of Granite and Synthesis of the JAW Paste

As described previously in Section 4.0, the low reactivity of untreated granite may result in low and very slow early strength development when used as a precursor [111-118]. On the other hand, granite is rich in aluminosilicates, it may be capable of providing the necessary elements for participating in geopolymerization reaction when involving a highly alkaline medium and an activation mechanism [114].

Furthermore, normalizing the cationic content of granite-based geopolymers with a rich calcium content substance may be enough to perform properly and to develop sufficient early strength and mechanical properties in due time [115-118].

Therefore, GGBFS was selected to normalize the chemical composition and mineralogy of the granite to compensate for its low early-strength development. GGBFS content ranged from 0 % to 90 % of the total weight of the precursor. Additionally, fluid-state and solid-state characteristics of the mixes were studied including consistency, thickening time, uniaxial and ultrasonic compressive strength, and composition analysis. Table 9 presents the mixes and their classification.

Table 9: Mix design for one-part AAM mixes.

Mix design name*[1,2]	GGBFS (wt.%) in Precursor	Classification
GGBFS-0%	0	Granite-based JAW
GGBFS-10%	10	Granite-based JAW
GGBFS-20%	20	Granite-based JAW
GGBFS-25%	25	Granite-based JAW
GGBFS-30%*[3]	30	Granite-based JAW
GGBFS-33%	33	Granite-based JAW
GGBFS-36%	36	Granite-based JAW
GGBFS-40%	40	Granite-based JAW
GGBFS-43%	43	Granite-based JAW
GGBFS-47%*[4]	47	Granite-based JAW
GGBFS-50%	50	AAM JAW
GGBFS-60%	60	Slag-based JAW
GGBFS-70%	70	Slag-based JAW
GGBFS-80%	80	Slag-based JAW
GGBFS-90 %	90	Slag-based JAW

***1- All recipes had the same water-to-solid and solid activator-to-precursors ratios, 0.33 and 0.20, respectively.**

***2- All recipes had the same microsilica content, 4.3 wt.% of the precursors.**

***3- GGBFS-30% is the so-called JAW-a. which is a comparable back-calculated two-part granite-based geopolymer mix formulation.**

***4- GGBFS-47 % is the so-called JAW-b, which is the neat one-part granite-based geopolymer.**

6.1.1 Consistency and Thickening Time

Consistency profiles of the normalized granite-based JAW mixes at 50 ℃ bottom hole circulating temperature (BHCT) are given in Figures 14 and 15. As mentioned previously in the methodology section, the 40 Bc consistency value was selected as a cut-off point for the workability benchmark for all investigated slurries.

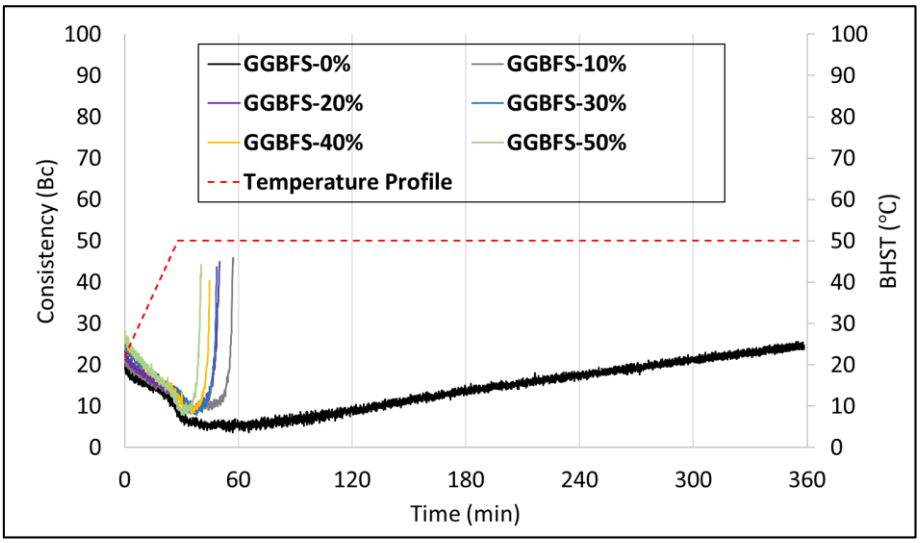

Figure 14: Consistency development profile of the granite-based geopolymers slurries at 50℃ BHCT. (Paper I)

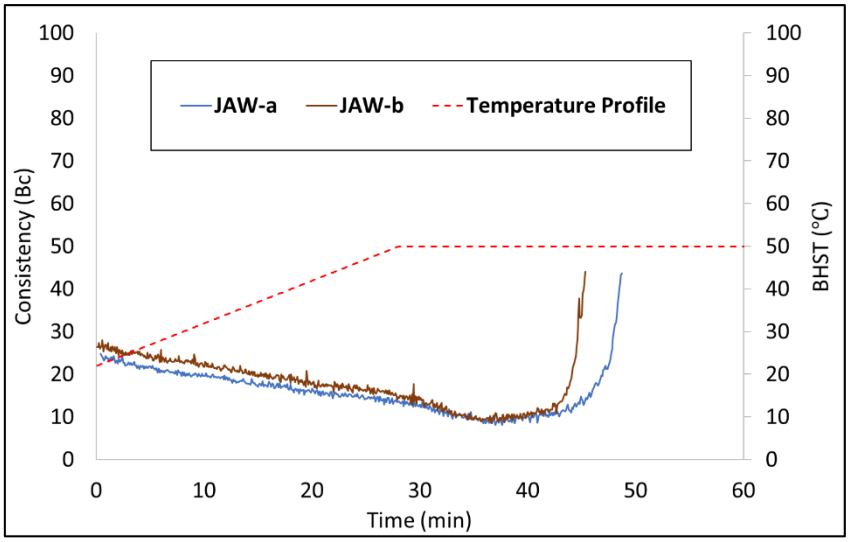

Figure 15: Consistency development profile of the two neat one-part granite-based geopolymers recipes at 50 ℃ BHCT. (Paper I)

Figure 14 shows the consistency profile of the GGBFS-0% mix that could not be set nor hardened within 6 hours of pumpability at 50 ℃

BHCT. However, as shown on the black curve at 60 min and onwards, its consistency gradually increased. Thus, the GGBFS-0% recipe does not fulfil an acceptable pumping time for well cementing applications where the circulating temperature is around 50 ℃ of BHCT.

The introduction of GGBFS to the granite-based slurry has shown its impact in two ways: on the pumping time and consistency values. On one hand, the GGBFS reduces pumping time of the given granite-based mix to a range between 41 – 57 minutes at 50 ℃ BHCT. All the granite-based mixes which contained GGBFS experienced a rapid gain in consistency or the so-called "right-angle set". On the other hand, it increased the initial consistency from 17 for GGBFS-0% to 28 Bc for GGBFS-50%. A trend was observed with increasing the partial replacement of granite by GGBFS in the precursor phase; by increasing the GGBFS content, the slurries become thicker and the initial consistency values were increased. Consequently, in addition to the shorter pumping time down to 43 minutes, shorter setting and hardening time were observed, as shown in Appendix 3; Table 10. Moreover, the right-angle-set behaviors were identified.

To better present the results from Figure 14, Figure 15 shows that JAW-b recipe with GGBFS-47% had higher initial consistency, shorter setting time and workability than JAW-a with lower GGBFS content (GGBFS-30%). These two granite-based mixes performed acceptable workability according to the operators' criteria due to their rapid gelation time or so-called right-angle-set behaviors upon reaching 30 Bc.

Considering the consistency profiles, the presence of GGBFS facilitates oligomerization and polycondensation mechanisms for the JAW mix design. This will be further investigated through this dissertation.

6.1.2 Uniaxial and Sonic Strength Development

Uniaxial and sonic compressive strengths of the JAW mixes were revealed as a function of the GGBFS content. Figure 16 illustrates the effect of increasing the partial replacement of GGBFS to granite on 1-day UCS for the heat-cured specimens at 70 ℃ bottom hole static temperature (BHST) which is equivalent to 50 ℃ bottom hole circulating temperature (BHCT). Figure 17 shows the 7-day sonic strength development of GGBFS-0%, JAW-a with GGBFS-30% and JAW-b with GGBFS-47% at 70 ℃ and 13.7 MPa.

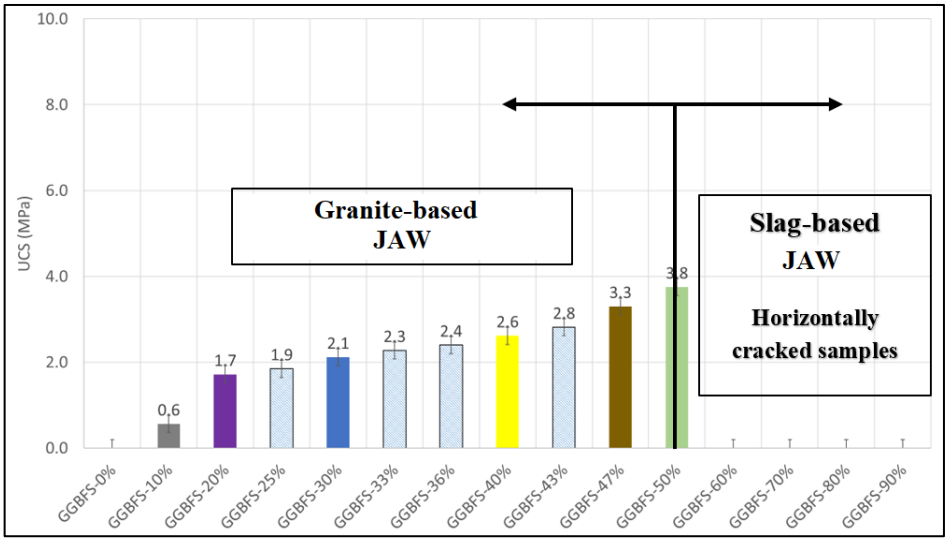

Figure 16: 1-day UCS data for heat cured samples, 70 ℃. (Paper I)

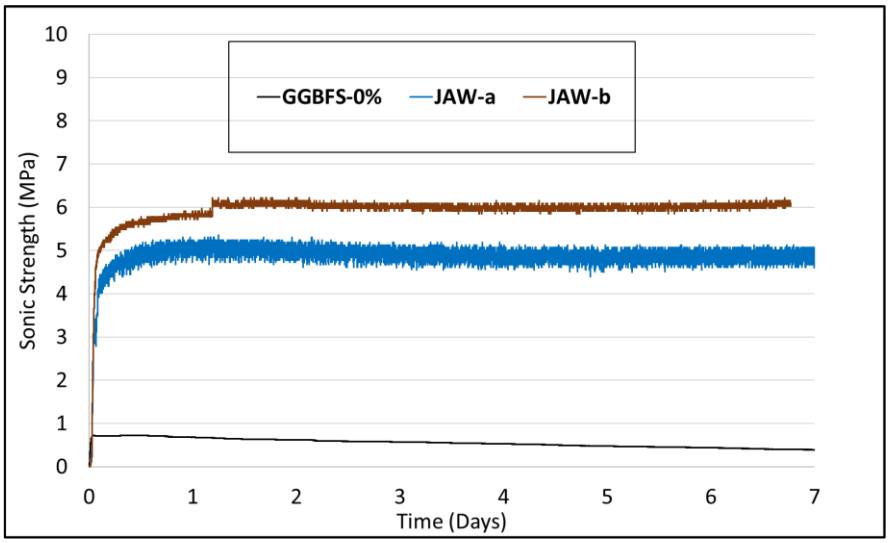

Figure 17: Sonic strength development for GGBFS-0%, JAW-a and JAW-b. (Paper I)

Figures 16 and 17 revealed how beneficial is the utilization of GGBFS for providing early-age strength development. GGBFS-0% could not set nor withstand sufficient compressive strength. On the other hand, the partial replacement and normalization of granite by GGBFS up to 50 wt.% showed a significant improvement in UCS and UCA data.

Nevertheless, the replacement of granite with more than 50 wt.% by GGBFS in the precursor phase could not be examined for UCA nor UCS due to the presence of horizontal cracks and observable 3D expansion in the specimens right after setting. In line with other researchers, they also observed cracks in their GGBFS-based samples, that might be caused by chemical shrinkage or dry shrinkage [28, 119-120]. Figure 18 shows the observed horizontal cracks in the specimens that contain more than or equal to 50 wt.% of GGBFS in the precursor phase. These cracks could also be due to the specimen expansion rooted in the high magnesium content of the used GGBFS. The utilized GGBFS was rich in expanding components including magnesium oxide (see Table 2). Li et al. [121] presented magnesium oxide as an expansive agent after its hydration. Its hydration product is magnesium hydroxide ($Mg(OH)_2$). Once $Mg(OH)_2$

produced crystals are confined, their volume increase and their crystallization pressure may cause expansion of the hardened cement paste.

Although the early-age strength of the mixes was improved by the use of the GGBFS, in well construction activities, the 1-day strength at corresponding downhole conditions should be over 7 MPa, which could not be achieved by only the normalization of granite with GGBFS and microsilica. Therefore, further development was suggested, see Section 6.2.

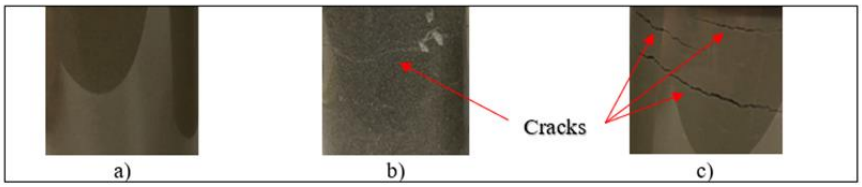

Figure 18: Three vertical sample pictures (4 x 4 cm); a) GGBFS-47% (without horizontal cracks), b) GGBFS-50% (a small horizontal crack on the surface), c) GGBFS-60% (with observable large horizontal cracks) after heat curing at 70 ℃ for 1-day (Paper I)

6.1.3 Compositional Analysis XRD

According to Bowen's reactions series, each mineral has a stability region when considering pressure and temperature [122]. The used granite is a highly crystalline material which also contains clay minerals in addition to quartz. It might be fair to assume that granite-based precursor mixes produce low amorphous content geopolymers. In other words, part of the crystalline phases may be consumed during the geopolymerization reaction. While a considerable amount of these crystals can remain unreacted. Hence, the precursor normalization by GGBFS which is a highly amorphous material can lead to achieving a higher amorphous geopolymer system. Figure 19 and Table 10 show XRD patterns and XRD crystallinity quantification, respectively, of GGBFS-0%, JAW-a with GGBFS-30% and JAW-b with GGBFS-47%.

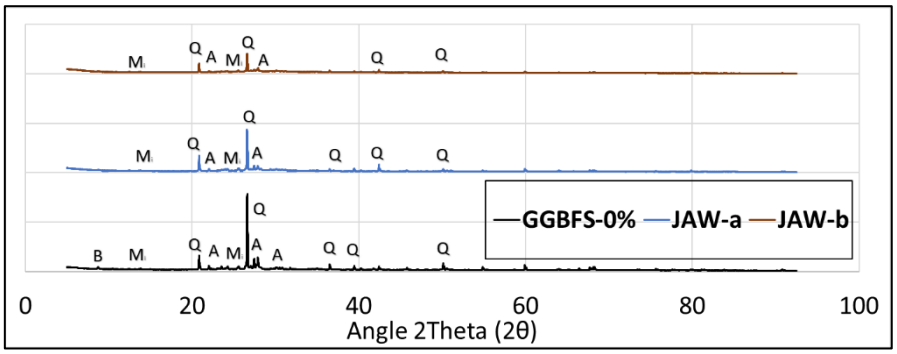

Figure 19: XRD patterns of selected mixtures after 7 days of heat curing at 70°C BHST, Q: Quartz, A: Albite, M: Microcline, B: Biotite. (Paper I)

Table 10: XRD crystallinity quantification of JAW samples using "EVA v5" software. (Paper I)

Mix Design	GGBFS in the precursor (wt.%)	Crystalline content (wt.%)	Amorphous content (wt.%)
Granite Powder	0	79.9	20.1
GGBFS-0%	0	75.2	24.8
JAW-a	30	64.9	35.1
JAW-b	47	51.7	48.3

From Figure 19 and Table 10, the higher the granite content, the higher the remaining crystalline phases. GGBFS-0% mix had the highest granite content in the precursor phase without any addition of GGBFS. It got the highest intensity of the major crystalline peaks such as quartz, Albite, and minor peaks such as Microcline and Biotite. This XRD pattern is very comparable to the stand-alone granite powder pattern. JAW-a (i.e., GGBFS-30%) had less XRD spectrum intensity if it is compared with GGBFS-0%. JAW-b (GGBFS-47%) had the lowest XRD pattern intensity with the highest GGBFS normalization to the granite-based precursor. Additionally, JAW-b got the highest detectable amorphous content after geopolymerization reaction if it is compared with GGBFS-0% and JAW-a.

In the case of JAW-a and JAW-b, their geopolymerization reactions lowered down and diminished the presented minor crystalline phases in granite such as albite, microcline, and biotite. One may conclude that the higher the granite content in the precursor phase, the higher the remaining crystalline phases in the matrix, and vice versa for GGBFS. These observations match the detected high PSD of granite, at which over D50 of granite can be considered as non-reactive particles and large crystalline filler in the JAW matrix. Thus, this partial granite replacement or its normalization by GGBFS is decisive for synthesizing the granite-based JAW system.

6.2 Screening and Developing JAW

One should note that 1-day strength development is critical for well construction purposes. Therefore, it was considered in this work. Based on the outcomes of normalization and synthesis of the JAW system, subsection 6.1 and Paper I, the selected chemical composition for the developed mix design of JAW is presented in Table 7. In this subsection, the objective is to further develop the neat JAW granite-based geopolymer. It shows the effect of water content and different chemical admixtures on the early-age performance of the JAW system.

6.2.1 Effect of Water Content

Park & Pour-Ghaz [57] suggested that water only provides a medium for the dissolution and restructuring of aluminosilicate sources into geopolymer. It was proven that the effect of water content on the strength development of geopolymers could be negative [44-45]. Hence, the kinetics of the geopolymerization reaction and concentrations of the activator are negatively affected while having high water content (i.e., diluting effect). It means that if gels (e.g., N/K-A-S-H, C-A-S-H, or C-S-H) are not produced enough, water can have a detrimental effect on mechanical properties and early-age strength development of

geopolymers. Figures 20-22 reveal the effect of water content on the synthesized JAW system.

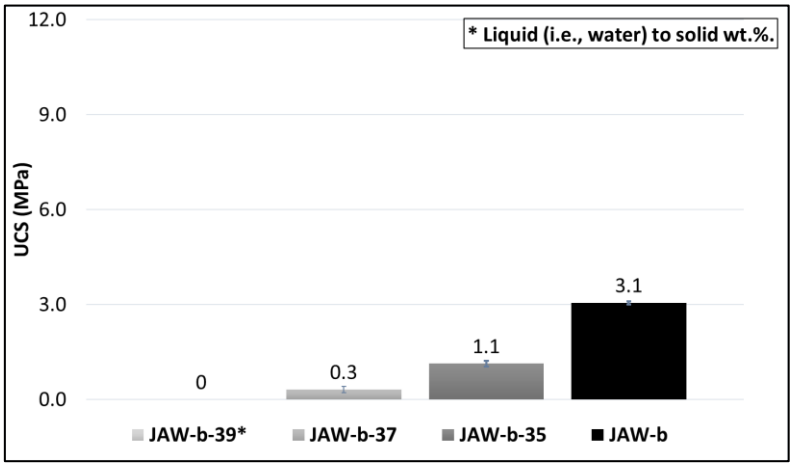

Figure 20: Effect of water content on 1-Day UCS of the JAW system at 70 °C BHST. (Paper III)

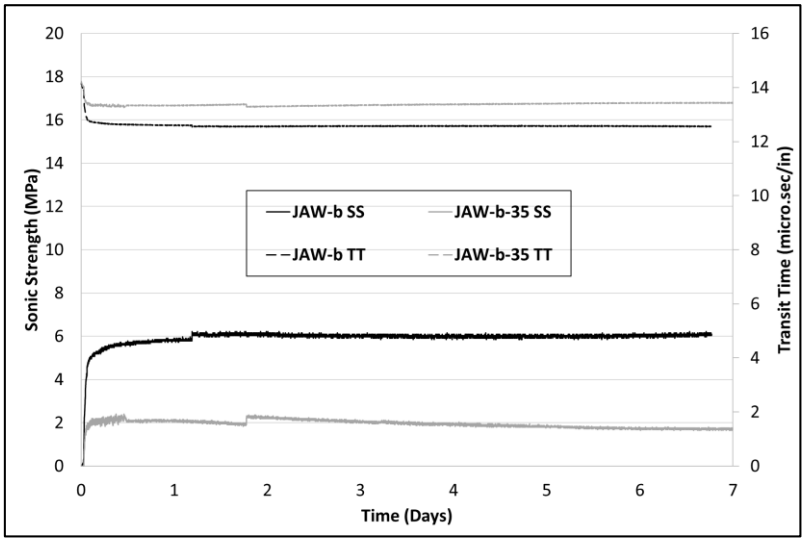

Figure 21: UCA for JAW with two different water content; SS: sonic strength, TT: transit time; JAW-b (33% w/s) and JAW-b-35 (35% w/s). (Paper II)

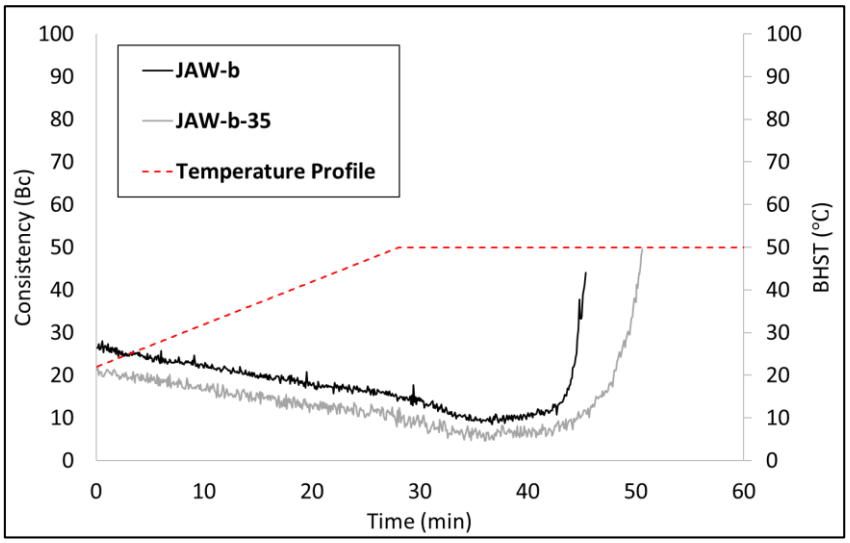

Figure 22:Effect of water content on the consistency of JAW at 50 ℃ BHCT; JAW-b (33% w/s) and JAW-b-35 (35% w/s).

The given JAW mix with higher water content than 35 % liquid-to-solid ratio (i.e., JAW-b-39 & JAW-b-37) could not set nor develop any reliable compressive strength. In addition, JAW-b-35 (i.e., 35 % w/s, grey color bar) was much weaker than JAW-b (i.e., 33 % w/s, black color bar). The obtained UCS results indicate that the optimum water content for this JAW system is below 33 % of the total solid powder. The measured sonic strength data agrees with the trend of the measured UCS values with higher water content. Both data show and prove the severe effect of water content on the JAW system.

JAW-b-35 had higher water content, it had lower initial consistency by 74 % and a longer pumpability profile by 111% than JAW-b with 33 % w/s ratio. JAW-b was a much thicker slurry with higher initial consistency right after mixing. Thus, a superplasticizer might be required to improve the rheology and lower the initial consistency of JAW-b.

6.2.2 Screening of Chemical Admixtures

From Table 6, five chemical admixtures were investigated and examined in this research. These admixtures were added to the neat slurry of JAW-b to improve its early-age strength in the same quantities between 0-1.14 wt.% to the total solid mix as given in Paper II and Appendix 4. These chemical admixtures include Calcium Oxide (CaO, JAW-b-CO), Calcium Carbonate (CaCO3, JAW-b-C), Sodium Hydroxide (NaOH, JAW-b-N), Aluminum Hydroxide ($Al(OH)_3$, JAW-b-Al) and Zinc Oxide (ZnO, JAW-b-Z). The samples were then screened to identify the most effective early-age strength booster for JAW-b. Figure 23 illustrates UCS results for the utilized 0.14 wt.% chemical admixtures after 1- and 7 days of heat curing at 70 ℃.

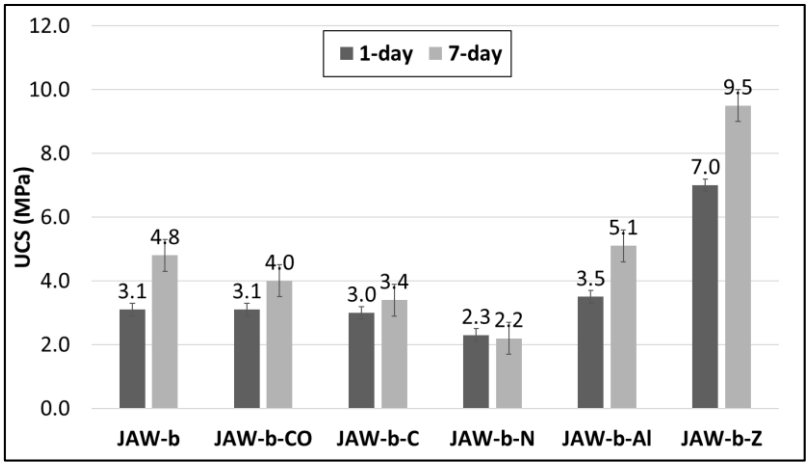

Figure 23: The effect of 0.14 wt.% chemical admixtures on 1- and 7-Day UCS at 70 ℃ BHST; Please consult the text for a description of the different samples. (Papers II and III)

Calcium Oxide (CaO, JAW-b-CO), Calcium Carbonate ($CaCO_3$, JAW-b-C), Sodium Hydroxide (NaOH, JAW-b-N) and Aluminum Hydroxide ($Al(OH)_3$, JAW-b-Al) could not improve the early-age strength when comparing the results with the neat JAW-b mix design. In fact, most of them had either a negligible or negative effect on the early strength. This could be due to the production of gels or products that depleted the

system from silicates while conserving the molar ratio at 2.4 [132]. Conducting an experimental sensitivity analysis, it was revealed that by an increase of the dosage of these admixtures, the early-age strength development rate was reduced for JAW-b-C, JAW-b-CO and JAW-b-N [44-45, 132].

On the other hand, the addition of Zinc Oxide (ZnO) remarkably improved the early-age strength of the system. Unlike the other utilized chemical admixtures, the addition of 0.86 wt.% ZnO facilitated achieving the highest 1- and 7-day UCS up to 10-13 MPa. JAW-b-Z had more than two to three times higher 1-day UCS than the neat JAW-b [44-45].

6.2.3 Effect of ZnO

Based on the positive 1-day UCS results obtained by utilization of Zinc Oxide (see Figure 24), this mix design was further investigated and analyzed. To simplify the naming of mix designs, from now on JAW-b-Z is called JAW-Z.

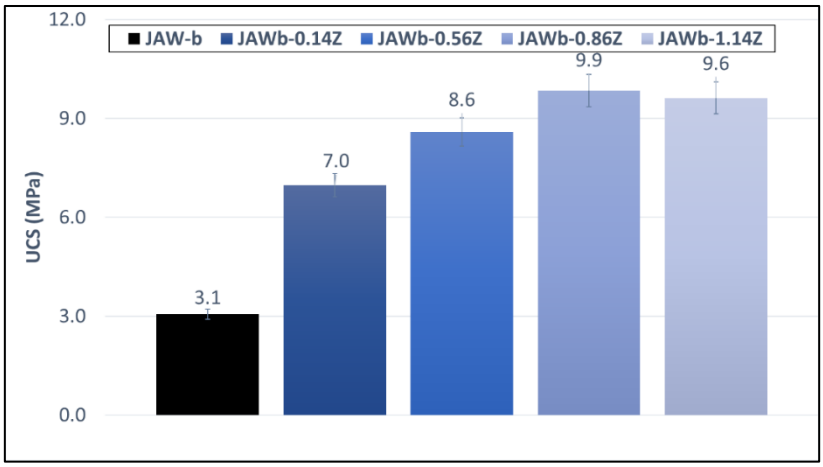

Figure 24:Effect of ZnO on JAW for 1-Day UCS at 70 °C BHST (Papers II and III).

Zailian et al. [123] showed that utilization of ZnO as a chemical admixture with low concentrations in the solid phase mixture could enhance the geopolymeric properties by positively controlling the formation of K-Z-Al-S-H, (N, K)-Z-S-H and/or C-Z-A-S-H gels through a complete geopolymerization reaction. This admixture may improve the thermodynamics of the geopolymerization reaction to achieve higher early strength [44-45, 123-124].

Figure 25 presents the sonic strengths of JAW-b and JAW-Z mix designs where ZnO shows its performance in the first hours of curing at 70 °C.

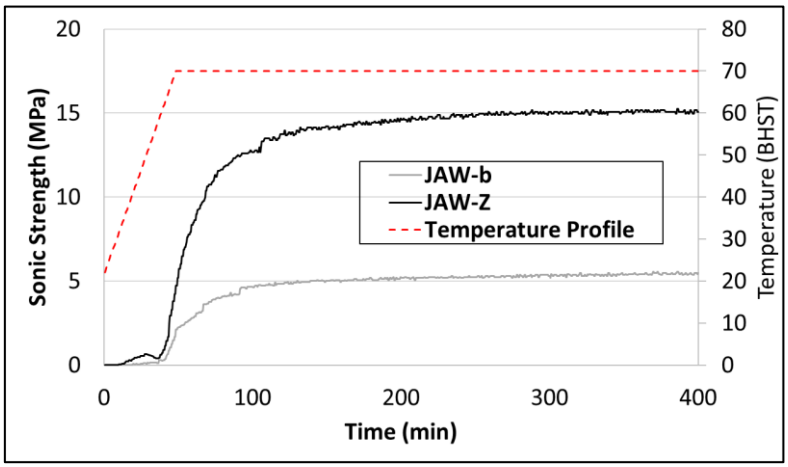

Figure 25: Sonic strength profile of JAW-b (neat) & JAW-Z (JAW-b + 0.86 wt.% ZnO). (Paper VI).

Considering the sonic strengths measured at 70 °C, zinc oxide containing mix design (JAW-Z) achieved around 8.5 MPa strength during the first heat curing hour which was three times higher than the neat one (JAW-b). It also achieved around 15.7 MPa strength within the first 5 hours while JAW-b got around 5.8 MPa after the same duration. Thus, ZnO can be considered an early-age strength booster for the JAW system developed in this research. Additionally, these observations, the early-age strength development studies, match the DSC results presented in subsection 6.3.2.

One may note that zinc (Zn) is a heavy transition metal, and its application can be challenged in Oil & Gas industry. This required further assessments; however, this is outside the scope of this work.

6.2.4 Effect of Superplasticizers

As above-mentioned, water content shall be optimum to facilitate the geopolymerization reaction. After lowering the water-to-solid ratio of the JAW system from 0.35 to 0.33, to ensure suitable rheological behaviour, various types of superplasticizers were examined. These superplasticizers were two naphthalene-based superplasticizers and a Na-based lignosulfonate superplasticizer. These superplasticizers were investigated separately after blending 1 wt.% by weight of the total solid in the JAW-Z mix design.

The selection of these three superplasticizers was based on their stability and effectiveness in high alkaline medium, especially for the given granite-based geopolymer system [108]. Figures 26 and 27 present the effect of these superplasticizers on the rheological and mechanical performance of JAW-Z. Tables 11 and 12 show their rheological and electrokinetic potential measurements, respectively.

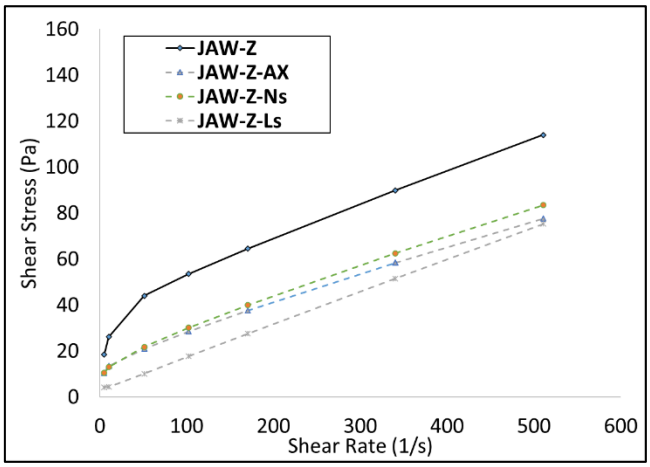

(a)

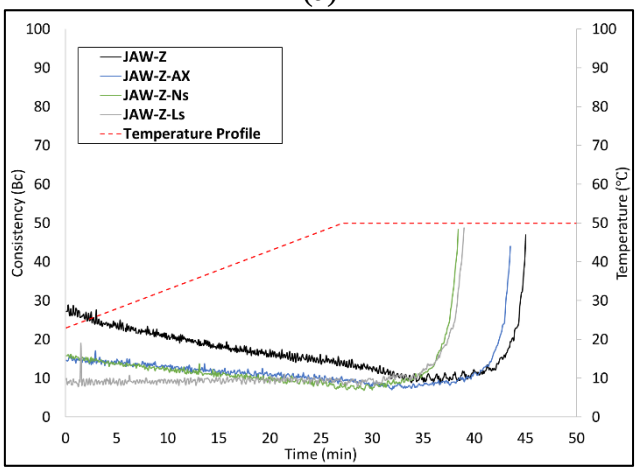

(b)

Figure 26: (a) Shear stress - Shear rate curves of JAW-Z with 1 wt.% superplasticizer, (b) consistency profile of JAW-Z with 1 wt.% superplasticizer at 50 °C BHCT. AX: Auxilchem Naphthalene-based powder, Ns: Sodium Poly-Naphthalene- sulphonate powder, Ls: Sodium Lignosulfonate. (Paper VI)

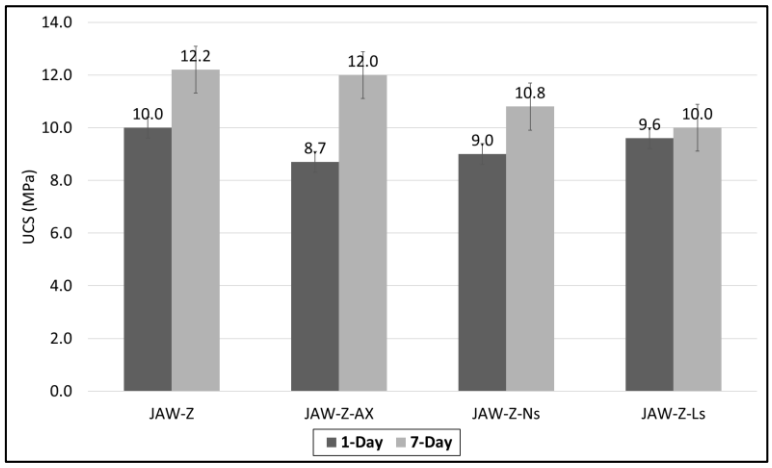

Figure 27: Uniaxial compressive strength of JAW-Z with 1 wt.% superplasticizer after 1- and 7-day at 70 °C BHST.

Table 11: Yield stress and API Gel-strength results of JAW with 1 wt.% superplasticizer. (Paper VI)

Recipes	Superplasticizer	10 sec API Gel-strength [Pa]	10 min API Gel-strength [Pa]	Estimated Yield Stress [Pa]	Flow Index
JAW-Z	---	18.5	19.1	15.4	0.37
JAW-Z-Ns	Naphthalene-SP	10.5	10.6	8.5	0.44
JAW-Z-AX	Auxilchem NS181	10.4	11.3	8.5	0.42
JAW-Z-Ls	Lignosulfonate-SP	5.6	6.9	4.1	0.64

Table 12: Zeta potential measurements of JAW with 1 wt.% superplasticizer. (Paper VI)

Recipes	ZP (mV)	Standard Deviation
JAW-Z	-25.4	± 0.3
JAW-Z-Ns	-27.9	± 1.3
JAW-Z-AX	-31.7	± 0.6
JAW-Z-Ls	-33.1	± 0.7

The rheology profile of the geopolymer slurries revealed non-Newtonian shear-thinning behavior for mixes with and without the superplasticizers. It was also observed that the absolute zeta potential value of these mixes was increased after the utilization of these superplasticizers. Considering the zeta potential and geochemistry of the precursors (see subsection 4.1), adsorption of these superplasticizers on the surfaces of GGBFS might have increased the magnitude of double-layer repulsive forces and then effectively reduced their yield stress and API gel strengths. Moreover, the addition of these superplasticizers efficiently lowered the initial viscosity and initial consistency of the slurries.

Furthermore, utilization of these admixtures had a negligible effect on the early-age strength development of JAW-Z (see Figure 27). Thus, these results show a stable and effective plasticizing behavior of these three superplasticizers, especially Lignosulfonate-SP.

6.3 Characterization of the JAW System - Short-term

Building on the work done on screening and developing JAW granite-based geopolymer mixes, JAW-b and JAW-Z were selected for characterization. Motivated by that, this subsection presents properties of JAW-b and JAW-Z (containing 0.86 wt.% of ZnO to the precursor) at 20-50 ℃ BHCT (i.e., 25-70 ℃ BHST).

The main objective was to understand each phase of geopolymerization, starting from the dissolution, reorganization, and then polycondensation phases of JAW-b and JAW-Z. Table 13 presents their formulations. JAW-Z contains 0.86 wt.% of ZnO to the total precursor content equivalent to 0.7 wt.% to the total solid content including precursors and activators.

Table 13: Formulations of JAW-b and JAW-Z. (Paper VII)

Composition (wt.%*)	Precursor Components	Activator	ZnO	Water / TSP
JAW-b	80.3	19.7	0.0	0.33
JAW-Z	79.8	19.5	0.7	0.33

*** By weight of the total mixture of all solid components (TSP).**

6.3.1 Dissolution of JAW

ICP-MS was utilized to study the dissolution stage of JAW components and their mixes. More ICP-MS details are provided in Appendix 8 and Paper VI regarding the pore solutions preparation and extraction from JAW system. Tables 14 and 15 provide the measured dissolutions. The pure solid activator dissolution data was used as the concertation baseline for silicon and potassium. In this evaluation, the given components and mixes had the same amount of solid activator and water.

Table 14: ICP evaluation for JAW components (Paper VI).

Material*	Silicon (mg/l)	Aluminum (mg/l)	Potassium (mg/l)	Sodium (mg/l)	Zinc (mg/l)
Activator	750	0.7	20000	100	0.7
Granite	1200	6.5	20000	110	5.2
GGBFS	220	23.0	19000	110	1.2
Microsilica	2800	2.1	20000	100	3.0

*** By weight of precursor used on each paste**

The ICP results showed that granite increases the concentration of silicon in the solution, perhaps due to mechanical friction between granite particles with the activator. On the other hand, although GGBFS was supposed to increase the silicon content, due to its reactivity and mixing condition, silicon containing products were precipitated, i.e., silicon being consumed. This observation could be due to the possible adsorption of silicates on the surfaces of GGBFS particles [17]. It could be also due to the formation of C-S-H or C-A-S-H gels. The microsilica

was effectively dissolved into the provided alkaline medium. Despite having comparable alumina content in granite and GGBFS (see Table 2), GGBFS released more aluminium than granite.

The extracted pore solution of JAW-b and JAW-Z was also investigated using ICP analysis, see Figure 28 and Table 15.

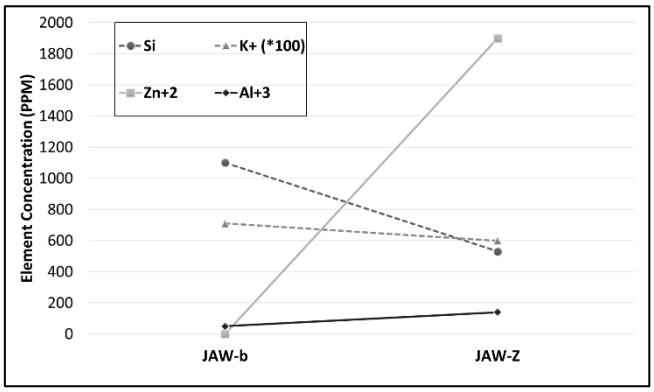

Figure 28: ICP analysis (Dissolution) of the pore solutions of JAW-b vs JAW-Z. (Paper VII)

Table 15: ICP evaluation for JAW recipes (Paper VI)

Material	Silicon (mg/l)	Aluminum (mg/l)	Potassium (mg/l)	Sodium (mg/l)	Zinc (mg/l)
JAW-b	1100	94	71000	540	0.6
JAW-Z	530	140	60000	530	1900

The ICP results show a lower silicon concentration for JAW-b and JAW-Z when they are compared with the utilized granite and microsilica themselves. The phenomenon of consuming the silicate as it was released could be due to adsorption on the GGBFS surface or the formation of gels. Contrary to the sum of the precursors, more aluminum dissolved from JAW-b and JAW-Z pastes. This dissolution may favour JAW system towards adjusting the silicon-aluminum ratio. Additionally, the dissolution of JAW-b and JAW-Z resulted in higher potassium concentrations than their granite-based precursors and the activator. The pastes` dissolved potassium content was more than 75%

mainly coming from the utilized activator. Thus, this increase in the free dissolved potassium could be due to the improvement in the solubilization of the potassium-based activator.

The main effect of zinc oxide in JAW-Z was a further decrease in or consumption of the free silicates. In addition, the dissolution of JAW-Z showed a small increase in aluminium content and a decrease in potassium concentrations. The addition of ZnO to the JAW system forms zincate and then captures silicates in the form of zincate-silicate complexes. Furthermore, the consumption of silicon and potassium concentrations for JAW-Z could be also due to the formation of potassium zincate-silicates. The ICP results and observations for JAW-Z are in line with the XRD pattern with the presence of crystalline tracers of additional potassium and zinc containing species and crystals, see Figure 29.

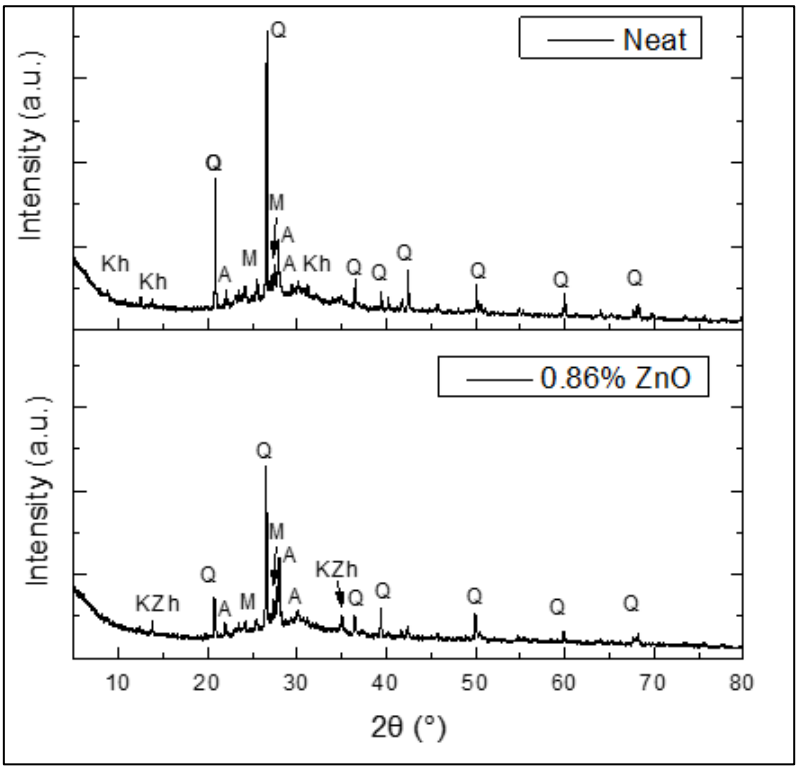

Figure 29: XRD mineralogical characterization of JAW-b (neat) and JAW-Z (JAW-b + 0.86 wt.% ZnO of the precursor). (A) Albite, (Kh) Potassium containing species/crystals, (KZh) Zinc containing species/crystals, (M) Microcline and (Q) Quartz. (Paper VI)

6.3.2 Kinetics of JAW

Differential Scanning Calorimetry (DSC) technique was used to analyze the heat release of the JAW system after being normalized by the total amount of each tested paste. Figures 30 and 31 show the DSC curves of JAW main precursors and mixes, respectively. All heat flow curves of the JAW components and mixes showed exothermic reactions. Moreover, a big difference in the heat release rate between 25 and 50 ℃ curves was noticed. At 50 ℃, the observed single peak was earlier with higher intensity, and had larger total heat released. This behaviour reveals the dependency of the JAW geopolymer system on the total cumulative heat.

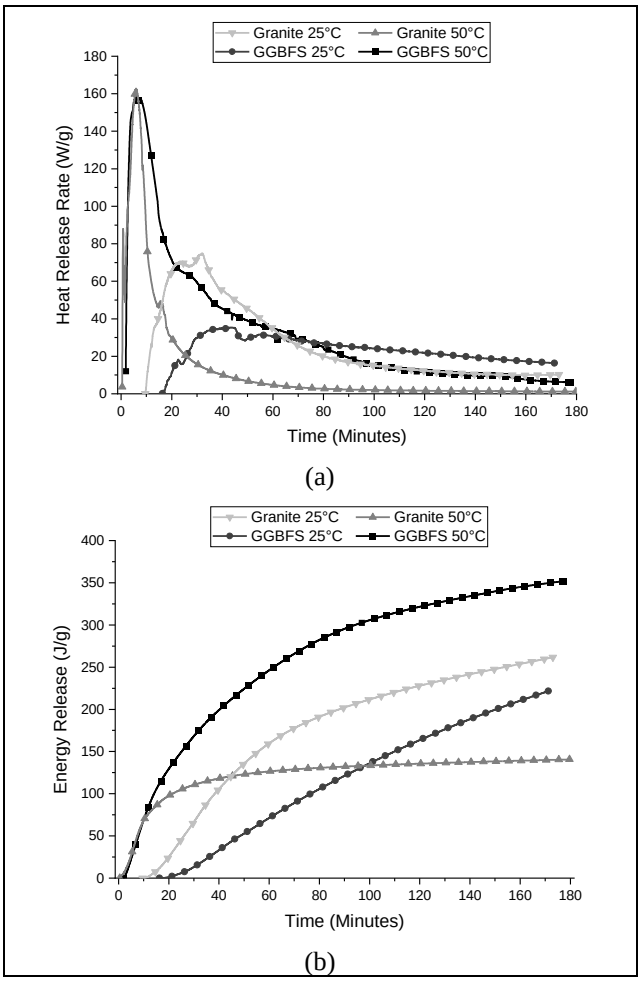

Figure 30: Differential scanning calorimetry data of Granite vs GGBFS; (a) heat rate (b) energy release. (Paper VI)

The DSC analysis of the granite and GGBFS showed that GGBFS reacts quickly and releases more heat, especially at 25 ℃. As mentioned before, unlike the highly crystalline granite, GGBFS is characterized by its high amorphous content and is more readily available for reaction. Furthermore, it can further react for much longer times than the given 3 hours. At 50 ℃, the GGBFS sustained a longer geopolymerization reaction than the granite. Hence, granite's total heat evolution was much lower than GGBFS. It means that the granite needs to be further

activated so that its reaction to take place at the same time or the total heat release of the system to be increased.

In the case of JAW mixes and by comparing the heat evolution curves of JAW-b and JAW-Z, utilization of the strength booster in JAW-Z provided earlier, higher, and wider heat release peaks with a higher total amount of heat release than the neat JAW mix (JAW-b). In addition, a significant positive effect of temperature on the heat release rates and total energy releases from both mixes was expected. Nevertheless, the precursors and mixes were observed to yield a single heat release peak in agreement with the literature [74, 125-126]. It could be fair to assume that this exothermic peak could be an indication of the occurrence of the geopolymerization reaction [125-126]. Both the dissolution and formation of geopolymers may occur simultaneously right after the initial mixing [125-126].

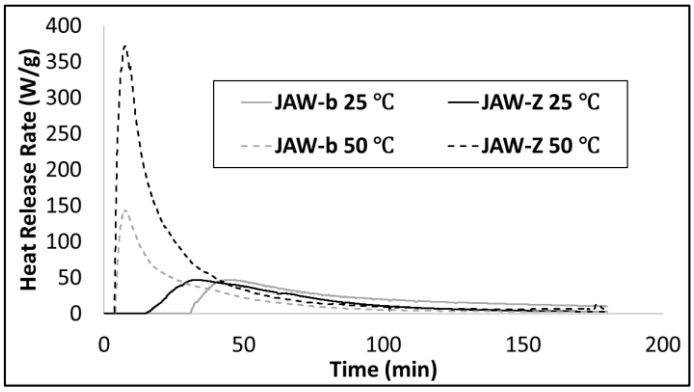

(a)

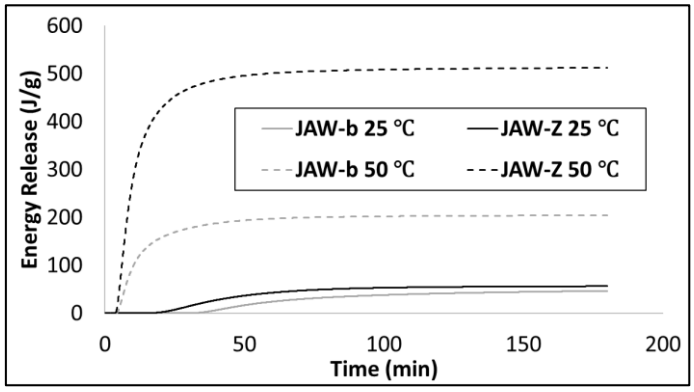

(b)

Figure 31: Differential scanning calorimetry data of the developed JAW; (a) heat rate (b) energy release; JAW-b & JAW-Z. (Paper VII).

6.3.3 Workability of JAW-b vs JAW-Z

An atmospheric consistometer was used to study the effect of circulating temperature between 20-50 ℃ BHCT on the workability of JAW-b and JAW-Z (See Figure 32).

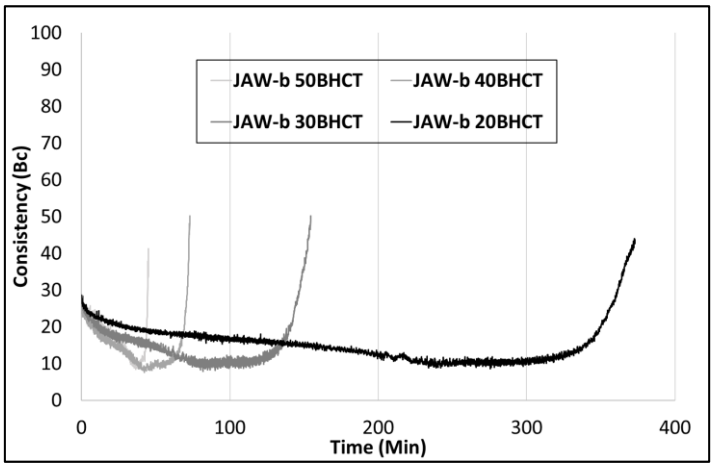

(a)

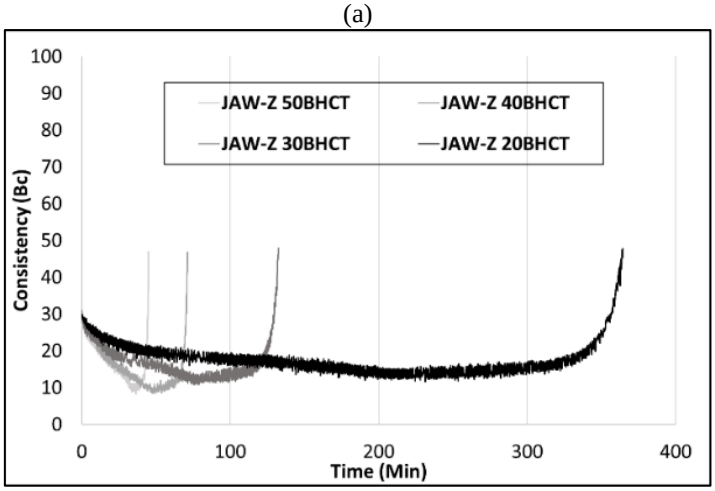

(b)

Figure 32: Consistency of the slurries (a) JAW-b and (b) JAW-Z. (Paper VII)

Both JAW mixes had very comparable consistency behaviour even at different circulating temperatures. The circulating temperature had a significant effect on pumpability and workability of the geopolymers. In line with Salehi et al. [35], geopolymers are significantly temperature dependent whereas the reduction in temperature prolongs the pumping time. However, the temperature dependency of the JAW system is not linear whereas 40 °C seems to be the critical temperature. The longest

observed pumpability up to 6 hours was at 20 ℃, while the shortest down to 45 minutes was at 50 ℃.

As a result, these consistency observations match their DSC profiles, where the dissolution of the JAW system was accelerated by increasing the conditioning temperature. This phenomenon could be due to speeding up the dissolution and solubility of aluminosilicates and silica ions at higher temperatures, i.e., higher cumulative heat given to the slurries. This could lead to accelerating the geopolymerization reaction and then shortening the setting time [125, 127].

6.4 Preliminary Study on Aging of JAW

Researching the properties of the aged geopolymers is a must when considering the integrity of wellbores[‡]. This alongside the limited available research on the JAW geopolymer systems highlights the necessity for further investigating and studying the durability of the developed geopolymers. Accordingly, this subsection is to study the properties and performance of the aged geopolymers. The aged geopolymers (i.e., JAW-b and JAW-Z) were mechanically and structurally analyzed over the given temperature ranges in the previous subsection 6.3, 25-70 ℃ bottom hole static temperature (BHST).

6.4.1 Uniaxial & Sonic Strength Development

Uniaxial compressive strength and sonic strength of geopolymers were examined for up to two months. Figures 33 and 34 show the uniaxial compressive strength of the JAW specimens after being cured at 25 ℃ and 70 ℃ in atmospheric pressure, and the extended sonic strength tests at 70 ℃ BHST and 13.8 MPa hydraulic pressure.

‡ Controlling fluid flow in wellbores during life cycle of wells.

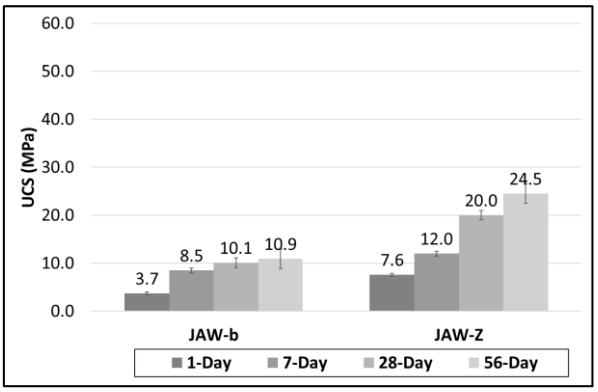

a) UCS of 25 ℃ BHST cured samples.

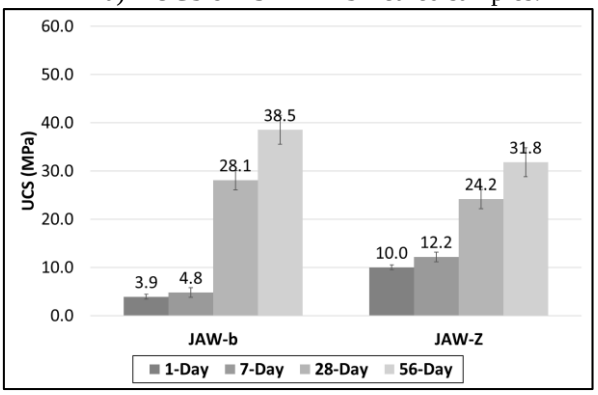

b) UCS of 70 ℃ BHST cured samples.

Figure 33: UCS data for JAW-b vs JAW-Z for up to two months of curing. (Paper VII)

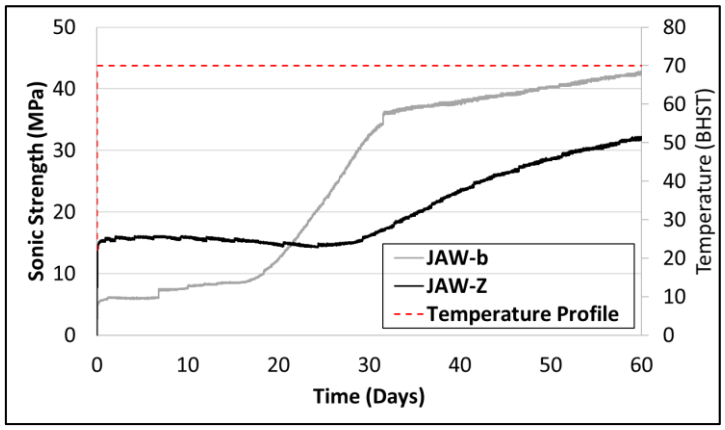

Figure 34: UCA profiles for JAW and JAW-Z up to two months; JAW-b (neat) & JAW-Z (JAW-b + 0.86 wt.% ZnO). (Paper VII).

The compressive strength of the JAW mixes was improved with ageing for longer curing time at 25 ℃ and 70 ℃. Additionally, higher curing temperatures with longer ageing improved the compressive strength of both JAW-b and JAW-Z. Considering 25 ℃ as a curing condition, the effect of ZnO as a strength booster for the JAW system was still significant and crucial to develop compressive strength, both early- and long-term. Appendix 1 includes extended UCA and UCS data for up to three and four months, respectively.

Furthermore, it was observed that the uniaxial compressive strength of JAW-b was higher than JAW-Z after a month when the sample was cured at 70 ℃. Consistent with the UCS data, the UCA profiles show a positive overcoming and higher sonic strength for JAW-b than JAW-Z after three weeks of heat curing at 70 ℃ and 13.6 MPa. Hence, at 70 ℃ BHST, two strength regimes were identified for the JAW mixes. The early-age sonic strength curve lasted for two weeks for JAW-b and three weeks for JAW-Z. While the second development curve was a continuously increasing long-term strength development for more than two months for both mixes.

This long-term development curve could be an indication of participation of the remaining unreacted precursor particles such as granite and/or could be an additional internal structural reorganization within the formed geopolymerization network. This ageing of the JAW system at high curing temperatures could result in a more favourable long-term maturation of the geopolymerization products (in agreement with subsections 6.4.3) and then yield effective improvements for strength development. One should note that when compressive strength started to improve, other properties such as matrix permeability, volume change, etc. may also be affected. However, studying these properties have not been the objective of this study.

An extended ICP pore solution study was performed to examine the dissolution of JAW after curing for 0.5-, 1-, 3-, 7-, 14- and 28-day, see Figure 35. Unlike the dissolution trend of the other elements and in line with the extended UCA and UCS observations, silicon concentration was the only element which was significantly increased again after two weeks of curing. This could be an additional indication for the additional dissolution of granite and then its participation in the long-term strength development of the synthesized JAW system.

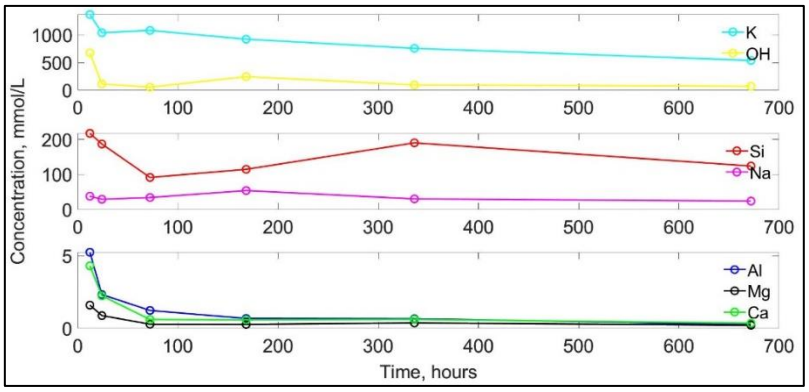

Figure 35: JAW dissolution behavior between 0.5-28 days.

6.4.2 Hydraulic Sealability and Morphology of Geopolymer Plug

To study the performance of the JAW mixes and their ability to withstand pressures at the geopolymer-casing interface, hydraulic sealability tests were performed, see Figure 36.

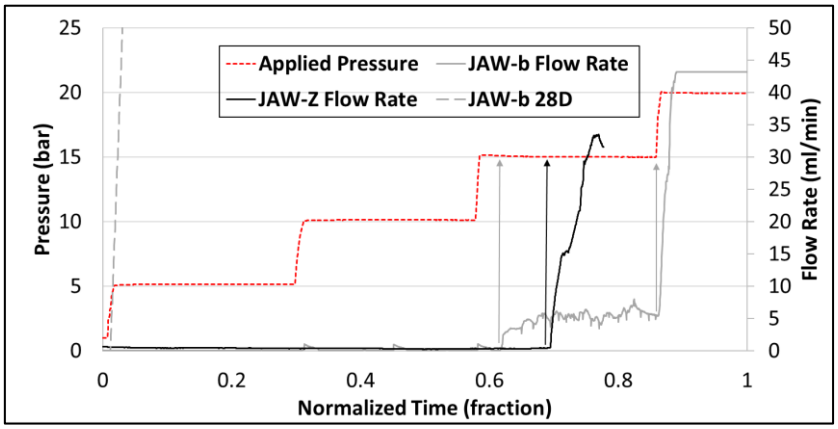

Figure 36: Hydraulic Sealability for JAW after 7-day & 28-day and JAW-Z after 7-day. (Paper VII)

This sealability test showed that the JAW system could withstand gas pressure before the complete gas breakthrough at the geopolymer-casing interface. After 7-day curing, the JAW mixes could withstand up to 15 bars of pressure at 25 ℃. These sealability results can be considered positive indications for the JAW mixes since they are comparable to the performance of neat API class G cement used in well-cementing applications [128].

Despite the positive sealability results after 7-day curing, the aged JAW system cured for 28 days could not withstand any pressure with a gas breakthrough at the geopolymer-casing interface. In addition, a clear gas breakthrough at the geopolymer-casing interface was observed, see Figure 37. This phenomenon could be due to the shrinkage of the aged JAW system after 1 month of curing at 25 ℃ and 3.4 MPa. This

observation matches Salehi et al. [35], who studied the volumetric shrinkage of low calcium fly ash geopolymers. Their study showed that geopolymers continuously shrink with ageing for two weeks up to 2.5 v.%.

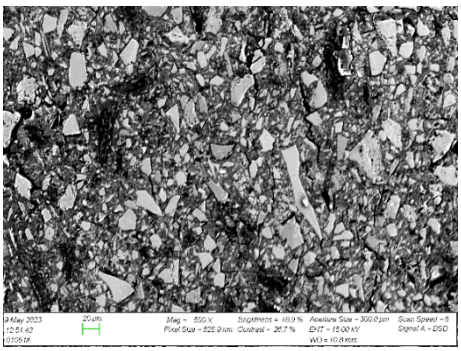

a) mainly geopolymer reactants after 7-day curing

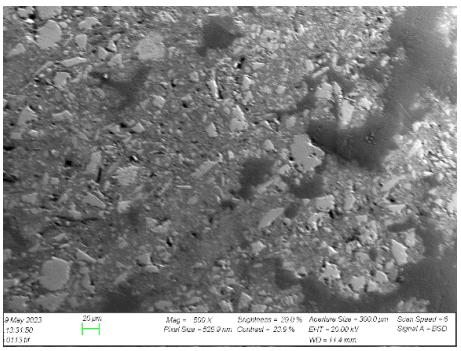

b) mainly geopolymer products after 28-day curing

c) gas breakthrough at the interface

Figure 37: a) SEM image of early-age JAW mix, b) SEM image of aged JAW mix, c) Top view of the sealability cell after gas breakthrough of the aged JAW. (Paper VII)

The reason behind this shrinkage could be a chemical shrinkage after the consumption of the aged JAW reactants during the geopolymerization reaction as shown in the SEM images in Figure 37.

As a result, it is necessary to have or consider utilizing an expansive agent for the JAW system to improve its long-term hydraulic sealability. In addition, further shrinkage quantification and evaluation tests are needed to study volume change of the geopolymers over a longer period.

6.4.3 Fourier Transform Infrared Spectroscopy (FTIR) and X-ray Diffraction (XRD)

FTIR and XRD were used and characterized to identify JAW`s functional groups and crystalline materials, respectively. Furtherly, they were integrated to confirm the geopolymerization products from JAW after 7-, 28- and 56-days of curing at 25 ℃ and 70 ℃, see Figures 38-40.

In the FTIR spectra, the T-O-T (T is a tetrahedral Si or Al) band position (in the range of 1400 – 700 cm^{-1}) could be an indication of aluminosilicate source dissolution, gelatinous product formations and/or degree of geopolymerization network crosslinking. This is a critical region of interest to identify chemical bonding and peak shifts for the geopolymer formulations. Hence, the O-C-O adsorption band (in the range of 1500 – 1400 cm^{-1}) is allocated to the calcium and/or carbonates groups' existence. Furthermore, the broad hump intensities (in the range of 3600-3000 cm^{-1} and 1700-1600 cm^{-1}) are correlated to the stretching vibrations of H-OH groups [47, 129].

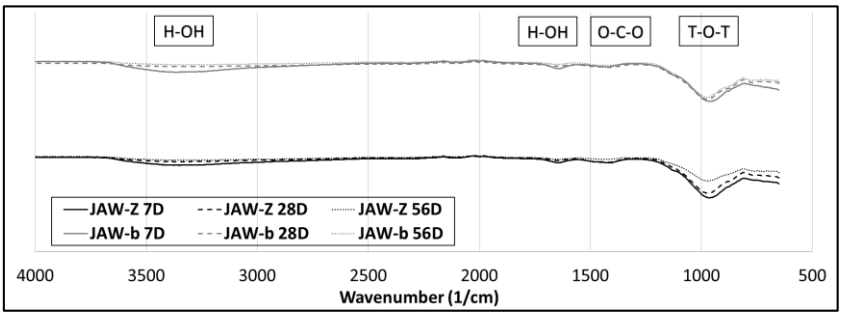

(a)

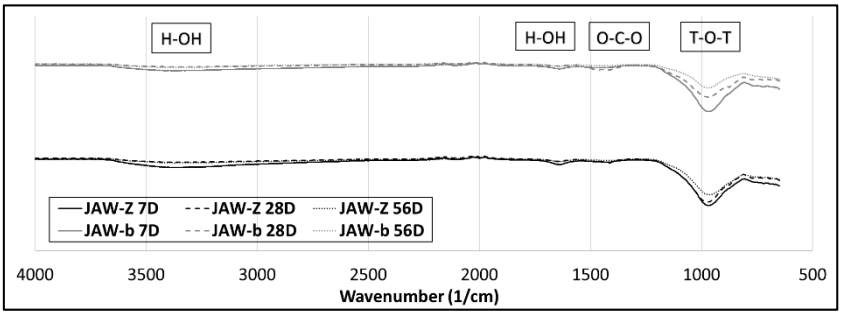

(b)

Figure 38: FTIR patterns of JAW-b and JAW-Z at 25 and 70 ℃. (Paper VII)

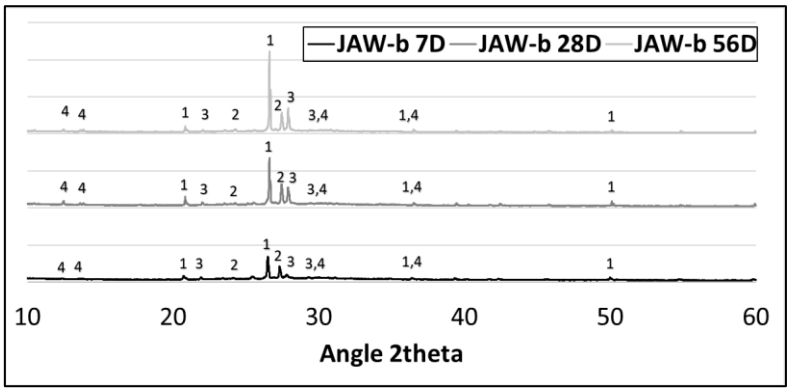

a) JAW-b at 25 ℃

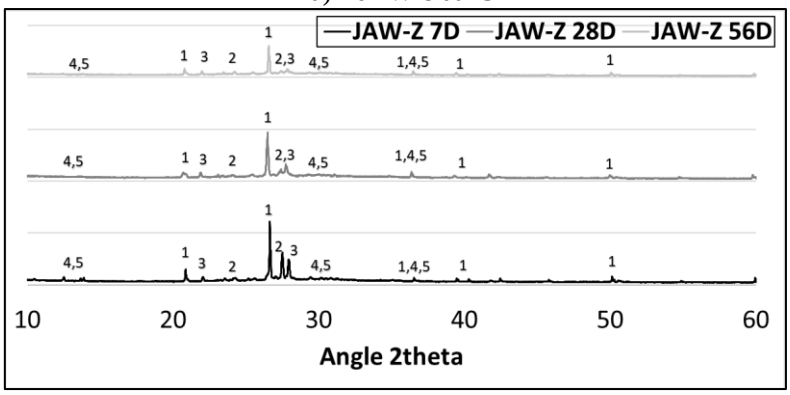

b) JAW-Z at 25 ℃

Figure 39: XRD patterns: a) JAW-b and b) JAW-Z, both cured at 25 ℃ BHST. 1: Quartz, 2: Microcline, 3: Albite, 4: Potassium containing species/crystals, 5: Zinc containing species/crystals. (Paper VII)

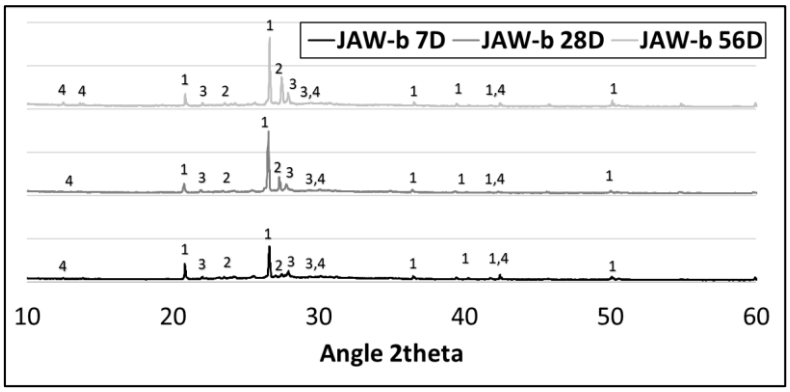

a) JAW-b at 70 ℃

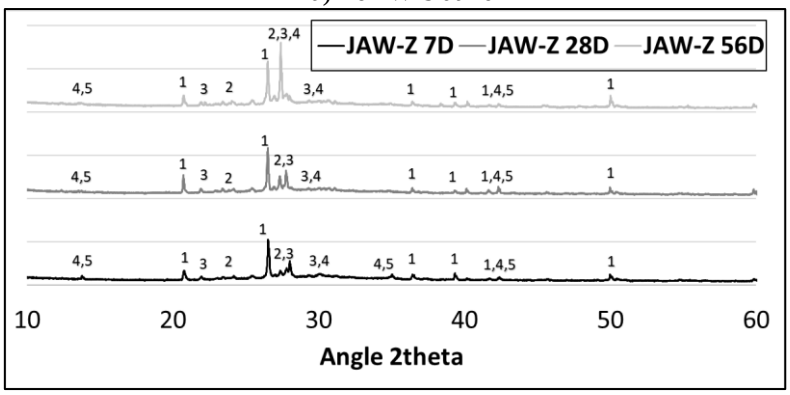

b) JAW-Z at 70 ℃

Figure 40: XRD patterns: a) JAW-b and b) JAW-Z, both cured at 70 ℃ BHST. 1: Quartz, 2: Microcline, 3: Albite, 4: Potassium containing species/crystals, 5: Zinc containing species/crystals. (Paper VII)

From FTIR spectra of the aged geopolymers, JAW spectra were affected and shifted by the ageing duration and curing temperature. At 25 ℃, there was a detectable shift in the wavelength of the T-O-T bands (between 1400 – 700 cm^{-1}) for both mixes from 962-966 cm^{-1} after 7-day to be centered around 975 cm^{-1} after 56-day of curing. This shift could be an indication of the aluminosilicate source dissolution (i.e., granite or activator) and formation of a higher crosslinking degree of geopolymers, CASH, NASH, and/or other aluminium silicate hydrates [46-47, 129]. Additionally, all T-O-T spectra bands hump were getting smaller in size with longer ageing, see Appendix 2; Figure 45. This could be due to the further dissolution and participation of granite or activator within the geopolymerization network. This observation is also in accordance with the presence of the second strength development regime for the aged JAW system.

On the other hand, the O-C-O adsorption band was negligible or undetectable for the given JAW mixes. This could be due to the low calcium content in the developed JAW mixes. Moreover, the concentration of ZnO was very low in the system, it did not give a detectable influence on FTIR spectra around 1100 – 1000 cm^{-1}.

In the case of the stretching vibrations of H-OH groups, both JAW mixes spectra were similar because of having comparable compositions and concentrations of the geopolymerization products. However, a higher wavelength shifting in their T-O-T and H-OH bands after ageing and curing at 70 ℃ was observed. Compliant with Shah et al. [130], these lateral shifts could be an indication of a higher degree of polymerization for the geopolymerization products at elevated curing temperatures. Thus, it is favourable for the JAW system to be aged and cured at elevated temperatures to achieve more geopolymerization products.

XRD patterns were also helpful in characterizing the effects of ageing and curing temperatures on the geopolymers. Both ageing and curing temperatures provided a detectable effect on the peaks` intensity of the

XRD patterns of the JAW system. The higher curing temperature with longer ageing duration gave higher and more crystalline XRD peak intensities. These observations match with other studies [46, 125, 131]. Additionally, they showed that alkali-activated materials with low calcium content have an overlapping of the natural (i.e., Quartz, Microcline & Albite) and synthesized potassium and zinc containing species and crystal structures in their XRD patterns.

Appendix 2 includes SEM micrographs that reveal the formation of geopolymerization products as a function of curing temperature for the aged JAW system. Elevated curing temperature accelerated the formation of denser structures. Moreover, longer ageing of JAW mixes also had a low presence of unreacted particles of the granite and GGBFS. This phenomenon is also in line with the FTIR and XRD data.

7. Summary & Conclusion

7.1 Summary

One-part granite-based geopolymers (JAW) mixes have been synthesised and then developed for well-cementing applications. JAW mixes were studied and developed under a wide range of curing durations and temperatures. They have been characterized chemically, physically, mechanically, rheologically, structurally, and morphologically.

It started with the synthesis and selection of an applicable neat one-part granite-based geopolymer recipe for well-cementing applications by screening and improving the early age performance. GGBFS and micro-silica were utilized as normalizers within the solid precursor. Their effect on fluid-state and solid-state properties such as precursors, slurry characterizations, mineralogy, morphology, compressive strength, sonic strength, and pumpability were characterized.

Afterwards, various chemical admixtures (including strength boosters and superplasticizers) and water concentrations were screened and then investigated to improve the early-age performance of the synthesized neat JAW under wellbore conditions.

Zinc Oxide (ZnO) as a strength booster showed the best early-age development performance on JAW to establish the so-called JAW-Z. Additionally, a Na-based lignosulfonate admixture was an effective superplasticizer for JAW-Z. Because of its positive early-age performance and strength development, JAW-Z has a promising potential to be utilized in well construction and well abandonment applications.

Consequently, further investigations were done on JAW-b (neat) and JAW-Z (developed JAW) to examine their durability including the effect of temperature and aging on the JAW system.

7.2 Conclusion

The main conclusion of this research can be summarized in the following points per each result and discussion subsection:

7.2.1 Normalization of Granite and Synthesis of the JAW Paste

- The utilized pure granite was considered as insufficient reactive in the geopolymer system, especially during the early-age performance.
- The low early strength of the granite-based geopolymer required modification with an amorphous phase containing cationic and silicate content such as GGBFS and microsilica.
- Partial replacement of granite with a cationic-rich source such as GGBFS is necessary to obtain a satisfactory reactive precursor system.
- This normalization helps to achieve acceptable early-age cementing properties.
- GGBFS-47% (neat, JAW-b) was considered a sweet spot for a neat one-part granite-based geopolymer mix design to be further developed.

7.2.2 Screening and Developing JAW

- The higher water content in the one-part granite-based geopolymer system negatively affected the early strength and setting time.
- Utilization of calcium-based admixtures can negatively impact on early strength of the geopolymers.
- ZnO was an effective early strength development booster.

- The top candidate recipes were having lower water content (0.33) and especially with lower concertation of ZnO chemical admixture than 1.14 wt%.
- ZnO might have a role in the polycondensation phase in the geopolymer system.

7.2.3 Short-term Characterization of the Developed JAW

- The addition of zinc oxide powder as a strength booster increases the rate of heat evolution and improves the early-age strength of the geopolymers.
- The higher the heat and energy evolution from the geopolymerization reaction, the higher the early strength.
- Utilization of zinc oxide decreases the silicate concentration and increases the aluminate content.
- Moreover, the addition of zinc oxide powder does not have any effect on the slurry properties nor show a retardation effect.

7.2.4 Preliminary Study on Aging of JAW

- The utilization of ZnO as a strength booster is very crucial to develop acceptable and durable mechanical properties for low-temperature well cementing applications.
- The longer the ageing duration, the denser, harder and then stronger the JAW matrix becomes.
- Late dissolution of the granite after two weeks of ageing and then its participation in the long-term strength development was experienced.
- Heat curing favours the geopolymerization reaction resulting in a reduction of unreacted precursor particles.

- Heat curing improves long-term strength development and helps in the formation of denser structures and higher crystalline products.
- The geopolymers shrink and this is intensified with curing time.

8. Recommendations

The granite-based JAW showed a positive potential as a replacement for cement in well-cementing applications to provide environmentally- and user-friendly cementitious material. Nevertheless, more investigations and studies are still needed to fully understand the complexity behind the JAW system.

It would be interesting to further consider and study the following:

- Thermal and mechanical activation of granite and investigating its particle size distribution (PSD).
- Development of a numerical microstructure simulation to predict any possible reactions and calculate stable phases of the products from the geopolymerization reaction to properly design/optimize JAW.
- Investigating the applicability of JAW for CCS applications.
- Investigating various expansive agents to avoid chemical shrinkage and to ensure JAW`s aging durability.
- Investigating the effect of inorganic and organic retarders on JAW to control its pumpability, especially at elevated temperatures.
- Investigating the utilization of seawater for the JAW system.
- Optimization of the JAW system towards more viable and sustainable development to be cheaper than OPC.

9. Reference

1- Wang, Y., & Salehi, S. (2015). Application of real-time field data to optimize drilling hydraulics using neural network approach. Journal of Energy Resources Technology, 137(6). https://doi.org/10.1115/1.4030847

2- Salehi, S., & Kiran, R. (2016). Integrated experimental and analytical wellbore strengthening solutions by mud plastering effects. Journal of Energy Resources Technology, 138(3). https://doi.org/10.1115/1.4032236

3- Salehi, S., Khattak, M. J., Ali, N., Ezeakacha, C., & Saleh, F. K. (2017). Study and use of geopolymer mixtures for oil and gas well cementing applications. Journal of Energy Resources Technology, 140(1). https://doi.org/10.1115/1.4037713

4- Kamali, M. (2022). Materials for Well Integrity: Performance of Setting Materials for Well Cementing. University of Stavanger, 2022 (PhD thesis UiS, no. 642)

5- Chamssine, F. (2023). Instituting Retarders for Geopolymers Developed for Downhole Applications. University of Stavanger, 2023 (PhD thesis UiS)

6- Sabins, F. L. (1990). Problems in Cementing Horizontal Wells. Journal of Petroleum Technology, 42(04), 398–400. https://doi.org/10.2118/20005-pa

7- Sweatman, R. (2000). Overview: Cementing technology. Journal of Petroleum Technology, 52(08), 22–22. https://doi.org/10.2118/0800-0022-jpt

8- Cowan, M. (2007). Field study results improve squeeze-cementing success. All Days. https://doi.org/10.2118/106765-ms

9- Dahi Taleghani, A., Li, G., & Moayeri, M. (2017). Smart expandable cement additive to achieve better wellbore integrity. Journal of Energy Resources Technology, 139(6). https://doi.org/10.1115/1.4036963

10- Nelson, E.B., & Guillot, D. (2006). Well Cementing, 2nd ed. Schlumberger.
11- Khalifeh, M., & Saasen, A. (2020). Introduction to Permanent Plug and Abandonment of Wells, Ocean Engineering & Oceanography. Springer International Publishing, Cham, Switzerland. https://doi.org/10.1007/978-3-030-39970-2
12- NORSOK-D-010 (2013). Well integrity in drilling and well operations. Standard Norway.
13- Oil & Gas UK (2015). Guidelines on Qualification of Materials for the Abandonment of Wells-Issue 2, OIL & GAS UK, London.
14- American Petroleum Institute, A. (2010). API Spec 10A, Specification for Cements and Materials for Well Cementing. Washington DC: API.
15- American Petroleum Institute, A. (2019). API RP 10B-2, Recommended Practice for Testing Well Cements. Washington DC: API.
16- American Petroleum Institute, A. (2017). API TR 10TR7. Mechanical Behavior of Cement. Washington DC: API.
17- Hewlett, P., C. (2001). Lea's Chemistry of Cement and Concrete. 4th ed. Butterworth-Heinemann, Oxford, UK.
18- Taylor, H., F., W. (1997). Cement Chemistry. 2nd ed. Thomas Telford Publishing.
19- Deshpande, A., Chiney, A., Patil, S., Paiva, M., D., M., Ravi, K., Aiex, C., Campos, G. (2015). Long-Term Study of Effects of CO2 Exposure on Cement Integrity Under Downhole Conditions. SPE. https://doi.org/10.2118/174329-MS
20- Simão, C., A., Folsta, M., G., Campos, G., Yerubandi, K., B., Patil, S., Jandhyala, S., R., K., Deshpande, A., Paiva, M., & Ravi, K. (2016). Cementing Solutions for Salt- and CO2-Laden Presalt Zones. SPE Deepwater Drilling and Completions Conference. Society of Petroleum Engineers. https://doi.org/10.2118/180336-MS

21- Bergen, S., L., Zemberekci, L., & Nair, S., D. (2022). A review of conventional and alternative cementitious materials for geothermal wells. Renewable and Sustainable Energy Reviews. https://doi.org/10.1016/j.rser.2022.112347
22- Andrew, R., M. (2019). Global CO2 emissions from cement production, 1928–2018. Earth Syst Sci Data 11, 1675–1710. https://doi.org/10.5194/essd-11-1675-2019
23- Damtoft, J., S., Lukasik, J., Herfort, D., Sorrentino, D., & Gartner, E., M. (2008). Sustainable development and climate change initiatives. Cem Concr Res 38, 115–127. https://doi.org/10.1016/j.cemconres.2007.09.008
24- IEA (2021). Net Zero by 2050 - A Roadmap for the Global Energy Sector.
25- Fantilli, A., Mancinelli, O., & Chiaia, B. (2019). The carbon footprint of normal and high-strength concrete used in low-rise and high-rise buildings. Case Studies in Construction Materials, 11: e00296.
26- Khalifeh, M. (2016). Materials for optimized P&A performance: Potential utilization of geopolymers. University of Stavanger, 2016 (PhD thesis UiS, no. 292)
27- Provis, J. L., & Bernal, S. A. (2014). Geopolymers and related alkali-activated materials. Annual Review of Materials Research, 44(1), 299–327. https://doi.org/10.1146/annurev-matsci-070813-113515
28- Yousefi Oderji, S., Chen, B., Ahmad, M. R., & Shah, S. F. (2019). Fresh and hardened properties of one-part fly ash-based geopolymer binders cured at room temperature: Effect of slag and alkali activators. Journal of Cleaner Production, 225, 1–10. https://doi.org/10.1016/j.jclepro.2019.03.290
29- Nodehi, M., & Taghvaee, V. M. (2021). Alkali-activated materials and geopolymer: A review of common precursors and activators addressing circular economy. Circular Economy and

Sustainability, 2(1), 165–196. https://doi.org/10.1007/s43615-021-00029-w

30- Provis, J. L. (2013). Geopolymers and other alkali activated materials: Why, how, and what? Materials and Structures, 47(1–2), 11–25. https://doi.org/10.1617/s11527-013-0211-5

31- Flatt, R., J., Roussel, N., & Cheeseman, C., R. (2012). Concrete: An eco material that needs to be improved. J Eur Ceram Soc 32, 2787–2798. https://doi.org/10.1016/j.jeurceramsoc.2011.11.012

32- McLellan, B., C., Williams, R., P., Lay, J., van Riessen, A., & Corder, G., D. (2011). Costs and carbon emissions for geopolymer pastes in comparison to ordinary portland cement. J Clean Prod 19, 1080–1090. https://doi.org/10.1016/j.jclepro.2011.02.010

33- Pacheco-Torgal, F., Labrincha, J., Leonelli, C., Palomo, A., & Chindaprasit, P. (2014). Handbook of Alkali-activated Cements, Mortars and Concretes. Woodhead Publishing.

34- Salehi, S., Khattak, J., Saleh, F., K., Igbojekwe, S. (2019). Investigation of mix design and properties of geopolymers for application as wellbore cement. J Pet Sci Eng 178, 133–139. https://doi.org/10.1016/j.petrol.2019.03.031

35- Salehi, S., Khattak, M., J., Ali, N., Ezeakacha, C., Saleh, F., K. (2018). Study and Use of Geopolymer Mixtures for Oil and Gas Well Cementing Applications. J Energy Resour Technol 140, 1–12. https://doi.org/10.1115/1.4037713

36- Krishna, R., S., Mishra, J., Zribi, M., Adeniyi, F., Saha, S., Baklouti, S., Shaikh, F., U., A., Gökçe, H., S. (2021). A review on developments of environmentally friendly geopolymer technology. Materialia (Oxf) 20, 101212. https://doi.org/10.1016/j.mtla.2021.101212

37- Alvi, M., A., A., Khalifeh, M., Agonafir, M., B. (2020). Effect of nanoparticles on properties of geopolymers designed for well cementing applications. J Pet Sci Eng 191, 107128. https://doi.org/10.1016/j.petrol.2020.107128

38- Khalifeh, M., Saasen, A., Larsen, H. B., & Hodne, H. (2017). Development and characterization of norite-based cementitious binder from an ilmenite mine waste stream. Advances in Materials Science and Engineering, 2017, 1–7. https://doi.org/10.1155/2017/6849139

39- Khalifeh, M., Saasen, A., Vrålstad, T., Larsen, H. B., & Hodne, H. (2015). Experimental study on the synthesis and characterization of aplite rock-based geopolymers. Journal of Sustainable Cement-Based Materials, 5(4), 233–246. https://doi.org/10.1080/21650373.2015.1044049

40- Shilar, F. A., Ganachari, S. V., & Patil, V. B. (2022). Investigation of the effect of granite waste powder as a binder for different molarity of geopolymer concrete on fresh and mechanical properties. Materials Letters, 309, 131302. https://doi.org/10.1016/j.matlet.2021.131302

41- Barlet-Gouedard, V., Zusatz-Ayache, B., Porcherie, O. (2008). Pumpable geopolymer Formulation for Oilfield Application. WO 2008/017414 A1.

42- Mahmoudkhani, A., H., Huynh, D., N., T., Sylvestre, C., & Schneider, J. (2008). New Environment-Friendly Cement Slurries With Enhanced Mechanical Properties, in: All Days. SPE. https://doi.org/10.2118/115004-MS

43- Wan-En, O., Yun-Ming, L., Cheng-Yong, H., Ho, L., N., al Bakri Abdullah, M., M., bin Khalid, M., S., Foo, K., L., Ong, S.-W., Tan, P., S., Hang, Y., J., & Zulkifly, K. (2022). Towards greener one-part geopolymers through solid sodium activators modification. J Clean Prod 134370. https://doi.org/10.1016/j.jclepro.2022.134370

44- Omran, M., & Khalifeh, M. (2022). Development of Low Carbon Dioxide Intensive Rock-Based Geopolymers for Well Cementing Applications – One-Part Geopolymer, in: Volume 10: Petroleum Technology. American Society of Mechanical Engineers, Hamburg, Germany. https://doi.org/10.1115/OMAE2022-78535

45- Omran, M., & Khalifeh, M. (2023). Development of one-part rock-based Geopolymers for downhole cementing applications. Journal of Energy Resources Technology, 145(10). https://doi.org/10.1115/1.4062250
46- Hajimohammadi, A., Provis, J. L., & van Deventer, J. S. (2008). One-part geopolymer mixes from geothermal silica and sodium aluminate. Industrial & Engineering Chemistry Research, 47(23), 9396–9405. https://doi.org/10.1021/ie8006825
47- Ma, C., Long, G., Shi, Y., & Xie, Y. (2018). Preparation of cleaner one-part geopolymer by investigating different types of commercial sodium metasilicate in China. Journal of Cleaner Production, 201, 636–647. https://doi.org/10.1016/j.jclepro.2018.08.060
48- Ke, X., Bernal, S. A., Ye, N., Provis, J. L., & Yang, J. (2014). One-part geopolymers based on thermally treated Red Mud/NaOH blends. Journal of the American Ceramic Society, 98(1), 5–11. https://doi.org/10.1111/jace.13231
49- Hajimohammadi, A., & van Deventer, J. S. (2016). Characterisation of one-part geopolymer binders made from Fly Ash. *Waste and Biomass Valorization*, *8*(1), 225–233. https://doi.org/10.1007/s12649-016-9582-5
50- Hajimohammadi, A., Provis, J. L., & van Deventer, J. S. J. (2011). Time-resolved and spatially-resolved infrared spectroscopic observation of seeded nucleation controlling geopolymer gel formation. Journal of Colloid and Interface Science, 357(2), 384–392. https://doi.org/10.1016/j.jcis.2011.02.045
51- Davidovits, J. (2017). Geopolymers: Ceramic-like inorganic polymers. Journal of Ceramic Science and Technology 8, 335–350. https://doi.org/10.4416/JCST2017-00038
52- Davidovits, J. (2013). Geopolymer Cement a review. Institut Geopolymer 1–11.
53- Davidovits, J. (2008). Geopolymer: Chemistry & Applications.

54- Davidovits, J. (1991). Geopolymers: Inorganic polymeric new materials. Journal of Thermal Analysis 37, 1633–1656. https://doi.org/10.1007/BF01912193

55- Pacheco-Torgal, F., Castro-Gomes, J., & Jalali, S. (2008). Alkali-activated binders: A review. Part 1. Historical background, terminology, reaction mechanisms and hydration products. Constr Build Mater 22, 1305–1314. https://doi.org/10.1016/j.conbuildmat.2007.10.015

56- Komnitsas, K. A. (2011). Potential of geopolymer technology towards Green Buildings and Sustainable Cities. Procedia Engineering, 21, 1023–1032. https://doi.org/10.1016/j.proeng.2011.11.2108

57- Park, S., & Pour-Ghaz, M. (2018). What is the role of water in the geopolymerization of Metakaolin? Construction and Building Materials, 182, 360–370. https://doi.org/10.1016/j.conbuildmat.2018.06.073

58- Gislason, S. R., & Oelkers, E. H. (2003). Mechanism, rates, and consequences of basaltic glass dissolution: II. an experimental study of the dissolution rates of basaltic glass as a function of ph and temperature. Geochimica Et Cosmochimica Acta, 67(20), 3817–3832. https://doi.org/10.1016/s0016-7037(03)00176-5

59- Oelkers, E. H., Schott, J., & Devidal, J.-L. (1994). The effect of aluminum, ph, and chemical affinity on the rates of aluminosilicate dissolution reactions. Geochimica Et Cosmochimica Acta, 58(9), 2011–2024. https://doi.org/10.1016/0016-7037(94)90281-x

60- Duxson, P., & Provis, J. L. (2008). Designing precursors for Geopolymer cements. Journal of the American Ceramic Society, 91(12), 3864–3869. https://doi.org/10.1111/j.1551-2916.2008.02787.x

61- Oelkers, E. H., & Gislason, S. R. (2001). The mechanism, rates and consequences of basaltic glass dissolution: I. an experimental study of the dissolution rates of basaltic glass as a function of

aqueous al, si and oxalic acid concentration at 25°C and ph = 3 and 11. Geochimica Et Cosmochimica Acta, 65(21), 3671–3681. https://doi.org/10.1016/s0016-7037(01)00664-0

62- Rees, C. A., Provis, J. L., Lukey, G. C., & van Deventer, J. S. J. (2008). The mechanism of geopolymer gel formation investigated through seeded nucleation. Colloids and Surfaces A: Physicochemical and Engineering Aspects, 318(1-3), 97–105. https://doi.org/10.1016/j.colsurfa.2007.12.019

63- Weng, L., & Sagoe-Crentsil, K. (2007). Dissolution processes, hydrolysis and condensation reactions during geopolymer synthesis: Part I—low si/al ratio systems. Journal of Materials Science, 42(9), 2997–3006. https://doi.org/10.1007/s10853-006-0820-2

64- Sagoe-Crentsil, K., & Weng, L. (2006). Dissolution processes, hydrolysis and condensation reactions during geopolymer synthesis: Part II. High Si/Al Ratio Systems. Journal of Materials Science, 42(9), 3007–3014. https://doi.org/10.1007/s10853-006-0818-9

65- Shi, C. (1997). Early hydration and microstructure development of alkali-activated slag cement pastes, Proceedings of the 10th International Congress on the Chemistry of Cement, Gothenburg, Sweden, 1997, pp. 3ii099.

66- Gruskovnjak, A., Lothenbach, B., Holzer, L., Figi, R., & Winnefeld, F. (2006). Hydration of alkali-activated slag: Comparison with ordinary Portland Cement. Advances in Cement Research, 18(3), 119–128. https://doi.org/10.1680/adcr.2006.18.3.119

67- Swaddle, T. (2001). Silicate complexes of aluminum(iii) in aqueous systems. Coordination Chemistry Reviews, 219-221, 665–686. https://doi.org/10.1016/s0010-8545(01)00362-9

68- Duxson, P., Provis, J. L., Lukey, G. C., Mallicoat, S. W., Kriven, W. M., & van Deventer, J. S. J. (2005). Understanding the relationship between geopolymer composition, microstructure

and mechanical properties. Colloids and Surfaces A: Physicochemical and Engineering Aspects, 269(1-3), 47–58. https://doi.org/10.1016/j.colsurfa.2005.06.060

69- Ma, C., Long, G., Shi, Y., & Xie, Y. (2018). Preparation of cleaner one-part geopolymer by investigating different types of commercial sodium metasilicate in China. Journal of Cleaner Production, 201, 636–647. https://doi.org/10.1016/j.jclepro.2018.08.060

70- Ma, C., Zhao, B., Guo, S., Long, G., & Xie, Y. (2019). Properties and characterization of green one-part geopolymer activated by composite activators. Journal of Cleaner Production, 220, 188–199. https://doi.org/10.1016/j.jclepro.2019.02.159

71- Zuo, Y., & Ye, G. (2021). GeoMicro3D: A novel numerical model for simulating the reaction process and microstructure formation of alkali-activated slag. Cement and Concrete Research, 141, 106328. https://doi.org/10.1016/j.cemconres.2020.106328

72- Zuo, Y. (2019). Experimental Study and Numerical Simulation of the Reaction Process and Microstructure Formation of Alkali-Activated Materials. (1 ed.). Delft University of Technology. https://doi.org/10.4233/uuid:193a4016-5fc7-401b-babe-722ff6a95a6c

73- Deir, E., Gebregziabiher, B. S., & Peethamparan, S. (2014). Influence of starting material on the early age hydration kinetics, microstructure and composition of binding gel in alkali activated binder systems. Cement and Concrete Composites, 48, 108–117. https://doi.org/10.1016/j.cemconcomp.2013.11.010

74- Chithiraputhiran, S., & Neithalath, N. (2013). Isothermal reaction kinetics and temperature dependence of alkali activation of slag, fly ash and their blends. Construction and Building Materials, 45, 233–242. https://doi.org/10.1016/j.conbuildmat.2013.03.061

75- Cai, J., Li, X., Tan, J., & Vandevyvere, B. (2020). Thermal and compressive behaviors of fly ash and Metakaolin-based

geopolymer. Journal of Building Engineering, 30, 101307. https://doi.org/10.1016/j.jobe.2020.101307

76- Gao, X., Yu, Q. L., & Brouwers, H. J. H. (2015). Reaction kinetics, gel character and strength of ambient temperature cured alkali activated slag–fly ash blends. Construction and Building Materials, 80, 105–115. https://doi.org/10.1016/j.conbuildmat.2015.01.065

77- Provis, J. L., & Bernal, S. A. (2014). Geopolymers and related alkali-activated materials. Annual Review of Materials Research, 44(1), 299–327. https://doi.org/10.1146/annurev-matsci-070813-113515

78- Fernández-Jiménez, A., & Palomo, A. (2005). Composition and microstructure of alkali activated fly ash binder: Effect of the activator. Cement and Concrete Research, 35(10), 1984–1992. https://doi.org/10.1016/j.cemconres.2005.03.003

79- Rowles, M. R., & O'Connor, B. H. (2009). Chemical and structural microanalysis of aluminosilicate Geopolymers synthesized by sodium silicate activation of Metakaolinite. Journal of the American Ceramic Society, 92(10), 2354–2361. https://doi.org/10.1111/j.1551-2916.2009.03191.x

80- Ranjbar, N., Kuenzel, C., Spangenberg, J., & Mehrali, M. (2020). Hardening evolution of geopolymers from setting to equilibrium: A Review. Cement and Concrete Composites, 114, 103729. https://doi.org/10.1016/j.cemconcomp.2020.103729

81- Fernández-Jiménez, A., Palomo, A., Sobrados, I., & Sanz, J. (2006). The role played by the reactive alumina content in the alkaline activation of Fly Ashes. Microporous and Mesoporous Materials, 91(1-3), 111–119. https://doi.org/10.1016/j.micromeso.2005.11.015

82- Duxson, P., Fernández-Jiménez, A., Provis, J. L., Lukey, G. C., Palomo, A., & van Deventer, J. S. (2006). Geopolymer technology: The current state of the art. Journal of Materials

Science, 42(9), 2917–2933. https://doi.org/10.1007/s10853-006-0637-z

83- White, C. E., Provis, J. L., Proffen, T., & Van Deventer, J. S. (2010). The effects of temperature on the local structure of Metakaolin-based geopolymer binder: A neutron pair distribution function investigation. Journal of the American Ceramic Society, 93(10), 3486–3492. https://doi.org/10.1111/j.1551-2916.2010.03906.x

84- Puligilla, S., & Mondal, P. (2015). Co-existence of aluminosilicate and calcium silicate gel characterized through selective dissolution and FTIR spectral subtraction. Cement and Concrete Research, 70, 39–49. https://doi.org/10.1016/j.cemconres.2015.01.006

85- Ismail, I., Bernal, S. A., Provis, J. L., San Nicolas, R., Hamdan, S., & van Deventer, J. S. J. (2014). Modification of phase evolution in alkali-activated blast furnace slag by the incorporation of Fly Ash. Cement and Concrete Composites, 45, 125–135. https://doi.org/10.1016/j.cemconcomp.2013.09.006

86- Myers, J. S., & Watkins, K. P. (1985). Origin of granite-greenstone patterns, Yilgarn Block, Western Australia. Geology, 13(11), 778. https://doi.org/10.1130/0091-7613(1985)13<778:oogpyb>2.0.co;2

87- Shang, X., Zhang, Z., Xu, X., Liu, T., & Xing, Y. (2019). Mineral composition, pore structure, and mechanical characteristics of pyroxene granite exposed to heat treatments. Minerals, 9(9), 553.

88- Clemens, J. D., Holloway, J. R., & White, A. J. R. (1986). Origin of an A-type granite; experimental constraints. American Mineralogist, 71(3-4), 317-324.

89- Whalen, J. B., Currie, K. L., & Chappell, B. W. (1987). A-type granites: geochemical characteristics, discrimination and petrogenesis. Contributions to mineralogy and petrology, 95(4), 407-419.

90- Chappell, B. W., & Stephens, W. E. (1988). Origin of infracrustal (I-type) granite magmas. Earth and Environmental

Science Transactions of the Royal Society of Edinburgh, 79(2-3), 71-86.

91- Castro, A., Moreno-Ventas, I., & De La Rosa, J. D. (1991). H-type (hybrid) granitoids: a proposed revision of the granite-type classification and nomenclature. Earth-science reviews, 31(3-4), 237-253.

92- Rosing-Schow, N., Andersen, T., & Müller, A. (2022). Lead Isotopes and the Sources of Granitic Magmas: The Sveconorwegian Granite and Pegmatite Province of Southern Norway. Minerals, 12(7), 878.

93- Heldal, T. & Neeb, P. R. (2000). Natural stone in Norway: production, deposits and developments. Norges geologiske. undersøkelse Bulletin 436, 15-26.

94- Geological Survey of Norway, NGU (2022). ANALYSERESULTATER FOR PUKKOMRÅDE, Pukkdatabasen: Velde pukkverk. Sandnes, Rogaland.

95- Kovler. (2012). 8 - Radioactive materials. In Toxicity of building materials (pp. 196–240). essay, Woodhead Publishing.

96- Shilar, F. A., Ganachari, S. V., Patil, V. B., Nisar, K. S., Abdel-Aty, A. H., & Yahia, I. S. (2022). Evaluation of the Effect of Granite Waste Powder by Varying the Molarity of Activator on the Mechanical Properties of Ground Granulated Blast-Furnace Slag-Based Geopolymer Concrete. Polymers, 14(2), 306.

97- Nath, P., & Sarker, P. K. (2014). Effect of GGBFS on setting, workability and early strength properties of fly ash geopolymer concrete cured in ambient condition. Construction and Building materials, 66, 163-171.

98- Aliabdo, A., Elmoaty, M., & Salem, H. (2016). Effect of cement addition, solution resting time and curing characteristics on fly ash based geopolymer concrete performance. Journal of Canadian Petroleum Technology 123: 581—593.

99- Saha, S., & Rajasekaran, C. (2017). Enhancement of the properties of fly ash based geopolymer paste by incorporating ground granulated blast furnace slag. Journal of Construction and Building Material 146: 615—620.

100- Luukkonen, T., Abdollahnejad, Z., & Yliniemi, J. (2018). One-part alkali-activated materials: A review. Cement and Concrete Research 103: 21—34.

101- Sasaki, K., Kurumisawa, K., & Ibayashi, K. (2019). Effect of retarders on flow and strength development of alkali-activated fly ash/blast furnace slag composite," Construction and building materials, vol. 216, pp. 337-346, 2019.

102- Mahya, A., Zhong, T., & Bijan, S. (2019). Mix composition and characterization of one-part geopolymer with different activators. Journal of Construction and Building Materials 225: 526—537.

103- Jingming, C., Xiaopeng, L., & Jiawei, T. (2020). Thermal and compressive behaviors of fly ash and metakaolin-based geopolymer. Journal of Building Engineering 30 (101307).

104- Singh, N. B. & Middendorf, B. (2020). Geopolymers as an alternative to Portland cement: An overview. Construction and Building Materials 237 (117455).

105- Omran, M., Hjelm, S., Khalifeh, M., & Salehi, S. (2023). Synthesis of sustainable one-part geopolymers for well cementing applications. Geoenergy Science and Engineering, 211822. https://doi.org/10.1016/j.geoen.2023.211822

106- Omran, M., Paiva, M. & Khalifeh, M. (2023). Design and Early Age Performance of Sustainable One-part Geopolymers for Well Cementing. SPE Journal (SPE-215825-PA).

107- Onutai, S., Jiemsirilers, S., Thavorniti, P., & Kobayashi, T. (2015). Aluminium hydroxide waste based geopolymer composed of fly ash for Sustainable Cement Materials. Construction and Building Materials, 101, 298–308. https://doi.org/10.1016/j.conbuildmat.2015.10.097

108- Omran, M., Khalifeh, M., & Saasen, A. (2022). Influence of Activators and Admixtures on Rheology of Geopolymer Slurries for Well Cementing Applications. SPE-210698-MS, Presented at the SPE Asia Pacific Oil & Gas Conference and

Exhibition 2022, Adelaide, Australia, 17 - 19 Oct 2022. https://doi.org/10.2118/210698-MS

109- Hjelm, S. (2022). Revealing the Effect of Superplasticizers on Viscosity and Yield Stress of Geopolymers. Bachelor project a Dept. of Energy and Petroleum Eng., University of Stavanger, Spring 2022.

110- Oderji, S. Y., Chen, B., Shakya, C., Ahmad, M. R., & Shah, S. F. (2019). Influence of superplasticizers and retarders on the workability and strength of one-part alkali-activated fly ash/slag binders cured at room temperature. Construction and Building Materials, 229, 116891. https://doi.org/10.1016/j.conbuildmat.2019.116891

111- Bacarji, E., Toledo Filho, R. D., Koenders, E. A. B., Figueiredo, E. P., & Lopes, J. L. M. P. (2013). Sustainability perspective of marble and granite residues as concrete fillers. Construction and Building materials, 45, 1-10.

112- Vijayalakshmi, M., & Sekar, A. S. S. (2013). Strength and durability properties of concrete made with granite industry waste. Construction and Building Materials, 46, 1-7.

113- Jain, K. L., Sancheti, G., & Gupta, L. K. (2020). Durability performance of waste granite and glass powder added concrete. Construction and Building Materials, 252, 119075.

114- Coppola, B., Tulliani, J. M., Antonaci, P., & Palmero, P. (2020). Role of natural stone wastes and minerals in the alkali activation process: A review. Materials, 13(10), 2284.

115- Khalifeh, M., Saasen, A., Hodne, H., & Motra, H. B. (2019). Laboratory evaluation of rock-based geopolymers for zonal isolation and permanent P&A applications. Journal of Petroleum Science and Engineering, 175, 352–362. https://doi.org/10.1016/j.petrol.2018.12.065

116- Khalifeh, M., Hodne, H., Saasen, A., Integrity, O., & Eduok, E. I. (2016). Usability of geopolymers for oil well cementing applications: Reaction mechanisms, pumpability, and

properties. SPE Asia Pacific Oil & Gas Conference and Exhibition. https://doi.org/10.2118/182354-ms

117- Khalifeh, M., Todorovic, J., Vrålstad, T., Saasen, A., & Hodne, H. (2016). The long-term durability of rock-based geopolymers aged at downhole conditions for oil well cementing operations. Journal of Sustainable Cement-Based Materials, 6(4), 217–230. https://doi.org/10.1080/21650373.2016.1196466

118- Khalifeh, M., Motra, H. B., Saasen, A., & Hodne, H. (2018). Potential utilization for a rock-based geopolymer in oil well cementing. Volume 8: Polar and Arctic Sciences and Technology; Petroleum Technology. https://doi.org/10.1115/omae2018-78305

119- Lea, F. M., Hewlett, P. C., & Liska, M. (2019). Lea's chemistry of cement and concrete. Butterworth-Heinemann.

120- Saasen, A., Salmelid, B., Blomberg, N., Hansen, K., Young, S. P., & Justnes, H. (1994). The use of blast furnace slag in North Sea Cementing applications. All Days. https://doi.org/10.2118/28821-ms

121- Li, S., Feng, Y., & Yang, J. (2021). Expansion mechanism and properties of magnesium oxide expansive hydraulic cement for engineering applications. Advances in Materials Science and Engineering, 2021, 1–9. https://doi.org/10.1155/2021/5542072

122- Yoder, Jr., H. (1992). Norman L. Bowen (1887-1956), MIT class of 1912, first Predoctoral fellow of the Geophysical Laboratory. Earth Sciences History, 11(1), 45–55. https://doi.org/10.17704/eshi.11.1.u8w2610560328526

123- Zailan, S. N., Bouaissi, A., Mahmed, N., & Abdullah, M. M. (2019). Influence of zno nanoparticles on mechanical properties and photocatalytic activity of self-cleaning zno-based geopolymer paste. Journal of Inorganic and Organometallic Polymers and Materials, 30(6), 2007–2016. https://doi.org/10.1007/s10904-019-01399-3

124- Nivethitha, D., & Dharmar, S. (2016). Influence of zinc oxide nanoparticle on strength and durability of cement mortar. Int. J. Earth Sci. Eng. 9(3), 175–181 (2016).

125- Pilehvar, S., Sanfelix, S. G., Szczotok, A. M., Rodríguez, J. F., Valentini, L., Lanzón, M., Pamies, R., & Kjøniksen, A.-L. (2020). Effect of temperature on geopolymer and Portland cement composites modified with micro-encapsulated phase change materials. Construction and Building Materials, 252, 119055. https://doi.org/10.1016/j.conbuildmat.2020.119055

126- Siyal, A. A., Azizli, K. A., Man, Z., & Ullah, H. (2016). Effects of parameters on the setting time of Fly Ash based Geopolymers using Taguchi method. Procedia Engineering, 148, 302–307. https://doi.org/10.1016/j.proeng.2016.06.624

127- Chen, A. L., Xu, D., Chen, X. Y., Zhang, W.Y., & Liu, X. H. (2012). Measurements of zinc oxide solubility in sodium hydroxide solution from 25 to 100 °c. Transactions of Nonferrous Metals Society of China (English Edition) 22, 1513–1516. https://doi.org/10.1016/S1003-6326(11)61349-6

128- Gomado, F. D., Khalifeh, M., & Aasen, J. A. (2023). Expandable geopolymers for improved zonal isolation and plugging. SPE/IADC International Drilling Conference and Exhibition, Day 3 Thu, March 09, 2023. https://doi.org/10.2118/212493-ms

129- Ma, C., Zhao, B., Guo, S., Long, G., & Xie, Y. (2019). Properties and characterization of green one-part geopolymer activated by composite activators. Journal of Cleaner Production, 220, 188–199. https://doi.org/10.1016/j.jclepro.2019.02.159

130- Shah, S. F., Chen, B., Oderji, S. Y., Haque, M. A., & Ahmad, M. R. (2020). Improvement of early strength of fly ash-slag based one-part alkali activated mortar. Construction and Building Materials, 246, 118533. https://doi.org/10.1016/j.conbuildmat.2020.118533

131- Samantasinghar, S., & Singh, S. P. (2019). Fresh and hardened properties of fly ash–slag blended geopolymer paste

and mortar. International Journal of Concrete Structures and Materials, 13(1). https://doi.org/10.1186/s40069-019-0360-1

132- Zhang, B., Zhu, H., Feng, P., & Zhang, P. (2022b). A review on shrinkage-reducing methods and mechanisms of alkali-activated/geopolymer systems: Effects of Chemical Additives. Journal of Building Engineering, 49, 104056. https://doi.org/10.1016/j.jobe.2022.104056

10. Appendices

Appendix 1 – Extended UCA & UCS Profiles

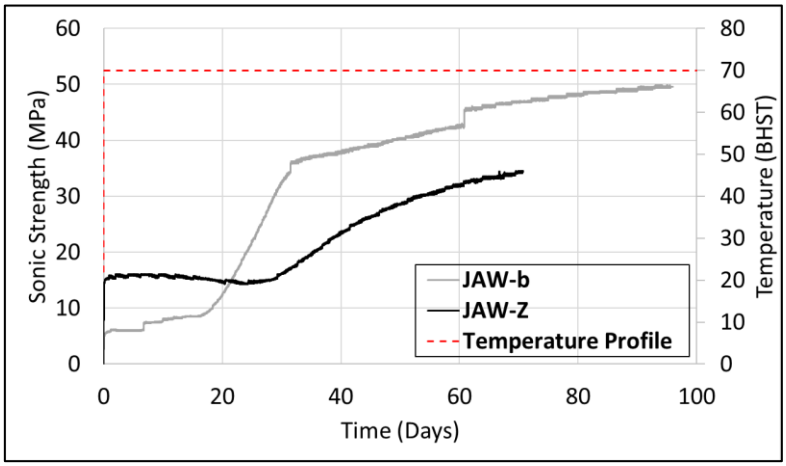

Figure 41: Extended UCA data for JAW-b vs JAW-Z.

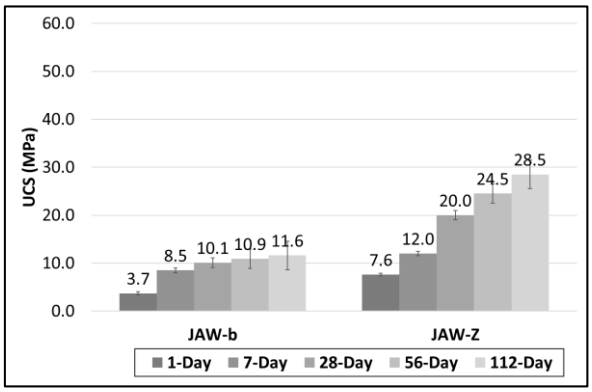

a) UCS of 25 °C BHST cured samples

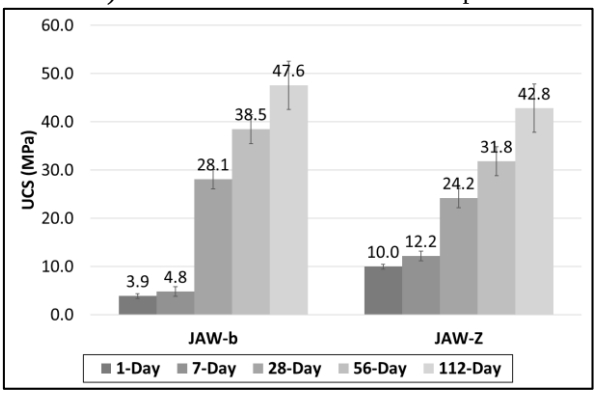

b) UCS of 70 °C BHST heat-cured samples

Figure 42: Extended UCS data for JAW-b Vs JAW-Z.

Appendix 2 – Additional Structural Characterizations

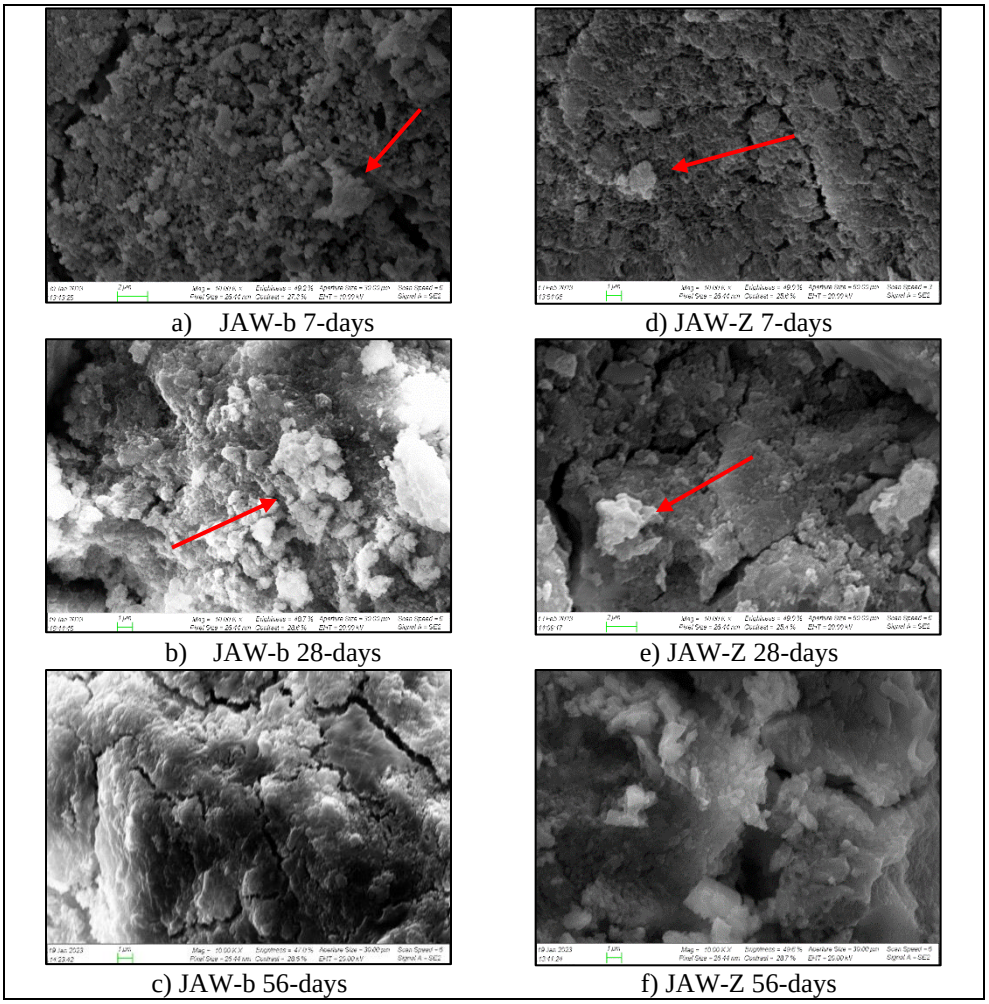

Figure 43: SEM after curing at 25 °C BHST, Magnification of 10 K.X. Results of curing time up to two months. The red arrow points towards unreacted particles.

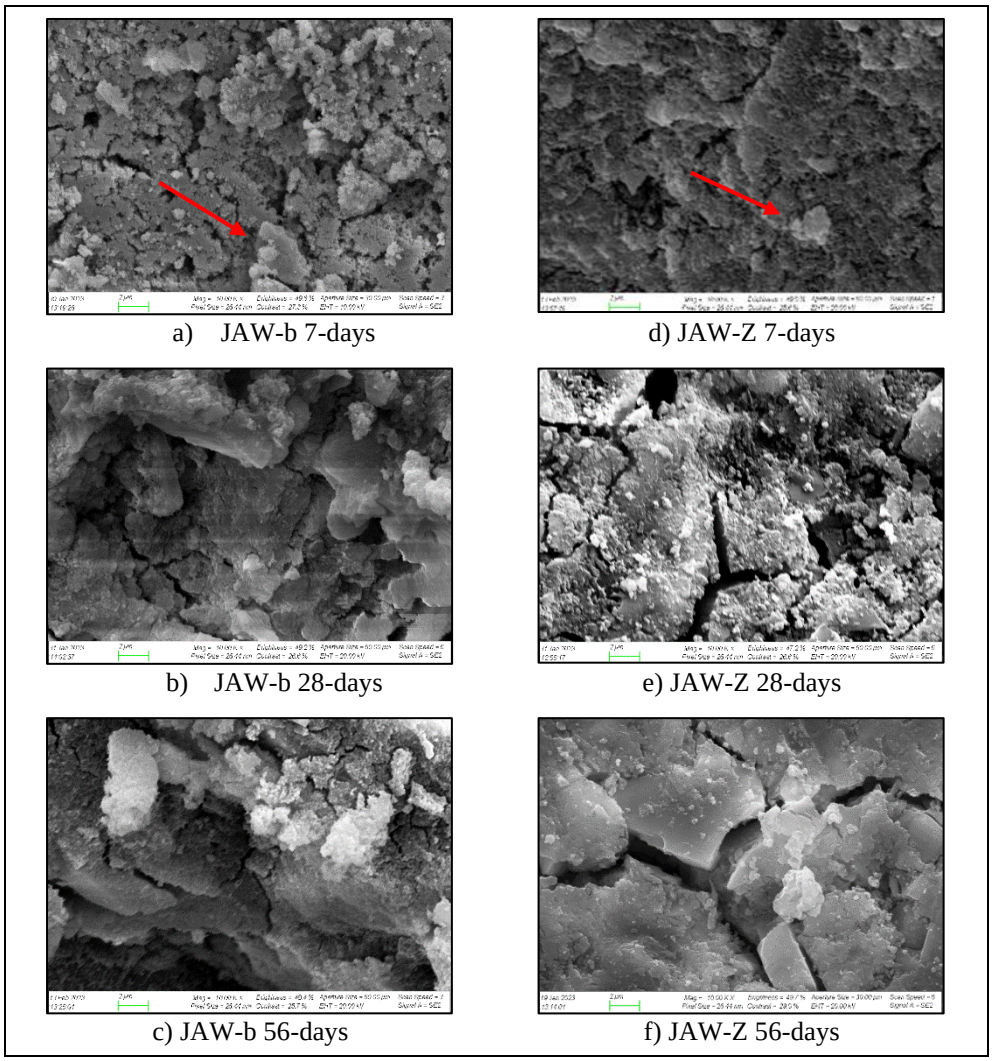

Figure 44: SEM after curing at 70 °C BHST, Magnification of 10 K.X. Results of curing time up to two months. The red arrow points towards unreacted particles.

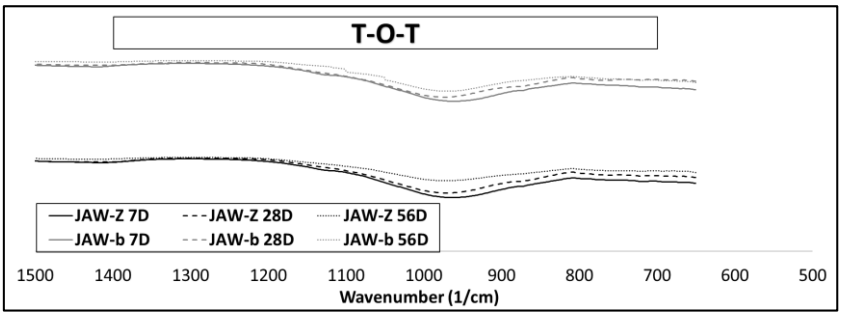

a) 25 ℃

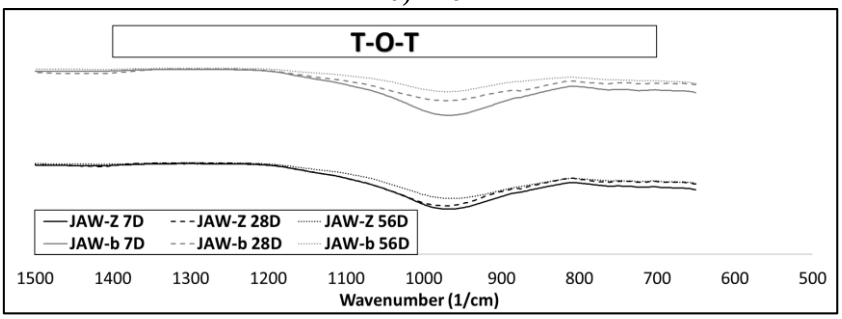

b) 70 ℃

Figure 45: FTIR patterns from 1500-500 cm^{-1} of JAW-b and JAW-Z at 25 and 70 ℃.

Appendix 3 – Paper I

227 (2023) 211822

Contents lists available at ScienceDirect

Geoenergy Science and Engineering

journal homepage: www.sciencedirect.com/journal/geoenergy-science-and-engineering

Synthesis of sustainable one-part geopolymers for well cementing applications

Mohamed Omran [a,*], Sondre Hjelm [a], Mahmoud Khalifeh [a], Saeed Salehi [b]

[a] Department of Energy and Petroleum Eng., Faculty of Science and Technology, University of Stavanger, 4036, Stavanger, Norway
[b] University of Oklahoma, Oklahoma, USA

ARTICLE INFO

Keywords:
One-part
Granite-based geopolymer
Well cementing
Chemical composition modification
Role of slag

ABSTRACT

This work describes the synthesis of a novel one-part granite-based geopolymer mix design for well cementing applications by screening and improving the early-age performance of the geopolymers. The dissolution rate of granite and potassium silicate (K_2SiO_3) is slightly enhanced when they are blended, compared to the situation when granite was mixed with alkali solution. It was revealed that the chemical composition of granite requires modification. Ground granulated blast-furnace slag (GGBFS) was incorporated up to 90% of total weight (wt.%) within the solid precursor to find out the optimum design, based on its effect on fluid-state and solid-state properties. Pumpability and strength development of the slurries were studied to establish the applicability of the mix designs. To further characterize the final products, the mineralogy and morphology of the specimens were examined. The use of GGBFS, to modify the chemical composition of the granite, reduces the pumping time significantly. Moreover, the use of GGBFS increases the density and initial consistency value of the slurry proportionally to the increase in GGBFS content. Additionally, a threshold effect was observed in the mechanical strength development. The higher the GGBFS content (up to 50 wt%), the higher the early-age compressive strength. The highest measured compressive strength for the neat rock-based geopolymer recipe was around 6 MPa within 1-day to 7-day for a mix of 47 wt% GGBFS to the solid precursor, while its optimized mix was around 12 MPa within the same period.

1. Introduction

Granite is one of the most abundant rock-type found on the earth's crust, and it is available globally, although its mineralogy could be different. Granite is an igneous rock and possesses several characteristics based on where it is located, and how the environment has affected the rock. A granitic rock's main characteristics and components are mineral crystals made up of a combination of quartz, feldspar, mica, hornblende, or pyroxene (Myers and Watkins, 1985). The proportion of minerals present in the granitic rock is divided into several different types. The dominant minerals in granite are normally a combination of quartz and feldspar, which make up almost 90% of the rock composition. Feldspar, an aluminosilicate, contains the elements calcium, potassium, and sodium. Based on the three elements, feldspar is divided into two main groups: potassium alkali feldspar, and plagioclase. Increasing or decreasing the ratio of these elements present in the granite will result in different granite families (i.e., granodiorite, syenite, and quartz monzonite), which all represent a granitic rock, but with different elemental compositions (Shang et al., 2019).

To differentiate between the different types of granite, a classification system was first proposed by Chappell and White in 1974. Chappell and White (Clemens et al., 1986), through extensive research of two specific granite types, agreed upon dividing the granites into an igneous source, and a sedimentary source granite, referred to as I-Type and S-Type, respectively. The list has been extended in recent years to further differentiate the granites. Using this classification made it easier to distinguish which type of granite is one of the interests based on the composition of the rock. The classifications are briefly described as follows in Table 1.

Granite is commonly found where two continental plates have collided. Following the tectonic plate movements, it reveals where and how easily accessible granite is all around the world (Myers and Watkins, 1985). Some continents are prone to have a higher content of alkali felspar, while other continents may have granite containing a mix of potassium feldspar and/or plagioclase. Following the use of modern technology, global industry, global production, and exporters located at

* Corresponding author.
E-mail address: mohamed.a.omran@uis.no (M. Omran).

https://doi.org/10.1016/j.geoen.2023.211822
Received 16 October 2022; Received in revised form 16 February 2023; Accepted 18 April 2023
Available online 22 April 2023
2949-8910/© 2023 The Authors. Published by Elsevier B.V. This is an open access article under the CC BY license (http://creativecommons.org/licenses/by/4.0/).

Table 1
Different types of granite and their description.

Classification	Description
I-Type	Orogenic, and have high sodium and calcium. (Clemens et al., 1986)
S-Type	Sodium-poor and aluminum-rich. (Clemens et al., 1986)
A-Type	Particularly high silicon and potassium at the expense of calcium and magnesium. (Whalen et al., 1987)
M-Type	Crystallized mafic magmas are generally sourced from the mantle. (Chappell and Stephens, 1988)
H-Type	Hybrid – Result of mixing two different magma sources. (Castro et al., 1991)

larger facilities have made granite easily accessible. Countries like Brazil, China, Canada, Italy, India, Sweden, and Norway are just a few of the larger exporters of granite (Castro et al., 1991; Granite and crude or roughly trimmed, 2022; Rosing-Schow et al., 2022).

Focusing on the Sveconorwegian orogenic belt of granite originating in the South of Norway and the South-Western side of Sweden, it reveals several larger deposits of granitic rock types such as pegmatites and A-Type granites, which dates back to about 1 billion years ago. From these deposits, especially around the coast of southern Norway, one may come across granitic rock types such as larvikite, gneiss and Drammensgranitt composed of, monzonite, migmatite, and biotite, respectively (Granite and crude or roughly trimmed, 2022; Rosing-Schow et al., 2022). Each of these granitic rock types is made up of a different composition of feldspar, quartz, and plagioclase mentioned in the section above. With the easily accessible granite available, research and development facilities have had the opportunity to be selective to what kind of granite-specific characteristics they would like to approach, and what their granitic composition should contain.

Pure granite is considered a non-reactive aggregate for geopolymerization, meaning that granite by itself will not readily react in alkaline medium. If the granite does not react with the other components i.e., in terms of geopolymer mixes, the early mechanical compressive strength may not sufficiently develop, and the granite will be deemed as not applicable for the geopolymer system (Bacarji et al., 2013). However, depending on the mineral composition of granite, it may provide the necessary aluminosilicates to be able to commence a chemical reaction involving the alkali-silica reaction (Coppola et al., 2020). The alkali-silica reaction has a significant effect on the durability of mechanical strength.

The common problem behind granite, being a non-reactive material, results in very low early strength (Vijayalakshmi and Sekar, 2013), this has been a challenge for a long time. Researchers have tried to activate and utilize granite in slag-based geopolymers and alkali-activated materials (Jain et al., 2020). Of the activation mechanisms, one may refer to chemical, thermal, and mechanical activation; however, each has a certain performance on the activation of granite due to its quartz and feldspar content.

Ground granulated blast furnace slag (GGBFS) is used in the geopolymer system when low calcium and magnesium content of the precursor is a concern (Shilar et al., 2022). GGBFS is a by-product of the steel industry and it contains large amounts of amorphous silicon dioxide, calcium oxide, and sometimes magnesium oxide, which play a huge role in the alkali-activated geopolymer system. C–S–H and C-A-S-H gels are formed when GGBFS is introduced to water, which acts as the primary binding component in cementitious materials (Shilar et al., 2022; Nath and Sarker, 2014). GGBFS as a by-product has not been serving any major use other than in smaller, specific concrete systems i.e., Portland cement and other pozzolanic materials. This is due to the low hydraulic properties of GGBFS when compared to Portland cement. The utilization of GGBFS as a combined-, or stand-alone product to fly ash and red mud, has given way for new research to explore the possibilities within the development and research of geopolymer concrete (Nath and Sarker, 2014).

Several studies have thoroughly investigated the use of slag in geopolymers, and alkali-activated materials (AAM), which concluded the potential use of GGBFS as a strength booster (Aliabdo et al., 2016; Saha and Rajasekaran, 2017; Luukkonen et al., 2018; Sasaki et al., 2019; Mahya et al., 2019; Jingming et al., 2020; Singh and Middendorf, 2020). Together with several alternative approaches to alkali-activated geopolymers, materials such as fly ash, rice husk ash and red mud have been mentioned in Table 2. GGBFS has often been introduced together with, i.e., fly ash, but until recent years was not tested as a stand-alone component for the geopolymer system. Table 2 presents a list of

Table 2
Examples of published literature reviews and articles on the role of calcium-rich byproducts used in one-part alkali-activated geopolymer concrete and cement.

Title	Significant Outputs
Effect of cement addition, solution resting time and curing characteristics on fly ash-based geopolymer concrete performance (Aliabdo et al., 2016).	By introducing Portland cement to fly ash-based geopolymers, compressive strength, tensile strength and modulus elasticity of the product were increased. In addition, it reduced water adsorption and resulted in a denser structure.
Synthesizing one-part geopolymers from rice husk ash (Sturm et al., 2016).	Observations on the reaction of rice husk ash containing silicates when introduced to a geopolymer system in combination with sodium aluminate to compensate for the lack of aluminium needed to initiate geopolymerization reaction.
Compressive strength of one-part alkali activated fly ash using red mud as alkali supplier (Choo et al., 2016).	Used red mud as the alkali supplier, and fly ash as a source of aluminosilicates in the geopolymer system, revealing an almost linear increase in the Uniaxial Compressive Strength (UCS) when considering the Na/Si ratio relation.
Enhancement of the properties of fly ash based geopolymer paste by incorporating ground granulated blast furnace slag (Saha and Rajasekaran, 2017).	Significant decrease in setting time when GGBFS was introduced to a fly ash-based geopolymer. Scanning electron microscope (SEM) images reveal a much denser structure when increasing the amount of GGBFS present in the system. It also enhanced the compressive strength of the samples.
One-part alkali-activated materials: A review (Luukkonen et al., 2018).	A review of one-part alkali-activated materials introduced the idea to use GGBFS as a stand-alone instead of mixing it with fly ash in both a liquid and solid activator. Ball-milling of the precursors and solid activator is a promising way of mechanochemical activation.
Effect of retarders on flow and strength development of alkali-activated fly ash/blast furnace slag composite (Sasaki et al., 2019).	Observing how excessive GGBFS in a geopolymer system may lead to a too rapid setting time. Introducing different chelators as retarders to prolong the setting time. Adding higher concentrations of GGBFS is revealed to create calcium aluminium silicate hydrate "C-A-S-H" gels which improve strength development.
Mix composition and characterization of one-part geopolymer with different activators (Mahya et al., 2019).	Alternating between different activators in solid form with the use of GGBFS combined with fly ash in geopolymer concrete. UCS of the concrete was observed to be positively affected for both early as well as final strength development, compared to the reference mix. The use of slag increased the formation of C-A-S-H gels.
Thermal and compressive behaviors of fly ash and metakaolin-based geopolymer (Jingming et al., 2020).	The use of GGBFS increases heat evolution and subsequently reduces the setting time and increases the early strength development of a fly ash-based geopolymer.
Geopolymers as an alternative to Portland cement: An overview (Singh and Middendorf, 2020).	An overview of geopolymers as an alternative to Portland cement. Explain the role of GGBFS in geopolymers due to its reactive amorphous phase, aluminosilicates needed for the geopolymerization reaction to take place.

scientific literature supporting the research of calcium-rich, and other components for the development of geopolymer mixes while focusing on high early strength, workability, and setting time.

Rock-based geopolymers have previously been studied thoroughly in the literature (Kamali et al., 2022). These geopolymers may not perform properly without normalizing the cationic content (Kamali et al., 2022; Omran et al., 2023, Omran and Khalifeh, 2023; Omran et al., 2022a). Because of their crystalline content and low calcium content, they may not develop sufficient early strength in due time. On the other hand, GGBFS slag can help with achieving early strength development and sustainability goals for rock-based geopolymers. One of the main challenges in front of geopolymers and alkali-activated materials (AAM) is the alkaline liquid hardener, which limits the commercialization of these products. This challenge becomes amplified when they are to be shipped offshore for well-cementing operations.

Therefore, this work describes the synthesis of a one-part granite-based geopolymer for use in well-cementing applications, intending to meet the early-age well-cementing properties outlined in the American Petroleum Institute (API) standard 10B-2 (API and R.P., 2019). This examines both the pumping time and solid-state properties of the mix design by varying and normalizing the chemical composition of the granite using ground granulated blast furnace slag (GGBFS). The utilization of GGBFS is to compensate for the low early-strength development of granite, GGBFS content ranges from 0% to 90% of the total weight of the precursor. Furthermore, the study investigates the effect of incorporating GGBFS as a normalizer on the mineralogy and mechanical properties of the granite-based geopolymer.

2. Materials and methods

2.1. Materials

Granite is a widely available rock in the south of Norway (Granite and crude or roughly trimmed, 2022; Rosing-Schow et al., 2022) and is considered a rich source of aluminosilicate (Kovler, 2012; Heldal and Neeb, 2000). According to the Geological Survey of Norway, granite from Norway is classified as a massive structure, medium to coarse-grained with no weathering, and medium grey in color. The mineral composition of granite mainly consists of feldspar and quartz as the dominant crystalline minerals. Other, minor minerals commonly found in that include plagioclase, muscovite, and biotite (Rosing-Schow et al., 2022; Geological Survey of Norway and NGU, 2022).

The one-part granite-based geopolymer formulation is based on solid rock-based precursors and a solid potassium-based activator with a molar ratio at $SiO_2/K_2O = 2.4$, mixed with water to initiate the geopolymerization reaction, producing the geopolymer cementing system. The materials present in the precursor were ground granite acting as the rock-based aluminosilicate material; GGBFS as calcium and magnesium-rich silicate material; and microsilica as a pure amorphous silica normalizer by 4.3 wt% of the precursor content. The chemical composition of the precursors is presented in Table 3. All the precursors' mineralogy and components of one-part granite-based geopolymers have previously been thoroughly studied (Kamali et al., 2022).

2.2. Methods

All the geopolymer recipes were prepared in a laboratory following the recommended API mixing procedures and in compliance with the API RP 10B-2 (API and R.P., 2019). This standard specifies methods and provides recommendations for testing of cement slurries and related materials under simulated well conditions. The experimental phase was conducted in the following order: atmospheric consistometer, calorimetric characterization, curing of samples for strength development, and compositional analysis of the solidified samples. However, the calorimetric characterization is not in this standard.

2.2.1. Mix design and formulations

Mix design entails preparing the solid phase of various alkali-activated or geopolymer recipes. The mix design was prepared in a stepwise manner with different concentrations of GGBFS ranging from 0 to 90 wt% of the precursor. Additionally, granite was compensated with GGBFS for the remainder of the total weight of the precursor. First, having obtained enough components, solids (precursors and the activator) were mixed in a clean plastic container. Following API Specification 10, the solid precursor and activator were combined with water through blending. Table 4 presents the different setups of recipes, and their total amount of GGBFS in the precursor, each with their recipe's name and classification, respectively.

2.2.2. Mixing and conditioning procedures

A commercial Constant Speed Blender, specified in API 10B-2 (API and R.P., 2019), was utilized for the preparation of the slurry. The precursor material and solid activator were introduced to distilled water in 15 s at 4000 rpm, and then the slurry was sheared for 35 s at 12,000 rpm.

Subsequently, an atmospheric consistometer was utilized for both conditioning and determining the thickening time for all the slurries at 50 °C, Bottom Hole Circulating Temperature (BHCT). This temperature

Table 4
Mix design for one-part rock-based geopolymer mixes.

Mix design name[a,b]	GGBFS (wt.%) in Precursor	Classification
GGBFS-0%	0	Rock-based geopolymer
GGBFS-10%	10	Rock-based geopolymer
GGBFS-20%	20	Rock-based geopolymer
GGBFS-25%	25	Rock-based geopolymer
GGBFS-30%[c,d]	30	Rock-based geopolymer
GGBFS-33%	33	Rock-based geopolymer
GGBFS-36%	36	Rock-based geopolymer
GGBFS-40%	40	Rock-based geopolymer
GGBFS-43%	43	Rock-based geopolymer
GGBFS-47%[d,e]	47	Rock-based geopolymer
GGBFS-50%	50	Alkali-activated material
GGBFS-60%	60	Slag-based AAM
GGBFS-70%	70	Slag-based AAM
GGBFS-80%	80	Slag-based AAM
GGBFS-90%	90	Slag-based AAM

[a] All recipes had the same water-to-solid and solid activator-to-precursors ratios, 0.33 and 0.20, respectively.
[b] All recipes had the same microsilica content, 4.3 wt% of the precursors.
[c] GGBFS-30% is the so-called OP-a, which is based on a back-calculated two-part granite-based geopolymer recipe from Omran et al. (2022b).
[d] GGBFS-47% is the so-called OP-b recipe, which is the neat one-part granite-based geopolymer recipe.
[e] A strength booster 0.06 wt.% in solid precursors of pure bulk aluminium hydroxide or zinc oxide. Both were added separately to OP-a and OP-b.

Table 3
Chemical composition of the precursors from a geochemical analysis (Omran et al., 2022a).

Chemical composition (wt.%)	SiO_2	Al_2O_3	Fe_2O_3	MgO	CaO	Na_2O	K_2O	TiO_2	MnO	LOI[a]
Granite (Norway)	73.44	13.33	2.06	0.44	1.12	3.12	5.11	0.23	0.04	0.9
GGBFS (Sweden)	35.78	12.72	0.18	12.77	33.74	0.55	0.82	2.23	0.58	0.3
Microsilica (Norway)	95.50	0.70	0.30	0.50	0.40	0.40	1.00	0.00	0.00	0.6

[a] Loss on ignition.

was chosen to simulate the conditions at the casing shoe of an intermediate casing string in offshore Norway, which is representative for 70 °C Bottom Hole Static Temperature (BHST).

2.2.3. Curing of samples

All samples were cured at atmospheric pressure in a preheated oven at 70 °C BHST. Cylindrical plastic molds equipped with end lids to avoid water evaporation, were used for storing and curing the samples. A cutter machine was used to flatten both ends of the cured samples. The dimensions for the cured samples used for the uniaxial compressive strength tests were 51 mm in diameter and 80 mm in height.

2.2.4. Scanning electron microscopy (SEM)

A scanning Electron Microscope machine was employed for examining the precursors and geopolymer surfaces topography. SEM analysis was conducted on all solid precursors prior to mixing and on crushed geopolymer samples after 7 days of curing. The samples were vacuum-dried for 1-day and then coated with an 11 nm layer of palladium plasma to prevent electrical charging.

2.2.5. Ultrasonic and uniaxial compressive strength

A high pressure high temperature (HPHT) ultrasonic cement analyzer (UCA) was applied to non-destructively measure the sonic strength development of the geopolymer at conditions of 13.7 MPa and 70 °C for a 7-day period (Omran et al., 2023, Omran and Khalifeh, 2023). Uniaxial compressive strength (UCS) tests were conducted according to API RP 10B-2 (API and R.P., 2019). The 70 °C heat-cured samples were crushed by availing a compressional mechanical tester, at a constant loading rate of 10 kN/min, and then correlated to the sonic strength data obtained from the UCA.

2.2.6. Compositional analysis using X-ray diffraction (XRD)

Bruker-AXS Micro-diffractometer D8 Advance with CuKα radiation (40.0 kV, 25.0 mA) and an angle 2theta (2θ) range from 5 to 92° with 1°/min step and 0.010° increment was used to analyze the crystalline phases by following relevant procedures were used in previous studies (Kamali et al., 2022; Omran et al., 2023). Only the main peaks of the XRD patterns have been considered due to the minor differences that can occur during sample preparation, or random distribution of minerals, in addition to the complexity of their chemical composition (Kamali et al., 2022; Omran et al., 2023, Omran and Khalifeh, 2023).

3. Result & discussion

3.1. Dissolution and early strength development of granite

3.1.1. Dissolution and characteristics of precursors

Granite (Norway) powder from a landfill in Norway was used to synthesize the one-part rock-based geopolymer mixes, while GGBFS and microsilica were used as normalizers for these mixes. Tables 5 and 6 illustrate the particle-size distribution (PSD) and electrokinetic potential of the precursors. Moreover, the morphology of the granite, GGBFS, microsilica and their mix after solidification is shown in Fig. 1.

Comparing the PSD results in Table 5 with the SEM images in Fig. 1, one may argue that granite has the largest PSD and more irregular shapes than the other two components. Only 50%, by volume, of the particles in granite, are less than, or equal to 21 μm. In addition, the granite's irregular particle shapes directly influence the dissolution phase, where it follows a set of surface-controlled reactions. This means that the other 50% of PSD of the granite particles can be considered large-size non-reactive fillers in the precursor with the lowest specific surface area (see Table 5, Fig. 1-a and 1-d) in agreement with Moosberg-Bustnes et al. (2004).

Table 5
Particle-size distribution of the precursors.

Material/ Powder	Specific Surface Area (m^2/kg)	Density (SG)	Dv (10)[a] (μm)	Dv (50)[a] (μm)	Dv (90)[a] (μm)
Granite	630.8	2.63	3.52	21.1	131.0
GGBFS	943.7	2.90	2.79	15.9	46.6
Microsilica	19,320	2.29	0.19	0.34	0.60

[a] Dv: Volume Median Diameter from PSD indicating the size below which 10%, 50% or 90% of all particles can be found.

Table 6
The Electrokinetic potential of the precursors by Omran et al. (2022b).

Material/ Powder	Particle Refractive Index	Zeta Potential (mV)	Standard Deviation of Zeta Potential (mV)
Granite	1.59	−9.61	±1.74
GGBFS	1.52	−20.77	±3.00
Microsilica	1.46	−33.53	±0.33

On the other hand, GGBFS and microsilica yield higher specific surface area values and much lower PSD. Furthermore, 90% by volume of the irregular shape particles of GGBFS, and spherical shape particles of microsilica, are smaller than, or around 47 and 0.6 μm, respectively (Fig. 1-b and 1-c). Thus, GGBFS and microsilica can be considered as more reactive having an excelled reaction phase compared to granite. The higher PSD with a low specific surface area will result in lower chemical reactivity and weaker solid-solid and solid-liquid interactivity (Oderji et al., 2019). The electrokinetic data of the given precursors agree with the PSD data in Tables 5 and 6 The granite is also observed to have the lowest absolute zeta-potential value out of the three materials measured, Table 6, implementing that granite is proven to have the least interactive particles among the other precursors in the early phase of strength development.

Omran et al. (2022a) presented the compositional analysis and dissolution rates for a one-part rock-based geopolymer system. The same activator and precursors were used, and it was shown that the used granite was highly crystalline, up to 80%, and had fewer reactive components. This observation also matches the SEM image of granite, as seen in Fig. 1-a. This granite is mainly composed of crystalline phases including quartz, albite, and microcline as major peaks with tracers of biotite peaks, while GGBFS and microsilica are amorphous and reactive components. For GGBFS, tracers of akermanite crystalline peaks could barely be detected.

Table 7 presents a dissolution rate analysis of the same one-part rock-based geopolymer system. The dissolution of granite increased the silicon concentration of the solid activator from 750 to 1200 ppm. On the other hand, GGBFS decreased the silicone concentration to 220 ppm. This could be either due to the adsorption of silicates on the surface of GGBFS particles or the formation of calcium silicate hydrates (C–S–H) bonds, which could be consuming the silicate as it is released (Hewlett, 2001; Haha et al., 2011, 2012; Ma et al., 2019). Moreover, the utilized microsilica was observed to be very effective in releasing silica into the solution without any observable effect on the potassium levels. Although alumina contents in GGBFS and granite are comparable as seen in Table 3, GGBFS released 4 times more reactive aluminum-free ions than granite (see Tables 7 and 8). This may be explained by noting that the decrease in silicate concentration favors the dissolution of aluminosilicates (Ma et al., 2019). Furthermore, the surface area of the particles directly influences their dissolution rates within the alkaline medium as mentioned previously. Therefore, granite particles, having the lowest specific surface area, yield the lowest dissolution rates, while microsilica particles have the largest specific surface area implementing the fastest dissolution rates.

Table 8 presents the dissolution behavior of the same precursors mentioned in a 4 Molar KOH activator system from Omran et al. (2022b). Tables 7 and 8 present the main differences in the dissolution of silicate-based (K-silicate) versus hydroxide-based (KOH) activators. In the hydroxide-based system, the activator is highly rich in free

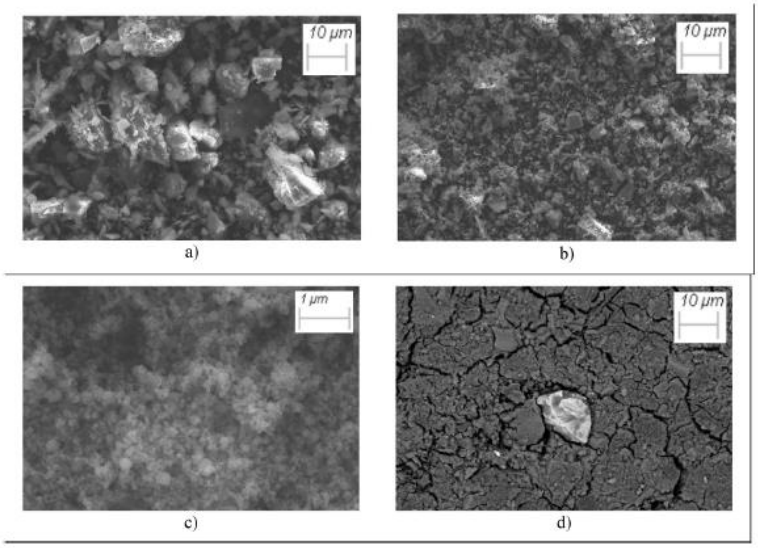

Fig. 1. SEM images of the precursors: a) granite, b) GGBFS, c) microsilica, and d) their mix after solidification.

Table 7
Dissolution results of the precursors using Inductively Coupled Plasma (ICP) analysis from (Omran et al., 2022a) in a potassium silicate-based activator.

Material[a,c]	Silicon (ppm)	Aluminum (ppm)	Potassium (ppm)	Sodium (ppm)
K_2SiO_3-based Activator	750	0.74	20,000	100
Granite	1200	6.50	20,000	110
GGBFS[a,b]	220	23.00	19,000	110
Microsilica[a,c]	2800	2.10	20,000	100

[a] Granite and GGBFS were added with a comparable weight% in the solution.
[b] Most likely the reactive silicate phases precipitated, and they were not detected through the ICP analysis.
[c] Microsilica was 10 times less than the weight of granite and GGBFS in the solution.

Table 8
Dissolution results of the same precursors (ICP analysis) in a hydroxide-based activator.

Material[a]	Silicon (ppm)	Aluminum (ppm)	Potassium (ppm)	Sodium (ppm)
KOH-based Activator	0	0	140,000	0
Granite	92	32.0	130,000	580
GGBFS	300	190.0	110,000	540
Microsilica	17,000	9.9	110,000	360

[a] These components were added with the same weight% in the activator solution.

hydroxide ions that strongly affect the dissolution rate of the silicon ions from the precursors. During the time, the given potassium silicate-based activator acted as an additional source of free silicon ions, or as the silicate provider itself in the dissolution phase. Comparing granite data in Tables 7 and 8, our measurements indicate that either granite gets more dissolved when K-silicate in a powder form is used or the powder silicate gets more dissolved in the presence of granite. Furthermore, dissolution data for GGBFS is a matter of discussion as the dissolution and oligomerization of silicates may take place and result in deposition of phases, which subsequently results in lower freed silicon ions in the samples solutions.

The silicate powder does not contain hydroxide (OH-) ions, but it has the potential to hydrolyze water into OH- and hydrogen (H^+) ions. Subsequently, OH- will attack the silicate species present in the precursor phase. The silica-rich medium could have the potential to directly affect the formation of geopolymer gels or the final product. Hence, faster consumption of the silica ions could happen, especially in the presence of GGBFS (Haha et al., 2011, 2012; Ma et al., 2019). The geopolymerization is accelerated at a high concentration of silicate oligomers and calcium (Ca^{2+}) ions. The higher their concentrations, the more mature C-A-S-H or potassium aluminum silicate hydrate (K-A-S-H) bonds can be produced, in agreement with Ma et al. (2019). Therefore, in the potassium silicate-based activator, the geopolymer system undergoes through a higher degree of geopolymerization reaction complexity at which dissolution and gel products or formations may happen in parallel.

3.1.2. Sonic strength development of the pure granite

GGBFS-0% is a zero wt.% slag in a granite-based geopolymer recipe. For this given granite-based recipe, the sonic strength development at 70 °C and 13.7 MPa was measured over the span of 7 days. The experiment was to track both setting-, and hardening time without the presence of GGBFS, see Fig. 2.

UCA data for the GGBFS-0% recipe matches the previous observations regarding the need for high reactive, and amorphous materials

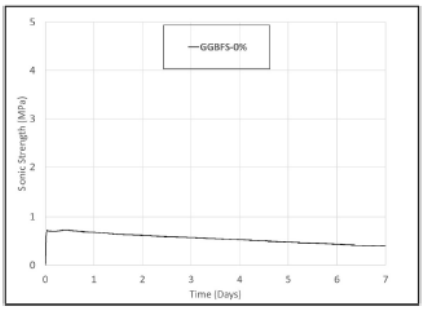

Fig. 2. Sonic strength development curves for GGBFS-0% recipe, cured at 70 °C and 13.7 MPa.

such as GGBFS and microsilica to be utilized in the granite-based geopolymer system. In agreement with Bacarji et al. (2013), the dissolution of granite by itself is not fast nor reactive enough to be integrated within the early reaction phases of the geopolymerization. Thus, this can present the impracticability for the geopolymer cement to develop acceptable early-stage mechanical properties for well-cementing applications. Without the normalization, this granite-based geopolymer would not be capable to achieve any strength developments higher than 0.4–0.6 MPa within the 7 days of heat curing at 70 °C and 13.7 MPa.

3.2. Normalisation of the granite

3.2.1. Uniaxial compressive strength (UCS)

Fig. 3 and Table 9 illustrate the uniaxial compressive strength of the various mixes of the given precursors as a function of GGBFS content after 1-day of heat curing at 70 °C and atmospheric pressure. All mix designs contain microsilica, 4.3 wt% in the solid precursors as shown in Table 4.

The UCS data reveal a threshold effect, and how increasing the GGBFS content benefits the early strength in the rock-based geopolymer recipes. GGBFS-0% recipe did not set and could not withstand any compressive stress during the first 24 h. After the addition of GGBFS by replacing the granite content stepwise up to 50 wt%, revealed a trend illustrating that the higher the GGBFS content, the stronger the samples' capability withstand compressive stresses up to 3.8 MPa. GGBFS-50% recipe can be considered an alkali-activated material and a threshold peak point for the GGBFS content in the granite-based geopolymer.

For GGBFS content above 50 wt% in the precursors, horizontal macrocracks were easily observable with the naked eye, and the samples were observed to be self-sliced into three and four parts horizontally (see Fig. 4). This phenomenon could suggest an expansion in the highly rich GGBFS content samples. The utilized GGBFS was rich in expanding components, such as magnesium oxides (see Table 2). The higher the GGBFS content, the higher the samples' expansion, and the bigger the observable horizontal crack propagations.

Fig. 5 shows the 1-day, and 7-day uniaxial compressive strength of the two selected neat, one-part rock-based recipes after heat curing at 70 °C. The selected neat recipes are "OP-a" and "OP-b". OP-a was the GGBFS-30% mix. The GGBFS-30% precursor mix has been already studied for conventional two-part geopolymers in literature (Omran et al., 2022b). OP-b is the GGBFS-47% mix that is close to the threshold GGBFS content for the rock-based geopolymer system. Thus, it compares the mechanical performance of these two mixes to clarify the effect of the GGBFS content in the precursors both with and without a strength booster. It also illustrates the possibilities for early strength optimization after introducing a strength booster admixture to either of the neat geopolymer systems.

The UCS results reveal a clear effect in the partial replacement of granite by GGBFS on the rock-based geopolymer system. Moving from replacing 30 wt% to 47 wt% of granite by GGBFS led to 157% and 130%, increases in 1-day and 7-day UCS, respectively, which is in agreement with the findings of previous studies (Saha and Rajasekaran, 2017; Luukkonen et al., 2018; Sasaki et al., 2019; Mahya et al., 2019; Jingming et al., 2020; Singh and Middendorf, 2020). Additionally, the addition of the strength boosters, especially zinc oxide, led to a doubling and

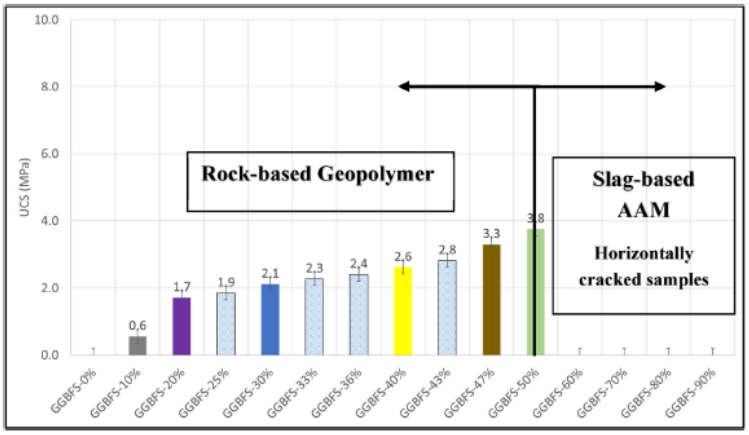

Fig. 3. UCS data for 1-day 70 °C heat cured samples.

Table 9
UCS data for 1-day 70 °C heat cured samples.

Mix design name	UCS 1-day (MPa)	Color Code
GGBFS-0%*1	N/A	**Black**
GGBFS-10%	0.6	**Grey**
GGBFS-20%	1.7	**Purple**
GGBFS-25%	1.9	N/A
GGBFS-30%*2	2.1	**Blue**
GGBFS-33%	2.3	N/A
GGBFS-36%	2.4	N/A
GGBFS-40%	2.6	**Yellow**
GGBFS-43%	2.8	N/A
GGBFS-47%*3	3.3	**Brown**
GGBFS-50%	3.8	**Green**
GGBFS-60%*4	N/A	N/A
GGBFS-70%*4	N/A	N/A
GGBFS-80%*4	N/A	N/A
GGBFS-90%*4	N/A	N/A

*1- GGBFS-0% did not set after 1-day 70°C heat curing.
*2- GGBFS-30% is OP-a recipe. OP-Da and OP-Za are based on OP-a mix with either 0.86 wt.% aluminium hydroxide or zinc oxide as strength boosters, respectively.
*3- GGBFS-47% is OP-b recipe. OP-Db and OP-Zb are based on OP-b mix with either 0.86 wt.% aluminium hydroxide or zinc oxide as strength boosters, respectively.
*4- All were horizontally cracked samples.
N/A: Not Available

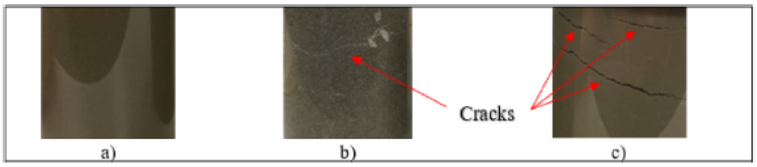

Fig. 4. Three vertical sample pictures (4 × 4 cm); a) GGBFS-47% (without horizontal cracks), b) GGBFS-50% (a small horizontal crack on the surface), c) GGBFS-60% (with observable large horizontal cracks) after heat curing at 70 °C for 1-day.

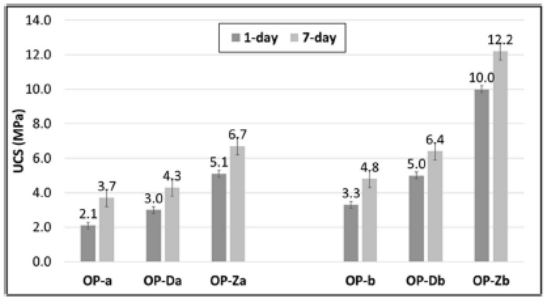

Fig. 5. UCS data for 1-day and 7-day for 70°C heat-cured geopolymer neat recipes: OP-a and OP-b with and without the early strength boosters.

tripling of the early strength development for both neat recipes, as observed in previous studies (Omran et al., 2023, Omran and Khalifeh, 2023; Omran et al., 2022a).

3.2.2. Sonic strength

Sonic strength curves were also investigated for the two neat geopolymer mixes at 70 °C and pressurized to 13.7 MPa for 7 days (see

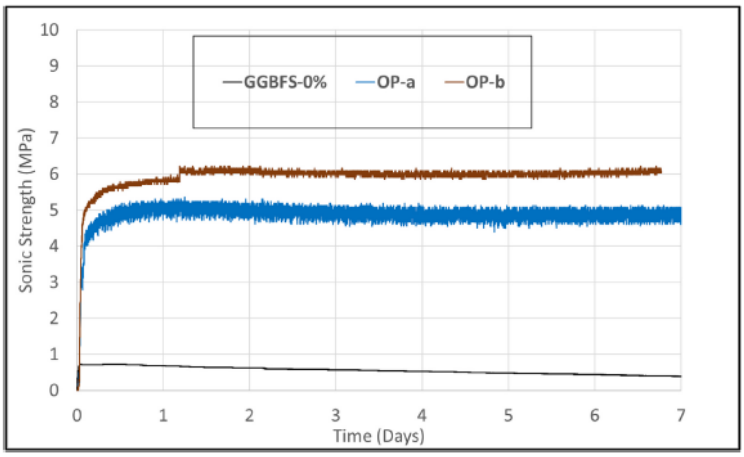

Fig. 6. Sonic strength development curves for GGBFS-0%, OP-a and OP-b.

Fig. 6). Table 10 shows the conventional setting and hardening times, defined as the time it requires the geopolymer cement to reach a sonic strength at 100 psi and 500 psi, and the sonic strength development at both 1-day, and 7-day.

The UCA results both confirm and match the UCS observations with respect to the effect of partially replacing granite with GGBFS for the rock-based geopolymer mixes. The higher the GGBFS content in the rock-based precursors, the higher the early strength development. OP-b (with a GGBFS content of 47 wt% in the precursor) provided a higher early strength development up to 7 days, in addition to an accelerated hardening time when compared to the OP-a recipe (with lower GGBFS content). On the other hand, GGBFS-0% had never managed to harden, or even reach 500 psi within the 7-day UCA test.

3.2.3. Consistency & thickening time

According to API standards (API and R.P., 2019), cement slurry should conserve its fluidity until being placed correctly at the desired depth. The cement is required to develop sufficient early strength to continue well operations without unnecessary long wait-on-cement. The consistency curves seen in Fig. 7 illustrates these three geopolymerization reaction stages. First, the dissolution of the precursors into monomers can be observed as a decrease in consistency while the temperature is ramping up. Second, the reorganization stage can be initiated by the reorganization of the dissolved monomers to form oligomers, which occurs at the lowest consistency ranges. Finally, the polycondensation stage starts, when the slurry coagulates and transforms into a gel with the formation of a three-dimensional (3D) network polymeric structure of the formed oligomers. This rapid gain in consistency is usually called a "right-angle set", and is a desirable property for a well-cementing slurry (Omran et al., 2022a).

Figs. 7 and 8 present the consistency profile in Bearden units (Bc) at a bottom hole circulating temperature of 50 °C, for the given rock-based geopolymer mixes. A consistency of 40 Bc was selected as a reference for the pumpability period for the geopolymer slurries. Tables 11 and 12 show the initial consistency and pumpability duration for each of the given rock-based geopolymer recipes.

From the workability results (see Fig. 7 and Table 11), the given rock-based slurries are observed to have pumpability times ranging from 41 to 57 min after utilizing different GGBFS concentrations. Additionally, the six geopolymer mixes all experienced a rapid gain in consistency, or the so-called "right-angle set". On the other hand, the consistency data of the GGBFS-0% recipe also experienced oligomerization at which its consistency gradually increased after the dissolution. This can be seen on the black curve at 60 min and onwards. This GGBFS-0% recipe had a very long pumpability time. It did not even manage to set nor reach 40 Bc within 6 h of conditioning at 50 °C BHCT. It is not an acceptable pumpability for any well-cementing slurry if it cannot be set nor hardened for more than 6 h.

The partial replacement of granite by GGBFS drastically increased the initial consistency for all slurries up to 158%. GGBFS-50% slurry was

Table 10
Summary of UCA data.

Mix Design	Setting Time to 100 psi (min)	Hardening Time to 500 psi (min)	Sonic strength (Mpa) for 1-day	Sonic strength (Mpa) for 7-day
GGBFS-0%*	720	10080+	0.68	0.40
OP-a	44	109	5.11	5.10
OP-b	43	66	5.85	6.10

*After 7 days of curing at 70°C and 13.7 MPa, turned the slurry into a gel-like structure which did not manage to harden.

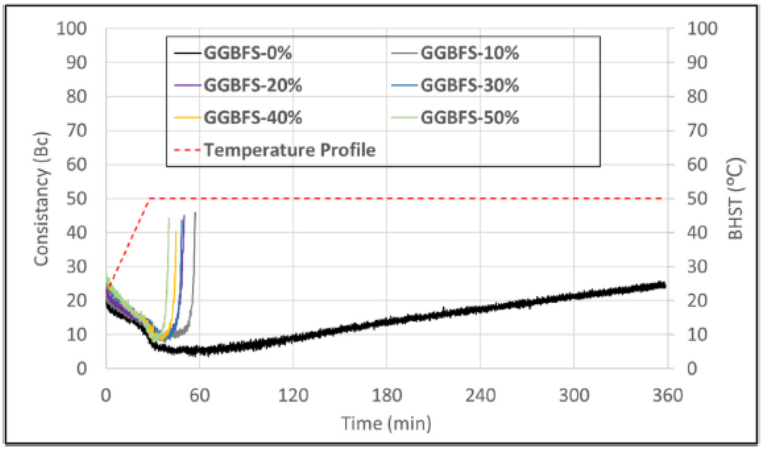

Fig. 7. Consistency development profile of the rock-based geopolymers slurries at BHCT 50 °C.

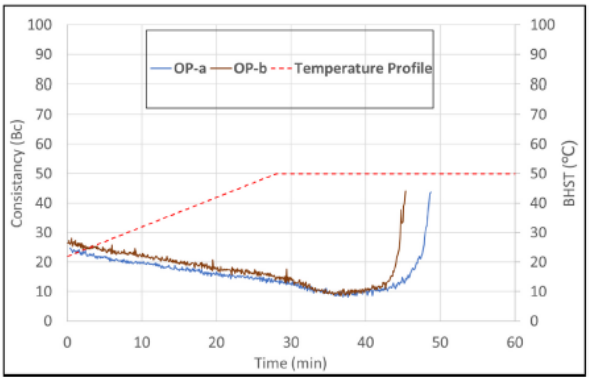

Fig. 8. Consistency development profile of the two neat one-part rock-based geopolymers recipes at BHCT 50 °C.

Table 11
Summary of consistency data for rock-based geopolymers slurries at BHCT 50 °C.

Recipe	GGBFS-0%	GGBFS-10%	GGBFS-20%	GGBFS-30%	GGBFS-40%	GGBFS-50%
Initial Consistency (Bc)	17.8	19.6	21.0	22.9	25.1	28.1
Pumpability (min)	360+	56.9	49.7	48.4	44.8	41.7

Table 12
Summary of consistency data for the two neat rock-based geopolymers recipes.

Recipe	OP-a	OP-b
GGBFS wt.%	30	47
Slurry density (SG)	1.78	1.87
Initial Consistency (Bc)	22.9	26.4
Reorganization period (min)	~10	~5
Polycondensation period (min)	~8	~4
Pumpability (min)	48.4	45.2

much thicker when compared with GGBFS-0%. Thus, a noticeable trend can be detected from the utilization of GGBFS with various concentrations in the precursors. The higher the content of GGBFS in the rock-based mixes, the higher the initial consistency and the thicker geopolymer slurries. These trends and observations also match the literature (Luukkonen et al., 2018; Sasaki et al., 2019; Mahya et al., 2019; Jingming et al., 2020; Singh and Middendorf, 2020; Yousefi Oderji et al., 2019; Oderji et al., 2019).

Fig. 8 and Table 12 present the consistency data for the selected neat rock-based recipes. Both the neat rock-based recipes had acceptable and comparable workability with a "right-angle set". The same trend was additionally observed and matched with the shown consistency profile in Fig. 7, and Table 11. OP-b, with higher GGBFS content, had higher initial consistency than the compared to OP-a. The reason behind this behavior may be because of a higher specific surface area for the given GGBFS. In addition the increase in density of the solid precursors after adding a higher amount of GGBFS in OP-b. This can be also due to the higher density of GGBFS when compared to granite. Hence, the behavior behind granite having the lowest solid-fluid interactivity, and electro-kinetic potential, may be revealed to how easy it is for the granite to segregate rather than integrate into the system. Furthermore, the higher the GGBFS content, the more rapid the reorganization phase and poly-condensation of the geopolymer slurry (Saha and Rajasekaran, 2017; Luukkonen et al., 2018; Sasaki et al., 2019; Mahya et al., 2019; Jingming et al., 2020; Singh and Middendorf, 2020).

3.2.4. Compositional analysis XRD

Others have investigated the XRD spectra of the given precursors (Kamali et al., 2022; Omran et al., 2023, Omran and Khalifeh, 2023; Omran et al., 2022a). Their studies show that granite has a very high crystalline content of up to 80% (Omran et al., 2023, Omran and Khalifeh, 2023; Omran et al., 2022a). It may be fair to assume that the rock-based precursor produces geopolymers with low amorphous content. In other words, the geopolymerization reaction consumes part of the crystalline phases in the precursors due to their dissolution within a highly alkaline medium. After the normalization of cations by GGBFS, the rock-based geopolymer mixes were observed to achieve a higher amorphous content. Fig. 9 presents the XRD spectra of GGBFS-0%, OP-a and OP-b. Table 13 summarizes crystallinity phase quantification by EVA v5 software.

GGBFS-0% and OP-a recipes have higher granite content in the precursors' mix, where all major peaks of crystalline phases, such as quartz, were lowered for OP-a, but not as lowered as for OP-b. In addition, the ongoing geopolymerization reaction lowers down and diminishes the presented minor crystalline phases in granite such as albite, microcline, and biotite for OP-a and OP-b mixes. It is here through the XRD spectra and the crystalline content observed that the higher the content of granite, the higher the remaining crystalline phases in the mix, and vice versa for the GGBFS content in the precursors' mix. This trend also matches the high PSD of granite, where a considerable amount of granite can be considered as a non-reactive, large crystalline filler in the geopolymer system. Thus, this partial granite replacement by GGBFS is deemed to be crucial for synthesizing an early reactive rock-based geopolymer system and to able to achieve acceptable early-age development for well-cementing applications.

4. Conclusion

The granite used in this study has a high particle size distribution, and over 50% volume of granite can be considered a non-reactive filler in the geopolymer system, especially in early-age performance. The dissolution rate of potassium silicate and/or granite is increased when these two are present in the system.

The low early strength of the granite-based geopolymer requires modification with an amorphous phase containing cationic content. Partial replacement of granite with a cationic-rich source such as GGBFS is necessary to obtain a satisfactory reactive precursor system. This normalization helps to achieve acceptable early-age well-cementing properties. The utilization of a higher content of GGBFS in the granite precursors' mix, up to 47 wt%, yielded higher early strength development up to 6 MPa for 1 day of curing. However, the higher the content of GGBFS, up to 47 wt%, the shorter the workability, and the faster the setting time, down to 9 min combined. Negative threshold effects were observed when more than 50 wt% of the granite was replaced by GGBFS. A consequence of increasing the GGBFS content more than or equal to 50 wt% is obvious expansion caused by magnesium content in GGBFS. This expansion resulted in large horizontal cracks. GGBFS-47% can be considered a sweet spot for a neat one-part granite-based geopolymer

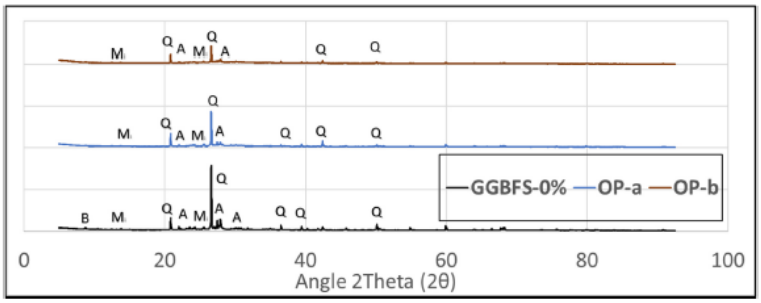

Fig. 9. XRD patterns of selected mixtures after 7 days of heat curing at 70 °C BHST. Q: Quartz, A: Albite, M: Microcline, B: Biotite.

Table 13
XRD crystallinity quantification using "EVA v5" software.

Mix Design	GGBFS in the precursor (wt.%)	Crystalline content (wt.%)	Amorphous content (wt.%)
GGBFS-0%	0	75.2	24.8
OP-a	30	64.9	35.1
OP-b	47	51.7	48.3

mix design to be further developed.

Credit author statement

Mohamed Omran: Conceptualization, Methodology, Investigation, Data Curation, Writing- Original draft preparation, Writing- Reviewing and Editing.; **Sondre Hjelm:** Investigation and Writing- Original draft preparation.; **Mahmoud Khalifeh:** Writing- Reviewing and Editing, Investigation, Resources, Supervision, Project administration, and Funding acquisition; **Saeed Salehi:** Writing- Reviewing and Editing, Investigation, and Supervision.

Data availability

Data will be made available on request.

Acknowledgement

The authors gratefully acknowledge TotalEnergies, AkerBP, ConocoPhillips and the Research Council of Norway for financially supporting the SafeRock KPN Project (RCN #319014- New Cementitious Material for Oil Well Cementing Applications – SafeRock) at the University of Stavanger, Norway. In addition, the authors would like to acknowledge Dr Mohammadreza Kamali and Mr Fawzi Chamssine for their lab support.

References

Aliabdo, A., Elmoaty, M., Salem, H., 2016. Effect of cement addition, solution resting time and curing characteristics on fly ash based geopolymer concrete performance. J. Can. Petrol. Technol. 123, 581—593.
API, R.P., 2019. 10B-2, Recommended Practice for Testing Well Cements. API, Washington, DC.
Bacarji, E., Toledo Filho, R.D., Koenders, E.A.B., Figueiredo, E.P., Lopes, J.L.M.P., 2013. Sustainability perspective of marble and granite residues as concrete fillers. Construct. Build. Mater. 45, 1–10.
Castro, A., Moreno-Ventas, I., De La Rosa, J.D., 1991. H-type (hybrid) granitoids: a proposed revision of the granite-type classification and nomenclature. Earth Sci. Rev. 31 (3–4), 237–253.
Chappell, B.W., Stephens, W.E., 1988. Origin of infracrustal (I-type) granite magmas. Earth and Environmental Science Transactions of the Royal Society of Edinburgh 79 (2–3), 71–86.
Choo, H., Lim, S., Lee, W., et al., 2016. Compressive strength of one-part alkali activated fly ash using red mud as alkali supplier. Journal of Construction and Building Materials 125, 21—28.
Clemens, J.D., Holloway, J.R., White, A.J.R., 1986. Origin of an A-type granite; experimental constraints. Am. Mineral. 71 (3–4), 317–324.
Coppola, B., Tulliani, J.M., Antonaci, P., Palmero, P., 2020. Role of natural stone wastes and minerals in the alkali activation process: a review. Materials 13 (10), 2284.
Geological Survey of Norway, NGU, 2022. ANALYSERESULTATER for PUKKOMRÅDE, Pukkdatabasen: Velde Pukkverk. Sandnes (Rogaland).
Granite, crude or roughly trimmed. (n.d.). Retrieved September 16, 2022, from https://oec.world/en/profile/hs/granite-crude-or-roughly-trimmed#:~:text=Granite%2C%20crude%20or%20roughly%20trimmed%20are%20the%20world's%202091st%20most,%2C%20and%20Spain%20(%2425M).
Haha, M.B., Le Saout, G., Winnefeld, F., Lothenbach, B., 2011. Influence of activator type on hydration kinetics, hydrate assemblage and microstructural development of alkali activated blast-furnace slags. Cement Concr. Res. 41 (3), 301–310. https://doi.org/10.1016/j.cemconres.2010.11.016.
Haha, M.B., Lothenbach, B., Le Saout, G., Winnefeld, F., 2012. Influence of slag chemistry on the hydration of alkali-activated blast-furnace slag — part II: effect of al2o3. Cement Concr. Res. 42 (1), 74–83. https://doi.org/10.1016/j.cemconres.2011.08.005.
Heldal, T., Neeb, P.R., 2000. Natural stone in Norway: production, deposits and developments. Norges geologiske. Undersøkelse Bulletin 436, 15–26.
Hewlett, P.C. (Ed.), 2001. Lea's Chemistry of Cement and Concrete, fourth ed. Butterworth-Heinemann, Oxford, UK.
Jain, K.L., Sancheti, G., Gupta, L.K., 2020. Durability performance of waste granite and glass powder added concrete. Construct. Build. Mater. 252, 119075.
Jingming, C., Xiaopeng, L., Jiawei, T., et al., 2020. Thermal and compressive behaviors of fly ash and metakaolin-based geopolymer. J. Build. Eng. 30, 101307.
Kamali, M., Khalifeh, M., Saasen, A., 2022. Bonding mechanism of zonal isolation materials to clean and rusted casing. SPE J. 1–15. https://doi.org/10.2118/209812-pa.
Kovler, 2012. 8 – radioactive materials. In: Toxicity of Building Materials. Woodhead Publishing, Essay, pp. 196–240.
Luukkonen, T., Abdollahnejad, Z., Yliniemi, J., et al., 2018. One-part alkali-activated materials: a review. Cement Concr. Res. 103, 21—34.
Ma, C., Zhao, B., Guo, S., Long, G., Xie, Y., 2019. Properties and characterization of green one-part geopolymer activated by composite activators. J. Clean. Prod. 220, 188–199. https://doi.org/10.1016/j.jclepro.2019.02.159.
Mahya, A., Zhong, T., Bijan, S., et al., 2019. Mix composition and characterization of one-part geopolymer with different activators. Journal of Construction and Building Materials 225, 526—537.
Moosberg-Bustnes, H., Lagerblad, B., Forssberg, E., 2004. The function of fillers in concrete. Mater. Struct. 37 (2), 74–81. https://doi.org/10.1007/bf02486602.
Myers, J.S., Watkins, K.P., 1985. Origin of granite-greenstone patterns, yilgarn block, western Australia. Geology 13 (11), 778–780.
Nath, P., Sarker, P.K., 2014. Effect of GGBFS on setting, workability and early strength properties of fly ash geopolymer concrete cured in ambient condition. Construct. Build. Mater. 66, 163–171.
Oderji, S.Y., Chen, B., Shakya, C., Ahmad, M.R., Shah, S.F., 2019. Influence of superplasticizers and retarders on the workability and strength of one-part alkali-activated fly ash/slag binders cured at room temperature. Construct. Build. Mater. 229, 116891 https://doi.org/10.1016/j.conbuildmat.2019.116891.
Omran, M., Paiva, M., Khalifeh, M., 2022a. Design and early age performance of one-Part Rock-based geopolymer for oil well cementing operations. SPE J. (Submitted, Under review).
Omran, M., Khalifeh, M., 2023. Development of one-part rock-based Geopolymers for downhole cementing applications. Journal of Energy Resources Technology 145 (10). https://doi.org/10.1115/1.4062250.
Omran, M., Khalifeh, M., Saasen, A., 2022b. Influence of Activators and Admixtures on Rheology of Geopolymer Slurries for Well Cementing Applications. SPE-210698-MS, Presented at the SPE Asia Pacific Oil & Gas Conference and Exhibition 2022. Adelaide, Australia. https://doi.org/10.2118/210698-MS, 17 – 19 Oct 2022.
Omran, M., Paiva, M., Khalifeh, M., 2023. Design and Early Age Performance of Sustainable One-Part Rock-based Geopolymers. SPE Journal (SJ-1222-0039, Under review).
Rosing-Schow, N., Andersen, T., Müller, A., 2022. Lead isotopes and the sources of granitic magmas: the sveconorwegian granite and pegmatite province of southern Norway. Minerals 12 (7), 878.
Saha, S., Rajasekaran, C., 2017. Enhancement of the properties of fly ash based geopolymer paste by incorporating ground granulated blast furnace slag. Journal of Construction and Building Material 146, 615—620.
Sasaki, K., Kurumisawa, K., Ibayashi, K., 2019. Effect of retarders on flow and strength development of alkali-activated fly ash/blast furnace slag composite. Construct. Build. Mater. 216, 337–346.
Shang, X., Zhang, Z., Xu, X., Liu, T., Xing, Y., 2019. Mineral composition, pore structure, and mechanical characteristics of pyroxene granite exposed to heat treatments. Minerals 9 (9), 553.
Shilar, F.A., Ganachari, S.V., Patil, V.B., Nisar, K.S., Abdel-Aty, A.H., Yahia, I.S., 2022. Evaluation of the effect of granite waste powder by varying the molarity of activator on the mechanical properties of ground granulated blast-furnace slag-based geopolymer concrete. Polymers 14 (2), 306.
Singh, N.B., Middendorf, B., 2020. Geopolymers as an alternative to Portland cement: an overview. Construct. Build. Mater. 237 (117455).
Sturm, P., Gluth, G.J.G., Brouwers, H.J.H., et al., 2016. Synthesizing one-part geopolymers from rice husk ash. Journal of Construction and Building Materials 124, 961–966. https://doi.org/10.1016/j.conbuildmat.2016.08.017.

Appendix 4 – Paper II

Development of Low Carbon Dioxide Intensive Rock-Based Geopolymers for Well Cementing Applications – One-Part Geopolymer

Mohamed Omran & Mahmoud Khalifeh

Peer-reviewed conference paper presented at the ASME 2022 41st International Conference on Ocean, Offshore and Arctic Engineering, Hamburg, Germany, 5–10 June

DOI: https://doi.org/10.1115/OMAE2022-78535.

This paper is not available in Brage due to copyright.

Appendix 5 – Paper III

Development of One-Part Rock-Based Geopolymers for Downhole Cementing Applications

Mohamed Omran[1]
Department of Energy and Petroleum Engineering (IEP),
University of Stavanger,
Kjølv Egelands House,
Kristine Bonnevies vei 22,
Stavanger 4021, Norway
e-mail: mohamed.a.omran@uis.no

Mahmoud Khalifeh
Department of Energy and Petroleum Engineering (IEP),
University of Stavanger,
Kjølv Egelands House,
Kristine Bonnevies vei 22,
Stavanger 4021, Norway
e-mail: mahmoud.khalifeh@uis.no

The use of geopolymers as a full replacement for cement in oil well cementing applications requires the development of not only environmentally friendly but also user-friendly cementitious materials. This study aims to investigate the early-age mechanical and chemical properties of synthesized one-part geopolymers, which are heat-cured rock-based products. These geopolymers were synthesized from granite-based precursors and were activated by solid powders of potassium silicate, with a small portion of potassium hydroxide (KOH) as an accelerator to enhance the setting time and early strength. The mechanical and chemical properties of the one-part geopolymers were characterized, and the mineralogy of the solidified samples was analyzed through crystallography to better understand their microstructure. The study found that the investigated one-part geopolymer mixes, which were activated by a solid activator with a modulus ratio of 2.4, developed acceptable compressive strength of around 7 to 13 MPa within 24 h and up to 7 days. The use of one-part geopolymers has the potential to provide environmentally- and user-friendly slurries that can facilitate their utilization for large-scale in-situ applications in the petroleum and civil engineering sectors. [DOI: 10.1115/1.4062250]

Keywords: geopolymer review, well integrity, water content, chemical admixture, just add water, petroleum engineering, petroleum wells-drilling/production/construction

Downloaded from http://asmedigitalcollection.asme.org/energyresources/article-pdf/145/10/103201/7008056/ert_145_10_103201.pdf by Stavanger University user on 26 July 2023

1 Introduction

The demand for Ordinary Portland Cement (OPC) and the consumption of limestone reserves are increasing very rapidly. These demands besides the high increases in carbon taxes have been tightly challenging the concrete industry on daily basis [1]. Several mandatory carbon emissions reduction policies have been introduced by governments and regulators. These regulations are to support the cementing industry toward more focusing on stimulating investment and innovation by researching and adopting these carbon emissions reduction policies [2,3]. OPC production and processing operations are dependent on the decarbonation of limestone and fuel used during the calcination and production of cement which releases high carbon dioxide emissions. OPC has been considered one of the main contributors to global carbon dioxide emissions with up to 8% [4,5]. It is very viable to develop low-carbon and low-energy types of cement alternatives to reduce the greenhouse effect [4,5]. Geopolymers are a type of cementitious material with the potential to fully replace OPC while having the potential to significantly reduce carbon dioxide emissions. In a study by McLellan et al. [6], the costs and greenhouse gas emissions of geopolymers were compared to OPC. The study found that geopolymer emits between 14 and 97 wt% less carbon dioxide than OPC. However, there is some uncertainty surrounding this finding due to the difficulty distinguishing between geopolymers and alkali-activated-based types of cement [7].

According to Duxson et al. [8], geopolymers are considered third-generation cement after OPC and lime. The term "geopolymer" generally refers to partially amorphous and partially crystalline solid aluminosilicate materials in tetrahedral form, also known as inorganic polymers. Some researchers do not distinguish between geopolymers and alkali-activated cement. Geopolymers are low calcium content systems consisting of sialate monomers as repeating units (O–Si–O–Al–O). Several solid aluminosilicate materials such as feldspar, metakaolin, industrial residues, and solid wastes have been utilized as solid geopolymer precursors. However, these precursors have different reactivity depending on their chemical composition, mineralogy, morphology, and fineness [8,9]. The main criteria for producing and developing stable geopolymer is the solid precursor should be highly amorphous or reactive, have consistent chemical composition, and have low water content demand with a water-to-solid precursor ratio of less than 0.4 [10,11].

Geopolymer could be designed to obtain desired mechanical properties compared to OPC, including higher acidic attack resistance, heat resistance, higher mechanical strength, and lower chemical shrinkage [12,13]. Furthermore, it is important to prepare and select each component's proper type and dose, such as alkali-silicate activator, precursors, and admixtures [14]. Moreover, geopolymer technology could be useful for allowing waste beneficiation routes, known as circular economy, for using various industrial wastes and unused by-products [15,16]. However, supply chain availability for geopolymer precursor materials, suitable admixtures for these materials, and examining protocols are still inadequate to be generalized and standardized globally [17].

Binders were mainly formed from the chemical reaction between the alkali activation source and the aluminosilicate precursor, which were patented in 1908 by Kuhl [18]. Afterward, several pioneering developments were done by Glukhovsky [19], Krivenko [20], Davidovits [21], and Palomo et al. [22], respectively. Table 1 presents some historical reviews and recent overview articles on geopolymer and alkali-activated materials.

Various types of raw materials have been utilized for synthesizing geopolymers, which may contain other types of synthetic powder precursors [29]. In the context of geopolymer synthesis, the most commonly used materials as powder precursors are metallurgical slags and fly ash. Metallurgical slags such as blast furnace slags (Ground Granulated Blast Furnace Slag, GGBFS) are mixtures of poorly crystalline materials with depolymerized calcium silicate glasses to control the strength development profile as is

[1]Corresponding author.

Contributed by the Petroleum Division of ASME for publication in the JOURNAL OF ENERGY RESOURCES TECHNOLOGY. Manuscript received January 3, 2023; final manuscript received February 24, 2023; published online April 17, 2023. Assoc. Editor: Lukasz Szablowski.

Copyright © 2023 by ASME; reuse license CC-BY 4.0

Table 1 Examples of published literature reviews and articles on alkali-activated materials and geopolymers

Title	Significant outputs
Mechanism of geopolymerization and factors influencing its development: a review [23]	A review of the development of geopolymers, including chemical reactions, source materials roles and effects, and mix compositions and combinations.
Alkali-activated binders: A review; (Part 1) historical background terminology reaction mechanisms and hydration products [24]; (Part 2) About materials and binders manufacture [25]	A general review of alkali-activated binders, including historical background, terminology, hydration products, materials and binders manufacture, and properties and durability
Mechanism and chemical reaction of fly ash geopolymer cement: A review [26]	An overview of utilization of fly ash geopolymer cement as alkali-activated binders
Geopolymer concrete: A review of some recent developments [10]	A review of utilization and development of geopolymer concrete as a potential construction material in several applications
Materials for optimized P&A performance: Potential utilization of geopolymers [27]	Development and utilization of rock-based geopolymers for zonal isolation and well abandonment were presented. Viscosity, pumpability, fluid loss, strength development, and durability of the geopolymers were studied
One-part alkali-activated materials: A review [28]	A review of the currently published state-of-art in the development of one-part geopolymer admixtures, including the employed solid precursors, activators, admixtures, mixing designs, and resulting binding materials

done in OPC [30]. Fly ash (FA) is a mixture of clay, sand, and organic matter that is presented in coal, produced as a by-product during the combustion process. These compounds are melted in a furnace and then quenched rapidly in air to obtain small spherical particles [31].

In geopolymer synthesis, there are two main classes for FA that can be used, which are dependent on their calcium content; Class F contains low calcium according to ASTM C618, and Class C contains high calcium content. However, Class C FA is rarely utilized in geopolymer synthesis as Class C could be classified compositionally comparable to some mixtures of Class F and GGBFS [32,33]. Moreover, fly ash class F and GGBFS mixtures are more preferred in the synthesis of geopolymers, where Class C fly ash is less abundant than fly ash Class F [7,10].

The nomenclature and terminology regarding geopolymers and alkali-activated materials are still subject to ongoing debates in the literature. The former is characterized by a three-dimensional tetrahedral silica structure with high content Q4(2Al) and Q4(3Al) centers and low calcium content. In contrast, the latter is characterized by lower silicon coordination, which is Q2 and Q2(1Al) centers, and higher calcium content [34].

Conventional geopolymers, also referred to as two-part geopolymers, are typically produced by partially dissolving solid precursors containing reactive aluminosilicates (known as part one) in a concentrated alkali solution. The alkali solution can include alkali silicate, carbonate, sulfate, or a combination of these compounds, which act as part two of the reaction [35,36]. However, the use of highly alkaline or alkaline silicate solutions poses logistical and environmental challenges. Thus, the development of one-part geopolymers that only require the addition of water has become crucial in recent years [9].

Purdon [37] prepared a mortar mixture by dry mixing sodium hydroxide powder, and slag and then adding water. A patent in the 1980s presented a dry mixture of metakaolin, amorphous silica, furnace slag, potassium silicate, and hydroxide, in addition to adding either fly ash, or calcined clay before and then adding water [38]. Another patent showed a mixture of amorphous silica from fly ash with sulfuric or hydrochloric acid [39].

In the 1970s, Davidovits conducted research on the formulation of one-part geopolymers by reacting metakaolin, alkali metal disilicate, and slag. He proposed the capability that sodium or potassium silicate powder could be used as solid activators due to their wide availability and unique activation properties [40].

Duxson and Provis [9] have presented other general specifications and approaches for one-part geopolymer mixtures. For instance, precursors can be prepared by melting feldspar with high calcium content before the combustion process. Reducing the amount of water in the mixture is also desired to conserve concrete properties and improve environmental sustainability. A lower water-to-binder ratio results in lower porosity and permeability of the concrete. As a result, a one-part geopolymer design should have a low water-to-binder ratio and fine spherical particles [7].

Currently, two-part geopolymers have been implemented in various large-scale applications in Australia and Ukraine as evidenced by studies [28,41]. However, the challenges regarding the transportation and handling of corrosive alkaline solutions needed for mixing conventional geopolymers are a major drawback. These challenges highlight the importance of not only environmentally friendly cementing materials but also to be user-friendly ones. Thus, the development of user-friendly geopolymers is a crucial strategy to facilitate the utilization of geopolymers as a full replacement of cement for oil well cementing applications.

One-part "just add water" geopolymers are user-environmentally friendly cementing materials. They are more promising for in-situ applications due to overcoming the impracticalities of conventional two-part geopolymers [17,35,42]. However, they still need extensive investigations and developments to be more applicable for industrial use.

In this article, the aim is to provide a prior state-of-the-art in the development of one-part rock-based geopolymer mixtures. This study discusses the early-age effect of water content and four different chemical admixtures on the geopolymerization mechanisms, hydrated products, and their mechanical properties.

2 Materials and Methods

This study involves the solid phase, which consists of precursors, a solid activator, and admixtures, and the liquid phase, which contains deionized water and an accelerator. The precursors are obtained from granite rock and by-product materials. For the solid activator, anhydrous potassium silicate in powder form with a molar ratio (MR) of 3.92 was utilized. Four admixtures are used in this study: sodium hydroxide in pellet form, calcium carbonate in powder form, calcium oxide in powder form, and zinc oxide powder. Additionally, a small amount of 12M potassium hydroxide (KOH) solution is used as an accelerator. The chemical composition of the neat recipe (granite is a source of aluminosilicate, GGBFS is a calcium- and magnesium-rich material and amorphous aluminosilicate, and microsilica is a pure amorphous silicate material) is shown in Table 2, indicating the weight percentage of the three precursors in the mixture. The mineralogy of the precursors has been studied in detail [27,43–45].

2.1 Experimental Equipment. *API Mixer—A high-shear API cement blender was used for mixing all the components to form the slurry in each experiment following API 10B-2* [27].

Curing of samples—All samples were heat cured in an oven at 70 °C Bottom hole circulating temperature (BHST). The samples

Downloaded from http://asmedigitalcollection.asme.org/energyresources/article-pdf/145/10/103201/7000306/er_145_10_103201.pdf by Stavanger University user on 26 July 2023

Table 2 Chemical composition of the precursor in wt%

Chemical composition (wt%)	SiO_2	Al_2O_3	Fe_2O_3	MgO	CaO	Na_2O	K_2O	TiO_2	MnO	LOI[a]
Precursor mix	56.63	12.47	1.09	6.23	16.45	1.77	2.87	1.16	0.29	0.6

[a]Loss on ignition.

were cured inside cylindrical plastic molds and covered with plastic lids.

Uniaxial compressive strength (UCS)—A cutter machine was used to flatten both sides of the samples to be prepared for running UCS. The dimensions of these samples were 51 mm in diameter and about 80-85 mm in height. UCS tests were performed following API Spec 10A [46]. *The samples were placed under compression using a mechanical tester with a loading rate of 10 kN/min.*

Sonic Strength—To measure the sonic strength of the materials, an ultrasonic cement analyzer (UCA) specified in API 10B-2 [27] was employed to measure sonic strength development by use of sonic impedance at 14 MPa and 70 °C for 7 days. The equipment is designed and calibrated to test OPC [47]. Therefore, for any new material, new algorithms should be generated and applied in the custom algorithm option. The same equipment was used for all the materials to minimize any errors in the system.

Compositional Analysis—The accuracy of X-ray diffraction (XRD) data is dependent on various parameters including XRD instrumental intensity, time-steps, incremental angle, testing conditions, etc. In this study, XRD samples were dried in an oven at 30 °C overnight. Afterward, these specimens were kept in a vacuum dryer for one day to maximize the removal of water particles and to prepare them for XRD testing.

The crystalline phases of the sample were analyzed by a Bruker-AXS Micro-diffractometer D8 Advance, which uses CuKα radiation (40.0 kV, 25.0 mA) with a 2θ range from 5 deg to 92 deg with 1 deg/min step and 0.010 deg increment. The main crystalline XRD patterns have been highlighted and investigated. EVA v5 software was used to analyze the crystalline components and to estimate the degree of crystallinity.

Table 3 Mix design for the given rock-based 1P GP

Mix design name[a,b]	Additives (wt%)	Additives in millimoles
W1P[c]	Non	Zero
W1Pb	Non	Zero
W1Pb-C02	0.14 wt% CaO	35.71
W1Pb-C04	0.57 wt% CaO	71.43
W1Pb-C06	0.86 wt% CaO	107.14
W1Pb-C08	1.14 wt% CaO	142.86
W1Pb-C2	0.14 wt% CaCO3	19.98
W1Pb-C4	0.57 wt% CaCO3	39.96
W1Pb-C6	0.86 wt% CaCO3	59.94
W1Pb-C8	1.14 wt% CaCO3	79.92
W1Pb-Z2	0.14 wt% ZnO	24.57
W1Pb-Z4	0.57 wt% ZnO	49.14
W1Pb-Z6	0.86 wt% ZnO	73.71
W1Pb-Z8	1.14 wt% ZnO	98.28
W1Pb-N2[d]	0.14 wt% NaOH	50.03
W1Pb-N4[d]	0.57 wt% NaOH	100.07
W1Pc[e]	Non	Zero

[a]All recipes had the same Activator and Accelerator to Solid precursors ratio, 0.20.
[b]All recipes had the same free water content, 88.19 wt% in the liquid phase.
[c]W1P has 35 wt% liquid-to-solid ratio. However, all W1Pb recipes have 33 wt% liquid-to-solid ratio.
[d]The addition of NaOH pellets was considered as a partial substitution to the KOH solution to conserve MR = 2.4.
[e]W1Pc has the same mix design as W1Pb with a solid accelerator either KOH or NaOH pellets instead of the liquid accelerator. The addition of these hydroxide pellets was considered as a complete substitution to the KOH solution with conserving MR at 2.4.

2.2 Experimental Procedures.

The candidate recipes were mixed in the laboratory according to the recommended procedures [27,43,46,48]. The mixing procedures for all recipes were as follows: the precursors were mixed including chemically normalized components. The activator was a potassium silicate anhydrous powder with a molar ratio (MR = SiO2/K2O) of 3.9. A small portion of potassium hydroxide 12M solution (as an accelerator) was used to lowering down the molar ratio to 2.4.

2.2.1 Mixing. Mix design entails preparing the solid and liquid phases of the neat recipe, with and without adding admixtures to the solid phase, and at the end, combining all of them by blending. First, having obtained enough components, solids and liquids are mixed separately in a clean bucket and plastic container, respectively. Regarding admixtures, for each experiment, each admixture in powder form between 0.14 and 1.14 wt% equivalent to the solid precursor was added to the solid phase in the initial mix design. Table 3 presents the type and total amount of additives added to the rock-based geopolymer with their recipes' names.

3 Results and Discussion

3.1 Uniaxial Compressive Strength Test.

All recipes in Table 3 were investigated for Uniaxial compressive Strength (UCS); each recipe includes three samples for each mix design, which were prepared and cured at 70 °C, at atmospheric pressure. All samples were tested after 1 day of curing. Furthermore, the top 1-day UCS recipes were also investigated after 7 days of curing. Figures 1–5 present the average compressive strength of the materials given in Table 3 after a 1-day curing period. Moreover, the top comparable recipes (with 0.14 wt% chemical admixture) from 1-day UCS results in addition to W1P (W1P-35%) were selected for further investigation for 7-day UCS data as shown in Figs. 6 and 7, respectively. One should note that 1-day strength development is critical for drilling purposes. Therefore, it was considered in this work.

UCS results show the effect of water content on the given mix design as shown in Fig. 1. It has been suggested that water only provides a medium for the dissolution and restructuring of aluminosilicate sources into geopolymer [49]. The given one-part rock-based

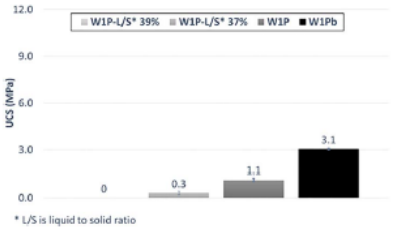

Fig. 1 The effect of water content on 1-day UCS

Downloaded from http://asmedigitalcollection.asme.org/energyresources/article-pdf/145/10/103201/7008036/ert_145_10_103201.pdf by Stavanger University user on 26 July 2023

Fig. 2 The effect of chemical admixture CO on 1-day UCS

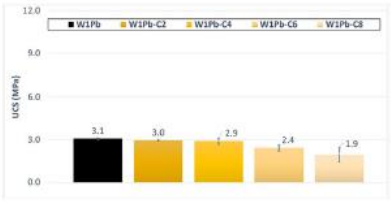

Fig. 3 The effect of chemical admixture C on 1-day UCS

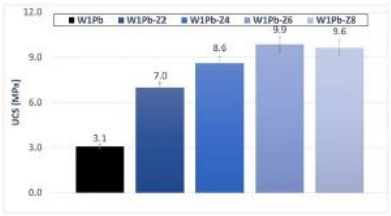

Fig. 4 The effect of chemical admixture Z on 1-day UCS

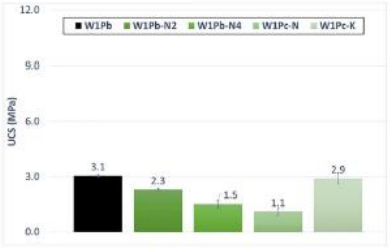

Fig. 5 The effect of NaOH and KOH pellets on 1-day UCS

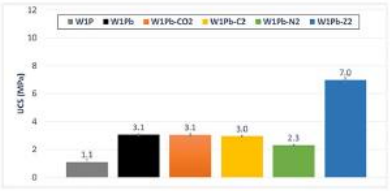

Fig. 6 The effect of various 0.14 wt% chemical admixtures on 1-day UCS

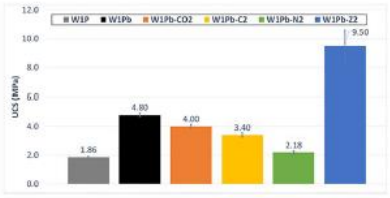

Fig. 7 The effect of various 0.14 wt% chemical admixtures on 7-day UCS

geopolymer recipes with higher water content than the 35% liquid-to-solid ratio could not set nor develop any reliable compressive strength within 1-day of heat curing at 70 °C. In addition, W1P (35% w/s, grey color bar) was much weaker than W1Pb (33% w/s, black color bar). The higher the water content, the lower the 1-day and 7-day UCS. W1Pb has almost triple the UCS value of W1P in agreement with the negative effect of water content on the geopolymer system in the literature [49].

Various chemical admixtures were added to the neat recipe to investigate each chemical admixture and its content on the neat one-part rock-based geopolymer recipe, W1Pb. A trend was obviously to be detected as the higher the content of chemical admixture the lower the 1-day UCS for chemical admixtures CaO, CaCO3, and NaOH. Therefore, with higher chemical admixtures content, it has also a negative effect on 1-day UCS and early strength development.

In the case of the addition of NaOH Pellets, both partial and complete replacement of the accelerator solution by NaOH pellets had a severe decrease in 1-day UCS (Fig. 5). This effect was observed to lose down to two-thirds of the UCS of W1Pb. This could happen due to the substitution of the KOH accelerator solution with NaOH pellets by conserving the modulus ratio at 2.4. However, the rate of dilution of NaOH pellets is much slower than the utilization of any alkali solution with free ions. NaOH pellets need a longer time to be dissolved in the distilled water medium to be fully activated or so-called concentrated water for the 1P GP system. While the complete replacement of the KOH liquid accelerator by KOH pellets had a comparable 1-day UCS with the neat recipe W1Pb.

Unlike the other chemical admixtures, the utilization of chemical admixture Z has a weight content threshold to reach the highest 1-day UCS of 10 MPa after the addition of 0.86wt% Z to neat recipe W1Pb and then 1-day UCS decreased with higher Z content. A similar trend was also observed by Ali [50] and Zailan et al. [51].

Zinc oxide is partially soluble in an alkaline medium, but its solubility increases at elevated temperatures up to 100 °C [52]. It is an amphoteric oxide, formed by bonding the cation Zn^{+2} with the anion O^{-2}. These elements can be presented in two possible structures: cubic and hexagonal as shown in Fig. 8.

Downloaded from http://asmedigitalcollection.asme.org/energyresources/article-pdf/145/10/103201/7009036/er1_145_10_103201.pdf by Stavanger University user on 26 July 2023

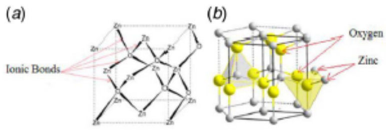

Fig. 8 Structures of ZnO: (a) cubic and (b) hexagonal [51]

ZnO can with MOH (M = K or Na) produce $ZnOH^+$, $Zn(OH)_3^-$, and $Zn(OH)_4^{-2}$ within the alkali pH range up to pH 14. At a high alkaline medium, the reaction between zinc oxide and alkali metal hydroxides (Am) produces two zincate-based anions: $MZn(OH)_3$ and $M_2Zn(OH)_4$. Figure 9 shows the chemical structure of Zincate [Zn (OH)3-]n polymeric anion. The presence of Zincate anions within the geopolymerization reaction may promote more favorable geopolymerization products

$$MOH + ZnO + H_2O = MZn(OH)_3 \quad (1)$$

$$2MOH + ZnO + H_2O = M_2Zn(OH)_4 \quad (2)$$

Other researchers observed not only a decrease in UCS at high concentrations of zinc oxide but also a threshold of the addition of zinc oxide to increase the compressive strength. Zinc oxide has been observed to play a role in the polycondensation phase by creating a more basic environment in the geopolymer system [51,53]. In a study by Zailan et al. [51], it was found that low concentrations of ZnO could fully control the formation of K(N)–A–S–H or C–A–S–H gels, from the complete geopolymerization reaction. It was also observed that more K(N)–A–S–H gel was formed than C–A–S–H gel during the geopolymerization process due to the low calcium content in the raw. However, it should be noted that these gel phases are indications of an incomplete geopolymerization reaction.

At higher concentrations of ZnO, UCS reduction could be due to the negative action of ZnO on the geopolymeric system, which might affect the condensation process and inhibit the formation of geopolymer gels [51]. The water molecules released during geopolymerization could introduce in reduction potential reaction with ZnO as shown in the following reversible chemical reaction [51]:

$$ZnO + H_2O + 2e^- \rightleftharpoons Zn_{(s)} + 2OH^- \quad (3)$$

Therefore, the utilization of low concentrations of ZnO can improve the chemical kinetics of geopolymerization reaction to get higher and earlier strength development as observed for the addition of 0.14 wt% (equivalent to 25 mmol) up to 0.86 wt% (equivalent to 74 mmol) of ZnO to neat recipe W1Pb in Fig. 4.

3.2 Nondestructive Compressive Strength. According to API standards [48], the cement should harden after the well placement process within the first 12–24 h more than 3.5 MPa (500 psi) as a minimum requirement for UCA and UCS. In this study, 6.89 MPa (1000 psi) is considered an acceptable UCA and UCS of the given mix design for oil well cementing applications.

The given algorithms provided by UCA have been developed for OPC, and they are not reliable for estimating the strength

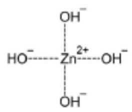

Fig. 9 Chemical structure of Zincate-based anion

Table 4 A polynomial equation for one-part rock-based geopolymers to estimate sonic strength from transit time data [11]

Mix design	Polynomial equation	R-Square value
W1P	$Y = 211.28X^2 - 6220X + 45677$	$R^2 = 96.12\%$

development of other materials such as one-part rock-based geopolymers [47,54].

The estimated sonic strengths showed that the development of algorithms to estimate the sonic strength from transit time is important. The speed of the compressional sonic wave is strongly affected by the chemistry of the under-investigated geopolymers [47].

A new empirical equation was developed by plotting the average compressive strength values versus measured transit time by the UCA equipment [11]. The equation is a polynomial equation for one-part rock-based geopolymers (Table 4).

Figures 10 and 11 present the sonic strength development curves based on the generated polynomial equation in Table 4.

Table 5 presents setting time data to reach 50 and 500 psi, besides, sonic strength data that has been observed after 1- and 7 days.

The estimated UCA data agree with the measured UCS values for the top candidate recipes for 1- and 7-day UCS as given in Figs. 6, 7 and 11. In Table 5, W1Pb-Z2 has the shortest time to reach 0.35 and 3.5 MPa. W1P with higher water content has the longest time to reach 0.35 and 3.5 MPa, which it was taking up to 19 days to reach 3.5 MPa. However, W1Pb was taking just one hour and six

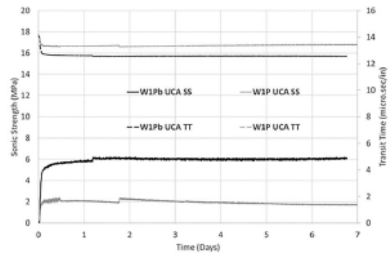

Fig. 10 UCA Data for the net recipe with two different water content, samples cured up to 7 days

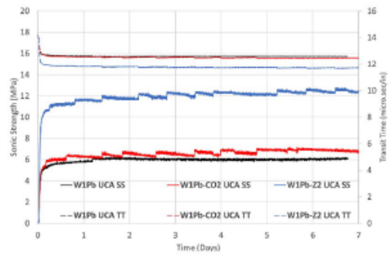

Fig. 11 UCA Data for samples containing 0.14 wt% chemical admixtures, cured up to 7 days

Downloaded from http://asmedigitalcollection.asme.org/energyresources/article-pdf/145/10/103201/7009386/jert_145_10_103201.pdf by Stavanger University user on 26 July 2023

Table 5 Summary of UCA data for the selected 1P GP recipes

Mix design	Setting time (min) to 0.35 MPa (50 psi)	Setting time (min) to 3.5 MPa (500 psi)	SS (MPa) for 1 day	SS (MPa) for 7 days
W1P	46	27,540	1.68	2.11
W1Pb	40	66	5.85	6.10
W1Pb-CO2	38	60	6.22	6.74
W1Pb-Z2	37	47	11.55	12.76

minutes to reach the same sonic strength value. This shows and proves the severe effect of water content on geopolymers as shown in Fig. 10 and Table 5.

Furthermore, the estimated sonic strength for 1- and 7-day is slightly higher than the measured compressive strength for 1- and 7-day UCS. This could be due to the addition of pressure ca. 13.8 MPa while curing in UCA; however, the UCS samples were cured at ambient pressure [55].

3.3 Composition Analysis, X-Ray Diffraction. Generally, geopolymers are known to contain amorphous content, especially at low curing temperatures; however, the amorphous content is diminished at elevated curing temperatures [11,36,56–58]. Khalifeh et al. [57] studied the mineralogy of rock-based geopolymers synthesized by the use of potassium silicate solution as an activator. They found that quartz was a major phase, and albite and microcline were minor phases.

Figure 12 presents the peaks observed in the spectra of the given geopolymer precursors. It shows the phases originally found in the rock precursors of the granite, GGBFS, and microsilica, where granite has high crystalline content of up to 80%. On the other hand, GGBFS and microsilica are considered for their highly amorphous content and observable amorphous hump as given in Fig. 12. For GGBFS, akermanite crystalline mineral could be barely detected in addition to other trace minerals/contaminants. However, in the case of microsilica, there was not any detectable crystalline peak as shown in Fig. 12.

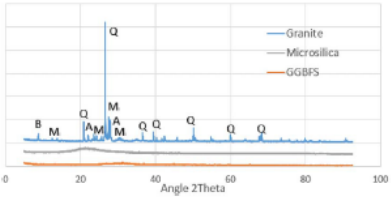

Fig. 12 Compositional analysis XRD for 1P GP precursor components

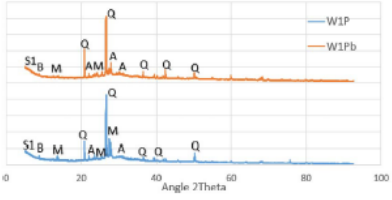

Fig. 13 XRD Compositional analysis for W1P versus W1Pb

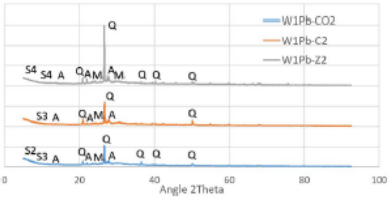

Fig. 14 XRD Compositional analysis for W1Pb* recipes

Granite main peaks correspond to quartz (SiO_2), microcline as an alkali feldspar ($KAlSi_3O_8$), and albite as a plagioclase feldspar ($NaAlSi_3O_8$). In addition, the precursor also contains biotite ($K(Mg,Fe)_3AlSi_3O_{10}(F,OH)_2$). However, Biotite mineral is not found or neglected in the spectra of any of the finished products as shown in Figs. 13 and 14. Table 6 indicates the computed crystalline and amorphous content for granite, the two neat recipes, and the developed recipes with chemical admixtures.

XRD Analysis shows similar patterns for the neat samples of the same original composition in Figs. 12 and 13. Figure 13 shows negligible major changes can be observed over the 7 days of curing, and no significant differences were found because of the differences in water content between W1P and W1Pb. Both neat recipes contain Quartz, Albite, Microcline, and tracers of Biotite and synthetic potassium aluminum-silicates hydrates (S1), but W1Pb has lower microcline and biotite content than W1P.

Figure 14 presents the differences in the compositional analysis of W1Pb with the 0.14wt% chemical additives of calcium oxide (CO), calcium carbonate (C), and zinc oxide (Z). These W1Pb* modified recipes also have Quartz, Albite and Microcline similar to the W1Pb neat, in addition to three synthetic crystals or hydrates. W1Pb-CO2 has two synthetic hydrates as tracers are Potassium–Sodium–Calcium–Aluminum–Silicate hydrates (S2) and Sodium–Calcium–Magnesium–Aluminum–Silicate hydrates (S3). W1Pb-C2 has tracers of synthetic Sodium–Calcium–Magnesium–Aluminum–Silicate hydrate (S3) only. While W1Pb-Z2 has just tracers of Potassium Zinc Aluminum–Silicate hydrates (S4).

Two trends were visible in the geopolymer samples. Over time, the composition changes slightly, and the presence of feldspar reduces in agreement with [11,36,56,57] and the presence of synthetic hydrates as a function of each added chemical admixture

Table 6 Degree of crystallinity analysis for granite and the selected recipes

Mix design	Crystallinity (%)	Amorphousity (%)
Granite	79.9	20.1
W1P	52.1	47.9
W1Pb	51.7	48.3
W1Pb-CO2	53.2	46.8
W1Pb-C2	50.1	49.9
W1Pb-Z2	53.0	47.0

Downloaded from http://asmedigitalcollection.asme.org/energyresources/article-pdf/145/10/103201/7009036/er_145_10_103201.pdf by Stavanger University user on 26 July 2023

even if as tracers. For W1P and W1Pb cured at 70 °C, there were little peaks of feldspar crystals after the 7 days of curing (Fig. 13). Similarly, W1Pb* recipes also have little trace of feldspar crystals after 7 days of curing, while the main peak of Biotite seemed to be diminished over the 7 days of heat curing (Fig. 14).

Therefore, this can suggest a chemical reaction between the geopolymer, chemical admixtures, and the feldspars (Albite and Microcline) present in the precursor. The absence of biotite in all products may also suggest a chemical reaction between the mixtures and biotite, but this absence can also be related to a lesser amount of biotite relative to that total in the final mix, thus making it difficult to differentiate in the XRD spectra.

The results also indicate that different types of feldspar react differently with and without the chemical admixtures put into the geopolymers. In addition, three new synthetic hydrates were observed after the addition of the investigated chemical admixtures (CO, C, and Z).

Further examinations and future studies are still needed to fully understand these complex chemical investigations and their economic feasibility. These studies should investigate and verify the geopolymerization process of these one-part geopolymer recipes, especially after adding ZnO as a strength booster. This investigation can be done by studying each stage of the geopolymerization reaction and by integrating other physical and chemical characterizations.

4 Conclusion

The development of an applicable mix design for one-part geopolymers is crucial to fit for offshore oil well cementing applications. The investigated geopolymers were heat-cured rock-based one-part recipes. They can be eligible for the development of short-term mechanical and chemical properties of cementing material. The developed W1Pb-Z recipes have the potential to be utilized in well construction and well abandonment applications. Furthermore, the higher water content in the one-part rock-based geopolymer system negatively affected the early strength development and setting time. Moreover, the higher the concentration of the given chemical admixtures, the lower the 1-day strength development. The top candidate recipes were having lower water content and especially with lower concertation of ZnO chemical admixture, as ZnO might have a role in the polycondensation phase in the geopolymer system. This can be due to the formation of the polymeric anions of zincate. Thus, ZnO can be considered an early strength development booster. Further investigations are still needed to fully understand the complexity behind the one-part rock-based geopolymerization process.

Acknowledgment

The authors gratefully acknowledge TotalEnergies, AkerBP, ConocoPhillips, and the Research Council of Norway for financially supporting the SafeRock KPN Project (RCN #319014) at the University of Stavanger, Norway. In addition, the authors would like to acknowledge Ms. Mya Chordar for her lab contribution.

Conflict of Interest

There are no conflicts of interest.

Data Availability Statement

The data sets generated and supporting the findings of this article are obtainable from the corresponding author upon reasonable request.

Nomenclature

Acronyms

- A = albite
- C = calcium carbonate
- CO = calcium oxide
- CuKα = copper k-alpha radiation
- FA = fly ash
- GGBFS = ground granulated blast furnace slag
- K = potassium
- M = alkali metal
- Mi = microcline
- Mmol = millimoles
- MPa = mega Pascal
- MR = modulus ratio
- N = sodium hydroxide
- Na = sodium
- OPC = Ordinary Portland Cement
- P&A = plugging and abandonment
- Q = quartz
- S1 = synthetic potassium aluminum silicates hydrates
- S2 = synthetic potassium sodium calcium aluminum silicate hydrates
- S3 = synthetic sodium calcium magnesium aluminum silicate hydrates
- S4 = synthetic potassium zinc aluminum silicate hydrates
- SS = sonic strength
- TT = transient time
- UCA = ultrasonic cement analyzer
- UCS = uniaxial compressive strength
- W1Pb* = W1Pb modified recipes with 0.14wt% chemical admixtures
- W1Pc = "Just Add Water" rock-based geopolymer mix design
- XRD = X-ray diffraction
- Z = zinc oxide
- 2θ = two theta angle
- 1P GP = one-part geopolymer

References

[1] Cement industry News and Events From World Cement With the Latest News Updates. World Cement. (n.d.). https://www.worldcement.com/
[2] IEA. (n.d.). Net Zero Emissions by 2050 Scenario (NZE)—Global Energy and Climate Model—Analysis. IEA. https://www.iea.org/reports/global-energy-and-climate-model/net-zero-emissions-by-2050-scenario-nze
[3] Liu, Y., and Rui, Z., 2022, "A Storage-Driven CO2 EOR for a net-Zero Emission Target," Engineering, **18**, pp. 79–87.
[4] Andrew, R., 2021, Review of "Cdiac-ff: Global and National CO2 emissions From Fossil Fuel Combustion and Cement Manufacture: 1751-2017", ESSD-2020-337.
[5] Damtoft, J. S., Lukasik, J., Herfort, D., Sorrentino, D., and Gartner, E. M., 2008, "Sustainable Development and Climate Change Initiatives," Cem. Concr. Res., **38**(2), pp. 115–127.
[6] McLellan, B. C., Williams, R. P., Lay, J., van Riessen, A., and Corder, G. D., 2011, "Costs and Carbon Emissions for Geopolymer Pastes in Comparison to Ordinary Portland Cement," J. Cleaner Prod., **19**(9–10), pp. 1080–1090.
[7] Provis, J. L., and Van Deventer, J., 2009, *Geopolymers: Structures, Processing, Properties and Industrial Applications*, Woodhead, Oxford.
[8] Duxson, P., Fernández-Jiménez, A., Provis, J. L., Lukey, G. C., Palomo, A., and van Deventer, J. S., 2006, "Geopolymer Technology: The Current State of the Art," J. Mater. Sci., **42**(9), pp. 2917–2933.
[9] Duxson, P., and Provis, J. L., 2008, "Designing Precursors for Geopolymer Cements," J. Am. Ceram. Soc., **91**(12), pp. 3864–3869.
[10] Singh, B., Ishwarya, G., Gupta, M., and Bhattacharyya, S., 2015, "Geopolymer Concrete: A Review of Some Recent Developments," Const. Build. Mater., **85**, pp. 78–90.
[11] Omran, M., and Khalifeh, M., 2022, "Development of Low Carbon Dioxide Intensive Rock-Based Geopolymers for Well Cementing Applications—One-Part Geopolymer," Proceedings of the ASME 2022 41st International Conference on Ocean, Offshore and Arctic Engineering. Volume 10: Petroleum Technology, Hamburg, Germany, June 5–10, 2022. p. V010T11A043.
[12] Sagoe-Crentsil, K., Brown, T., and Taylor, A., 2013, "Drying Shrinkage and Creep Performance of Geopolymer Concrete," J. Sustain. Cem. Based Mater., **2**(1), pp. 35–42.
[13] Bakri, A. M., Kamarudin, H., Binhussain, M., Nizar, I. K., Rafiza, A. R., and Zarina, Y., 2013, "Comparison of Geopolymer Fly Ash and Ordinary Portland Cement to the Strength of Concrete," Adv. Sci. Lett., **19**(12), pp. 3592–3595.

Downloaded from http://asmedigitalcollection.asme.org/energyresources/article-pdf/145/10/103201/7000306/ert_145_10_103201.pdf by Stavanger University user on 26 July 2023

[14] Shi, C., Shi, Z., Hu, X., Zhao, R., and Chong, L., 2015, "A Review on Alkali-Aggregate Reactions in Alkali-Activated Mortars/Concretes Made With Alkali-Reactive Aggregates," Mater. Struct., **48**(3), pp. 621–628.
[15] Mehta, A., and Siddique, R., 2016, "An Overview of Geopolymers Derived From Industrial By-Products," Construct. Build. Mater., **127**, pp. 183–198.
[16] Khalifeh, M., Saasen, A., Larsen, H. B., and Hodne, H., 2017, "Development and Characterization of Norite-Based Cementitious Binder From an Ilmenite Mine Waste Stream," Adv. Mater. Sci. Eng., **2017**, pp. 1–7.
[17] Van Deventer, J. S. J., Provis, J. L., and Duxson, P., 2012, "Technical and Commercial Progress in the Adoption of Geopolymer Cement," Miner. Eng., **29**, pp. 89–104.
[18] Kühl, H., 1908, Slag Cement and Process Making the Same, US Patent No. 900,939.
[19] Glukhovsky, V. D., 1959, Soil Silicates. Gostroiizdat Publish, Kiev, 1959.
[20] Krivenko, P. V., 1986, "Synthesis of Cementitious Materials of the Me2O-MeO-Me2O3-SiO2- H2O System With Required Properties," D.Sc. (Eng) thesis, KISI Public, Kiev.
[21] Davidovits, J., 1991, "Geopolymers," J. Therm. Anal., **37**(8), pp. 1633–1656.
[22] Palomo, A., Blanco-Varela, M. T., Granizo, M. L., Puertas, F., Vazquez, T., and Grutzeck, M. W., 1999, "Chemical Stability of Cementitious Materials Based on Metakaolin," Cem. Concr. Res., **29**(7), pp. 997–1004.
[23] Khale, D., and Chaudhary, R., 2007, "Mechanism of Geopolymerization and Factors Influencing Its Development: A Review," J. Mater. Sci., **42**(3), pp. 729–746.
[24] Pacheco-Torgal, F., Castro-Gomes, J., and Jalali, S., 2008, "Alkali-activated Binders: A Review," Construct. Build. Mater., **22**(7), pp. 1305–1314.
[25] Pacheco-Torgal, F., Castro-Gomes, J., and Jalali, S., 2008, "Alkali-Activated Binders: A REVIEW. Part 2. About Materials and Binders Manufacture," Construct. Build. Mater., **22**(7), pp. 1315–1322.
[26] Al Bakri, A. M., Kamarudin, H., Bnhussain, M., Nizar, I. K., and Mastura, W., 2011, "Mechanism and Chemical Reaction of Fly Ash Geopolymer Cement: A Review," J. Asian Sci. Res., **1**(5), pp. 247–253. Retrieved from https://archive.aessweb.com/index.php/5003/article/view/3292
[27] API, R.P 10B-2, 2013, *Recommended Practice for Testing Well Cements*, API, Washington, DC.
[28] Luukkonen, T., Abdollahnejad, Z., Yliniemi, J., Kinnunen, P., and Illikainen, M., 2018, "One-Part ALKALI-ACTIVATED Materials: A Review," Cem. Concr. Res., **103**, pp. 21–34.
[29] Hos, J. P., McCormick, P. G., and Byrne, L. T., 2002, "Investigation of a Synthetic Aluminosilicate Inorganic Polymer," J. Mater. Sci., **37**, pp. 2311–2316.
[30] Wang, D., and Chen, Z., 1997, "On Predicting Compressive Strengths of Mortars With Ternary Blends of Cement, Gghfs and Fly Ash," Cem. Concr. Res., **27**(4), pp. 487–493.
[31] Nugteren, H. W., 2007, "Coal Fly Ash: From Waste to Industrial Product," Part. Part. Syst. Charact., **24**(1), pp. 49–55.
[32] Puertas, F., Martínez-Ramírez, S., Alonso, S., and Vázquez, T., 2000, "Alkali-Activated Fly Ash/Slag Cements," Cem. Concr. Res., **30**(10), pp. 1625–1632.
[33] Li, C., Sun, H., and Li, L., 2010, "A Review: The Comparison Between Alkali-Activated Slag (si+ca) and Metakaolin (Si+Al) Cements," Cem. Concr. Res., **40**(9), pp. 1341–1349.
[34] Rahier, H., Van Mele, B., and Wastiels, J., 1996, "Low-Temperature Synthesized Aluminosilicate Glasses," J. Mater. Sci., **31**(1), pp. 80–85.
[35] Provis, J. L., 2018, "Alkali-Activated Materials," Cem. Concr. Res., **114**, pp. 40–48.
[36] Omran, M., Khalifeh, M., and Hjelm, S., 2022, Role of Zeta Potential on Rheology of One-Part Geopolymer Slurries-Influence of Superplasticizers. I: Annual Transactions the Nordic Rheology Society. ISBN 978-82-692721-2-3. s.15-22.
[37] Purdon, A. O., 1940, "The Action of Alkalis on Blast-Furnace Slag," J. Soc. Chem. Ind.
[38] Heitzmann, R. F., Fitzgerald, M., and Sawyer, J. L., 1987, Mineral Binder and Compositions Employing the Same, Mineral Binder and Compositions Employing the Same. US Patent No. 4,642,137.
[39] Schwarz, W., and Lerat, A., 1994, Tectoaluminosilicate Cement and a Process for Its Manufacture, Tectoaluminosilicate Cement and a Process for Its Manufacture. U.S. Patent No. 5,372,640.
[40] Davidovits, J., 1994, Method for Obtaining a Geopolymeric Binder Allowing to Stabilize, Solidify and Consolidate Toxic or Waste Materials, Method for Obtaining a Geopolymeric Binder Allowing to Stabilize, Solidify and Consolidate Toxic or Waste Materials. U.S. Patent No. 5,349,118.
[41] Glasby, T., Day, J., Genrich, R., and Aldred, J., 2015, "EFC Geopolymer Concrete Aircraft Pavements at Brisbane West Wellcamp Airport," Proceedings of the 27th Biennial National Conference of the Concrete Institute of Australia in Conjunction With the 69th RILEM Week, Melbourne, Australia, Aug. 30–Sept. 2, Concrete Institute of Australia, Sydney.
[42] Palomo, Á, Fernández Jiménez, A., López Hombrados, C., and Lleyda, J. L., 2007, "Railway Sleepers Made of Alkali Activated fly ash Concrete," Rev. Ing. De Constr., **22**(2).
[43] Norsok, D., 2013, Well Integrity in Drilling and Well Operations. Standards Norway, Rev, 4. Lysaker, Norway.
[44] Haghighat-Nejad, F., 2019, *Flexible Geopolymer for Oil and Gas Well Cementing: An Experimental Study*, University of Stavanger, Norway.
[45] Khalifeh, M., 2016, "Materials for Optimized P&A Performance: Potential Utilization of Geopolymers," PhD thesis UiS, University of Stavanger, Norway.
[46] API Spec 10A, 2015, *Specification for Cements and Materials for Well Cementing*, 23rd ed., American Petroleum Institute, Washington, DC.
[47] Kamali, M., Khalifeh, M., Saasen, A., and Delabroy, L., 2020, "Materials for Well Integrity: Characterization of Short-Term Mechanical Properties," Proceedings of the ASME 2020 39th International Conference on Ocean, Offshore and Arctic Engineering. Volume 11: Petroleum Technology, Virtual, Online. Aug. 3–7, ASME, p. V011T11A035.
[48] API RP 10B-2, 2019, *Recommended Practice for Testing Well Cements*, American Petroleum Institute, Washington, DC.
[49] Park, S., and Pour-Ghaz, M., 2018, "What Is the Role of Water in the Geopolymerization of Metakaolin?," Constr. Build. Mater., **182**, pp. 360–370.
[50] Pathak, A., 2017, "Effect of Zinc Oxide Nanoparticle on Compressive Strength and Durability of Concrete," Int. J. Res. Appl. Sci. Eng. Technol., V(VIII), pp. 683–687.
[51] Zailan, S. N., Bouaissi, A., Mahmed, N., and Abdullah, M. M., 2019, "Influence of Zno Nanoparticles on Mechanical Properties and Photocatalytic Activity of Self-Cleaning Zno-Based Geopolymer Paste," J. Inorg. Organomet. Polym. Mater., **30**(6), pp. 2007–2016.
[52] Chen, A.-l., Xu, D., Chen, X.-y., Zhang, W.-y., and Liu, X.-h., 2012, "Measurements of Zinc Oxide Solubility in Sodium Hydroxide Solution From 25 to 100 °C," Trans. Nonferr. Metals Soc. China, **22**(6), pp. 1513–1516.
[53] Nivethitha, D., and Dharmar, S., 2016, "Influence of Zinc Oxide Nanoparticle on Strength and Durability of Cement Mortar," Int. J. Earth Sci. Eng., **9**(3), pp. 175–181.
[54] Khalifeh, M., Saasen, A., and Vrålstad, T., 2014, "Potential Utilization of Geopolymers in Plug and Abandonment Operations," Proceedings of the SPE Bergen One Day Seminar, Bergen, Norway, Apr. 2.
[55] Scherer, G. W., Funkhouser, G. P., and Peethamparan, S., 2010, "Effect of Pressure on Early Hydration of Class H and White Cement," Cem. Concr. Res., **40**(6), pp. 845–850.
[56] Chamssine, F., Khalifeh, M., Eid, E., Minde, M. W., and Saasen, A., 2021, "Effects of Temperature and Chemical Admixtures on the Properties of Rock-Based Geopolymers Designed for Zonal Isolation and Well Abandonment," Proceedings of the ASME 2021 40th International Conference on Ocean, Offshore and Arctic Engineering. Volume 10: Petroleum Technology, Virtual, Online. June 21–30, ASME, p. V010T11A031.
[57] Khalifeh, M., Saasen, A., Vrålstad, T., Larsen, H. B., and Hodne, H., 2016, "Experimental Study on the Synthesis and Characterization of Aplite Rock-Based Geopolymers," J. Sustain. Cem. Based Mater., **5**(4), pp. 233–246.
[58] Omran, M., Khalifeh, M., and Saasen, A., 2022, "Influence of Activators and Admixtures on Rheology of Geopolymer Slurries for Well Cementing Applications," Proceedings of the SPE Asia Pacific Oil & Gas Conference and Exhibition, Adelaide, Australia, Oct. 17–19.

Downloaded from http://asmedigitalcollection.asme.org/energyresources/article-pdf/145/10/103201/7003036/ert_145_10_103201.pdf by Stavanger University user on 26 July 2023

Appendix 6 – Paper IV

ANNUAL TRANSACTIONS OF THE NORDIC RHEOLOGY SOCIETY, VOL. 30, 2022

Role of Zeta Potential on Rheology of One-part Geopolymer Slurries – Influence of Superplasticizers

Mohamed Omran[1], Mahmoud Khalifeh[1], and Sondre Hjelm[1]

[1] Department of Energy and Petroleum Engineering, Faculty of Science and Technology, University of Stavanger, Stavanger, Norway.

ABSTRACT

One-part geopolymers have great potential as an alternative cementitious material to replace ordinary Portland cement (OPC). They are more convenient to be utilized in cast-in-situ applications than the conventional two-part geopolymers as well. Superplasticizers are admixtures that plasticize and fluidize the cementitious slurry through steric and electrostatic mechanisms that apply repulsion forces between the slurry particles. They are commonly used to improve the workability of cement and conventional geopolymer slurries. However, the most developed superplasticizers are suitable for Ordinary Portland cement. Zeta potential measurements of geopolymer slurries can be used in the evaluation of superplasticizers. Therefore, the effect of zeta potential on rheological properties of one-part geopolymer slurries due to the influence of three different superplasticizers is presented. The results show that lignosulfonate-based material could be an effective superplasticizer for Just Add Water geopolymer slurries. It gave the lowest yield stress and API gel strength while having the highest absolute zeta potential value.

Introduction

Superplasticizers are admixtures which plasticize and fluidize cement slurries by means of electrostatic and steric repulsion mechanisms that apply repulsion forces between the slurry particles. They are commonly used to improve the workability of cement and geopolymer pastes. They are used to control the flow properties and allow the possibility of reducing the water to solid ratio without affecting their workability to achieve high mechanical strength and long-term durability. These admixtures have several chemical bases such as lignosulfonates, naphthalene, melamine, polycarboxylates, etc [1-5].

Lignosulphonates were used not only as superplasticizers but also as retarders to enhance the viscosity and pumpability of OPC. Naphthalenes and melamines are superplasticizers that influence dispersing of cementitious particles through electrostatic repulsion mechanisms. Polycarboxylates are other types of superplasticizers that have electrostatic repulsion mechanisms like naphthalenes and melamines, in addition to applying the steric repulsion mechanism due to the long lateral chains of ether on the molecules [1-4].

Davidovits et al. [6] introduced the geopolymers with chemical designation as polysialates, where sialate is the silicon-oxygen-aluminate network [-Si-O-Al-O-]. This network is a tetrahedra SiO4 and AlO4 structure linked by sharing all oxygens. Hence, positive ions such

as alkali metal cations (e.g., potassium ion K^+ and sodium ion Na^+) have to be presented within the structure cavities for balancing negative charges of A13+ in the IV-fold coordination. Geopolymers have generally low calcium content [6-8]. Therefore, the available superplasticizers for OPC may not influence them properly [5].

Although several articles focus on controlling the reaction, setting time and strength development of geopolymer mixes [6-13], few studied the effect of superplasticisers on one-part geopolymer slurries. Several variables affect the geopolymeric structure such as particle size and shape, and solid phase volume fraction besides surface effects such as electrostatic forces and adsorption of ions between the particles [3-9]. Hence, Superplasticisers as surfactants may be more suitable candidates for enhancing the rheology of the geopolymeric slurries, due to their structures' compatibility with the geopolymer structures.

A study conducted by Palacios et al. [10] shows that the pH of the slurry significantly impacts the performance of the superplasticizers. At pH values below 11.7, most of the superplasticizers perform better on alkali-activated-based materials. However, at higher pH values, especially above 13.6, most of the superplasticizers get unstable and do not perform properly. One should note that naphthalene-based admixtures are stable in high pH environments. The reader should distinguish between alkali-activated-based materials and geopolymers whereas geopolymers are a sub-group of alkali-activated materials. Thus, geopolymer properties like pH of the slurry and size and surface potential of the geopolymer particles have a significant role in controlling the adsorption rate of the superplasticizers [10].

This work aims to present the effect of utilization of three different superplasticizers by utilization of the electrokinetic potential of the slurries. In addition, it will discuss their zeta potential role in the rheology of geopolymer slurries, especially on viscosity and yield stress of one-part rock-based geopolymer recipe at varying shear rates for well construction in the petroleum industry.

Experimental Materials

This research is based on selecting one of the top candidate one-part geopolymer recipes from Omran & Khalifeh[11], "W1Pb-Z6" or so-called in this paper "OP-Z" as the neat recipe. The solid phase includes a precursor, a solid activator, and a superplasticiser. The liquid phase includes distilled water. The chemical composition and mineralogy of the powder mix have been thoroughly studied [11-14].

Furthermore, 1 wt.% solid powder of three different superplasticizers (two naphthalene-based and a Na-based lignosulfonate superplasticizer) are used separately to enhance the rheology of one-part rock-based OP-Z neat geopolymer mix design. The chemical structure of the superplasticizers is given in Figure 1. The selection of the superplasticizers is based on selecting the most stable superplasticizers that can be utilized and worked effectively for rheology enhancement in high pH environments.

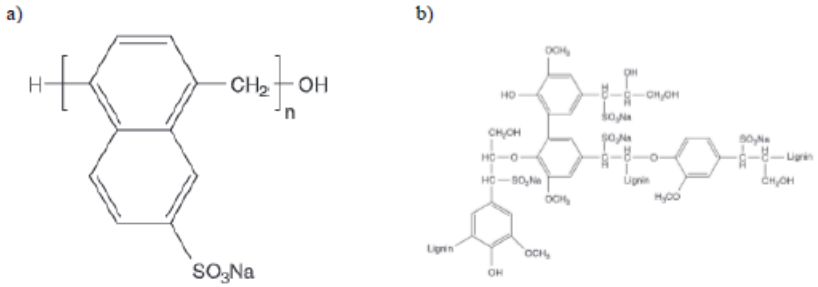

Figure 1: Chemical structure of the superplasticizers: a) naphthalene derivate, b) lignosulfonate molecule [16].

Experimental Methods

All the experiments and preparation of the slurries were conducted according to the international standard [16]. A high-shear cement blender, the OFITE Model 20 Constant Speed Blender, was used for mixing all the components to form the slurry in each experiment.

An atmospheric consistometer, OFITE Model 60, was employed for conditioning all the given slurries in ambient conditions. A non-pressurized rotational viscometer, OFITE 900, was used for the viscosity measurement. Shear stresses of the slurries were recorded in $lb_f/100\ ft^2$.

The zeta potential of the geopolymer slurries was examined at ambient temperature (25°C) by Electrophoretic Light Scattering (ELS) using a Zetasizer Nano ZS (Malvern) equipped with a laser source (wavelength 633 nm) at a scattered angle of 13°.

Results

The shear stress and viscosity of the slurries were studied to investigate the impact of the superplasticizers on the neat geopolymer slurry OP-Z (see Figures 2-4). The pH of the neat slurry after conditioning was measured to be 13.94.

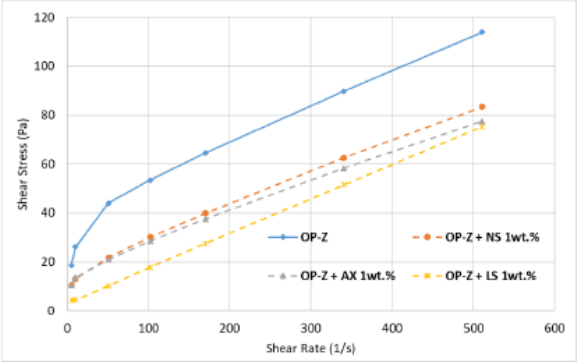

FIGURE 2: Shear stress - Shear rate curves of neat slurry with 1 wt.% superplasticizer in solid form.

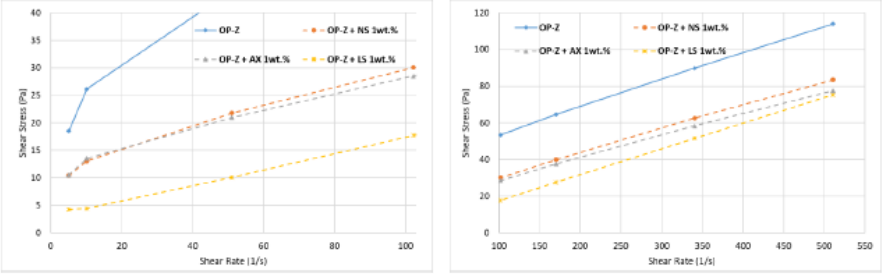

FIGURE 3: Shear stress - Shear rate curves of neat slurry with 1 wt.% superplasticizer in solid form; Left) shear rates below 100 1/s, and Right) shear rates above 100 1/s.

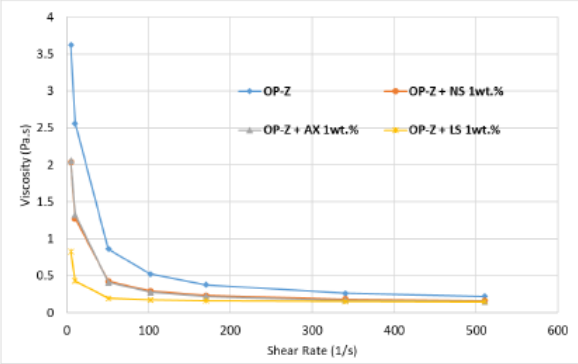

FIGURE 4: Viscosity profiles of neat slurry with 1 wt.% superplasticizer in solid form.

Hershel-Bulkley model was used to estimate yield stress for all geopolymer mixtures as linear scaling regression analysis between 5.11 to 10.2 1/s shear rates as given in Table 1. This model could fit the given shear stress vs shear rate profiles in Figure 1. The power-law index (flow index, n) was measured to indicate the changes in viscosity with shear rate. It was equivalated as the slope of the log-log shear stress to shear rate curve.

Table 1: Yield stress and API Gel-strength results

Recipes	*Superplasticizer*	*10 sec API Gel-strength [Pa]*	*10 min API Gel- strength [Pa]*	*Estimated Yield Stress [Pa]*	*Flow Index*
OP-Z	Non	18.5	19.1	15.4	0.37
OP-Z + NS 1wt.%	Naphthalene-SP	10.5	10.6	8.5	0.44
OP-Z + AX 1wt.%	Auxilchem NS181	10.4	11.3	8.5	0.42
OP-Z + LS 1wt.%	Lignosulfonate-SP	5.6	6.9	4.1	0.64

All given geopolymer recipes were examined for their zeta potential, which includes slurries with and without superplasticizers (see Table 2).

Table 2: Zeta potential measurements of the geopolymer slurries with and without superplasticizers.

Recipes	*ZP (mV)*	*Standard Deviation*
OP-Z	-25.4	± 0.29
OP-Z + NS 1wt.%	-27.9	± 1.32
OP-Z + AX 1wt.%	-31.7	± 0.65
OP-Z + LS 1wt.%	-33.1	± 0.66

Discussion

One-part geopolymeric slurries are non-Newtonian fluids in which the shear viscosity is no longer a material constant, as the viscosity is changing with changing shear rate and also with shearing time. Figure 2 shows shear-thinning behaviour for the examined one-part geopolymer recipes with and without adding superplasticizers. In addition, the flow indexes of the given slurries were 0.37 to 0.64, which were less than 1 ($n < 1$) for shear-thinning materials. It is observable that the absolute value of zeta potential for the slurries with superplasticizer can directly be correlated to the initial viscosity of the slurry, especially at 5 and 10 1/s shear rates as shown in Figures 2-4, below 100 s^{-1} shear rates.

From Figure 3, above 100 s^{-1} shear rates, zeta potential values might not be correlated with the viscous behaviour of the investigated geopolymer slurries anymore, especially at higher shear rates. The resistance of the formed particles network is weakened at which the shear rates increase and give rise to weaken the colloidal flocculent interactions [5, 13].

One-part rock-based geopolymers can be considered as being constructed by long-lasting time-dependent interactions and flow properties due to complex ongoing geopolymerization (i.e., dissolution and oligomerization) reactions. These interactions are replaced by a strong molecular network to form a gel structure [5-8].

Kashani et al. [17] have shown that when alkali silicate-based hardener is mixed with precursors, a negative zeta potential value is expected while for activators consisting of alkali solutions, the zeta potential value approaches positive values. In other words, when alkali silicate-based hardener is mixed with precursors, deflocculation of slag particulate suspensions occurs due to deflocculation and plasticizing effects of silicate anions, which is a result of repulsive forces. However, when alkali solution is used as an activator, the hydroxyl groups sit on precursors and create flocculation. Adsorption of the superplasticizer on the particles increases the magnitude of double-layer repulsive forces and subsequently reduces the yield stress of the slurry. Others presented the utilization of naphthalene-based superplasticizers for conventional geopolymer slurries had a great effect on lowering the yield stress and gel strength with the highest absolute zeta potential values [9-10, 17-20].

In this study, a lignosulfonate-based superplasticizer has been also investigated besides the two naphthalene-based superplasticizers. The results of these three superplasticisers show stable and effective plasticising behaviour to the given high pH rock-based OP-Z geopolymer recipe. Lignosulfonate-based superplasticizer gave the best effect on lowering the yield stress and gel strength with the highest absolute zeta potential value. It lowered the initial viscosity from 3.6 Pa.s for the neat recipe down to 0.8 Pa.s for OP-Z + LS 1wt.% mix design. It also lowered the yield stress and API gel strength by 73% and 70% respectively when it is compared with OP-Z neat recipe. The higher the absolute value of zeta potential, the better the colloidal effectiveness on the geopolymer slurry initially in static conditions. Hence, zeta potential measurements might be correlated to the initial rheological properties such as yield stress, without any considerable effect at high shear rates.

The observations show the presence of shear-thinning - thixotropic flow behaviour for the given one-part rock-based geopolymer recipe with naphthalene-based superplasticizers as time-dependent slurries. However, the Lignosulfonate-based superplasticizer gave Bingham Plastic behaviour. The investigated superplasticisers can be also applicable to be used for two-part geopolymer slurries, especially the lignosulfonate-based superplasticizer.

The recommended dosage of the superplasticizers is typically 0-1 wt.%, while below 0.5 wt.% is more of interest due to techno-economic reasons. Thus, a further investigation will be needed to study the effect of the weight content of these superplasticisers below 1 wt.% on the

one-part geopolymer system. In addition, it would be useful to further correlate these observations with interactive forces between geopolymer materials and these three superplasticizers.

Conclusion

From the experimental results, Naphthalene-based superplasticizers are good candidates for lowering yield stress, API gel-strength and viscous behaviour of one-part rock-based geopolymers as they work effectively with the conventional two-part geopolymer systems. However, the lignosulfonate-based superplasticizer gave the best effect on lowering the yield stress and gel strength with the highest absolute zeta potential values due to their particle's dispersion with the highest absolute zeta potential value. Both Na-based lignosulfonate and Naphthalene-based superplasticizers might be the most effective superplasticizers for one- and two-part rock-based geopolymer systems. Zeta potential measurements might be correlated to the initial rheological properties such as yield stress, without any considerable effect at high shear rates.

Acknowledgements

The authors also thank Aker BP, ConocoPhillips Norge, TotalEnergies, and the Research Council of Norway for their support through the SafeRock project (#319014—New Cementitious Material for Oil Well Cementing Applications—SafeRock). Special thanks to Laurent Delabroy and Roy Middleton for their technical inputs.

References

1. Burgos-Montes, O., Palacios, M., Rivilla, P., & Puertas, F. (2012). Compatibility between superplasticizer admixtures and cements with mineral additions. Construction and Building Materials, 31, 300–309. https://doi.org/10.1016/j.conbuildmat.2011.12.092
2. Gołaszewski, J., & Szwabowski, J. (2004). Influence of superplasticizers on rheological behaviour of fresh cement mortars. Cement and Concrete Research, 34(2), 235–248. https://doi.org/10.1016/j.cemconres.2003.07.002
3. Montes, C., Zang, D., & Allouche, E. N. (2012). Rheological behavior of fly ash-based geopolymers with the addition of superplasticizers. Journal of Sustainable Cement-Based Materials, 1(4), 179–185. https://doi.org/10.1080/21650373.2012.754568
4. Yamada, K., Takahashi, T., Hanehara, S., & Matsuhisa, M. (2000). Effects of the chemical structure on the properties of polycarboxylate-type superplasticizer. Cement and Concrete Research, 30(2), 197–207. https://doi.org/10.1016/s0008-8846(99)00230-6
5. Puertas, F., Santos, H., Palacios, M., & Martínez-Ramírez, S. (2005). Polycarboxylate superplasticiser admixtures: effect on hydration, microstructure and rheological behaviour in cement pastes. Advances in Cement Research, 17(2), 77–89. https://doi.org/10.1680/adcr.2005.17.2.77
6. Davidovits, M., Davidovits, N., & Davidovits, J. (1991). manufacture of alkali metal polysialate-disiloxo-type aluminosilicate geopolymers and the products obtained. FR Patent 2659319.
7. Masi, G., Rickard, W. D. A., Vickers, L., Bignozzi, M. C., & van Riessen, A. (2014). A comparison between different foaming methods for the synthesis of light weight geopolymers. Ceramics International, 40(9), 13891–13902. https://doi.org/10.1016/j.ceramint.2014.05.108
8. Khalifeh, M., Saasen, A., Hodne, H., & Motra, H. B. (2019). Laboratory evaluation of rock-based geopolymers for zonal isolation and permanent P&A applications. Journal of Petroleum Science and Engineering, 175, 352–362. https://doi.org/10.1016/j.petrol.2018.12.065
9. Zingg, A., Winnefeld, F., Holzer, L., Pakusch, J., Becker, S., & Gauckler, L. (2008). Adsorption of polyelectrolytes and its influence on the rheology, zeta potential, and microstructure of various cement and hydrate phases. Journal of Colloid and Interface Science, 323(2), 301–312. https://doi.org/10.1016/j.jcis.2008.04.052

10. Palacios, M., Houst, Y. F., Bowen, P., & Puertas, F. (2009). Adsorption of superplasticizer admixtures on alkali-activated slag pastes. Cement and Concrete Research, 39(8), 670–677. https://doi.org/10.1016/j.cemconres.2009.05.005
11. Omran, M., & Khalifeh, M. (2022). Development of Low Carbon Dioxide Intensive Rock-Based Geopolymers for Well Cementing Applications – One-Part Geopolymer. OMAE2022-78535. OMAE 41st International Conference on Ocean, Offshore & Arctic Engineering. Hamburg, Germany, Volume: 10, Petroleum Technology.
12. Khalifeh, M., (2016). "Materials for optimized P&A performance: Potential utilization of geopolymers."
13. Khalifeh, M., Saasen, A., Vrålstad, T., Larsen, H., & Hodne, H. (2016). "Experimental study on the synthesis and characterization of aplite rock-based geopolymers," Journal of Sustainable Cement-Based Materials, vol. 5, no. 4, pp. 233-246, 2016/07/03 2016, https://doi:10.1080/21650373.2015.1044049.
14. Khalifeh, M., Hodne, H., Saasen, A., Integrity, O., & Eduok, E. I. (2016). Usability of geopolymers for oil well cementing applications: Reaction mechanisms, pumpability, and properties. SPE Asia Pacific Oil & Gas Conference and Exhibition . https://doi.org/10.2118/182354-ms
15. Russell, N. (2012). Superplasticizers and the rheology of concrete. In Understanding the rheology of concrete (pp. 144–208). essay, Woodhead Publ.
16. API, R., "10B-2, Recommended Practice for Testing Well Cements. 2013," Washington, DC: API.
17. Kashani, A., Provis, J. L., Qiao, G. G., & van Deventer, J. S. J. (2014). The Interrelationship between surface chemistry and rheology in alkali activated slag paste. Construction and Building Materials, 65, 583–591. https://doi.org/10.1016/j.conbuildmat.2014.04.127
18. Khale, D., & Chaudhary, R. (2007). Mechanism of geopolymerization and factors influencing its development: A Review. Journal of Materials Science, 42(3), 729–746. https://doi.org/10.1007/s10853-006-0401-4
19. Omran, M., Khalifeh, M., & Saasen, A. (2022). Influence of Activators and Admixtures on Rheology of Geopolymer Slurries for Well Cementing Applications. SPE-210698-MS, to be presented at the SPE Asia Pacific Oil & Gas Conference and Exhibition 2022, Adelaide, Australia, 17 - 19 Oct 2022.
20. Oderji, S. Y., Chen, B., Shakya, C., Ahmad, M. R., & Shah, S. F. (2019). Influence of superplasticizers and retarders on the workability and strength of one-part alkali-activated fly ash/slag binders cured at room temperature. Construction and Building Materials, 229, 116891. https://doi.org/10.1016/j.conbuildmat.2019.116891

Appendix 7 – Paper V

Influence of Activators and Admixtures on Rheology of Geopolymer Slurries for Well Cementing Applications

Mohamed Omran, Mahmoud Khalifeh, & Arild Saasen

Paper presented at the SPE Asia Pacific Oil & Gas Conference and Exhibition, Adelaide, Australia, October 2022.

DOI: https://doi.org/10.2118/210698-MS

This paper is not available in Brage due to copyright.

Appendix 8 – Paper VI

Design and Early Age Performance of Sustainable One-Part Geopolymers for Well Cementing

Mohamed Omran[1]*, Maria Paiva[2], and Mahmoud Khalifeh[1]

[1]Department of Energy and Petroleum Engineering, University of Stavanger (UIS)
[2]Sustainable Materials Research Center (NUMATS), Federal University of Rio de Janeiro (UFRJ)

Summary

One-part geopolymers, known as "just add water" (JAW), alkali-activated formulation is presented in this work. This work reveals the design and development of short-term properties of JAW geopolymers for use in oilwell cementing and well abandonment. Granite-based mix designs normalized with a byproduct slag and a small amount of microsilica as precursors were developed. The solid activator is composed of potassium silicate and potassium hydroxide, which are mixed with the precursors to synthesize the JAW formulation. Zinc oxide is used as a strength booster admixture. The cementing properties of the developed granite-based mix designs were characterized by investigating reaction phases and mechanical properties. Dissolution, heat evolution, pumpability, strength development, and mineralogy are also studied. The results show that a positive correlation among all the given analyses for the final geopolymeric product is quite observable. Zinc oxide is favorable to be added for optimizing the given precursor mix design to enhance the solubility and leads to much higher heat evolutions. Furthermore, it develops early strength up to 16 MPa without any negative effect on the investigated one-part geopolymer slurries.

Downloaded from http://onepetro.org/SJ/article-pdf/doi/10.2118/215825-PA/3118828/spe-215825-pa.pdf/1 by Stavanger University Library user on 26 July 2023

Introduction

The primary objective of all cementing operations in the oil and gas industry is the effective placement of barrier materials that can fulfill their functions at downhole conditions. After setting, the hardened cement is expected to work as a physical barrier, providing proper long-term zonal isolation within the wellbore. Additionally, safe and economical cementing operations are other important requirements and key paths to improve the overall performance of well-cementing systems (Nelson and Guillot 2006; Khalifeh and Saasen 2020).

Within this context, ordinary Portland cement (OPC) is the prime material used for zonal isolation and well abandonment for more than a century, mainly due to its worldwide manufacturing infrastructure, raw materials, known chemistry, availability, and pricing (Hewlett 2001; Nelson and Guillot 2006; Taylor 1997). Even though OPC chemistry is well-known and developed, there are technical constraints reported in the literature regarding its short- and long-term properties (Deshpande et al. 2015; Simao et al. 2016). OPC durability limitations are even more challenging to overcome when considering the harsh conditions present in the oil and gas wells environment (Bergen et al. 2022; Kiran et al. 2017; Nelson and Guillot 2006). Moreover, its production contributes up to 8% of the global CO_2 emissions (Andrew 2019), from the decomposition of carbonates and high fossil fuel consumption. Altogether, these aspects represent a powerful driving force toward the development of cementitious materials with lower carbon footprint to achieve global carbon dioxide reduction goals (Damtoft et al. 2008; IEA 2021).

Geopolymers are a subcategory of alkali-activated based materials (Davidovits 2008; Palomo et al. 2014), which have been estimated to have between 70% and 80% lower CO_2 emissions per ton of produced material (Flatt et al. 2012; McLellan et al. 2011; Pacheco-Torgal et al. 2014). Practical application of geopolymers in well cementing has been proposed as early as 2008 by a cementing services company (Barlet-Gouedard et al. 2008), with reports of field tests dating from the same period (Mahmoudkhani et al. 2008). Despite fulfilling rheological and pumpability requirements, having excellent mechanical properties at the hardened state and high durability in wellbore conditions (Chamssine et al. 2022a; Khalifeh et al. 2014; Nasvi et al. 2014a, 2014b, 2014c, 2014d; Paiva et al. 2018; Salehi et al. 2017, 2018, 2019), compared to OPC well-cementing pastes, geopolymers are not in widespread use in the oilwell industry. Salehi et al. (2018) attribute this fact to uncontrolled thickening time at elevated temperatures.

In the field of geopolymer technology, geopolymers are classified as two-part system (conventional geopolymers) or one-part system (JAW). Conventional geopolymers are formed by mixing one or more of the raw materials (precursors) with a high alkaline activator solution, producing a cementitious material. Activator solutions are generally composed of alkali metal hydroxide solutions, alone or combined with alkali metal silicates (Davidovits 1991, 2013). Common precursors are natural minerals, such as kaolin, metakaolin, aplite, and granite; industrial wastes, such as ground granulated blast furnace slag (GGBFS); fuel ashes, including fly ash, rice husk, bamboo leaf, and palm oil ashes; demolition wastes; and, more recently, red mud waste (Krishna et al. 2021). Geopolymers derived from rock-based precursors, such as aplite (Khalifeh et al. 2016a, 2016b, 2017, 2018, 2019) and granite (Alvi et al. 2020; Chamssine et al. 2021, 2022a, 2022b; Kamali et al. 2020, 2022), combined with GGBFS, have also been investigated for oil and gas applications, aiming to minimize their CO_2 emissions, compared to calcined precursors such as metakaolin and fly ash.

Logistics, health, safety, and environmental aspects related to the transportation and handling of alkaline activator solutions needed for mixing the two-part geopolymers in offshore applications are drawbacks for their field applications. In addition, the transportation of large volumes of the liquid hardener phase can produce additional CO_2 emissions when compared to a single-phase geopolymer powder system. These challenges highlight the importance of developing the one-part geopolymers, as a crucial strategy for their offshore oilwell-cementing applications, promoting its commercialization. Researchers have come up with the one-part system, known as the JAW system. In the JAW system, the alkaline/alkali silicate solution is replaced with a powder phase and preblended with the precursors. So, only water

*Corresponding author; email: mohamed.a.omran@uis.no

Copyright © 2023 The Authors.
Published by the Society of Petroleum Engineers. This paper is published under the terms of a Creative Commons Attribution License (CC-BY 4.0).

Original SPE manuscript received for review 21 December 2022. Revised manuscript received for review 26 April 2023. Paper (SPE 215825) peer approved 18 May 2023.

is required to be introduced to the powder to produce the slurry. Such a product would then potentially be capable of being user-friendly at the same time as generating lower CO_2 emissions, rooted in the transportation of unnecessary liquid (Omran and Khalifeh 2023; Wan-En et al. 2022).

Pacheco-Torgal et al. (2008) and Singh and Middendorf (2020) discussed views on the geopolymerization reaction, summarizing the process as a dissolution of the precursors in the alkaline solution as the pH is raised, followed by the transport and reorganization of simple silica and alumina tetrahedra, condensation in dimers and oligomers, and polymerization of the aluminosilicate network **(Fig. 1).**

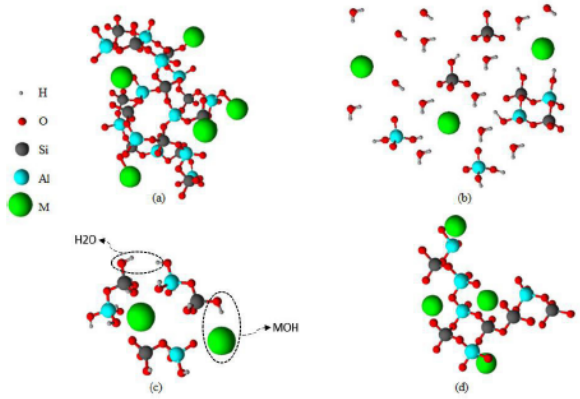

Fig. 1—Geopolymerization process steps: (a) geopolymer precursor prior dissolution, (b) dissolution and formation of monomers and dimers, (c) reorganization and condensation, and (d) geopolymerization.

The product of the geopolymerization process is a solid 3D network of silicate and aluminate tetrahedra, incorporating positively charged cations (mainly Na^+, K^+, and Ca^{2+}) to balance the charge of aluminate. Usually, the resulting network is denoted N-A-S-H (sodium ions), K-A-S-H (potassium ions), or (C, N)-A-S-H (calcium and sodium), where (H) represents free water in the nanopore space (Davidovits 2017; Khale and Chaudhary 2007). This must be distinguished from the C-S-H derived structures C-A-S-H and C-(N)-A-S-H, which form when enough calcium is present in solution. These structures maintain the classic lamellar structure of C-S-H, with partial replacement of silicate by aluminate tetrahedra and incorporation of sodium into the interlamellar solution (Myers et al. 2014). These products are more usually associated with alkali-activated materials, rather than geopolymers. Hybrid AAM-geopolymer pastes may form, with (C,N)-A-S-H slowly changing into C-(N)-A-S-H as the paste matures (García-Lodeiro et al. 2013).

The kinetics of geopolymer formation is still not completely understood, and there is no single technique that quantifies the reaction progress across all steps (Luukkonen et al. 2018; Zhang et al. 2012, 2013). Most often, the authors study the overall kinetics through practical measurements, such as the setting time and strength development rate, regardless of precursors, activators, and retarders used. Zhang et al. (2012) described the heat release rate of metakaolin-based geopolymer during isothermal calorimetry, identifying three distinct peaks. Peak I is a sharp peak that occurs after mixing, interpreted as the heat of dissolution of the precursors, followed by an intermediate period of lower heat release rate, during which reorganization and condensation occur. Peak II corresponds to geopolymerization and percolation of the solid phase. A third peak was observed, but its meaning is still unclear. This two-step heat release behavior was observed by other researchers too (Cai et al. 2020; Kumar et al. 2010; Paiva et al. 2021; Yao et al. 2009), sometimes with significant overlap between the two peaks. In contrast with OPC hydration, there is no direct proportion between heat release and reaction progress. The amount of heat reflects the enthalpy of formation of the specific products formed. In particular, K-A-S-H formation releases more heat than the equivalent amount of N-A-S-H (Paiva et al. 2021).

Nedunuri and Muhammad (2022) reviewed retarders for alkali-activated materials and reported that only zinc was able to delay setting by forming complexes with both silica and calcium ions. The authors studied the effect of up to 3% $ZnSO_4 \cdot 7H_2O$ on the properties of alkali-activated GGBFS and fly ash at room temperature, finding it very effective in increasing both initial and final setting times. However, increasing the concentration of zinc delayed strength development in the first 7 days, leading to a lower final strength. In extreme cases, formulations with 11% or less CaO in the precursor mix and 3% zinc did not develop any strength after 120 days, suggesting a poisoning effect. Zailan et al. (2020) were able to add up to 10% ZnO to a Type F fly ash-based geopolymer, with a decrease of 44% in the compressive strength at 28 days, but the authors did not report the effect in setting time. Wang et al. (2020) observed a significant increase in setting times after adding 25% ZnO by weight of metakaolin. The authors attribute the effect to the formation of sodium or potassium zincate, retarding the formation of geopolymer. However, the amount of zinc is much larger than typically used for retardation purposes, and the compressive strength was not reported.

The zinc retardation mechanism was studied by Garg and White (2017) in alkali-activated slag using ZnO, concluding that calcium zincate $Ca[Zn(OH)_3]_2 \cdot 2H_2O$ (CZ) precipitates as a metastable phase, delaying the formation of C-(N)-A-S-H. The authors did not observe any retardation of alkali-activated metakaolin, suggesting that retardation is dependent on the presence of calcium. After the ZnO is consumed, the calcium concentration rises, and C-(N)-A-S-H starts to form. At this point, CZ starts to dissolve, calcium is released, and zinc is incorporated into the C-(N)-A-S-H network, replacing silica tetrahedra (Tommaseo and Kersten 2002).

Downloaded from http://onepetro.org/SJ/article-pdf/doi/10.2118/218928/spe-218928-pa/3118928/spe-218928-pa.pdf by Stavanger University Library user on 26 July 2023

Considering there is no literature consensus on the zinc retardation mechanism and its optimal concentration for low-calcium geopolymer systems, Chamssine et al. (2021) studied a two-part low-calcium (10%) geopolymer well-cementing system. Their precursors were granite, GGBFS, and silica, and they found that the addition of $Zn(NO_3)_2{\cdot}6H_2O$ and $K(NO_3)$ was able to extend the setting time. Chamssine et al. (2022b) reported that the addition of 0.3% Zn^{2+} by weight of slurry as zinc salt extended significantly the thickening time at 50°C of bottomhole circulating temperature (BHCT) and 14 MPa of curing pressure. Chamssine et al. (2022a) increased the Zn^{2+} addition to 1.1% by weight of slurry and prolonged the pumpability at 60°C BHCT and 14 MPa.

One-part geopolymers are a more recent development, combining suitable precursors and activators in a solid mixture that forms a geopolymer by the simple addition of water (Luukkonen et al. 2018). The precursors can be any materials that form conventional geopolymers, and the activators can be prepared using the components of any two-part geopolymer activator solutions. Additionally, no differences were found in the reaction products of one- and two-part fly-ash geopolymers when prepared with similar mixing ratios (Suwan and Fan 2017). However, an important difference between two- and one-part geopolymers is the slow release and availability of alkali and free $HSiO_4^{3-}$ and $Al(OH)_4^-$, which may hinder or prevent the geopolymerization reaction. Mitigation techniques include adding reactive sources of silica and alumina, such as amorphous silica and sodium silicates and aluminates, calcinating the precursors, grinding the precursors to increase their surface area, and grinding the precursors with the alkali sources to obtain mechanochemical activation (Matalkah et al. 2017). However, finely ground precursors not only increase the availability of reactive species but also lead to worse rheological properties due to increased surface area. This is an important issue because commonly used OPC superplasticizers have mixed results for one- and two-part geopolymers, depending on alkalinity, activator type, precursor type, calcium content, and temperature (Nematollahi and Sanjayan 2014; Omran et al. 2022a, 2022b; Palacios and Puertas 2005). Finally, when the precursors are sufficiently reactive, the added dissolution heat of activators may lead to the early setting of one-part geopolymer mixes.

The development of user-friendly geopolymers is a crucial strategy to facilitate the use of geopolymers as a full replacement of cement for oilwell cementing applications. Thus, the development of one-part geopolymers that require only the addition of water has become crucial in recent years. One-part JAW geopolymers are user and environmentally friendly cementing materials. They are more promising for in-situapplications due to overcoming the impracticalities of conventional two-part geopolymers (Omran and Khalifeh 2022, 2023).

Building on the previous works, Omran and Khalifeh (2022, 2023) proposed a novel one-part geopolymer formulation based on granite, GGBFS, and microsilica, using anhydrous potassium silicate as a solid activator. Four different solid admixtures were individually investigated, namely, NaOH, $CaCO_3$, CaO, and ZnO, in quantities ranging from 0.14% to 1.14% by weight of precursor. In addition to distilled water, a small amount of KOH solution was used as an accelerator. The neat formulation (W1Pb) developed 4.8 MPa in 7 days of curing at 70°C and atmospheric pressure. The use of calcium oxide, calcium carbonate, and NaOH resulted in a reduction of early strength, up to 7 days, even in the smallest concentration (0.14%), with worse effects in larger concentrations. NaOH had the worst performance, yielding 2.2 MPa at 7 days. Zinc oxide significantly improved the mechanical strength, reaching 9.5 MPa in 7 days by only using 0.14% ZnO. The authors concluded that the formulations with zinc oxide addition less than or equal to 0.86% have the potential to be used in oilwell cementing. While the addition of ZnO higher than 1.0 wt% showed a negative effect on the 24-hour compressive strength at 70°C.

Motivated by that, this paper aims to thoroughly evaluate the early age properties and the mix design of one-part rock-based geopolymer systems with 0.57% and 0.86% of ZnO, by investigating their geopolymerization process under an oilwell cementing condition. Consequentially, it is to design a new one-part naturally occurring viable and sustainable granite-based geopolymer. It is focused on studying each stage of the geopolymerization process starting from the characterization of dissolution, reorganization, and then polycondensation processes, integrating them with a wide range of physical and chemical characterizations.

Materials and Methods

Materials. The JAW geopolymer formulation is based on solid precursors and activator components, which are mixed with water to produce the cementing system. The precursor materials used were ground granite (from Norway), a rock-based aluminosilicate material; GGBFS (from Sweden), a calcium silicate material rich in aluminum and magnesium; and a small portion of microsilica (MS, from Norway), an almost pure amorphous silica.

This study is a design of granite-based geopolymers where the base of the JAW system is granite, and due to its chemical composition, it is normalized with microsilica and slag. Unlike GGBFS-based geopolymers, granite-based geopolymers are characterized as aluminosilicate-rich materials with low calcium content and less calcium dependency on geopolymerization reaction. In other words, GGBFS and microsilica were incorporated as composition normalizers to the total weight of the granite-based precursor, to develop the required early-age well-cementing properties (Omran et al. 2023).

Chemical Composition (wt%)	Granite	GGBFS	Microsilica	JAW Precursor Mixture
SiO_2	73.44	35.78	95.50	56.63
Al_2O_3	13.33	12.72	0.70	12.47
Fe_2O_3	2.06	0.18	0.30	1.09
MgO	0.44	12.77	0.50	6.23
CaO	1.12	33.74	0.40	16.45
Na_2O	3.12	0.55	0.40	1.77
K_2O	5.11	0.82	1.00	2.87
TiO_2	0.23	2.23	0.00	1.16
MnO	0.04	0.58	0.00	0.29
LOI*	0.90	0.30	2.00	0.60

* Loss on ignition.

Table 1—Chemical composition of the precursors.

Downloaded from http://onepetro.org/SJ/article-pdf/doi/10.2118/216925-PA/2118928/spe-216925-pa.pdf/1 by Stavanger University Library user on 26 July 2023

The chemical composition, as well as the JAW precursor mixture composition, obtained through X-ray fluorescence analysis, is presented in **Table 1.** The physical properties of the precursors and other mixture components are presented in **Table 2.** Their specific gravities at 25°C were determined with an Ultrapyc 3000 Helium pycnometer from Anton Paar. The particle-size distributions of the solid precursors (**Fig. 2**) and their estimated specific surface areas were assessed through laser diffraction in water dispersion, using a Malvern Mastersizer 3000 particle size analyzer with size limitations over 3000 µm.

The activators were prepared using anhydrous potassium silicate with a molar ratio (SiO_2/K_2O) of 3.92 and ground potassium hydroxide pellets. When required by the specific formulation, KOH and distilled water were used to prepare a 12 M solution. Zinc oxide was

Physical Properties	SG (g/cm³)	d_{10} (µm)	d_{50} (µm)	d_{90} (µm)	SSA (m²/kg)
Granite	2.63	3.52	21.1	131	631
GGBFS	2.90	2.79	15.9	46.6	944
Microsilica	2.29	0.19	0.34	0.60	19 320
K_2SiO_3	2.37	ND	ND	ND	ND
KOH (anhydrous)	2.12	ND	ND	ND	ND
ZnO	5.61	ND	ND	ND	ND

ND, not determined; SG, specific gravity; SSA, specific surface area; d_{10}, d_{50}, d_{90}, particle-size distribution percentiles.

Table 2—Physical properties of the components.

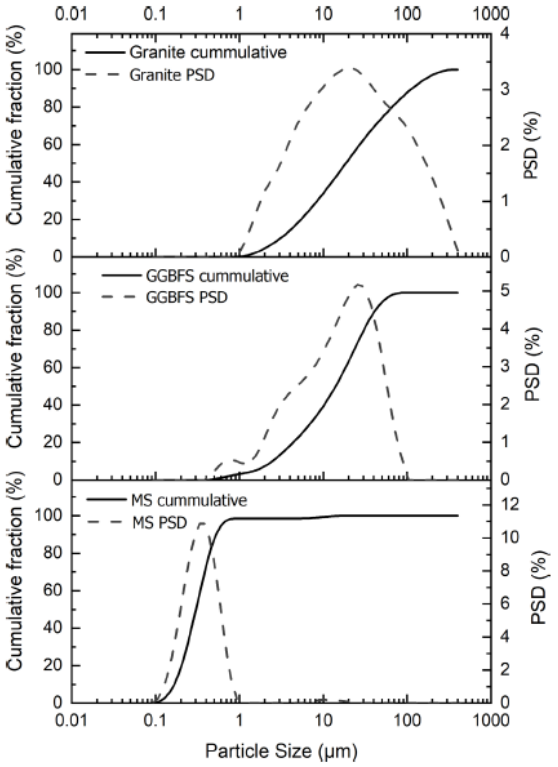

Fig. 2—Size distribution of precursors in aqueous dispersions.

Downloaded from http://onepetro.org/SJ/article-pdf/doi/10.2118/216925-PA/3118828/spe-216925-pa.pdf/1 by Stavanger University Library user on 26 July 2023

used as an additive to improve the mechanical properties and potentially retard the setting at high temperatures. Distilled water was used to prepare the samples. When the KOH solution was used, its water content was discounted from the added water.

Formulations. In this work, three previously developed formulations (W1Pb, W1Pb-Z4, and W1Pb-Z6) are studied using the following notation (neat, 0.57% ZnO, and 0.86% ZnO). Additionally, a true JAW neat formulation is introduced, in which the 12 M KOH solution is replaced by anhydrous potassium hydroxide and, therefore, only water is truly required in the liquid part. The silica modulus or molar ratio (SiO_2/K_2O) of the activator was kept constant at 2.40. The full compositions are listed in **Table 3,** while the molar ratios of those formulations, water-to-solid proportions, and their theoretical specific gravities are listed in **Table 4.**

Composition (% bwop*)	Granite	GGBFS	MS	K_2SiO_3	KOH (Anhydrous)	KOH (12 M Solution)	ZnO	Water
JAW	48.6	47.1	4.29	20.8	4.24	0.00	0.00	41.3
Neat	48.6	47.1	4.29	20.8	0.00	9.21	0.00	36.4
0.57% ZnO	48.6	47.1	4.29	20.8	0.00	9.21	0.57	36.4
0.86% ZnO	48.6	47.1	4.29	20.8	0.00	9.21	0.86	36.4

*By weight of precursor mixture (granite, GGBFS, and MS).

Table 3—Geopolymer formulations investigated in this study.

Molar Ratios	JAW	Neat	0.57% ZnO	0.86% ZnO
$SiO_{2,nominal}/Al_2O_3$	9.72	9.72	9.72	9.72
$SiO_{2,reactive}/Al_2O_3$	4.87	4.87	4.87	4.87
$SiO_{2,nominal}/CaO$	4.05	4.05	4.05	4.05
$SiO_{2,reactive}/CaO$	2.03	2.03	2.03	2.03
K_2O/Al_2O_3	1.07	1.07	1.07	1.07
Na_2O/Al_2O_3	0.23	0.23	0.23	0.23
$(K_2O + Na_2O)/Al_2O_3$	1.31	1.31	1.31	1.31
$ZnO/SiO_{2,nominal}$	–	–	0.00585	0.00877
$ZnO/SiO_{2,reactive}$	–	–	0.0117	0.0175
ZnO/CaO	–	–	0.0237	0.0355
H_2O/K_2O	17.75	17.78	17.78	17.78
KOH molarity (M)	–	12	12	12
Water/solids	0.338	0.338	0.336	0.335
Specific gravity (g/cm³)	1.88	1.90	1.90	1.89

Table 4—Oxide molar ratios, water-to-solid ratios, and theoretical density of geopolymer formulations.

Activation (pH) and dissolution [inductively coupled plasma mass spectrometry (ICP-MS)] studies were performed for a diluted version of the activator, for each individual precursor, for zinc oxide, and for the full formulations of **Table 3**. All solids were mixed with the diluted activator, as described in **Table 5.** For ICP-MS tests, the activator was diluted with double the amount of water.

The overall kinetics evaluation [differential scanning calorimetry (DSC)] used the same formulations of **Table 3** and additionally two individual precursor formulations presented in **Table 6.**

Mixing and Conditioning. Slurry preparation was performed by preblending all solid components with the activator (solid and/or solution) and adding the mixture to distilled water, in the amount indicated for each experiment. For pH, ICP-MS, and DSC tests, the solids were homogenized by mixing and shaking manually, then added to the activator in water, and hand mixed for 5 minutes.

For standard tests [e.g., thickening time, sonic strength (SS), and destructive compressive strength], the procedure recommended in API RP 10B-2 (2019) was followed. The OFITE Model 20 constant-speed blender was used for mixing all the slurry components. The preblend of geopolymer precursor and activator was poured in distilled water into the first 15 seconds at 4,000 rev/min, and then the slurry was sheared for 35 seconds at 12,000 rev/min.

A temperature of 50°C was chosen as BHCT and 70°C as the bottomhole static temperature (BHST). An atmospheric consistometer (API RP 10B-2 2019) was used for conditioning all slurries, at 50°C BHCT, prepared for measuring compressive strength.

X-Ray Diffraction. The mineralogical characterization of raw precursors **(Table 1)** and pastes **(Table 3)** was obtained by X-ray diffraction (XRD) and Rietveld analysis. Fractured paste samples from the uniaxial compressive strength (UCS) test were ground and dried in an oven at 30°C overnight, and then they were kept in a vacuum dryer for 1 day to maximize the removal of moisture. The analysis was conducted according to ASTM C1365-18 (2018) using a Bruker-AXS Microdiffractometer D8 Advance diffractometer, operating at 45 kV and 40 mA with CuKα radiation (λ = 1.5418 Å), a scanning range of 5–92° 2θ, and a step size of 0.01° 2θ.

Downloaded from http://onepetro.org/SJ/article-pdf/doi/10.2118/215825-PA/3118928/spe-215825-pa.pdf/1 by Stavanger University Library user on 26 July 2023

Mix (% bwop*)	Granite	GGBFS	MS	K_2SiO_3	KOH (Anhydrous)	KOH (12 M Solution)	ZnO	Water†
K_2SiO_3	0.0	0.0	0.00	20.8	0.00	0.00	0.00	166
Activator	0.0	0.0	0.00	20.8	0.00	9.21	0.00	166
Granite	48.6	0.0	0.00	20.8	0.00	9.21	0.00	166
GGBFS	0.0	47.1	0.00	20.8	0.00	9.21	0.00	166
Microsilica	0.0	0.0	4.29	20.8	0.00	9.21	0.00	166
0.86% ZnO‡	0.0	0.0	0.00	20.8	0.00	9.21	0.86	166
JAW	48.6	47.1	4.29	20.8	4.26	0.00	0.00	166
Neat	48.6	47.1	4.29	20.8	0.00	9.21	0.00	166
0.57% ZnO	48.6	47.1	4.29	20.8	0.00	9.21	0.57	166
0.86% ZnO	48.6	47.1	4.29	20.8	0.00	9.21	0.86	166

*By weight of precursor used in the JAW mixture.
†For dissolution (ICP-MS) measurements, the amount of water was doubled to 333% bwop.
‡This composition was only considered for pH measurements.

Table 5—Precursor and geopolymer formulations adopted for the pH and ICP-MS evaluations.

Mix (% bwop*)	Granite	GGBFS	MS	K_2SiO_3	KOH (Anhydrous)	KOH (12 M Solution)	ZnO	Water
Granite	100	0.0	0.00	20.8	0.00	9.21	0.00	36.4
GGBFS	0.0	100	0.00	20.8	0.00	9.21	0.00	36.4

*By weight of precursor used in the JAW mixture.

Table 6—Precursor formulations adopted for the kinetics evaluations.

Crystalline phases of precursors and pastes were identified using the EVA v5 Bruker software. Rietveld quantitative phase analysis of granite was conducted using the TOPAS v5 Bruker software and a PDF database. GGBFS and MS are approximately amorphous, based on the absence of major crystalline peaks in their respective diffractograms.

Fourier-Transform Infrared Spectroscopy. Aliquots from the samples prepared for XRD tests (raw precursors in **Table 1** and geopolymer pastes in **Table 3**) were used for Fourier transform infrared (FTIR) spectroscopy according to the ASTM C1365-18 (2018) standard, using an Agilent Cary 630 FTIR spectrometer equipped with a diamond composite attenuated total reflectance crystal. FTIR spectra were collected in transmittance mode from 4000 cm^{-1} to 600 cm^{-1} at a resolution of 1 cm^{-1}.

Alkalinity and Inductively Coupled Plasma. A Mettler Toledo SevenExcellence pH meter was used to measure the alkalinity of diluted mixes **(Table 5)** at room temperature (uncontrolled) and BHCT (50°C). ICP-MS was used to analyze the dissolution of each material and their mixes **(Table 5)** in the given alkaline medium following ASTM D5673-16 (2016). The ICP-MS samples were collected after performing a 30-minute static fluid loss test (API RP 10B-2 2019) at room temperature and 6.9 MPa for each of the formulations given in **Table 5**.

Isothermal Calorimetry. A DSC was used to obtain the isothermal calorimetry curves of the raw materials and geopolymer pastes (**Tables 3 and 6**, respectively) to study their kinetics. Studies were performed at room temperature (25°C) and at BHCT (50°C) for up to 180 minutes. The heat evolution exerted by them was evaluated according to ASTM C1702-17 (2017).

Thickening Time. The thickening time of all geopolymer formulations, presented in **Table 3**, was measured according to API RP 10B-2 (2019) using an atmospheric consistometer, ramping up from room temperature to 50°C BHCT at 1 °C/min. The pumpability time at 40 Bc was chosen for all pastes, and the tests were ended by that time.

Ultrasonic Compressive Strength. The SS development of the pastes **(Table 3)** was assessed according to API RP 10B-2 (2019), with an ultrasonic cement analyzer. The test was performed at 13.8 MPa and 70°C (BHST) for 7 days, with the temperature and pressure ramp-up rates of 1 °C/min, and 17.2 bar/min, respectively. SS was obtained from the transit time using the custom algorithm fitted by Omran and Khalifeh (2022), which correlates the destructive uniaxial strength with the ultrasonic cement analyzer transit time, for a very similar formulation.

Uniaxial Compressive Strength. Cylindrical samples for UCS (51 mm diameter and 80 mm height) were cast in plastic molds and cured at atmospheric pressure in an oven at 70°C (BHST) for 24 hours and 7 days. A cutter machine was used to flatten both ends of the cured samples. Six samples for each mix design of **Table 3** were prepared. UCS tests were performed according to ASTM C597-16 (2021), using a Toni Technik-H mechanical tester at a loading rate of 10 kN/min.

Downloaded from http://onepetro.org/SJ/article-pdf/doi/10.2118/218925-PA/3116828/spe-218925-pa.pdf by Stavanger University Library user on 26 July 2023

Results and Discussion

Characterization of Precursors and Pastes (Particle-Size Distribution and XRD). As seen in **Table 1**, the chemical composition of the granite precursor is mainly silica and alumina, with potassium, sodium, and iron oxide as minor components. Its particle-size distribution (**Table 2** and **Fig. 2**) is very coarse and wide, spanning from 3.5 μm to 131 μm, with a median diameter of 21 μm. GGBFS, on the other hand, is composed mainly of silica and calcium oxide, with similar amounts of aluminum and magnesium as secondary components. Its median particle size of 16 μm is similar to that of granite, with a narrower range. Microsilica is almost pure silicon oxide, much finer than the other two precursors, and with a narrow size distribution of around 0.34 μm.

XRD spectra of the precursors, characterized by Omran and Khalifeh (2022), are shown in **Fig. 3.** Granite has a very high crystalline content, whose mineralogy was reinterpreted and quantified, as detailed in **Table 7.** The major phases are quartz, feldspar (microcline and albite), and oligoclase, with biotite and chlorite as minor phases.

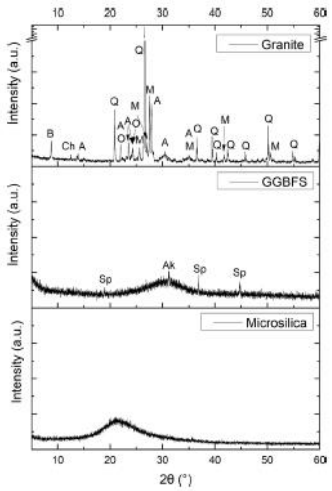

Fig. 3—XRD mineralogical characterization of the raw material precursors. (A) Albite, (Ak) Akermanite, (B) Biotite, (Ch) Chlorite, (M) Microcline, (O) Oligoclase, (Q) Quartz, and (Sp) Spinel.

Minerals	No.	Granite (%wt/wt)
Quartz	PDF 00-008-7651	35.693
Albite	PDF 00-009-0466	21.625
Microcline 1	CIF 9004191	16.059
Microcline 2	PDF 00-019-0932	11.918
Oligoclase	CIF 9011423	10.654
Biotite	PDF 04-013-2135	2.382
Chlorite	COD 9010163	1.669

Table 7—Granite mineralogy obtained from Rietveld quantification.

As GGBFS and microsilica exhibit mainly amorphous profiles, compared to granite, no Rietveld refinement was conducted for them. Qualitatively, GGBFS contains a minor amount of akermanite and spinel, as expected for typical blast furnace slags (Hewlett 2001).

XRD spectra of selected geopolymer pastes are shown in **Fig. 4.** In comparison with the solid precursors, the main peaks relative to granite (quartz, albite, and microcline) are still present, while the biotite peak disappeared. An additional hydrated K-A-S-H phase was observed in the pastes, JAW and neat. In 0.86% ZnO paste, an additional K-(K-Na)-Zn-A-S-H phase, with the presence of zinc, was detected. An amorphous hump is present in all pastes, which encompasses unreacted amorphous precursor phases, and possibly amorphous geopolymers and hydrated phases such as C-S-H, C-A-S-H, and C-(K, Na)-A-S-H.

FTIR Characterization of Precursors and Pastes. FTIR spectra were used to analyze the individual precursors and the dry potassium silicate activator at room temperature following ASTM E168-16 (2016). The broadband between 800 cm^{-1} and 1250 cm^{-1} is attributed

Downloaded from http://onepetro.org/SJ/article-pdf/doi/10.2118/215925-PA/3118928/spe-215925-pa.pdf/1 by Stavanger University Library user on 26 July 2023

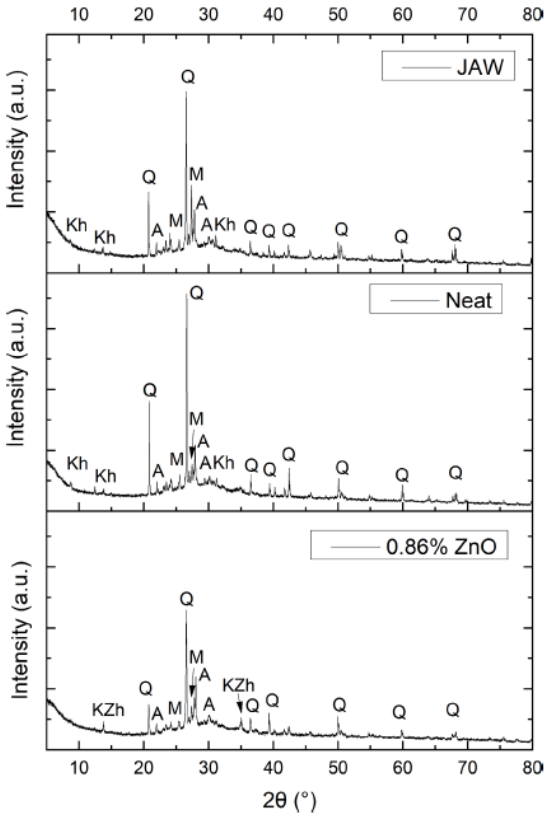

Fig. 4—XRD mineralogical characterization of selected geopolymers after 7 days of curing at 70°C. (A) Albite, (Kh) K-A-S-H, (KZh) (K-Na)-Zn-A-S-H, (M) Microcline and (Q) Quartz.

to the asymmetric stretching vibrations of the bond between silica tetrahedra or silica-alumina tetrahedra (Si-O-T, where T is either Si or Al) by Sturm et al. (2016). This band was observed for all materials, as shown in **Fig. 5**, with peaks varying from 990 cm^{-1} for granite to 872 cm^{-1} for GGBFS. Sturm et al. (2016) observed a peak at 1059 cm^{-1} for pure amorphous silica and a peak at 975 cm^{-1} for geopolymer, attributing the shift to the increasing fraction of alumina tetrahedra.

In the case of the silicate activators, Falcone et al. (2010) observed a shift from 1020 cm^{-1} toward lower wavenumbers with the increase in silica concentration. Therefore, the main absorption peak at 965 cm^{-1} is consistent with the high molar ratio (3.92) of the solid activator.

GGBFS also shows a small absorption peak at 1480 cm^{-1}, generally attributed to O–C-O bonds, such as those in calcium carbonate (Sturm et al. 2016). As GGBFS can form C-S-H, mild carbonation may have occurred in this precursor (Hewlett 2001).

FTIR spectra of the geopolymer pastes are presented in **Fig. 6.** The band between 800 cm^{-1} and 1250 cm^{-1}, corresponding to the stretching vibration mode of tetrahedral silica and alumina, was also observed. The peak at 965 cm^{-1} is located between the granite and GGBFS peaks and is consistent with the structure of geopolymers. The carbonate peak from GGBFS is still present around 1420 cm^{-1}, but less pronounced, suggesting that the geopolymer products are not suffering carbonation.

The broad hump between 2500 cm^{-1} and 3700 cm^{-1} corresponds to stretching vibrations of incorporated water and hydrated products (H–OH bonds). Together with the small O–H stretching peak around 1640 cm^{-1}, this peak around 3360 cm^{-1} represents the generation of geopolymeric products. Compared to JAW (dry activator), the peak area increases by 25% for the neat paste, due to the use of a liquid activator. The addition of zinc oxide does not shift any of the peaks but increases the area of the H–OH peak by 59% and 61% for 0.57% ZnO and 0.86% ZnO pastes, respectively, compared to the JAW one. The peak intensity follows the same trend.

Downloaded from http://onepetro.org/SJ/article-pdf/doi/10.2118/215825-PA/2118928/spe-215825-pa.pdf/1 by Stavanger University Library user on 26 July 2023

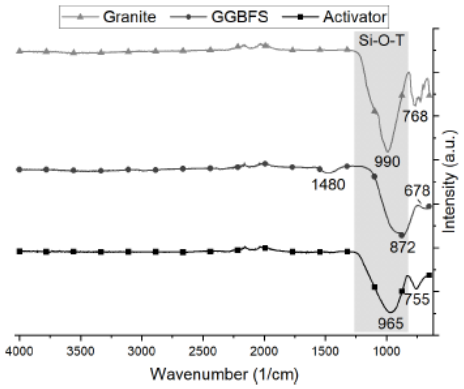

Fig. 5—FTIR spectra of the solid powder precursors.

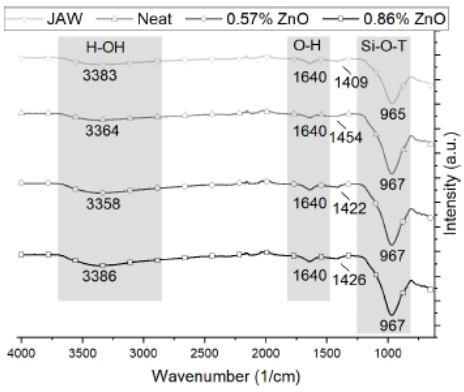

Fig. 6—FTIR spectra of the four geopolymer designs.

Activation of Precursors and Pastes (pH Evaluation). Table 8 presents the pH evolution in the first 10 minutes after mixing at room temperature. Pure silicate dissolves and generates a stable pH of 12.13. Therefore, in this dilute concentration, it is not sufficiently alkaline to be a standalone activator. The addition of KOH raised the pH to 13.48. Subsequent tests are analyzed with respect to this.

Granite initially increased the pH by +0.07 but then lowered by −0.02 after 10 minutes, showing some consumption of OH^- in the first minutes. GGBFS also reduced the pH by −0.05, a similar behavior. Microsilica had a stronger effect, lowering by −0.11, despite having less than 10% of the mass of the two other precursors. Zinc oxide also consumed alkalinity, lowering the pH by −0.05 despite its much smaller amount. This can be explained by its solubility in high pH. In this temperature and time scale, granite is less reactive than GGBFS, while microsilica seems to be more easily activated than the other two.

When combined, the precursors have a different effect on pH. Formulation JAW caused an initial decrease in pH but a final increase (+0.03), which can be explained by its use of solid KOH instead of the KOH solution used for the other tests. The dissolution of KOH can also explain the increase in solution temperature to 25.8°C. Formulation neat had an insignificant variation of pH. Mixes of 0.57% ZnO and 0.86% ZnO displayed an initial drop in pH, but 0.57% ZnO returned to the base value of 13.48. Only 0.86% ZnO lowered the pH by −0.08 after 10 minutes. As microsilica alone can lower the pH to 13.37 and each individual precursor can lower the pH below the base value, a competition effect must be inhibiting the activation of the mixes.

Table 9 presents the results at a temperature of 50°C. The results for precursors are analogous to those at room temperature. The baseline (pure activator) is pH 13.41 at 10 minutes. Granite had the smallest reduction (−0.03), GGBFS was again more reactive than granite (reduction −0.05) and microsilica had the largest effect (−0.11). Zinc oxide reduced the pH by −0.09, despite its very small amount. The formulations without zinc had an initial drop and stayed stable for 10 minutes at 13.30 (−0.11). The two formulations with zinc had a

Downloaded from http://onepetro.org/SJ/article-pdf/doi/10.2118/215825-PA/3118828/spe-215825-pa.pdf by Stavanger University Library user on 26 July 2023

Activators, Activated Materials, and Formulations	pH* (Initial)	pH* (10 Minutes)	T (°C) Average
K_2SiO_3	12.13	12.12	22.14
K_2SiO_3 + KOH (Activator)	13.50	13.48	22.53
Granite	13.55	13.46	22.43
GGBFS	13.50	13.43	22.47
Microsilica	13.47	13.37	22.55
0.86% ZnO†	13.47	13.43	23.00
Neat†	13.49	13.48	22.77
0.57% ZnO‡	13.45	13.48	22.87
0.86% ZnO‡	13.42	13.40	22.90
JAW‡	13.43	13.53	25.80

*pH meter has ±0.01 error margin.
†Same composition described in **Table 5**.
‡By weight of precursor used on each paste.

Table 8—Initial and final pH data at room temperature.

Activator, Activated Materials, and Formulations	Initial pH*	pH* After 10 minutes	pH Total Average
K_2SiO_3 + KOH (activator)	13.40	13.41	13.41
Granite	13.39	13.38	13.39
GGBFS	13.35	13.36	13.36
Microsilica	13.32	13.30	13.31
0.86% ZnO†	13.31	13.31	13.31
Neat‡	13.30	13.30	13.30
0.57% ZnO‡	13.27	13.26	13.27
0.86% ZnO ‡	13.27	13.25	13.26
JAW ‡	13.31	13.30	13.30

*pH meter has ±0.01 error margin.
†Same composition described iin **Table 5**.
‡By weight of precursor used on each paste.

Table 9—Initial and final pH data at 50°C.

slightly larger initial drop, ending with 13.26 (−0.15). This confirms that zinc oxide contributes to the reduction in pH, as suggested by the data at room temperature.

Dissolution of Precursors and Pastes (ICP Analysis). ICP-MS results for the activator, individual precursors with activator, and diluted geopolymer mixes are shown in **Table 10.** We use the pure activator (silicate and hydroxide solution) as the baseline for silicon (750 mg/L) and potassium (20 000 mg/L) concentrations because all mixes have the same amount of activator and dilution water. Granite increased the silicon concentration from 750 mg/L to 1200 mg/L, while GGBFS decreased it to 220 mg/L. A possible reason is the adsorption of silicate on the surface of GGBFS particles (Hewlett 2001) or formation of C-S-H. Microsilica, as observed in the pH studies, was very effective in releasing silica into the solution. Potassium levels were not affected within the precision of the method. Although

Material	Silicon (mg/L)	Aluminum (mg/L)	Potassium (mg/L)	Sodium (mg/L)	Zinc (mg/L)
Activator	750	0.74	20 000	100	0.68
Granite	1200	6.5	20 000	110	5.2
GGBFS	220	23	19 000	110	1.2
Microsilica	2800	2.1	20 000	100	3
JAW*	840	110	89 000	800	21
Neat*	1100	94	71 000	540	0.61
0.57% ZnO*	900	120	64 000	540	980
0.86% ZnO*	530	140	60 000	530	1900

*By weight of precursor used on each paste.

Table 10—ICP evaluation for precursors and geopolymer pastes.

Downloaded from http://onepetro.org/SJ/article-pdf/doi/10.2118/215825-PA/2118828/spe-215825-pa.pdf/1 by Stavanger University Library user on 26 July 2023

alumina contents in GGBFS and granite are similar (12.7% and 13.3%, respectively), GGBFS released much more aluminum (23 mg/L) than granite (6.5 mg/L).

Dilute geopolymer formulations show dissolution behaviors beyond the dissolution of each individual precursor. Notably, the silicon concentration of the mixes is smaller than that generated by granite by itself and much smaller than that of microsilica. Therefore, a phenomenon such as GGBFS surface adsorption or C-S-H formation must be consuming the silicate as it is released. On the other hand, all mixes release much more aluminate into the solution, compared to the sum of the precursors. This may be explained by noting that the decrease in silicate concentration favors the dissolution of silico-aluminates. The high amount of aluminum released by GGBFS may have the same origin. Potassium concentration is much higher for geopolymer mixes than for individual precursors and pure activators. About 77% of the potassium content of the mix comes from the activator; therefore, the increase in concentration must come from improved solubilization of solid potassium silicate.

The main effects of zinc oxide are a decrease in silicate concentration, a small increase in aluminate concentration, and a decrease in potassium concentration. Zinc oxide in water forms zincate, which captures silicate in zincate-silicate complexes. The simultaneous decrease in silicate and potassium concentration suggests the capture or precipitation of potassium zincate silicate, which would also explain the reduction in pH observed in the previous section. XRD analysis of cured geopolymers indicates the presence of a potassium-sodium zinc silicate hydrate (N, K)-Z-S-H, which could account for this observation. Aluminum concentration is not reduced, suggesting that aluminate is not being immobilized. Without calcium concentration measurements, it is not possible to confirm the precipitation of CZ, as suggested by Garg and White (2017), which would also be consistent with the observations.

Kinetics of Precursors and Pastes. For all DSC curves, the initial equilibration period is discarded, and the curves are shown after they become exothermal. The main difference in behavior between the curves at 25°C and the corresponding 50°C curves is that the main peak occurs earlier and has greater intensity and decays faster at 50°C, showing that the reactions are thermally activated. In most cases, the total heat released at 50°C is also larger during the first 3 hours.

Fig. 7 shows the heat evolution and accumulated heat released by precursors, for the first 3 hours after mixing. Compared to granite at 25°C, GGBFS reaches its peak heat release earlier and releases more heat during the study period. This can be understood as GGBFS has a significant amorphous fraction, which is more readily dissolved, compared to the mainly crystalline granite. At longer times, GGBFS releases more heat per unit weight, suggesting that the precursor can react further in the next hours. At 50°C, temperature activation makes both precursors approximately equivalent in peak heat release rate, but GGBFS sustains the reaction for longer. In fact, granite heat release appears to reach a plateau and the total energy is lower at 50°C than it is at 25°C.

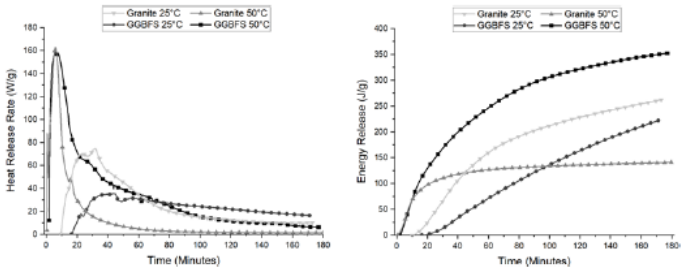

Fig. 7—DSC measurements of activated precursors at 25°C and 50°C.

As shown in **Fig. 8,** at 25°C, the neat paste with the liquid accelerator reacts earlier and has a larger heat release peak than the JAW paste with solid precursors. The total heat release is also higher for the neat slurry. This can be explained by the need to first dissolve the

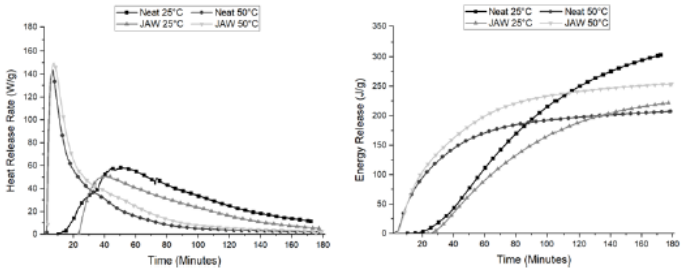

Fig. 8—DSC measurements of geopolymer formulations with liquid activator (neat) and solid activator (JAW) at 25°C and 50°C.

Downloaded from http://onepetro.org/SJ/article-pdf/doi/10.2118/215825-PA/3118829/spe-215825-pa.pdf/1 by Stavanger University Library user on 26 July 2023

solid activator, before ideal conditions for precursor dissolution and geopolymerization can be met. At 50°C, this first dissolution step happens very fast, and the JAW was able to release more heat than the neat, possibly because of the significant heat of dissolution of potassium hydroxide.

Fig. 9 compares the heat evolution of the neat formulation vs. the ones with 0.57% ZnO and 0.86% ZnO. As the amount of added zinc increases, the height and width of the peak increase and the total amount of heat also increases. However, this early energy release is followed by a period of low heat evolution.

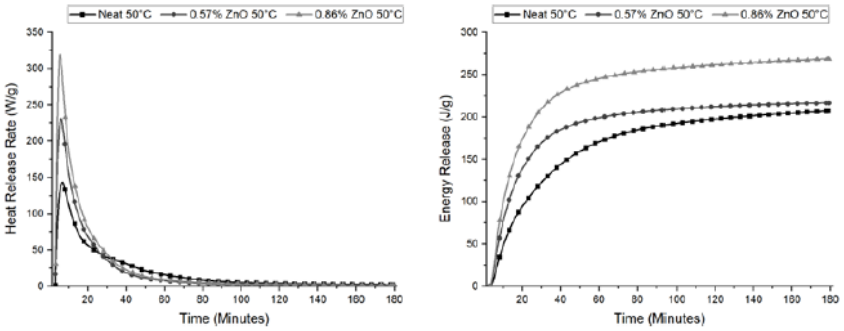

Fig. 9—Isothermal calorimetry measurements of geopolymer formulations with added zinc oxide at 50°C.

Table 11 summarizes the observations above in terms of the size and position of the peak in the heat evolution curve, as well as the total energy release for those pastes.

	Time at Maximum Heat Release Rate (minutes)		Maximum Heat Release Rate (mW/g)		Total Energy Release at 180 minutes (J/g)	
Material	25°C	50°C	25°C	50°C	25°C	50°C
Granite	44	6	35	152	216	140
GGBFS	24	6	65	162	257	347
JAW	39	8	50	140	217	251
Neat	52	8	57	143	298	205
0.57% ZnO	–	7	–	234	–	215
0.86% ZnO	–	7	–	317	–	267

Table 11—Heat and energy evolution parameters for the pastes.

Thickening Time. The consistency (in Bearden units) vs. time measurements at BHCT 50°C for the proposed geopolymer formulations are presented in **Fig. 10.** A consistency of 40 Bc was selected as a baseline for the pumpability period for geopolymer slurries. These consistency curves show the three geopolymerization reaction stages, starting from the dissolution of the precursors, observed as a decrease in consistency while the temperature is ramping up, until reaching the reorganization stage. The reorganization stage has the lowest consistency range. After that, the polycondensation stage starts, when the slurries coagulate and then transform into a gel with the formation of a 3D network polymeric structure. This rapid gain in consistency is usually called "right-angle set," and it is a desirable property in a well cementing slurry. Due to safety reasons, the tests were not followed up to 100 Bc.

These four rock-based slurries had pumpability times of 40 Bc ranging from 43 minutes to 45 minutes, as shown in **Fig. 10**. In addition, a right-angle set was observed for the four recipes. Compared to two-part rock-based slurries (Chamssine et al. 2021, 2022b), these recipes range from 64% to 72% of the pumpability time of those slurries. In contrast, the four mixes have initial consistencies from 17 Bc to 27 Bc, whereas the neat two-part slurry had initial consistency of around 37 Bc. Moreover, the JAW slurry had the lowest initial consistency among all one-part (neat, 0.57%, and 0.86% ZnO) rock-based geopolymer slurries due to the 100% free water content in liquid phase, while the rest have 88% free water content in liquid phase.

Ultrasonic Compressive Strength. Fig. 11 presents the SS development curves for the four geopolymer mixes at 70°C of BHST and pressurized to 2,000 psi (13.8 MPa). **Table 12** presents the conventional setting and hardening times, defined as the times to reach SSs of 100 psi and 500 psi (0.69 MPa and 3.45 MPa, respectively) in addition to the SS after 1 day and 7 days.

Uniaxial Compressive Strength. Fig. 12 shows the UCS of the geopolymer pastes after 1 day and 7 days of curing at 70°C and atmospheric pressure. JAW and neat slurries have similar strengths. Pastes with 0.57% and 0.86% ZnO have higher strength, almost

Downloaded from http://onepetro.org/SJ/article-pdf/doi/10.2118/215825-PA/3118828/spe-215825-pa.pdf by Stavanger University Library user on 26 July 2023

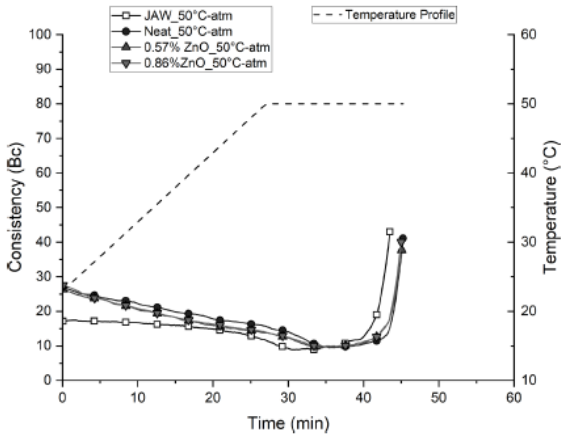

Fig. 10—Consistency evolution of geopolymer slurries at BHCT 50°C and atmospheric pressure.

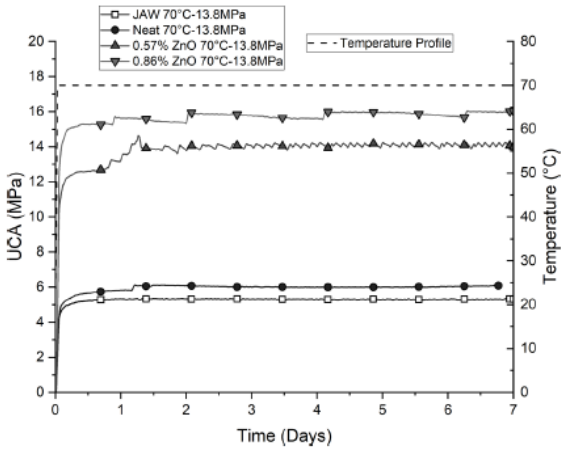

Fig. 11—SS development up to 7 days at 70°C and 13.8 MPa.

Mix Design	Setting Time to 100 psi (minutes)	Hardening Time to 500 psi (minutes)	SS (MPa) for 1 day	SS (MPa) for 7 days
JAW	44	68	5.36	5.42
Neat	43	66	5.85	6.10
0.57% ZnO	42	48	13.21	13.94
0.86% ZnO	38	46	15.65	16.04

Table 12—Summary of ultrasonic cement analyzer data for the four optimized mixes.

Downloaded from http://onepetro.org/SJ/article-pdf/doi/10.2118/215825-PA/3118828/spe-215825-pa.pdf/1 by Stavanger University Library user on 26 July 2023

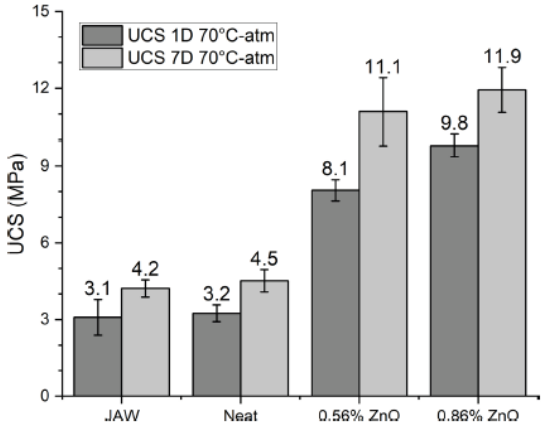

Fig. 12—UCS data cured at 70°C and atmospheric pressure.

three times the strength of the neat pastes. These results are in good agreement with those obtained using SS tests. Most of the strength development occurs within the first 12 hours.

Discussion

The JAW geopolymer formulation is a combination of two precursors with distinct natures and behaviors. Granite is a highly crystalline aluminosilicate material; therefore, it is slower to activate than amorphous precursors. Its silica/aluminum ratio is very high, compared to the ideal 2:1 ratio; therefore, geopolymerization in the form of K-A-S-H is limited by the low availability of aluminates in solution. On the other hand, GGBFS is a calcium-rich amorphous precursor, with less silica but similar aluminate content. It will dissolve earlier and supply free calcium to the solution. In low-pH silica-rich environments, this will lead to the formation of C-S-H (Myers et al. 2014), which will capture and precipitate silica, as observed through ICP **(Table 10)**.

Gasteiger et al. (1992) investigated the solubility of aluminosilicate materials in alkaline solutions, finding an equilibrium involving aluminate $Al(OH)_4^-$, orthosilicic acid $HSiO_4^{3-}$, and the solid phase present in the system, described by the solubility product [Si][Al]. In **Fig. 13,** the reduction in silica concentration will induce silicate-aluminate dissolution, especially after the addition of ZnO, favoring the silica/aluminum ratio close to the ideal ratio by increasing the availability of more free aluminum ions and enabling the formation of C-A-S-H, C-(K)-A-S-H, and (K-Na)-Zn-A-S-H.

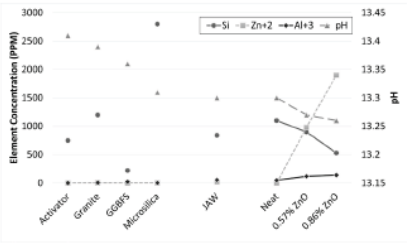

Fig. 13—Integrated analysis between pH and ICP for all given mixes.

When the precursors are combined in the JAW and neat formulations, it is observed through ICP-MS that higher silicate and aluminate concentrations can be obtained by the dissolution of silicate- and aluminate-rich granite, enhanced by the capture of silicates through C-S-H formation, using calcium from GGBFS, as seen in **Fig. 13**. Heat release peaks are broader than the respective peaks for each precursor, as the formulation starts to react earlier through the action of GGBFS and continues for longer as the granite fraction is consumed together with GGBFS.

At high pH, silica dimers and polymers tend to depolymerize. However, when sufficient aluminum and silica are present in solution, aluminosilicate dimers $[(OH)_3–Al–O–Si–(OH)_3]^-$ will form, reorganize, and condense in small aluminosilicate units (Gasteiger et al.

Downloaded from http://onepetro.org/SJ/article-pdf/doi/10.2118/215825-PA/3186828/spe-215825-pa.pdf by Stavanger University Library user on 26 July 2023

1992). In these conditions, zinc oxide is present as zincate, $Zn(OH)_3^-$ or $Zn(OH)_4^{2-}$ (Chen et al. 2012). Anseau et al. (2005) used ^{29}Si, ^{27}Al, and ^{67}Zn NMR in high pH solutions, to show that silicates in solution form complexes with both zincates and aluminates, in similar proportions. Each zincate ion can bind to a silicate monomer or dimer, while aluminates bind to a single silicate monomer. This competition may explain the retardation of low calcium geopolymers, as observed by Chamssine et al. (2022b).

In the case of 0.57% ZnO and 0.86% ZnO slurries, thickening time results did not show marked differences in setting time. The difference may be attributed to the smaller amount of zinc used in this work and the lower solubility of ZnO (Chen et al. 2012) compared to the zinc salt used by Chamssine et al. (2022a). Also, calorimetry shows that the initial effect of zinc was to increase the heat release rate. Through ICP-MS, it is seen that the effect of zinc was to decrease the silicate concentration and to increase the aluminate content (see **Fig. 13**). It is possible that there was excess free silica in solution; therefore, the complexation with zincates and precipitation as C-S-H worked to capture this excess of silica and induced the dissolution of aluminates. Therefore, the dissolution stage of geopolymerization was enhanced rather than retarded, precipitating larger amounts of (C,K)-A-S-H and C-(K)-A-S-H, as seen in both SS **(Fig. 11)** and UCS **(Fig. 12)** results. Only later, the retardation effect can be observed as a slowing of the heat release rate, as seen in **Fig. 14.**

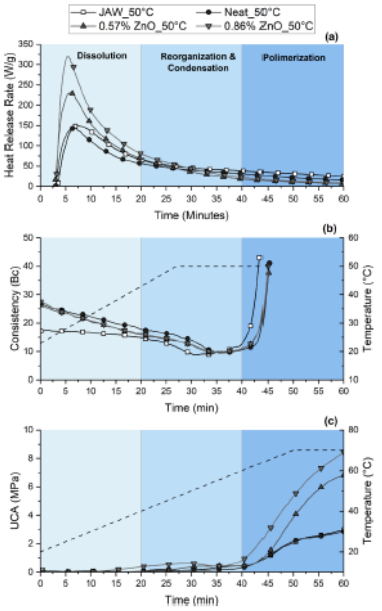

Fig. 14—Comparison between (a) heat release rate, (b) consistency profile, and (c) SS development, at the first hour after mixing, to understand the rock-based geopolymer kinetics.

From **Fig. 11** and **Table 12**, there was a small improvement from JAW (true one-part) to neat (formulation using KOH solution). Zinc addition, on the other hand, significantly improved the strength, with 0.86% ZnO paste giving the highest SS development up to 7 days, as well as the fastest setting and hardening times. Its SS is about three times that of the pure recipes JAW and neat. Omran and Khalifeh (2022) performed a wider study of the neat formulation, considering additional concentrations of zinc oxide and other additives, such as calcium oxide, calcium carbonate, and sodium hydroxide. Compared to those results, this work demonstrates that the new JAW formulation can reach strengths comparable to those of the neat one. The JAW formulation reaches a comparable strength after 1 day of curing, but the neat gains slightly less strength after 7 days. Formulations with zinc oxide suggest that the difference between 0.57% ZnO and 0.86% ZnO pastes becomes smaller after 7 days of curing, a result that was not seen in sonic strength curves. Higher concentrations did not increase the 1-day strength and therefore were not investigated in this work. However, the lack of retardation indicates that there is room to increase the ZnO content to increase the setting time.

Conclusions

Short-term chemical and mechanical properties of one-part geopolymer mixes were studied to obtain a better understanding of their geopolymerization mechanism for well-cementing applications. This investigation revealed some correlations between the chemical and mechanical properties of geopolymer cement. The addition of zinc oxide powder as a strength booster increases the rate of heat evolution and improves the early strength development. The higher the heat and energy evolution from geopolymerization reaction, the better the

Downloaded from http://onepetro.org/SJ/article-pdf/doi/10.2118/215925-PA/3118928/spe-215925-pa.pdf/1 by Stavanger University Library user on 26 July 2023

early strength development. Moreover, the addition of zinc oxide powder does not have any effect on the slurry properties without any retardation.

Acknowledgments

The authors gratefully acknowledge TotalEnergies, AkerBP, ConocoPhillips, and Research Council of Norway for financially supporting the SafeRock KPN Project (RCN #319014319014— New Cementitious Material for Oil Well Cementing Applications—SafeRock) at the University of Stavanger, Norway. In addition, the authors would like to acknowledge Professor Oscar Reales and Dr. Paulo Moreira for thier collaboration.

References

Alvi, M. A. A., Khalifeh, M., and Agonafir, M. B. 2020. Effect of Nanoparticles on Properties of Geopolymers Designed for Well Cementing Applications. *J Pet Sci Eng* **191**. https://doi.org/10.1016/j.petrol.2020.107128.

Andrew, R. M. 2019. Global CO2 Emissions from Cement Production, 1928–2018. *Earth Syst Sci Data* **11**: 1675–1710. https://doi.org/10.5194/essd-11-1675-2019.

Anseau, M. R., Leung, J. P., Sahai, N. et al. 2005. Interactions of Silicate Ions with Zinc(II) and Aluminum(III) in Alkaline Aqueous Solution. *Inorg Chem* **44** (22): 8023–8032. https://doi.org/10.1021/ic050594c.

API RP 10B-2, Recommended Practice for Testing Well Cements. 2019. Washington, DC., USA: American Petroleum Institute.

ASTM C1365-18, Standard Test Method for Determination of the Proportion of Phases in Portland Cement and Portland-Cement Clinker Using X-Ray Powder Diffraction Analysis. 2018. West Conshohocken, Pennsylvania, USA: ASTM: .

ASTM C1702-17, Standard Test Method for Measurement of Heat of Hydration of Hydraulic Cementitious Materials Using Isothermal Conduction Calorimetry. 2017. West Conshohocken, Pennsylvania, USA: ASTM.

ASTM C597-16, Standard Test Method for Pulse Velocity Through Concrete. 2021. West Conshohocken, Pennsylvania, USA: ASTM.

ASTM D5673-16, Standard Test Method for Elements in Water by Inductively Coupled Plasma—Mass Spectrometry. 2016. West Conshohocken, Pennsylvania: ASTM.

ASTM E168-16, Standard Practices for General Techniques of Infrared Quantitative Analysis. 2016. West Conshohocken, Pennsylvania, USA: ASTM.

Barlet-Gouedard, V., Zusatz-Ayache, B., and Porcherie, O. 2008. Pumpable Geopolymer Formulation for Oilfield Application. 2008/017414 A1. WO.

Bergen, S. L., Zemberekci, L., and Nair, S. D. 2022. A Review of Conventional and Alternative Cementitious Materials for Geothermal Wells. *Renew Sust Energ Rev* **161**. https://doi.org/10.1016/j.rser.2022.112347.

Cai, J., Li, X., Tan, J. et al. 2020. Thermal and Compressive Behaviors of Fly Ash and Metakaolin-Based Geopolymer. *J Build Eng* **30**. https://doi.org/10.1016/j.jobe.2020.101307.

Chamssine, F., Khalifeh, M., and Saasen, A. 2022a. Rheological and Mechanical Properties of Rock-Based Geopolymers Developed for Well Abandonment: Effect of Chemical Admixtures at Elevated Temperatures. Paper presented at the ASME 2022 41st International Conference on Ocean, Offshore and Arctic Engineering, Hamburg, Germany, 5–10 June. https://doi.org/10.1115/OMAE2022-78376.

Chamssine, F., Khalifeh, M., Eid, E. et al. 2021. Effects of Temperature and Chemical Admixtures on the Properties of Rock-Based Geopolymers Designed for Zonal Isolation and Well Abandonment. Paper presented at the ASME 2021 40th International Conference on Ocean, Offshore and Arctic Engineering, Virtual, Online, 21–30 June. https://doi.org/10.1115/OMAE2021-60808.

Chamssine, F., Khalifeh, M., Saasen, A. et al. 2022b. Effect of Zn^{2+} and K^{+} as Retarding Agents on Rock-Based Geopolymers for Downhole Cementing Operations. *J Energy Resour Technol* **144** (5). https://doi.org/10.1115/1.4053710.

Chen, A., Xu, D., Chen, X. et al. 2012. Measurements of Zinc Oxide Solubility in Sodium Hydroxide Solution from 25 to 100 °C. *Trans Nonferrous Met Soc China* **22** (6): 1513–1516. https://doi.org/10.1016/S1003-6326(11)61349-6.

Damtoft, J. S., Lukasik, J., Herfort, D. et al. 2008. Sustainable Development and Climate Change Initiatives. *Cem Concr Res* **38**: 115–127. https://doi.org/10.1016/j.cemconres.2007.09.008.

Davidovits, J. 1991. Geopolymers: Inorganic Polymeric New Materials. *J Therm Anal* **37**: 1633–1656. https://doi.org/10.1007/BF01912193.

Davidovits, J. 2008. *Geopolymer: Chemistry & Applications*. Saint-Quentin, Paris: Institut Geopolymer.

Davidovits, J. 2013. *Geopolymer Cement a Review*, 1–11. Saint-Quentin, Paris: Institut Geopolymer.

Davidovits, J. 2017. Geopolymers: Ceramic-like Inorganic Polymers. *J Ceram Sci Technol* **8**: 335–350. https://doi.org/10.4416/JCST2017-00038.

Deshpande, A., Chiney, A., Patil, S. et al. 2015. Long-Term Study of Effects of CO2 Exposure on Cement Integrity Under Downhole Conditions. Paper presented at the EUROPEC 2015, Madrid, Spain, 1–4 June. SPE-174329-MS. https://doi.org/10.2118/174329-MS.

Falcone, J. S., Bass, J. L., Angelella, M. et al. 2010. The Determination of Sodium Silicate Composition Using ATR FT-IR. *Ind Eng Chem Res* **49** (14): 6287–6290. https://doi.org/10.1021/ie1002747.

Flatt, R. J., Roussel, N., and Cheeseman, C. R. 2012. Concrete: An Eco Material That Needs to Be Improved. *J Eur Ceram Soc* **32** (11): 2787–2798. https://doi.org/10.1016/j.jeurceramsoc.2011.11.012.

García-Lodeiro, I., Fernández-Jiménez, A., and Palomo, A. 2013. Variation in Hybrid Cements over Time. Alkaline Activation of Fly Ash–Portland Cement Blends. *Cem Concr Res* **52**: 112–122. https://doi.org/10.1016/j.cemconres.2013.03.022.

Garg, N. and White, C. E. 2017. Mechanism of Zinc Oxide Retardation in Alkali-Activated Materials: An in Situ X-Ray Pair Distribution Function Investigation. *J Mater Chem A* **5** (23): 11794–11804. https://doi.org/10.1039/C7TA00412E.

Gasteiger, H. A., Frederick, W. J., and Streisel, R. C. 1992. Solubility of Aluminosilicates in Alkaline Solutions and a Thermodynamic Equilibrium Model. *Ind Eng Chem Res* **31** (4): 1183–1190. https://doi.org/10.1021/ie00004a031.

Hewlett, P. C., ed. 2001. *Lea's Chemistry of Cement and Concrete*, fourth edition. Oxford, UK: Butterworth-Heinemann.

IEA2021. Net Zero by 2050 - A Roadmap for the Global Energy Sector.

Kamali, M., Khalifeh, M., and Saasen, A. 2022. Bonding Mechanism of Zonal Isolation Materials to Clean and Rusted Casing. *SPE J* **27** (5): 2613–2627. SPE-209812-PA. https://doi.org/10.2118/209812-PA.

Kamali, M., Khalifeh, M., Saasen, A. et al. 2020. Materials for Well Integrity: Characterization of Short-Term Mechanical Properties. Paper presented at the ASME 2020 39th International Conference on Ocean, Offshore and Arctic Engineering, Virtual, 3–7 August. https://doi.org/10.1115/OMAE2020-18623.

Khale, D. and Chaudhary, R. 2007. Mechanism of Geopolymerization and Factors Influencing Its Development: A Review. *J Mater Sci* **42** (3): 729–746. https://doi.org/10.1007/s10853-006-0401-4.

Khalifeh, M. and Saasen, A. 2020. *Introduction to Permanent Plug and Abandonment of Wells, Ocean Engineering & Oceanography*. Cham, Switzerland: Springer International Publishing. https://doi.org/10.1007/978-3-030-39970-2.

Downloaded from http://onepetro.org/SJ/article-pdf/doi/10.2118/215825-PA/3188288/spe-215825-pa.pdf/1 by Stavanger University Library user on 26 July 2023

Khalifeh, M., Hodne, H., Saasen, A. et al. 2016a. Usability of Geopolymers for Oil Well Cementing Applications: Reaction Mechanisms, Pumpability, and Properties. Paper presented at the SPE Asia Pacific Oil & Gas Conference and Exhibition, Perth, Australia, 25–27 October. SPE-182354-MS. https://doi.org/10.2118/182354-MS.

Khalifeh, M., Motra, H. B., Saasen, A. et al. 2018. Potential Utilization for a Rock-Based Geopolymer in Oil Well Cementing. Paper presented at the ASME 2018 37th International Conference on Ocean, Offshore and Arctic Engineering, Madrid, Spain, 17–22 June. https://doi.org/10.1115/OMAE2018-78305.

Khalifeh, M., Saasen, A., Hodne, H. et al. 2019. Laboratory Evaluation of Rock-Based Geopolymers for Zonal Isolation and Permanent P&A Applications. *J Pet Sci Eng* **175**: 352–362. https://doi.org/10.1016/j.petrol.2018.12.065.

Khalifeh, M., Saasen, A., Vralstad, T. et al. 2014. Potential Utilization of Class C Fly Ash-Based Geopolymer in Oil Well Cementing Operations. *Cem Concr Compos* **53**: 10–17. https://doi.org/10.1016/j.cemconcomp.2014.06.014.

Khalifeh, M., Saasen, A., Vrålstad, T. et al. 2016b. Experimental Study on the Synthesis and Characterization of Aplite Rock-Based Geopolymers. *J Sustain Cem-Based Mater* **5** (4): 233–246. https://doi.org/10.1080/21650373.2015.1044049.

Khalifeh, M., Todorovic, J., Vrålstad, T. et al. 2017. Long-Term Durability of Rock-Based Geopolymers Aged at Downhole Conditions for Oil Well Cementing Operations. *J Sustain Cem-Based Mater* **6** (4): 217–230. https://doi.org/10.1080/21650373.2016.1196466.

Kiran, R., Teodoriu, C., Dadmohammadi, Y. et al. 2017. Identification and Evaluation of Well Integrity and Causes of Failure of Well Integrity Barriers (A Review). *J Nat Gas Eng* **45**: 511–526. https://doi.org/10.1016/j.jngse.2017.05.009.

Krishna, R. S., Mishra, J., Zribi, M. et al. 2021. A Review on Developments of Environmentally Friendly Geopolymer Technology. *Mater* **20**. https://doi.org/10.1016/j.mtla.2021.101212.

Kumar, S., Kumar, R., and Mehrotra, S. P. 2010. Influence of Granulated Blast Furnace Slag on the Reaction, Structure and Properties of Fly Ash Based Geopolymer. *J Mater Sci* **45** (3): 607–615. https://doi.org/10.1007/s10853-009-3934-5.

Luukkonen, T., Abdollahnejad, Z., Yliniemi, J. et al. 2018. One-Part Alkali-Activated Materials: A Review. *Cem Concr Res* **103**: 21–34. https://doi.org/10.1016/j.cemconres.2017.10.001.

Mahmoudkhani, A. H., Huynh, D. N. T., Sylvestre, C. et al. 2008. New Environment-Friendly Cement Slurries With Enhanced Mechanical Properties. Paper presented at the CIPC/SPE Gas Technology Symposium 2008 Joint Conference, Calgary, Alberta, Canada, 16–19 June. SPE-115004-MS. https://doi.org/10.2118/115004-MS.

Matalkah, F., Xu, L., Wu, W. et al. 2017. Mechanochemical Synthesis of One-Part Alkali Aluminosilicate Hydraulic Cement. *Mater Struct* **50** (1). https://doi.org/10.1617/s11527-016-0968-4.

McLellan, B. C., Williams, R. P., Lay, J. et al. 2011. Costs and Carbon Emissions for Geopolymer Pastes in Comparison to Ordinary Portland Cement. *J Clean Prod* **19** (9–10): 1080–1090. https://doi.org/10.1016/j.jclepro.2011.02.010.

Myers, R. J., Bernal, S. A., and Provis, J. L. 2014. A Thermodynamic Model for C-(N-)A-S-H Gel: CNASH-Ss. *Cem Concr Res* **66**: 27–47. https://doi.org/10.1016/j.cemconres.2014.07.005.

Nasvi, M. C. M., Ranjith, P. G., and Sanjayan, J. 2014a. Effect of Different Mix Compositions on Apparent Carbon Dioxide (CO2) Permeability of Geopolymer: Suitability as Well Cement for CO2 Sequestration Wells. *Appl Energy* **114**: 939–948. https://doi.org/10.1016/j.apenergy.2013.05.050.

Nasvi, M. C. M., Ranjith, P. G., Sanjayan, J. et al. 2014b. A Numerical Study of CO2 Flow through Geopolymer under Down-Hole Stress Conditions: Application for CO2 Sequestration Wells. *J Unconv Oil Gas Resour* **7**: 62–70. https://doi.org/10.1016/j.juogr.2014.01.002.

Nasvi, M. C. M., Ranjith, P. G., Sanjayan, J. et al. 2014c. Effect of Temperature on Permeability of Geopolymer: A Primary Well Sealant for Carbon Capture and Storage Wells. *Fuel* **117**: 354–363. https://doi.org/10.1016/j.fuel.2013.09.007.

Nasvi, M. C. M., Ranjith, P. G., Sanjayan, J. et al. 2014d. Mechanical Behaviour of Wellbore Materials Saturated in Brine Water with Different Salinity Levels. *Energy* **66**: 239–249. https://doi.org/10.1016/j.energy.2013.12.003.

Nedunuri, A. S. S. S. and Muhammad, S. 2022. The Role of Zinc Sulphate as a Retarder for Alkali Activated Binders and Its Influence on the Rheological, Setting and Mechanical Behaviour. *Constr Build Mater* **344**. https://doi.org/10.1016/j.conbuildmat.2022.128128.

Nelson, E. B. and Guillot, D., eds. 2006. *Well Cementing*, second edition. Houston, Texas, USA: Schlumberger.

Nematollahi, B. and Sanjayan, J. 2014. Effect of Different Superplasticizers and Activator Combinations on Workability and Strength of Fly Ash Based Geopolymer. *Mater & Des* **57**: 667–672. https://doi.org/10.1016/j.matdes.2014.01.064.

Omran, M. and Khalifeh, M. 2022. Development of Low Carbon Dioxide Intensive Rock-Based Geopolymers for Well Cementing Applications – One-Part Geopolymer, in: Volume 10: Petroleum Technology. Paper presented at the ASME 2022 41st International Conference on Ocean, Offshore and Arctic Engineering, Hamburg, Germany, 5–10 June. https://doi.org/10.1115/OMAE2022-78535.

Omran, M. and Khalifeh, M. 2023. Development of One-Part Rock-Based Geopolymers for Downhole Cementing Applications. *J Energy Resour Technol* **145** (10): 10. https://doi.org/10.1115/1.4062250.

Omran, M., Khalifeh, M., and Hjelm, S. 2022a. Role of Zeta Potential on Rheology of One-Part Geopolymer Slurries: Influence of Superplasticizers. In *Annual Transactions of the Nordic Rheology Society*, Vol. 30. Aarhus, Denmark: Nordic Rheology Society.

Omran, M., Khalifeh, M., and Saasen, A. 2022b. Influence of Activators and Admixtures on Rheology of Geopolymer Slurries for Well Cementing Applications. Paper presented at the SPE Asia Pacific Oil & Gas Conference and Exhibition, Adelaide, Australia, 17–19 October. SPE-210698-MS. https://doi.org/10.2118/210698-MS.

Omran, M., Hjelm, S., Khalifeh, M. et al. 2023. Synthesis of Sustainable One-Part Geopolymers for Well Cementing Applications. *Geoenergy Sci Eng* **227**. https://doi.org/10.1016/j.geoen.2023.211822.

Pacheco-Torgal, F., Castro-Gomes, J., and Jalali, S. 2008. Alkali-Activated Binders: A Review. *Constr Build Mater* **22** (7): 1305–1314. https://doi.org/10.1016/j.conbuildmat.2007.10.015.

Pacheco-Torgal, F., Labrincha, J., Leonelli, C. et al., eds. 2014. *Handbook of Alkali-Activated Cements, Mortars and Concretes*. Sawston, UK: Woodhead Publishing.

Paiva, M. D. M., Fonseca Rocha, L. D., Castrillon Fernandez, L. I. et al. 2021. Rheological Properties of Metakaolin-Based Geopolymers for Three-Dimensional Printing of Structures. *ACI Mater J* **118** (6). https://doi.org/10.14359/51733122.

Paiva, M. D. M., Silva, E. C. C. M., Melo, D. M. A. et al. 2018. A Geopolymer Cementing System for Oil Wells Subject to Steam Injection. *J Pet Sci Eng* **169**: 748–759. https://doi.org/10.1016/j.petrol.2018.06.022.

Palacios, M. and Puertas, F. 2005. Effect of Superplasticizer and Shrinkage-Reducing Admixtures on Alkali-Activated Slag Pastes and Mortars. *Cem Concr Res* **35**: 1358–1367. https://doi.org/10.1016/j.cemconres.2004.10.014.

Palomo, A., Krivenko, P., Garcia-Lodeiro, I. et al. 2014. A Review on Alkaline Activation: New Analytical Perspectives. *Mater Constr* **64**. https://doi.org/10.3989/mc.2014.00314.

Salehi, S., Khattak, M. J., Ali, N. et al. 2018. Study and Use of Geopolymer Mixtures for Oil and Gas Well Cementing Applications. *J Energy Resour Technol* **140** (1): 1–12. https://doi.org/10.1115/1.4037713.

Downloaded from http://onepetro.org/SJ/article-pdf/99/10.2118/215825-PA/3118828/spe-215825-pa.pdf/1 by Stavanger University Library user on 26 July 2023

Salehi, S., Khattak, M. J., Bwala, A. H. et al. 2017. Characterization, Morphology and Shear Bond Strength Analysis of Geopolymers: Implications for Oil and Gas Well Cementing Applications. *J Nat Gas Sci Eng* **38**: 323–332. https://doi.org/10.1016/j.jngse.2016.12.042.

Salehi, S., Khattak, J., Saleh, F. K. et al. 2019. Investigation of Mix Design and Properties of Geopolymers for Application as Wellbore Cement. *J Pet Sci Eng* **178**: 133–139. https://doi.org/10.1016/j.petrol.2019.03.031.

Simao, C. A., Folsta, M. G., Campos, G. et al. 2016. Cementing Solutions for Salt- and CO2-Laden Presalt Zones. Paper presented at the SPE Deepwater Drilling and Completions Conference, Galveston, Texas, USA, 14–15 September. SPE-180336-MS. https://doi.org/10.2118/180336-MS.

Singh, N. B. and Middendorf, B. 2020. Geopolymers as an Alternative to Portland Cement: An Overview. *Constr Build Mater* **237**. https://doi.org/10.1016/j.conbuildmat.2019.117455.

Sturm, P., Gluth, G. J. G., Brouwers, H. J. H. et al. 2016. Synthesizing One-Part Geopolymers from Rice Husk Ash. *Constr Build Mater* **124**: 961–966. https://doi.org/10.1016/j.conbuildmat.2016.08.017.

Suwan, T. and Fan, M. 2017. Effect of Manufacturing Process on the Mechanisms and Mechanical Properties of Fly Ash-Based Geopolymer in Ambient Curing Temperature. *Mater Manuf Process* **32**: 461–467. https://doi.org/10.1080/10426914.2016.1198013.

Taylor, H. F. W. 1997. *Cement Chemistry*, second edition. London, England: Thomas Telford Publishing. https://doi.org/10.1680/cc.25929.

Tommaseo, C. E. and Kersten, M. 2002. Aqueous Solubility Diagrams for Cementitious Waste Stabilization Systems. 3. Mechanism of Zinc Immobilizaton by Calcium Silicate Hydrate. *Environ Sci Technol* **36**: 2919–2925. https://doi.org/10.1021/es0102484.

Wan-En, O., Yun-Ming, L., Cheng-Yong, H. et al. 2022. Towards Greener One-Part Geopolymers through Solid Sodium Activators Modification. *J Clean Prod* **378**. https://doi.org/10.1016/j.jclepro.2022.134370.

Wang, L., Geddes, D. A., Walkley, B. et al. 2020. The Role of Zinc in Metakaolin-Based Geopolymers. *Cem Concr Res* **136**. https://doi.org/10.1016/j.cemconres.2020.106194.

Yao, X., Zhang, Z., Zhu, H. et al. 2009. Geopolymerization Process of Alkali–Metakaolinite Characterized by Isothermal Calorimetry. *Thermochim Acta* **493** (1–2): 49–54. https://doi.org/10.1016/j.tca.2009.04.002.

Zailan, S. N., Bouissi, A., Mahmed, N. et al. 2020. Influence of ZnO Nanoparticles on Mechanical Properties and Photocatalytic Activity of Self-Cleaning ZnO-Based Geopolymer Paste. *J Inorg Organomet Polym* **30** (6): 2007–2016. https://doi.org/10.1007/s10904-019-01399-3.

Zhang, Z., Provis, J. L., Wang, H. et al. 2013. Quantitative Kinetic and Structural Analysis of Geopolymers. Part 2. Thermodynamics of Sodium Silicate Activation of Metakaolin. *Thermochim Acta* **565**: 163–171. https://doi.org/10.1016/j.tca.2013.01.040.

Zhang, Z., Wang, H., Provis, J. L. et al. 2012. Quantitative Kinetic and Structural Analysis of Geopolymers. Part 1. The Activation of Metakaolin with Sodium Hydroxide. *Thermochim Acta* **539**: 23–33. https://doi.org/10.1016/j.tca.2012.03.021.

Downloaded from http://onepetro.org/SJ/article-pdf/doi/10.2118/215825-PA/3188288/spe-215825-pa.pdf/1 by Stavanger University Library user on 26 July 2023

Appendix 9 – Paper VII

Aging and Temperature Effects on the Performance of Sustainable One-part Geopolymers Developed for Well-Cementing Applications

Mohamed Omran, Mahmoud Khalifeh, & Maria Paiva

An accepted open-access Journal paper; in SPE Journal.

The SPE paper number assigned to the manuscript is SPE-217993-PA

Aging and Temperature Effects on the Performance of Sustainable One-part Geopolymers Developed for Well-Cementing Applications

M. Omran[1,1], UiS; **M. Khalifeh[1]**, UiS; and **M. D. M. Paiva[2]**, UFRJ.

1 Department of Energy and Petroleum Eng., Faculty of Science and Technology, University of Stavanger, 4036 Stavanger, Norway.
2 Sustainable Materials Research Center (NUMATS), Federal University of Rio de Janeiro, Rio de Janeiro, Brazil
❖ Corresponding author; E-mail address: mohamed.a.omran@uis.no (M. Omran)

Keywords: One-part Geopolymer; Compressive Strength; Strength Booster; Zinc Oxide; Aging Impact.

Abstract

This study elucidates the effects of aging and temperature over the performance of One-part 'just add water' (JAW) granite-based geopolymers for application in well cementing and well abandonment. Additionally, the investigation delves into the fluid-state and early-age solid-state properties of these geopolymers, with a particular emphasis on their performance after aging. The aging process extended up to 56 days for assessing mechanical properties and up to 28 days for evaluating hydraulic sealability through dedicated tests. The obtained results unveil a non-linear correlation between the designated temperature and pumping duration. Notably, the issue of fluid loss emerged as a significant concern for these geopolymers. The early-age strength development of the mix design containing zinc demonstrates adherence to industry norms by achieving minimal strength requirements within 24 hours of curing. Zinc plays a pivotal role as a strength enhancer during the initial curing stages of geopolymers, both under ambient conditions and at elevated temperatures (70 °C). However, upon extended curing at elevated temperatures, zinc's impact slightly diminishes compared to the unmodified mix design. After around the 30-days of curing, a consecutive reaction occurs in both the unmodified and zinc-modified mix designs. Aging leads to a decline in the material's hydraulic sealability that was initially established during the early stages of curing.

Introduction

In recent years, there has been a rapid increase in the demand for cement production. A 2016 report estimated that the emission of greenhouse gases from the cement industry alone could be responsible for up to 8% of global carbon dioxide (CO2) emissions (Gilfillan and Marland, 2021). Despite efforts to improve efficiency and promote cleaner cement production, the energy-intensive process of cement clinker calcination remains a necessity (Mo et al., 2010). Therefore, the development of sustainable and viable alternative materials that can fully replace Ordinary Portland Cement (OPC) while possessing equal or superior chemo-physical properties remains the most effective strategy (Luukkonen et al., 2018; Omran and Khalifeh, 2023).

[1] Corresponding author; E-mail address: mohamed.a.omran@uis.no (M. Omran)

Alkali-Activated Materials (AAM) and geopolymers have been recognized as environmentally friendly alternatives to replace OPC. It is believed that their production results in 50 to 70 percent lower CO2 emissions per ton of the produced material when compared to that of OPC (McLellan et al., 2011; Mellado et al., 2014). Moreover, the production of these materials aligns with the principles of circular economy when by-products are utilized as precursors. Extensive research has been conducted on various types of geopolymers. Depending on the specific type and mix design, geopolymers exhibit improved resistance to acids and sulfates, enhanced heat resistance, reduced chemical shrinkage, and stronger mechanical properties when compared to OPC(Luukkonen et al., 2018).

Conventional geopolymers are typically produced using a "Two-Part" mixture, consisting of an alkaline or alkali silicate solution and a solid precursor that contains amorphous aluminosilicates. While the two-part geopolymer exhibits excellent properties compared to OPC (Chamssine, 2023; Gomado et al., 2023; Khalifeh, 2016; Khalifeh et al., 2019, 2018; Paiva et al., 2018; Salehi et al., 2018) its application is limited to pre-cast operations due to logistical and health, safety, and environmental (HSE) constraints arising from the high pH of the activator solution. In other words, the drawback of the two-part geopolymer system is the requirement for a user-hostile and highly corrosive activator solution, which poses potential risks and restricts its use in mass production and large-scale applications, particularly in the oil and gas industry (Luukkonen et al., 2018; Nematollahi et al., 2015).

"One-part" also known as "Just Add Water" (JAW) geopolymers, can be seen as the evolution of two-part geopolymers, effectively addressing the limitations caused by the high pH liquid activator. Unlike two-part geopolymers, JAW geopolymers only require the addition of water along with the dry ingredients (Luukkonen et al., 2018; Nematollahi et al., 2015; Omran and Khalifeh, 2023; Singh and Middendorf, 2020). This concept was initially introduced by Hajimohammadi et al. (2008). Afterwards, extensive research and development have been carried out by various researchers on one-part geopolymers, leading to the proposal of different geopolymer mix designs. These investigations have focused on the geopolymer cement synthesis using industrial and natural aluminosilicates sources, mainly composed of fly ash slag and metakaolin, that are normalized when needed with complementary Si and Al reactive sources, like synthetic and agroindustrial ashes. More recently, various Al and Si-rich residues such as, mine tailings, bauxite, rock backfill, demolition waste, sewage and sludge materials have also been adopted as geopolymers precursors (Nematollahi et al., 2015; Singh and Middendorf, 2020).

Several factors including curing temperature and aging affect directly geopolymers through the geopolymerization process and its performance (Adam and Horianto, 2014; Cai et al., 2020; Chithiraputhiran and Neithalath, 2013; Hajimohammadi et al., 2011, 2008; Hajimohammadi and van Deventer, 2017; Ke et al., 2015; Kong and Sanjayan, 2010; Li et al., 2013; Luukkonen et al., 2018; Omran et al., 2023a, 2023b; Pilehvar et al., 2020; Rovnanik, 2010; Sun and Vollpracht, 2019). Table 1 presents a compilation of relevant literature from previous research endeavors, providing a summary of their significant findings in the respective field of study.

Table 1 Examples of published literature reviews and articles on the different effects of temperature, curing conditions, and curing duration on alkali-activated geopolymer cement.

Title	Geopolymer System	Significant Outputs
One-part geopolymer mixes from geothermal silica and sodium aluminate (Hajimohammadi et al., 2008)	One-Part	• Purified and milled geothermal silica was utilized as a Si-rich precursor and then activated by various concentrations of solid sodium aluminate and water-to-solid ratios. • Lower water content in the system increased the degree of crystallinity with two weeks of aging at 40°C. • The high aluminium content can hinder the geopolymerization reaction by causing the sorption of aluminium onto the silica surface, thereby impeding its dissolution.
One-part geopolymers based on thermally treated Red Mud/NaOH blends (Ke et al., 2015)	One-Part	• An Alkali-Thermal activation process was investigated for an aluminium- and calcium-rich red mud base JAW system. • Sodium hydroxide in pellet form was calcined with red mud at 800°C, leading to the formation of calcium-rich phases, such as C_3A, and α-C_2S. Additionally, this process promoted the formation of a partially peralkaline Na-aluminosilicate phase. • Na-rich aluminosilicate salts can supply an adequate number of alkalis during the dissolution process, thereby enhancing the reactivity. • The excess of alkalis in the system resulted in limited strength development and efflorescence, which were identified as shortcomings.
Characterisation of one-part geopolymer binders made from Fly Ash (Hajimohammadi and van Deventer, 2017)	One-Part	• A low calcium content fly ash was activated by various concentrations of solid sodium silicates and sodium hydroxide and different water contents. • The reaction mechanisms and physical properties of the system were investigated after curing the samples at 40°C for up to 3 weeks. • The higher the Si/Al ratio of the binder design, the denser the geopolymer microstructure. • A lower water content leads to increased participation of Si in the final geopolymer gel, thereby achieving optimal mechanical performance.
Time-resolved and spatially resolved infrared spectroscopic observation of seeded nucleation controlling geopolymer gel formation (Hajimohammadi et al., 2011)	One-Part	• A milled geothermal silica precursor and a solid sodium aluminate activator were seeded with various types of oxide nanoparticles, the samples were cured at 40 °C for up to three weeks. • The addition of ZnO nanoparticles enhances the mechanical properties of the JAW mix design, particularly during the early-age performance, when compared to the unseeded mix design. • The seeding process enhances the dissolution of silica and enables control over silica release rates in the initially aluminium-rich reaction mixture, thereby allowing engineering structure and physical properties of the geopolymers. • The seeding process enhances the geopolymer nucleation stage by hindering the sorption of aluminium on the silica surface.
Synthesis of sustainable one-part geopolymers for well cementing	One-Part	• Presents a synthesis of granite-based geopolymers normalized with slag in different ratios.

applications (Omran et al., 2023a)		• The use of slag increases the viscosity and consistency of the slurry, it has an optimum working range of up to 47 wt.%. • Exceeding the optimal slag content, over-expansion and detrimental physical properties are expected. • Considering the early-age properties of the geopolymers, granite mainly works as a filler.
Design and Early Age Performance of Sustainable One-part Geopolymers for Well Cementing (Omran et al., 2023b)	One-Part	• ZnO acts as an early strength booster by increasing the rate of heat evolution, thereby satisfying the early-age properties required for cementing wells. • The dissolution rate of the solid activator is a parameter that needs to be considered. • By combining the solid activator and granite, Si and Al are released, which is an indication of granite dissolution.
One part alkali-activated materials for construction – A review (Mahendra and Narasimhan, 2023)	One-Part	• The primary components of one-part geopolymers often consist of precursors such as fly ash and GGBFS. • The reaction can lead to the precipitation of various gel forms, including C/Na-A-S-H. • In comparison to two-part systems, the release rates of Si and Al species are generally slower in one-part systems. • Introducing water gradually has shown to be more efficacious than adding all the water at once.

To develop a commercially viable and sustainable geopolymer, one should consider the techno-economical aspects of the precursors to be used. One of the main drivers to make the geopolymers more attractive nowadays is to reduce the green-house gases emissions from their synthesis, the availability and transportation of the raw materials, and also their precursors beneficiation, as well as their activators preparations impacts. In an effort, Khalifeh (2016; 2019, 2018) first developed two-part granite-based geopolymers to replace OPC used in well construction and well abandonment operations.

As the HSE limitations of the two-part system were identified, Omran and Khalifeh (Omran and Kalifeh, 2022; Omran and Khalifeh, 2023) developed a one-part granite-based geopolymer. Omran et al (2023a, 2023b) performed further studies, in the fluid-state and early-age solid-state properties of the one-part granite-based geopolymers, revealing the potential of the developed technology for in-situ applications with adjustable properties. Experimental studies show that the use of sodium salts of naphthalene-sulfonic acid containing formaldehydes dispersants and sodium lignosulphonates are effective superplasticizers for this type of geopolymer (Hjelm, 2022; Omran et al., 2022a, 2022b).

The above-mentioned articles, along with the limited number of accessible papers on one-part geopolymers, highlight the need for further research on the topic of one-part geopolymers. Additionally, there is a lack of research on the impact of elevated temperature and long aging on the final properties of the developed geopolymers.

This work aims to investigate the effect of temperature and long curing time, on the properties and performance of the one-part granite-based geopolymers, in order to better understand the mechanism of zinc in the one-part geopolymer design.

Materials and Methods

Materials

The neat JAW geopolymer is based on both solid precursors and solid activator components, which together are mixed with distilled water to create the cementitious geopolymer system. The materials in the precursor were ground granite rock, a Ground Granulated Blast Furnace Slag (GGBFS) rich in aluminum, calcium and magnesium, and microsilica (MS), which is an almost pure amorphous silica source. The dissolution rate and their role in the mix design have been published in previous works (Omran et al., 2023a, 2023b; Omran and Khalifeh, 2023).

The chemical composition of the raw materials and the neat JAW precursor has been tabulated in Table 2. The activator was prepared using anhydrous potassium silicate and potassium hydroxide in powder form with a final molar ratio (SiO_2/K_2O) of 2.4. In addition to analyzing the neat JAW recipe, zinc oxide was introduced together with the precursor as an additive for improving the mechanical properties of the geopolymer cement. The physical properties of the precursor and other mixture components are presented in Table 3.

Table 2 – Chemical composition of the JAW geopolymer precursor (Omran et al., 2023b).

Chemical composition (wt.%)*	Granite	GGBFS	Microsilica	JAW Precursor Mixture
SiO_2	73.44	35.78	95.50	56.63
Al_2O_3	13.33	12.72	0.70	12.47
Fe_2O_3	2.06	0.18	0.30	1.09
MgO	0.44	12.77	0.50	6.23
CaO	1.12	33.74	0.40	16.45
Na_2O	3.12	0.55	0.40	1.77
K_2O	5.11	0.82	1.00	2.87
TiO_2	0.23	2.23	0.00	1.16
MnO	0.04	0.58	0.00	0.29
LOI**	0.90	0.30	2.00	0.60

*By weight of the total precursor mixture; **Loss of ignition

Table 3 – Physical properties of all components in the geopolymer system.

Physical properties	d_{10} (µm)	d_{50} (µm)	d_{90} (µm)	SG (g/cm^3)	SSA (m^2/kg)
Granite	3.52	21.1	131	2.63	631
GGBFS	2.79	15.9	46.6	2.90	944
Microsilica	0.19	0.34	0.60	2.29	19320
K_2SiO_3	5.16	33.3	101	2.37	487
ZnO	0.55	2.06	106	5.61	3810

SG, specific gravity; SSA, specific surface area; d10, d50, d90, particle-size distribution percentiles

Mix Design

In this work, two previously developed recipes "JAW" and "JAW-Z" have been studied (Omran et al., 2023a, 2023b) and listed in Tables 4 and 5. JAW-Z was selected among other ZnO concentrations evaluated previously because it showed the best early age performance.

Table 4 – Geopolymer formulations investigated in this study.

Composition (% bwop*)	JAW	JAW-Z (JAW + 0.86% ZnO)
Granite	48.6	48.6
GGBFS	47.1	47.1
MS	4.29	4.29
K_2SiO_3	20.8	20.8
KOH (anhydrous)	4.24	4.24
ZnO	0.00	0.86
Water	41.3	41.3
Source	(Omran et al., 2023b)	(Omran et al., 2023b)

* By weight of precursor mixture (granite, GGBFS and MS).

Table 5 – Oxide molar ratios, water-to-solids ratios and theoretical density of geopolymer formulations.

Molar ratios	JAW	JAW-Z
$SiO_{2,nominal}$ / Al_2O_3	9.72	9.72
$SiO_{2,reactive}$ / Al_2O_3	4.87	4.87
$SiO_{2,nominal}$ / CaO	4.05	4.05
$SiO_{2,reactive}$ / CaO	2.03	2.03
K_2O / Al_2O_3	1.07	1.07
Na_2O / Al_2O_3	0.23	0.23
(K_2O + Na_2O) / Al_2O_3	1.31	1.31
ZnO / $SiO_{2,nominal}$	–	0.0088
ZnO / $SiO_{2,reactive}$	–	0.0175
ZnO / CaO	–	0.0355
H_2O / K_2O	17.75	17.78
Water/Solids	0.33	0.33
Specific Gravity (g/cm^3)	1.88	1.89

Methods

Mixing procedure, thickening time (TT), differential scanning calorimetry (DSC), ultrasonic compressive strength (UCS), uniaxial compressive strength (UCS), alkalinity and inductively coupled plasma (ICP-MS), X-ray diffraction (XRD) and Fourier-transform Infrared Spectroscopy (FTIR) methodologies are described in detail on previous study (Omran et al., 2023b). A pressurized mud balance was used to estimate slurry density (API RP 10B-2, 2019). Hydraulic sealability test (HST) methodology, by the other hand, can be found in the work done by Gomado et al. (2023).

Viscosity & API Gel-Strength Measurements

The rheological behavior of the slurries was assessed at 25°C by using a VG-meter according to the specifications of the American Petroleum Institute API RP 10B-2 (2019). Omran et al. (2022a, 2022b) studied the rheology of granite-based geopolymers where the Hershel-Bulkley model was applied successfully.

Static Fluid Loss Test

An API fluid-loss test cell was used to measure the fluid loss at 69 bar (1000 psi) in ambient temperature (API RP 10B-2, 2019). A sieve with a mesh grid of 250 μm and a hardened filter was used together. The hardened filter was used to facilitate sampling for further analysis. The test was running for 30 minutes. Afterwards, the produced fluids have been collected and examined as pore solution for pH (see Table 6) and Inductively Coupled Plasma Spectroscopy (ICP) analysis (see Figure 2).

Hydraulic Sealability Test

Due to volume limitations, a Hobart N50-60 commercial mixer was used for hydraulic sealability tests. The precursors were introduced to deionized water at Level 1 stirring speed and then stirred continuously for 25 minutes at Level 2 stirring speed. Then, slurries were poured and cured inside hydraulic sealability test cells at 37.5 bar and 25°C. Once the geopolymer cement had fully cured, nitrogen gas was connected to the bottom of the test cell, which then is connected to the separator, flowmeters, and the data logging system. The plugs within the hydraulic test cell were then pressure tested with increments of 5 bar at a time to test their sealing ability. Details of the test setup and test protocols have been published by Gomado et al.(2023).

Scanning Electron Microscope

To analyze and reveal microstructure of the geopolymers, a Scanning Electron Microscope (SEM) was used at BSE and SE modes. SEM analysis was performed on the remains of each crushed geopolymer specimen after performing UCS tests at the final day of aging (7 days – 2 months). Prior to coating, all samples were dried the same way as the samples for XRD. Then, the samples were coated with an 11 nm palladium plasma to prevent the samples from charging during the experiment.

Results & Discussion

Early-age Properties Characterization

Slurry Characteristics

Figure 1 and Table 6 present the rheological properties of JAW and JAW-Z. Both recipes have very comparable rheological behavior. The slurries are both behaving shear thinning pastes. The measurements do not indicate sign of particle settling. Table 7 presents a summary of the other slurry properties measured right after mixing including slurries` pH, density, zeta potential and initial consistency. These parameters are also comparable for both mixes. Additionally, the pore solution was collected and examined for both mixes and the ones from (Omran et al., 2023b) after performing the fluid-loss test (FLT), which can be seen in Table 8 and Figure 2 below.

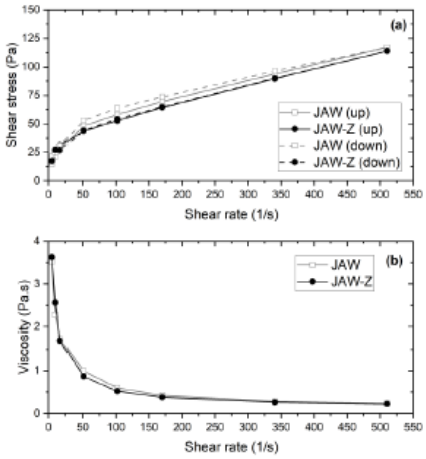

Figure 1: (a) Shear rate – Shear stress profiles and (b) Viscosity curves; JAW (neat) & JAW-Z (JAW + 0.86% ZnO).

Table 6: Rheological properties data in ambient conditions.

Mix Design	10-sec API Gel-strength [Pa]	10-min API Gel-strength [Pa]	Estimated Yield Stress [Pa]	Flow Index	Rheological Behavior
JAW	20.05	23.51	13.7	0.37	Shear thinning
JAW-Z	18.48	19.05	15.4	0.37	Shear thinning

Table 7: Slurry properties in ambient conditions.

Mix Design	Slurry Density (SG)	Slurry pH	Slurry Zeta Potential (mV)	Initial Consistency (Bc)
JAW	1.87	13.72 (±0.01)	-25.0 (±0.16)	26.4
JAW-Z	1.89	13.84 (±0.01)	-25.4 (±0.29)	27.2

Table 8: Fluid Loss test (FLT) and pore solution results.

Mix Design	FLT Volume (mL)	FLT Blowout Time (min)	Spurt Loss Volume (mL)	Pore Solution pH
JAW	27(±0.5)	6	120.75	14.0 (±0.1)
JAW-Z	25(±0.5)	6	111.80	14.0 (±0.1)

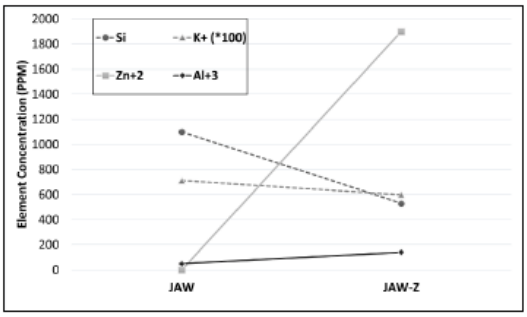

Figure 2: Dissolution ICP-MS analysis for pore solutions of JAW vs JAW-Z [24]; JAW (neat) & JAW-Z (JAW + 0.86% ZnO).

The static fluid loss for both neat and 0.86% ZnO JAW (as well as the ones from (Omran et al., 2023b)) reveals higher values than the limits outlined from API [28] and not observed at all for the two-part granite-based geopolymers (Chamssine, 2023). Thus, fluid loss control additives shall be tested in combination with the JAW geopolymers.

The ICP-MS analysis, see Figure 2, shows that the zinc contributes to facilitate the dissolution of aluminum species to some extent, while simultaneously lowers the availability of silicon species in the pore solution due to the consumption of free silicon ions through the formation of zincates. That was further investigated by (Anseau et al., 2005; Chen et al., 2012; Hajimohammadi et al., 2011; Mahendra and Narasimhan, 2023) and summarized by (Omran et al., 2023b). Thus, it favors the geopolymerization process by lowering the Si/Al ratio from 10 to 3.

Conditioning and Thickening time

Figure 3 and Table 9 show effect of 20, 30, 40 and 50°C BCHTs temperature on the thickening time for the given two recipes and the ones from (Omran et al., 2023b). All the examined slurries of the JAW system set and harden rapidly, typically within minutes, once they reach a consistency between 40-50 Bc. Therefore, 40 Bc was selected as the pumpability time for all pastes and the tests were concluded at this point. All JAW recipes exhibited a right-angle set phenomenon within a bottom hole circulating temperature range of 20-50°C.

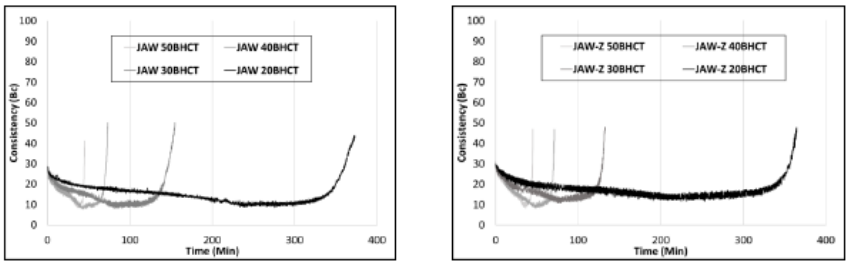

(a) (b)

Figure 3: Effect of temperature on consistency of the slurries (a) JAW and (b) JAW-Z; JAW (neat) & JAW-Z (JAW + 0.86% ZnO).

Table 9: Pumpability of JAW and JAW-Z at 40 Bc.

Recipe/ Circulating Temperature (°C BHCT)	20 °C BHCT	30 °C BHCT	40 °C BHCT	50 °C BHCT
JAW Pumpability (min)	369.5	151.8	72.4	45.2
JAW-Z Pumpability (min)	361.3	142.7	71.0	44.9

Both recipes have very comparable initial consistency results at each temperature assessed, as detailed in Table. Lower BHCT has a clear effect on elongating the pumpability duration for both recipes, i.e., the slurry is temperature sensitive. This behavior has been also observed by Salehi et al. (2018) and Paiva(2018), suggesting that geopolymers are temperature sensitive materials, independently of their neat designs. At 20 °C BHCT, both recipes had the longest pumpability duration up to 6 hours, while at 50 °C BHCT, they had the shortest pumpability duration down to 45 minutes. Although the 0.86% ZnO was not effective to further elongate the thickening time compared to the neat JAW, at any of the temperatures, it mildly accelerated the setting to reach an early and sustainable strength development. In accordance with the differential scanning calorimetry profiles shown below (Figure 4), the dissolution of geopolymer precursors is significantly accelerated at higher temperatures. This leads to an increase in the solubility of aluminosilicates and the availability of silica ions, thereby speeding up the geopolymerization reaction and reducing the setting time (Chen et al., 2012; Pilehvar et al., 2020).

Kinetics of Pastes

Figure 4 and Table 10 provide the DSC profiles and data for the two mixes and the ones from Omran (2023b) at 25 and 50 °C. The initial equilibration period was discarded for the given DSC curves.

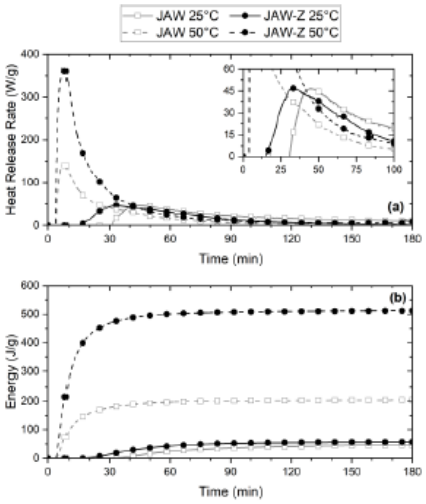

Figure 4: Differential scanning calorimetry data (a) heat rate (b) energy release; JAW (neat) & JAW-Z (JAW + 0.86% ZnO).

Table 10: Kinetics data for JAW and JAW-Z

Material	Time at maximum heat release rate (min)		Maximum heat release rate (mW/g)		Total energy release (J/g)	
	25 °C BHCT	50 °C BHCT	25 °C BHCT	50 °C BHCT	25 °C BHCT	50 °C BHCT
JAW	47	8	47	143	46	204
JAW-Z	33	7	47	372	56	512

Both mixes are observed to yield a single heat release peak. Chithiraputhiran & Neithalath (2013) observed a comparable single heat peak from 50 – 50 and 70 – 30 low calcium fly ash-slag geopolymers for the first 72 hours. Pilehvar et al. (2020) observed a shoulder-like shape overlapping with the single peak for a low calcium fly ash-slag geopolymer system. It would be reasonable to assume that the single peak can be identified as an indication that both the dissolution and formation of geopolymers may occur simultaneously, right after the initial mixing (Pilehvar et al., 2020; Siyal et al., 2016).

The main difference observed between the two DSC profiles in Figure 4 is regarding the heat release rates magnitudes and time by which they occur: The total heat released at 50°C is 5 to 10 times larger than the corresponding at 25°C during the first 3 hours for both mixes. This suggests a speed up rate of the dissolution and condensation processes. These observations indicate that overall geopolymerization reaction is thermally accelerated, by releasing more heat at early times and cumulative energy over time than what is observed at room temperature, as summarized in Table 9 and similarly reported by the literature (Cai et al., 2020; Chithiraputhiran and Neithalath, 2013; Ma et al., 2018; Najafi Kani et al., 2017; Omran et al., 2023b; Pilehvar et al., 2020).

At 25°C, JAW-Z paste oxide reacts earlier and has a slightly broader heat release peak than the one observed for the neat JAW at the same temperature in Figure 4. The total heat release is also observed to be higher for JAW-Z. At 50 °C, the first dissolution step is observed to happen very rapidly, and therefore JAW-Z paste was able to release more heat than the neat one at the same temperature. The DSC results are also in line with the early-age sonic strength development (see Figure 5). Omran et al. (2023b) investigated the effect of 0.5 and 0.86% ZnO in the same JAW system. They found that the higher the amount of added zinc, the higher the increase in the heat release magnitude, as well as the total amount of accumulated energy.

Early-age Sonic Strength

Figure 5 presents the early-age sonic compressive strength performance obtained by using an Ultrasonic cement analyzer (UCA). Both neat JAW and JAW-Z were measured during the first 8 hours at 70°C BHST, which is equivalent to that at 50 °C BHCT. Table 11 illustrates the results from the early-age UCA.

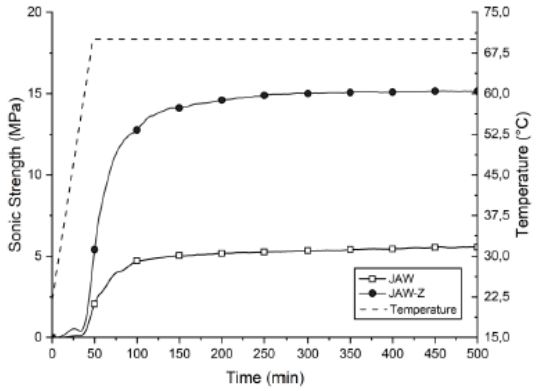

Figure 5: UCA early-age profile at 70 °C BHST and 13.8 MPa; JAW (neat) & JAW-Z (JAW + 0.86% ZnO).

Table 11: UCA early-age data; SS: Sonic Strength (Omran et al., 2023b).

Mix Design	Setting Time to 100 psi (min)	Hardening Time to 500 psi (min)	SS (MPa) for 1 hour	SS (MPa) for 5 hours
JAW	43	66	2.8	5.9
JAW-Z	38	46	8.5	15.7

Both recipes were observed to have comparable timing for developing strength during the initial 45 minutes, which is matching their consistency profiles and pumpability at 50 °C BHCT as explained previously (see Figure 3). This observation agrees with the DSC observations at 50°C BHCT, where the addition of zinc oxide is observed to have a clear effect on accelerating the early-age strength development for the JAW-Z contrary to that of the neat JAW.

JAW-Z was measured to have a sonic compressive strength development of up to 8.5 MPa during the first hour of heat curing, three times higher than that of neat JAW at the same time. Furthermore, JAW-Z was observed to have a shorter hardening time to reach 3.45 MPa (500 psi) and a higher sonic strength value of up to 15.7 MPa within the first 5 hours of curing than JAW. This addition of zinc oxide also tripled the sonic compressive strength of the neat mix.

Ageing Properties & Characterizations

Hydraulic Sealability Test (HST)

Figure 6 represents the hydraulic bond strength (HBS) profiles and breakthroughs for the injected N_2 gas over the two given JAW mix designs with the steel casing after 7 days of curing. It is important to study hydraulic bond strength to understand the ability of the systems to withstand pressure occurring at the cement-casing steel interface without producing a microannulus which would compromise their integrity capacities.

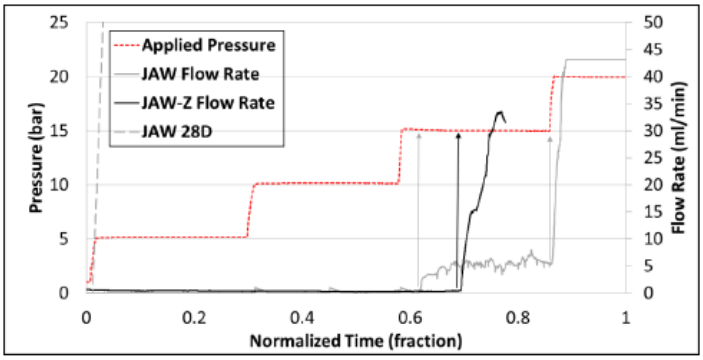

Figure 6: Hydraulic sealability for JAW and JAW-Z mixes. The first grey arrow is the partial initial breakthrough at 15 bars for the neat JAW; the second grey arrow is the complete breakthrough between 15- 20 bars for the neat JAW. The black arrow is the complete breakthrough at 15 bars for JAW-Z.

The conducted hydraulic bond strength test acknowledges the pressure required for fluid to break through the cement-steel casing interface, which was observed to happen after applying 15 – 20 bars for both mix designs. The observed results present a positive indication when being compared with the performance of Ordinary Portland Cement (OPC) for well-cementing applications (Gomado et al., 2023; Salehi et al., 2018).

On the other hand, the aged, cured JAW sample for one month could not withstand 5 bars with an observable de-bonding from the casing. Figure 7 presents the observed de-bonding and breakthrough of the injected gas at 5 bars from all sides of the geopolymer-casing interface. This de-bonding could be due to shrinkage of the slurries. Salehi et al. (Salehi et al., 2018) examined the shrinkage of geopolymers. They observed that geopolymers continuously shrink with time especially at higher curing temperatures, up to 2.5 % volumetric shrinkage after 14 days. However, some geopolymers shrink with lower rates compared to OPC-based cement (Salehi et al., 2018). The observed de-bonding or shrinkage could be due to the reactants` consumption during JAW geopolymerization process as shown in Figure 7. In line with the following FTIR and XRD results and characterizations, it could happen due to having the volume of the geopolymerization products less than the given reactants, or so-called chemical

shrinkage phenomenon, over time. The chemical shrinkage in geopolymers can be result of formation of K(Na)-A-S-H gels and/or water as by-product of the geopolymerization reaction.

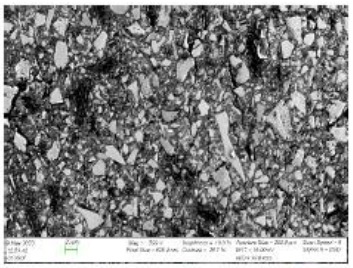

a) mainly geopolymer reactants

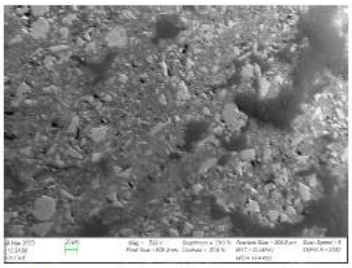

b) mainly geopolymer products

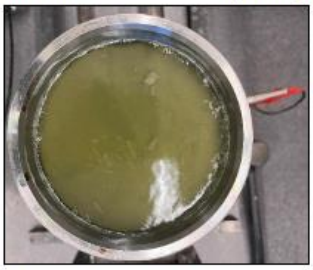

c) gas breakthrough during the hydraulic bond strength test

Figure 7: a) SEM image of early-age JAW mix, b) SEM image of aged JAW mix, c) Top view of the sealability cell after de-bonding of the aged JAW.

Hence, an expansive agent additive might be required to further improve the long-term hydraulic bond strength of the given JAW mixes. Additionally, cement slurry linear expansion and/or contraction test is required to quantify the shrinkage of the systems.

Uniaxial & Ultrasonic Strength Development

Figure 8 shows the uniaxial compressive strength of the geopolymer mixes (JAW and JAW-Z) after 1 day up to 56 days cured in atmospheric pressure, at 25 °C BHST and 70 °C BHST, respectively. Figure 9 and Table 12 present the extended sonic strength development profiles and data for JAW vs JAW-Z, at 70 °C BHST and pressurized to 13.8 MPa.

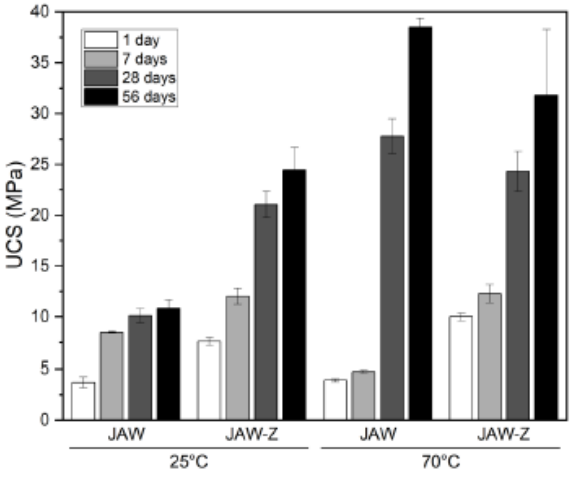

Figure 8: UCS data at 25 and 70 °C BHST.

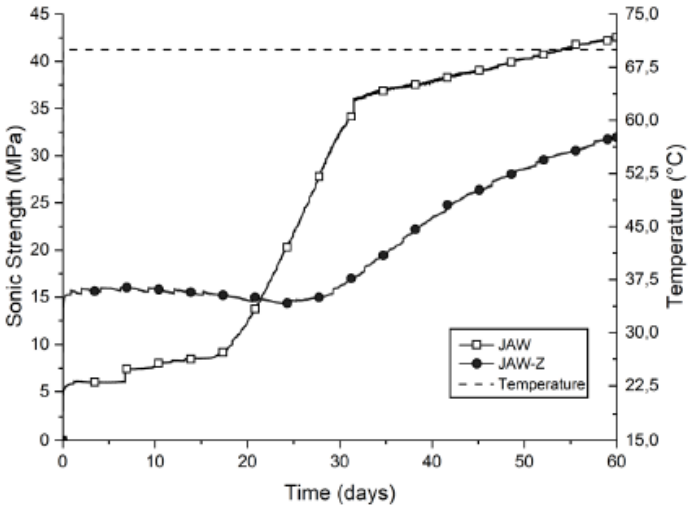

Figure 9: UCA profiles for JAW and JAW-Z; JAW (neat) & JAW-Z (JAW + 0.86% ZnO).

Table 12: Extended UCA sonic strength development data up to 2 months.

Sonic Strength (Day)	1D	7D	14D	28D	56D	60D
JAW (MPa)	5.8	7.4	8.5	28.4	41.8	42.4
JAW-Z (MPa)	15.8	16.0	15.7	15.5	30.7	31.9

At a fixed curing temperature, either 25 or 70 °C BHST, it is observed that the longer the specimen is allowed to cure, the higher the uniaxial compressive strength is obtained for both recipes, in line with (Chithiraputhiran and Neithalath, 2013). Hence, one may also conclude that with a higher curing temperature, higher geopolymer strength development should expect (Chithiraputhiran and Neithalath, 2013; Salehi et al., 2018). Furthermore, the addition of ZnO gave an effective and clear early-age strength booster effect on JAW-Z, in line with the discussed DSC results (see Figure 4). The addition of this strength booster has doubled and tripled the UCS after 1-day of curing in ambient and elevated temperatures, respectively. This observation agrees with the numbers obtained from the UCA data as seen previously in Figure 5. In addition, others have stated the positive effects of utilizing zinc compounds for alkali-activated materials that can improve the cementing properties including compressive strength development (Hajimohammadi et al., 2011; Luukkonen et al., 2018; Van Deventer et al., 2012). One may conclude that the addition of ZnO is very crucial to develop acceptable and durable mechanical properties for well cementing, especially for low to medium temperature applications.

From the extended UCA profiles seen in Figure 8, two sonic strength development zones can be identified for both recipes. The first development curve is observed to happen around the initial mixing and early-age curing which lasted for two weeks for JAW, and three weeks for JAW-Z. Continuing, the second development curve was observed to be a long-term asymptotically-like increasing function curve for both mixes. The presence of the second strength development curve could be an indication of an additional internal structural reorganization and participation of the remaining unreacted precursors particles, which is aligned with the hydraulic sealability data although in different time scales. This could be an interesting observation, especially considering quartz present in granite. Further investigation on the consecutive reaction could provide a better understanding of the product, resulting in more favorable long-term mature geopolymerization products, which yield favorable mechanical properties.

After 28 days of heat curing at 70 °C BHST, the UCS of JAW subdued the UCS for JAW-Z. This observation matches with the values obtained from the UCA, where JAW started to positively overcome JAW-Z. The sonic strength of the neat JAW after 28- and 56 days are 28 and 42 MPa, respectively, while for JAW-Z are 16 and 31 MPa, respectively. These extended UCA results are very comparable to the extended UCS results. A comparable trend was observed by (Van Deventer et al., 2012) in calcium-rich alkali-activated materials using ZnO as a chemical admixture.

Fourier Transform Infrared Spectroscopy (FTIR)

Figures 10 &11 and Tables 13-16 present the FTIR spectra and wave hollows data of the two recipes. The mix designs were studied after 7-, 28- and 56-days of curing at both 25 and 70 °C BHST, respectively. The band in the range of 1400 – 700 cm^{-1} is assigned to the T-O-T (T is a tetrahedral Si or Al) bonds asymmetric stretching vibrations. The T-O-T bands position

can indicate the dissolution of the aluminosilicate source, gelatinous product formations and degree of crosslinking within the geopolymerization network. Absorption O-C-O band between 1500 – 1400 cm^{-1} is assigned to the presence of calcium and CO_3^{-2} groups. The intensity of the broad hump in ranges of 3600-3000 cm^{-1} and 1700-1600 cm^{-1} is associated with the presence of H-OH groups stretching vibrations (Ma et al., 2019, 2018).

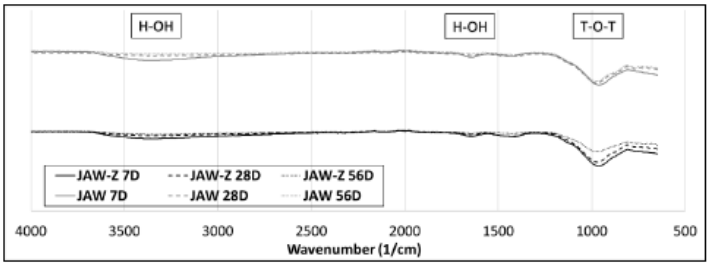

Figure 10: FTIR for JAW and JAW-Z at 25°C BHST.

Table 13: The wave hollows occurred for JAW at 25 °C BHST.

Mix Design (25°C)	Curing Duration	T-O-T (cm^{-1}) [1400-700]	H-OH (cm^{-1}) [1700-1600]	H-OH (cm^{-1}) [3600-3000]
JAW	7D	962	1642	3360
JAW	28D	975	1638	3381
JAW	56D	975	1638	3381

Table 14: The wave hollows occurred for JAW-Z at 25 °C BHST.

Mix Design (25°C)	Curing Duration	T-O-T (cm^{-1}) [1400-700]	H-OH (cm^{-1}) [1700-1600]	H-OH (cm^{-1}) [3600-3000]
JAW-Z	7D	966	1638	3375
JAW-Z	28D	974	1639	3386
JAW-Z	56D	975	1640	3386

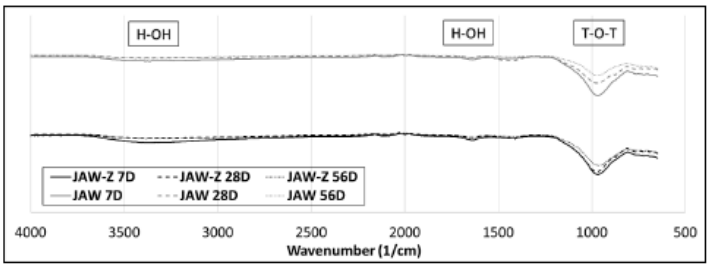

Figure 11: FTIR for JAW vs JAW-Z at 70°C BHST.

Table 15: The wave hollows occurred for JAW at 70 °C BHST.

Mix Design (70°C)	Curing Duration	T-O-T (cm^{-1}) [1400-700]	H-OH (cm^{-1}) [1700-1600]	H-OH (cm^{-1}) [3600-3000]
JAW	7D	969	1638	3366
JAW	28D	971	1646	3383
JAW	56D	972	1647	3388

Table 16: The wave hollows occurred for JAW-Z at 70 °C BHST.

Mix Design (70°C)	Curing Duration	T-O-T (cm^{-1}) [1400-700]	H-OH (cm^{-1}) [1700-1600]	H-OH (cm^{-1}) [3600-3000]
JAW-Z	7D	970	1642	3381
JAW-Z	28D	975	1646	3383
JAW-Z	56D	975	1653	3394

The results obtained from running FTIR show broad stretching vibrations and shifting in the bands' positions for JAW and JAW-Z as a function of curing time and curing temperature. At 25 °C, JAW and JAW-Z have the T-O-T stretching vibrations in ranges between 1400 – 700 (cm^{-1}), which are centered around 962-966 (cm^{-1}) after 7 days of curing for then to be centered around 975 (cm^{-1}) after 56 days. This shift in the wavelength of T-O-T bands for JAW and JAW-Z can be correlated to the dissolution of aluminosilicate precursor (Hajimohammadi et al., 2011), and the formation of CASH, NASH, or both gels with a higher crosslinking degree. Hence, the addition of admixtures could be low enough not to cause a significant influence on FTIR peaks around 1100 – 1000 cm^{-1} (Hajimohammadi et al., 2011). Interestingly, the size of T-O-T bands for both mixes with ageing was getting smaller which might be correlated to the further dissolution and participation of granite. This could define and be in line with the presence of the second sonic strength development zone in Figure 8.

The C-O-C vibration is hard to detect clearly due to the low calcium content in the mix designs, which agrees with previous studies (Omran et al., 2023b). The H-OH stretching at 3600 – 3000 cm^{-1} and 1700 – 1600 cm^{-1} are comparable for both JAW and JAW-Z. Hence, the resonance intensity differences are a function of the composition and concentration of the reaction products. This trend can be also observed at 70°C BHST curing, but with a higher shifting of the wavelengths for T-O-T and H-OH bands. These shifts indicate a higher degree of geopolymerization happening at elevated curing temperatures in agreement with Shah et al. (Shah et al., 2020). Therefore, the longer the specimen is allowed to cure while undergoing higher curing temperature, the higher the shifts in T-O-T, Si-O, and H-OH bonds are to be expected. Afterwards, the higher the formation of silicate hydration products in higher amounts could be produced and detected.

X-ray Diffraction (XRD)

Omran et al. (2023a, 2023b) characterized the precursors granite, GGBFS, and microsilica using XRD and Rietveld refinement. The results exhibited granite to be a highly crystalline precursor, rich in quartz, feldspar (microcline and albite), and oligoclase, with biotite and

chlorite as minor phases, with a crystalline content of around 80 % (see Table 17). While GGBFS and microsilica have highly amorphous content.

Table 17: Granite mineralogy obtained from Rietveld quantification [24].

Minerals	(#)	Granite (%wt/wt)
Quartz	PDF 00-008-7651	35.693
Albite	PDF 00-009-0466	21.625
Microcline 1	CIF 9004191	16.059
Microcline 2	PDF 00-019-0932	11.918
Oligoclase	CIF 9011423	10.654
Biotite	PDF 04-013-2135	2.382
Chlorite	COD 9010163	1.669

The XRD peaks and patterns of JAW and JAW-Z after 7D, 28D, and 56D under 25 and 70 °C BHST are illustrated in Figures 12 and 13, respectively.

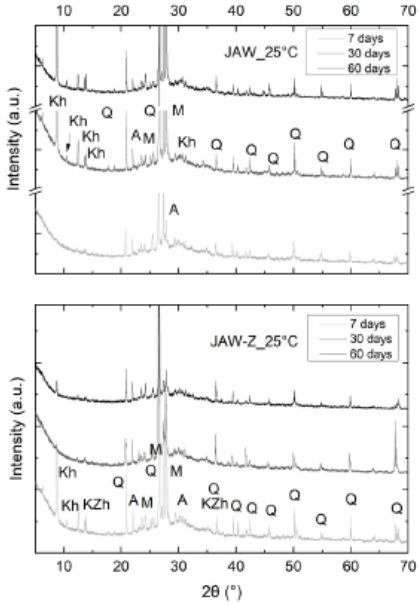

Figure 12: XRD patterns: a) JAW (neat) and b) JAW-Z (JAW + 0.86% ZnO), both cured at 25 °C BHST. Q: Quartz, M: Microcline, A: Albite, Kh: K-A-S-H or C-K-A-S-H, KZh: K-Z-A-S-H.

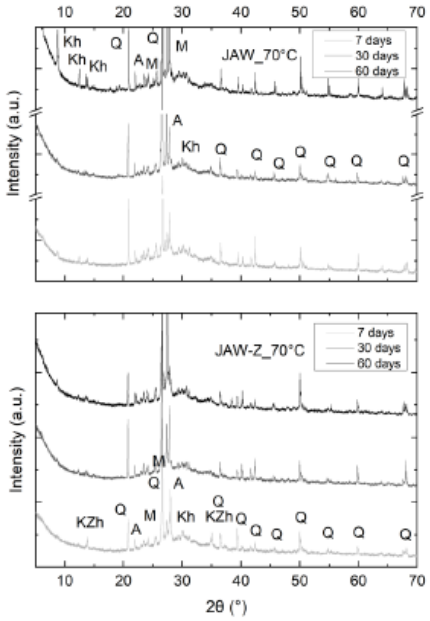

Figure 13: XRD patterns: a) JAW (neat) and b) JAW-Z (JAW + 0.86% ZnO), both cured at 70 °C BHST. Q: Quartz, M: Microcline, A: Albite, Kh: K-A-S-H or C-K-A-S-H, KZh: K-Z-A-S-H.

XRD spectra of JAW and JAW-Z have also been investigated as functions of curing time and curing temperature. The XRD peak intensities became higher and more crystalline by increasing both the curing period and curing temperature. These observed results match (Hajimohammadi et al., 2011; Pilehvar et al., 2020; Samantasinghar and Singh, 2019) considering low calcium content alkali-activated materials due to the overlaying of natural and synthesized crystals between angles 20-30° 2theta.

On the other hand, this trend could not be observed for the JAW-Z mix at 25 °C, where XRD reveals a much higher amorphous content. The presence of the amorphous phases can be due to the unreacted amorphous precursor phases. Both mixes may potentially contain amorphous geopolymers and hydrated phases such as C-A-S-H and C-(K, Na)-A-S-H, or a mix of both combined. Therefore, it would be fair to assume that JAW-Z could also contain an additional K-Zn-A-S-H phase as seen in Figures 10 and 11. These XRD observations are in line with previous studies (Omran et al., 2023b; Omran and Khalifeh, 2023).

Morphology - Scanning Electron Microscopy (SEM)

Granite has irregularly crystalline shaped particles mainly of quartz and feldspars. In addition, GGBFS and microsilica have a higher specific surface area and lower particle size distribution, when compared with granite (Omran et al., 2023a). Figures 14 and 15 include SEM micrographs of the two mixes cured at 25 and 70 °C, respectively, taken after 7D, 28D, and 56D of curing.

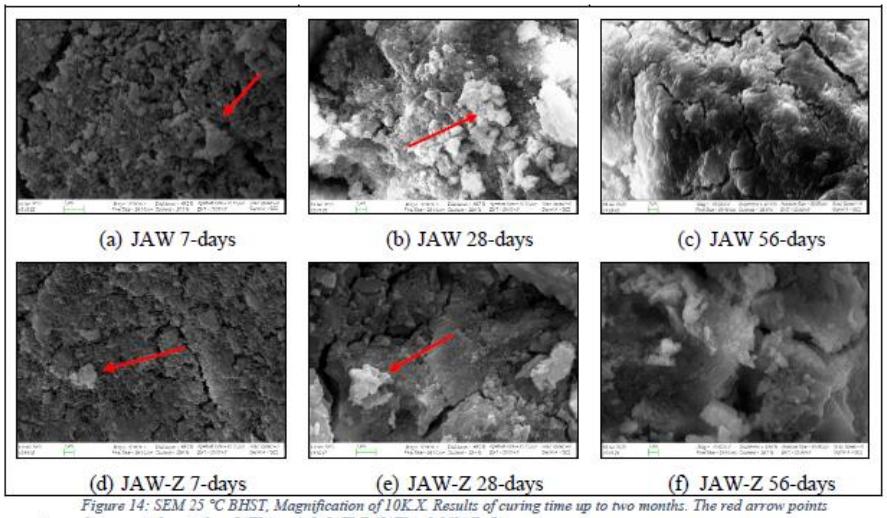

Figure 14: SEM 25 °C BHST, Magnification of 10K.X. Results of curing time up to two months. The red arrow points towards unreacted particles; JAW (neat) & JAW-Z (JAW + 0.86% ZnO).

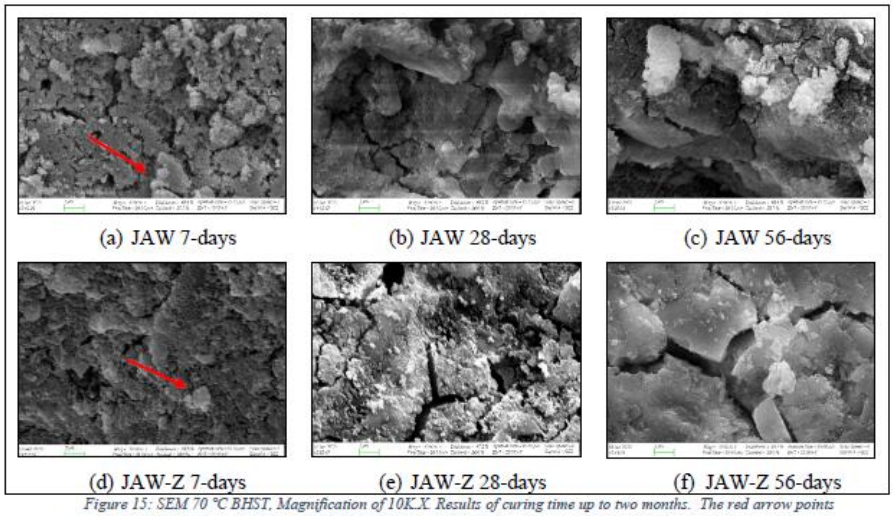

Figure 15: SEM 70 °C BHST, Magnification of 10K.X. Results of curing time up to two months. The red arrow points towards unreacted particles; JAW (neat) & JAW-Z (JAW + 0.86% ZnO).

The SEM images reveal that curing time and temperature have impact on the formation of more dense structures. Both mixes are observed to have a higher degree of incomplete geopolymerization reactions after 7D with fewer formation of gels. Unlike that of the 7 days of curing micrographs, the 28 and 56 days of curing indicate very low to the negligible presence of any remains of unreacted particles of granite and/or GGBFS. In addition, the longer the

curing duration, the lower the matrix porosity, and the denser and the harder the matrix gets for the two mixes. The dense matrices for JAW and JAW-Z match the results obtained from FTIR, and strength development evolutions over curing time.

The variation in curing temperature is also observed to have a clear effect on the SEM micrographs for both mixes. The samples cured at 25°C show larger amounts of unreacted particles and smaller amounts of geopolymer products. Contrary, the samples cured at 70°C are observed to have fewer remaining unreacted particles and larger amounts of geopolymer products being formed. Having the samples cured at elevated temperatures is observed to accelerate the geopolymerization reaction, which then helps the geopolymerization network in forming more complex 3D complex structures, and denser geopolymer matrixes. This trend is in line with the literature (Pilehvar et al., 2020; Salehi et al., 2018). Furthermore, the previously mentioned SEM observations also match the results and trends obtained from FTIR, and strength development evolution at prolonged curing and higher curing temperature.

Conclusion

Chemical properties and mechanical performance of aged granite-based JAW geopolymer were studied for well-cementing applications under a wide range of curing temperatures. High curing temperature favors the geopolymerization reaction, strongly impacts pumpability of the slurries, leaves fewer remaining unreacted precursor particles, improves strength development rate, and results in formation of denser structures and higher crystalline products. The use of ZnO as a strength enhancer was crucial for achieving acceptable mechanical properties in low-temperature well cementing applications, even though it may lead to a slight reduction in compressive strength compared to the neat mix design at a later stage. However, the hydraulic sealability of the system is negatively impacted with aging JAW mixes due to de-bonding at the geopolymer-casing interface. An expansive agent might be required to further improve the long-term hydraulic bond strength of JAW to avoid any possible chemical shrinkage with aging.

Acknowledgments

The authors gratefully acknowledge TotalEnergies, AkerBP, ConocoPhillips, and the Research Council of Norway for financially supporting the SafeRock KPN Project (RCN #319014- New Cementitious Material for Oil Well Cementing Applications - SafeRock) at the University of Stavanger, Norway. In addition, the authors would like to acknowledge Mr. Sondre Hjelm and Mr. Foster Gomado for their Lab contribution.

References

Adam, A.A., Horianto, X.X.X., 2014. The Effect of Temperature and Duration of Curing on the Strength of Fly Ash Based Geopolymer Mortar. Procedia Engineering 95, 410–414. https://doi.org/10.1016/j.proeng.2014.12.199

Anseau, M.R., Leung, J.P., Sahai, N., Swaddle, T.W., 2005. Interactions of silicate ions with zinc(II) and aluminum(III) in alkaline aqueous solution. Inorganic Chemistry 44, 8023–8032. https://doi.org/10.1021/ic050594c

API RP 10B-2, 2019. Recommended practice for testing well cements. American Petroleum Institute, Washington, DC.

Cai, J., Li, X., Tan, J., Vandevyvere, B., 2020. Thermal and compressive behaviors of fly ash and metakaolin-based geopolymer. Journal of Building Engineering 30, 101307. https://doi.org/10.1016/j.jobe.2020.101307

Chamssine, F., 2023. Instituting Retarders for Geopolymers Developed for Downhole Applications (PhD Thesis). University of Stavanger, Stavanger, Norway.

Chen, A.L., Xu, D., Chen, X.Y., Zhang, W.Y., Liu, X.H., 2012. Measurements of zinc oxide solubility in sodium hydroxide solution from 25 to 100 °c. Transactions of Nonferrous Metals Society of China (English Edition) 22, 1513–1516. https://doi.org/10.1016/S1003-6326(11)61349-6

Chithiraputhiran, S., Neithalath, N., 2013. Isothermal reaction kinetics and temperature dependence of alkali activation of slag, fly ash and their blends. Construction and Building Materials 45, 233–242. https://doi.org/10.1016/j.conbuildmat.2013.03.061

Gilfillan, D., Marland, G., 2021. CDIAC-FF: global and national CO₂ emissions from fossil fuel combustion and cement manufacture: 1751–2017. Earth Syst. Sci. Data 13, 1667–1680. https://doi.org/10.5194/essd-13-1667-2021

Gomado, F.D., Khalifeh, M., Aasen, J.A., 2023. Expandable Geopolymers for Improved Zonal Isolation and Plugging, in: Day 3 Thu, March 09, 2023. Presented at the SPE/IADC International Drilling Conference and Exhibition, SPE, Stavanger, Norway, p. D031S026R004. https://doi.org/10.2118/212493-MS

Hajimohammadi, A., Provis, J.L., van Deventer, J.S.J., 2011. Time-resolved and spatially-resolved infrared spectroscopic observation of seeded nucleation controlling geopolymer gel formation. Journal of Colloid and Interface Science 357, 384–392. https://doi.org/10.1016/j.jcis.2011.02.045

Hajimohammadi, A., Provis, J.L., van Deventer, J.S.J., 2008. One-Part Geopolymer Mixes from Geothermal Silica and Sodium Aluminate. Ind. Eng. Chem. Res. 47, 9396–9405. https://doi.org/10.1021/ie8006825

Hajimohammadi, A., van Deventer, J.S.J., 2017. Characterisation of One-Part Geopolymer Binders Made from Fly Ash. Waste Biomass Valor 8, 225–233. https://doi.org/10.1007/s12649-016-9582-5

Hjelm, S., 2022. Revealing the Effect of Superplasticizers on Viscosity and Yield Stress of Geopolymers. (Bachelor Thesis). University of Stavanger, Stavanger, Norway.

Ke, X., Bernal, S.A., Ye, N., Provis, J.L., Yang, J., 2015. One-Part Geopolymers Based on Thermally Treated Red Mud/NaOH Blends. J. Am. Ceram. Soc. 98, 5–11. https://doi.org/10.1111/jace.13231

Khalifeh, M., 2016. Materials for Optimized P&A Performance: Potential Utilization of Geopolymers (PhD Thesis). University of Stavanger, Stavanger, Norway.

Khalifeh, M., Saasen, A., Hodne, H., Godøy, R., Vrålstad, T., 2018. Geopolymers as an Alternative for Oil Well Cementing Applications: A Review of Advantages and Concerns. Journal of Energy Resources Technology 140, 092801. https://doi.org/10.1115/1.4040192

Khalifeh, M., Saasen, A., Hodne, H., Motra, H.B., 2019. Laboratory evaluation of rock-based geopolymers for zonal isolation and permanent P&A applications. Journal of Petroleum Science and Engineering 175, 352–362. https://doi.org/10.1016/j.petrol.2018.12.065

Kong, D.L.Y., Sanjayan, J.G., 2010. Effect of elevated temperatures on geopolymer paste, mortar and concrete. Cement and Concrete Research 40, 334–339. https://doi.org/10.1016/j.cemconres.2009.10.017

Li, X., Wang, Z., Jiao, Z., 2013. Influence of Curing on the Strength Development of Calcium-Containing Geopolymer Mortar. Materials 6, 5069–5076. https://doi.org/10.3390/ma6115069

Luukkonen, T., Abdollahnejad, Z., Yliniemi, J., Kinnunen, P., Illikainen, M., 2018. One-part alkali-activated materials: A review. Cement and Concrete Research 103, 21–34. https://doi.org/10.1016/j.cemconres.2017.10.001

Ma, C., Long, G., Shi, Y., Xie, Y., 2018. Preparation of cleaner one-part geopolymer by investigating different types of commercial sodium metasilicate in China. Journal of Cleaner Production 201, 636–647. https://doi.org/10.1016/j.jclepro.2018.08.060

Ma, C., Zhao, B., Guo, S., Long, G., Xie, Y., 2019. Properties and characterization of green one-part geopolymer activated by composite activators. Journal of Cleaner Production 220, 188–199. https://doi.org/10.1016/j.jclepro.2019.02.159

Mahendra, K., Narasimhan, M.C., 2023. One part alkali-activated materials for construction – A review. Materials Today: Proceedings S2214785323039871. https://doi.org/10.1016/j.matpr.2023.07.116

McLellan, B. C., Williams, R. P., Lay, J., van Riessen, A., & Corder, G. D. (2011). Costs and carbon emissions for geopolymer pastes in comparison to ordinary Portland Cement. Journal of Cleaner Production, 19(9–10), 1080–1090. https://doi.org/10.1016/j.jclepro.2011.02.010

Mellado, A., Catalán, C., Bouzón, N., Borrachero, M. V., Monzó, J. M., & Payá, J. (2014). Carbon footprint of Geopolymeric Mortar: Study of the contribution of the alkaline activating solution and assessment of an alternative route. RSC Adv., 4(45), 23846–23852. https://doi.org/10.1039/c4ra03375b

Mo, L., Deng, M., Tang, M., 2010. Effects of calcination condition on expansion property of MgO-type expansive agent used in cement-based materials. Cement and Concrete Research 40, 437–446. https://doi.org/10.1016/j.cemconres.2009.09.025

Najafi Kani, E., Allahverdi, A., Provis, J.L., 2017. Calorimetric study of geopolymer binders based on natural pozzolan. J Therm Anal Calorim 127, 2181–2190. https://doi.org/10.1007/s10973-016-5850-7

Nematollahi, B., Sanjayan, J., Shaikh, F.U.A., 2015. Synthesis of heat and ambient cured one-part geopolymer mixes with different grades of sodium silicate. Ceramics International 41, 5696–5704. https://doi.org/10.1016/j.ceramint.2014.12.154

Omran, M., Hjelm, S., Khalifeh, M., Salehi, S., 2023a. Synthesis of sustainable one-part geopolymers for well cementing applications. Geoenergy Science and Engineering 227, 211822. https://doi.org/10.1016/j.geoen.2023.211822

Omran, M., Kalifeh, M., 2022. Development of Low Carbon Dioxide Intensive Rock-Based Geopolymers for Well Cementing Applications – One-Part Geopolymer, OMAE2022-78535, in: 41st International Conference on Ocean, Offshore & Arctic Engineering. OMAE, Hamburg, Germany.

Omran, M., Khalifeh, M., 2023. Development of One-Part Rock-Based Geopolymers for Downhole Cementing Applications. Journal of Energy Resources Technology 145, 103201. https://doi.org/10.1115/1.4062250

Omran, M., Khalifeh, M., Hjelm, S., 2022a. Role of Zeta Potential on Rheology of One-part Geopolymer Slurries: Influence of Superplasticizers, in: Annual Transactions of the Nordic Rheology Society, Vol. 30. Nordic Rheology Society.

Omran, M., Khalifeh, M., Saasen, A., 2022b. Influence of Activators and Admixtures on Rheology of Geopolymer Slurries for Well Cementing Applications, in: Day 3 Wed, October 19, 2022. Presented at the SPE Asia Pacific Oil & Gas Conference and Exhibition, SPE, Adelaide, Australia, p. D031S012R003. https://doi.org/10.2118/210698-MS

Omran, M., Paiva, M., Khalifeh, M., 2023b. Design and Early Age Performance of Sustainable One-Part Geopolymers for Well Cementing. SPE Journal 1–18. https://doi.org/10.2118/215825-PA

Paiva, M.D.M.M.D.M., Silva, E.C.C.M.E.C.C.M., Melo, D.M.A.D.M.A., Martinelli, A.E.A.E., Schneider, J.F.J.F., 2018. A geopolymer cementing system for oil wells subject to steam injection. Journal of Petroleum Science and Engineering 169, 748–759. https://doi.org/10.1016/j.petrol.2018.06.022

Pilehvar, S., Sanfelix, S.G., Szczotok, A.M., Rodríguez, J.F., Valentini, L., Lanzón, M., Pamies, R., Kjøniksen, A.-L., 2020. Effect of temperature on geopolymer and Portland cement composites modified with Micro-encapsulated Phase Change materials. Construction and Building Materials 252, 119055. https://doi.org/10.1016/j.conbuildmat.2020.119055

Rovnaník, P., 2010. Effect of curing temperature on the development of hard structure of metakaolin-based geopolymer. Construction and Building Materials 24, 1176–1183. https://doi.org/10.1016/j.conbuildmat.2009.12.023

Salehi, S., Khattak, M.J., Ali, N., Ezeakacha, C., Saleh, F.K., 2018. Study and Use of Geopolymer Mixtures for Oil and Gas Well Cementing Applications. Journal of Energy Resources Technology, Transactions of the ASME 140, 1–12. https://doi.org/10.1115/1.4037713

Samantasinghar, S., Singh, S.P., 2019. Fresh and Hardened Properties of Fly Ash–Slag Blended Geopolymer Paste and Mortar. Int J Concr Struct Mater 13, 47. https://doi.org/10.1186/s40069-019-0360-1

Shah, S.F.A., Chen, B., Oderji, S.Y., Haque, M.A., Ahmad, M.R., 2020. Improvement of early strength of fly ash-slag based one-part alkali activated mortar. Construction and Building Materials 246, 118533. https://doi.org/10.1016/j.conbuildmat.2020.118533

Singh, N.B., Middendorf, B., 2020. Geopolymers as an alternative to Portland cement: An overview. Construction and Building Materials 237. https://doi.org/10.1016/j.conbuildmat.2019.117455

Siyal, A.A., Azizli, K.A., Man, Z., Ullah, H., 2016. Effects of Parameters on the Setting Time of Fly Ash Based Geopolymers Using Taguchi Method. Procedia Engineering 148, 302–307. https://doi.org/10.1016/j.proeng.2016.06.624

Sun, Z., Vollpracht, A., 2019. One year geopolymerisation of sodium silicate activated fly ash and metakaolin geopolymers. Cement and Concrete Composites 95, 98–110. https://doi.org/10.1016/j.cemconcomp.2018.10.014

Appendix 10 – A Filed Patent in Norway

ANKOM
BRANN
2022 -12- 23

patent trademark design
Norwegian Industrial
Property Office

BRANN AB
Box 3690
10359 STOCKHOLM
Sverige

Oslo, 2022.12.15

Your ref.: P3156ZNO
Application no.: 20220629 (please include in your reply)
Applicant: UNIVERSITETET I STAVANGER
Due date: 2023.06.15

KOPI

Office action in patent application no. 20220629

Basis of the opinion
Description received 2022.06.01
Claims received 2022.06.01
Drawings received 2022.06.01